Hydration mechanism of cements based on low-CO2 clinkers containing belite, ye'elimite and calcium alumino-ferrite

Jia Wang

THESE

présentée en vue de l'obtention du titre de

DOCTEUR DE L'UNIVERSITÉ LILLE 1 SCIENCES ET TECHNOLOGIES

Spécialité : Molécules et Matière condensée

par

Jia WANG

Hydration mechanism of cements based on low-CO_2 clinkers containing belite, ye'elimite and calcium alumino-ferrite

Soutenue le 05 Octobre 2010

Jury

M.SAKAI Etsuo	Professeur (Tokyo Institute of Technology)	Rapporteur
M.NONAT André	Directeur de recherche (CNRS)	Rapporteur
MELLE. CAU-DIT-CAUMES Céline	Ingénieur - Chercheur (CEA de Marcoule)	Examinateur
MME.SORRENTINO Danielle	Chercheur (MRPRO - HDR)	Examinateur
M.LAFHAJ Zoubeir	Professeur (Ecole Centrale Lille)	Examinateur
M.GARTNER Ellis	Principal Scientist (Lafarge – Dr)	Examinateur
M.SUI Tongbo	Professor (Chinese Ceramic Society)	Examinateur
M.DAMIDOT Denis	Professeur (Ecole des Mines Douai)	Examinateur

Abstract

The objective of this work was to better understand the hydration mechanisms of cements belonging to the family of BCSAF cement in order to develop simple mechanistic models which can help us to optimise mixtures of BCSAF clinker and other compounds for specific applications.

The studied cements were made from a clinker containing 52% of belite, 33% of ye'elimite and 14% of a ferrite phase and various amounts of anhydrite and limestone.

From the detailed investigation of the hydration of cement containing 95% of clinker and 5% of anhydrite, it has been demonstrated that the mechanism of hydration has two main successive periods of hydration: the beginning of hydration is controlled by ye'elimite and anhydrite, while the remaining of hydration is governed by belite and the ferrite phase that react with some of the hydrates formed during the first period. It is C_2ASH_8 nucleation rate that governs the beginning of the hydration of belite. The main parameter that governs the nucleation rate of strätlingite is $[SO_4]^{2-}$ that has to be low. C-S-H does not form as the initial hydrate for belite hydration because it is not saturated in the beginning due to low calcium and silicon concentration and its formation is further delayed later by the inhibition effect of high aluminate concentration on C-S-H nucleation. As a consequence, this is indirectly the sulphate concentration that controls the beginning of belite hydration and thus the reactions leading to its reduction, mainly the hydration of ye'elimite to form ettringite. Globally it is once ye'elimite has been completely reacted that strätlingite may nucleate. A synergy between the reactions of belite and ferrite is found to accelerate the formation of later hydrate, hydrogarnet and C-S-H at the expense of strätlingite.

A similar mechanism of hydration has been found for cements having higher anhydrite contents at the exception of cements that have more anhydrite than the theoretical anhydrite content to consume all ye'elimite to form ettringite. For the former cements, more anhydrite can strongly delay the second period of the hydration where both belite and ferrite react. In the later cases, the mechanism of hydration is quite different as belite does start to react till the beginning of hydration certainly forming either a Si containing ettringite or C-S-H.

The influence of 15% of limestone was investigated on the cement containing 95% of clinker and 5% of anhydrite. The results showed that limestone did not change the first period involving anhydrite and ye'elimite, but strongly delayed the beginning of the second period where both belite and ferrite hydrate. This may be due to a delayed nucleation of strätlingite induced by a longer period having higher $[SO_4]^{2-}$ as ettringite is stabilised by the precipitation of carbonated AFm at the expense of calcium monosulfoaluminate hydrate, thanks to the carbonate ions brought by limestone.

Finally some perspectives are given in order to reduce the duration of the first period and then to enable the hydration of both belite and ferrite more rapidly.

Keywords: Belite (C_2S), ye'elimite ($C_4A_3\$$), Ferrite (C_4AF), hydration, anhydrite, limestone

Résumé

L'objectif de ce travail a été d'apporter une meilleure compréhension des mécanismes réactionnels de l'hydratation de ciments appartenant à la famille de ciment BCSAF afin de développer des schémas réactionnels simplifiés permettant d'optimiser les ciments à base d'un clinker BCSAF et d'autres constituants pour des applications spécifiques.

Les ciments étudiés ont été réalisés à partir d'un clinker contenant 52% de belite, 33% de ye'elimite and 14% de ferrite et diverses quantités d'anhydrite et de calcaire.

A partir de l'étude détaillée de l'hydratation d'un ciment contenant 95% de clinker et 5% d'anhydrite, il a été démontré que le mécanisme de l'hydratation est constitué de deux périodes successives : le début de l'hydratation est contrôlé par l'hydratation de la ye'elimite réagissant avec l'anhydrite, tandis que la suite de l'hydratation est contrôlée par les hydratations de la belite et de la ferrite qui réagissent avec certains des hydrates formés lors de la première période. La vitesse de nucléation de la strätlingite contrôle le début de l'hydratation de la belite. Le principal paramètre qui contrôle cette dernière est la concentration en sulfate de la phase aqueuse qui doit être très faible. Ainsi C-S-H n'est pas formé au début de l'hydratation de la belite parce qu'elle n'est pas saturé à cause de faible concentration de calcium et silicon et sa formation est retardé plus tard à cause de l'inhibition de sa nucléation par de trop fortes quantités d'aluminate en solution. Par conséquence, c'est indirectement la concentration en sulfate de la solution qui contrôle le début de l'hydratation de la belite and ainsi les réactions conduisant à sa réduction à travers la précipitation de phase notamment lors de l'hydratation de la ye'elimite pour former de l'ettringite. Ainsi d'une façon générale, la strätlingite commence à nucléer quand la ye'elimite a complètement réagi. D'autre part, une synergie entre les hydratations de la belite et de la ferrite permet de former des hydrogrenats et des C-S-H à des temps longs au détriment de la strätlingite formée auparavant.

Un mécanisme d'hydratation similaire a été trouvé pour les ciments contenant des quantités plus importantes d'anhydrite à l'exception de ceux qui contiennent une quantité d'anhydrite supérieure que la quantité théorique permettant de faire réagir toute la ye'elimite en ettringite. Toutefois pour le premier type de ciments, une augmentation de la quantité d'anhydrite allonge à la fois le temps d'apparition de la seconde période et la durée des différentes étapes de cette dernière. Donc l'hydratation est globalement plus lente. Pour le second type de ciment, contenant de fortes quantités d'anhydrite, le mécanisme d'hydratation est assez différent car l'hydratation de la belite commence dès le début de l'hydratation et conduit à la formation, soit d'ettringite contenant Si, soit de C-S-H.

L'effet de 15% de calcaire a également été étudié pour le ciment contenant 95% de clinker et 5% d'anhydrite. Les résultats ont montré que le calcaire ne change pas la première période de l'hydratation mettant en jeu principalement la ye'elimite et l'anhydrite. Par contre la seconde période, durant laquelle la belite et la ferrite s'hydratent, est fortement retardée à son début. Ceci peut être dû à un retard de la nucléation de la strätlingite à cause de concentrations en sulfate de la solution restant plus longtemps élevées par le fait que l'ettringite est stabilisée en présence de carbonate par la formation de phases AFm carbonatées qui inhibent la formation de monosulfoaluminate de calcium hydraté.

Pour finir, des perspectives sont données notamment afin de réduire la durée de la première période de l'hydratation et ainsi permettre un démarrage plus rapide de l'hydratation de la belite et de la ferrite.

Keywords: Belite (C_2S), ye'elimite ($C_4A_3\$$), Ferrite (C_4AF), hydration, anhydrite, calcaire

Acknowledgments

Countless memories accumulated during the first year are made by pieces of unforgettable experience with countless people; even every person that I crossed in my way has already earned his place in my esteem.

My first thoughts are naturally given to my work team, Lafarge Research Centre (LCR).
Firstly, I would like to thank Paul ACKER, the organizer of the 'Lafarge Chair', who brought me into LCR and gave me the opportunity to continue my thesis in the hydration group.
To my industrial supervisor, Ellis GARTNER, I extend special thanks for his assistance, suggestions, and friendly counselling as I worked through problems, both in my research and my life. I also thank the BCSAF project leader Günter WALENTA, for his full support.
Additional thanks are due to Vincent MORIN, Cedric COMPARET, Blandine ALBERT, Jean-Michel CASABONNE, for many discussions, suggestions, recommendations, and supports; also, to Isabelle BACO, Veronique BROYER, Marie-Christine, Pascal BOST, Vincent BRIAUD, Aurélie MARTINS and Marie-France for guiding me on my experimental work, especially when I just arrived in the physical chemistry laboratory.

Then, I would like to show my sincere thanks to my French academic supervisor, Prof. Denis DAMIDOT, who impresses me with his inexhaustible energy and passion on research. I also thank all the members of the Civil Engineering Department of "Ecole des Mines de Douai" for their assistance during my stay in their laboratory.

I would also like to thank all my colleagues on the CBMA side. In particular, my Chinese supervisor, Vice president of CBMA, Prof. SUI, who helped immeasurably on my arrival at CBMA and my first bibliography study on Chinese CSA (Calcium Sulfo-aluminate) cement; President Cui QI, vice-president Guanghua LIU, for their help during my stay in Beijing; Senior Engineer, Zhaijun WEN, Xianbin WANG, Chao LIU and Zhijun XIN, for inspiring me on literature study and helping me to arrange the appointments with other people; Lei FAN, Wensheng ZHANG, Li TAN, Hongtao ZHANG, Juan LI, Chunying ZHOU, for their warm reception; and a special thanks to my office-mate, Min WANG, for all his care about my daily life, and especially for introducing me so many of his friends and his favourite restaurants.

Finally, I would like to thank for the support of my family far away from China, even they get more and more confused about what I am doing.

NOTATIONS

Oxide notation

C	CaO
A	Al_2O_3
S	SiO_2
F	Fe_2O_3
$	SO_3
H	H_2O
$\overline{C}$	CO_2

Notation and formulae for solid phases discussed in this report

Name	Formula	Name	Formula
Belite	C_2S	Monocarboaluminate	$C_3A.C\overline{C}.H_{11}$
Ye'elimite	$C_4A_3\$$	Hemicarboaluminate	$C_3A.\frac{1}{2}C\overline{C}.\frac{1}{2}CH.H_{11}$
Anhydrite	C$	Strätlingite	C_2ASH_8
Ferrite	$C_2A_xF_{(1-x)}$	Katoite (hydrogarnet)	$C_3A_{(1-y)}F_yS_zH_{(6-2z)}$
Ettringite	$C_3A.3C\$.H_{32}$	Calcite (limestone)	$C\overline{C}$
Monosulfoaluminate	$C_3A.C\$.H_{12}$	Gibbsite	AH_3

Sample coding

k165-400B-xA means that clinker k165 and anhydrite were ground separately to about 400m²/kg Blaine specific surface area in a lab ball mill, and then mixed in the ratio (100-x):x by mass. (x=0, 5, 10 and 20)

k165-400B-5A-15L means that limestone and cement k165-400B-5A were mixed in the ratio 100: 15 by mass.

Annex coding

Annex x-y means the Yst Annex mentioned in Chapter X.

Coding of Figures

Figure x-y means the Yst Figure mentioned in Chapter X.
Figure xAy-z means the Zst Figure mentioned in Annex x-y.
* note: Main Figures in Chapter 3, 4, 5 can be found in the end of the chapter.

Coding of Tables

Table x-y means the Yst Table mentioned in Chapter X.
Table xAy-z means the Zst Table mentioned in Annex x-y.
* note: Main Tables in Chapter 3, 4, 5 can be found in the end of the chapter.

LIST OF ANNEXES

Chapter 2

Chapter 5

LIST OF FIGURES

Chapter 1

Chapter 2

Chapter 3

Chapter 4

Chapter 5

LIST OF TABLES

Chapter 1

Chapter 2

Chapter 3

Chapter 4

Chapter 5

Chapter I

Introduction

1 Introduction

1.1 Political and social contexts

Today, it is widely accepted that a close link exists between increased concentrations of greenhouse gases and climate variability (Figure 1-1).

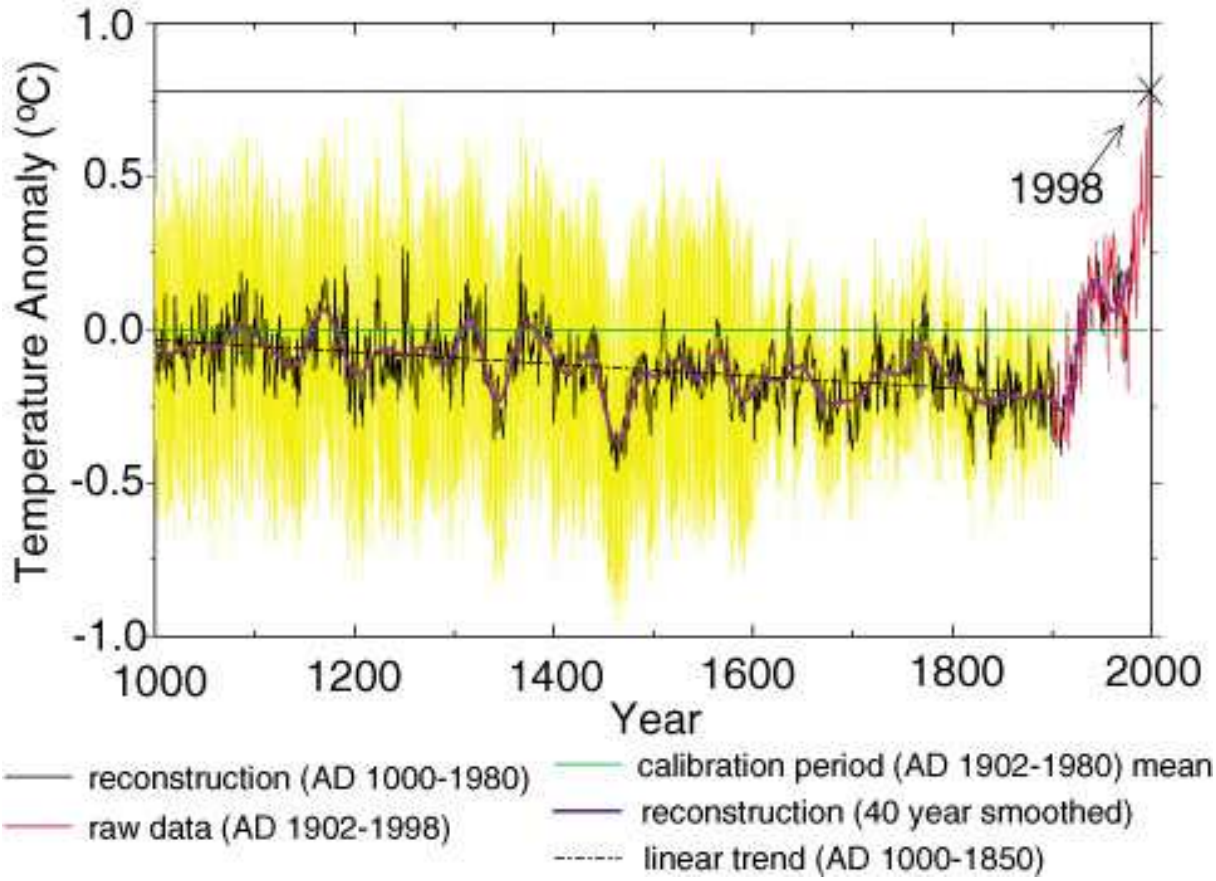

Figure 1-1: Average temperature in the northern hemisphere in the last millennium [1]

According to the Precautionary Principle, commitments to reduce greenhouse gas have been made in 1997 under the Kyoto Protocol.

1.2 Actuality of cement industry and the reaction of Lafarge

Cement production is regarded as the third largest source of CO_2 after the combustion of fossil fuels and deforestation. With the increasing requirement of cement, particularly in developing countries, it is expected that emissions of CO_2 related to cement manufacture and use will double by the middle of this century.

Lafarge, the world leader in construction materials, is the first industrial group to become a WWF Conservation Partner, with a relationship that began in 2000. Within the terms of this unique partnership, WWF is contributing to the expertise Lafarge that needs to develop in order to improve its environmental policies and practices and to raise awareness of the importance of sustainability and biodiversity conservation.

In November 2001, Lafarge made the important commitment to reduce its CO_2 emissions globally by 20% per ton of cement produced over the period 1990 - 2010. Lafarge also

committed to reducing its absolute CO_2 emissions by 10% in industrialized countries below 1990 levels by 2010.

To achieve this goal, Lafarge has to improve its energy efficiency, use alternative fuels and produce cement in ways that are less carbon-intensive. WWF will be strictly involved in the implementation and monitoring of the program.

Lafarge has also published its first sustainable development report, which concerns the economic, social and environmental issues related to the group's activities in 75 countries. Among environmental objectives, in addition to reducing emissions, the Lafarge group will:

- Audit all its production sites every 4 years to have an environmental assessment site by site (CO_2 emissions, water consumption, energy and raw materials used, etc.).
- Achieve a rate of 80% of operated quarries for the extraction of construction materials to have a rehabilitation plan.

1.3 Lafarge's approaches to reducing CO_2 emissions.

Numerous studies have been carried out in the European cement industry to reduce CO_2 emissions. The only current approaches are reducing the use of cement-based materials, replacing fossil fuels with renewable fuels and maximizing the thermal efficiency of the kiln. These three approaches probably reach their practical limits in the forthcoming decade, and new approaches will be needed in the long term.

During the formation of clinker, calcium carbonate is transformed into calcium oxide, which allows the escape of carbon dioxide (CO_2) contained in the limestone. This releases about 0.53 ton of CO_2 per ton of Portland cement. Moreover, energy consumption and electricity represents 65 to 70% of the cost of production [2].

The generation of carbon dioxide from decarbonation of raw materials ($RMCO_2$) was calculated by Gartner [2] for different minerals that can be found in cement (Table 1-1). For example, we can see that the $RMCO_2$ values of $C_4A_3\$$, C_2S and C_4AF are respectively 0.216, 0.511, 0.362 compared to 0.578 for C_3S, the phase which represents about 65 % of a typical Ordinary Portland Cement (OPC) [2].

Cement compound	Raw materials used	$RMCO_2$ (g/g)	$RMCO_2$ (g/ml)
M (magnesia, periclase)	Magnesite	1.092	3.91
C (calcia, quicklime)	Limestone	0.785	2.63
C_3S (alite)	Limestone + silica	0.578	1.80
β-C_2S (belite)	Limestone + silica	0.511	1.70
C_3A (tricalcium aluminate)	Limestone + alumina	0.489	1.50
C_4AF (calcium aluminoferrite)	As above + iron oxide	0.362	1.29
NS (sodium metasilicate)	Soda + silica	0.361	-
CA (monocalcium aluminate)	Limestone + alumina	0.279	0.83
$C_4A_3\$$ (calcium sulfoaluminate)	As above + anhydrite	0.216	0.56

Table 1-1: Raw Materials CO_2 per unit mass and volume for the major cement compounds of interest

Thus, classical calcium sulfoaluminate cements (CSA, see Table 1-2) based on ye'eliminte ($C_4A_3\$$) with lesser amounts of C_2S and C_4AF, should give lower raw materials-derived CO_2 emissions than OPC.

Type	$C_4A_3\$$	C_2S	C_4AF
CSA (low ferrite)	55 to 75	15 to 30	3 to 6
CSA (high ferrite)	35 to 55	15 to 35	15 to 30

Table 1-2: Typical phase composition of CSA cement products in China ([3] P. 33)

Also, considering that the thermal energy is mainly used for calcining limestone, the reduction of limestone content in the kiln feed creates a similar decrease in the energy needed for calcination. So the composition of CSA permits a production process that might be considered to be more "environmentally friendly," than that of OPC, because:

- The quantity of limestone in the raw materials of the kiln is reduced, hence both fuel-derived and raw-materials-derived CO_2 emissions are reduced;
- The maximum synthesis temperatures are at least 100°C lower than those required (1400°C - 1500°C) for OPC;
- The clinker is easier to grind (i.e. less energy is required for grinding);
- Industrial waste and secondary products can be reused more easily as raw materials [4].

CSA has been used in civil construction on a large scale since its invention at the CBMA (China Building Material Academy) in the 1970s [5], but its production has stayed stable around 1.2~1.3 millions tons since 2004 in China [6]. One of the main reasons is that more aluminium is needed in the raw material to produce CSA, which makes it more expensive to produce than OPC, and which has thus limited it to various "niche" applications which make use of special properties such as rapid hardening or self-stressing (depending on the cement formulation).

In 2004, Gartner [2] proposed that cements based on belite, ye'elimite and other phases could be of interest as low-CO_2 alternatives to Portland cement, and a Lafarge patent was filed based on this approach [9]. The clinkers proposed by Lafarge are referred to as "BCSAF" and are richer in belite than classical CSA, which allows the use of less expensive raw materials.

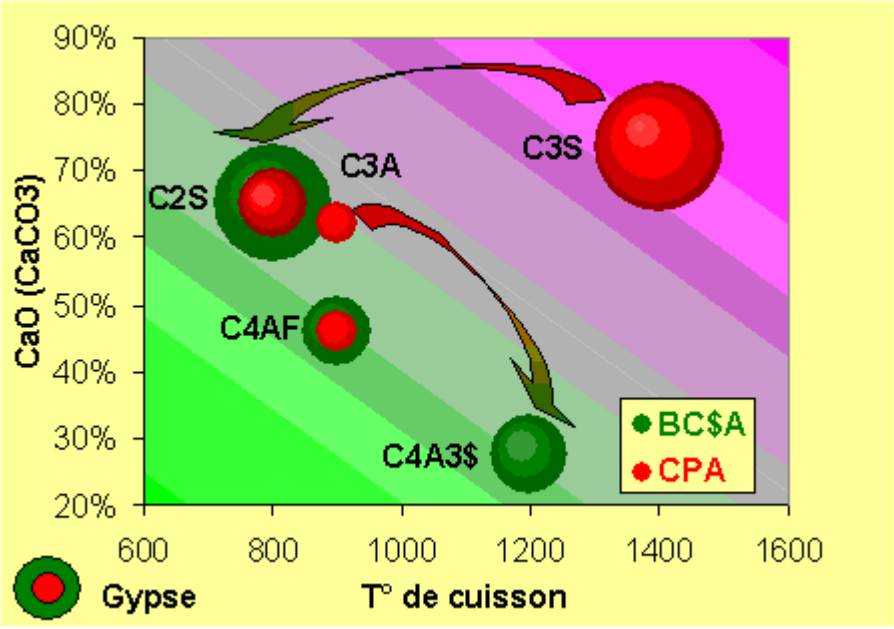

Figure 1-2: The conception of BCSAF cement

The preparation of BCSAF clinker and cement is described in the patent [7]. The raw

materials used in the patent examples were a relatively pure limestone, a kaolinite clay and gypsum. Iron was added as Fe_2O_3.

%	CaO	SiO_2	Al_2O_3	Fe_2O_3	SO_3	MgO	TiO_2	K_2O	Na_2O
BCSAF	52.48	17.60	16.90	7.79	4.51	0.21	0.37	0.08	0.06
%	"C_2S"		"$C_4A_3\$$"		Ferrite		Others		
BCSAF	51.4		28.6		19.3		0.7		

Table 1-3: The physical (calculated) and chemical (measured) composition of typical BCSAF [8]

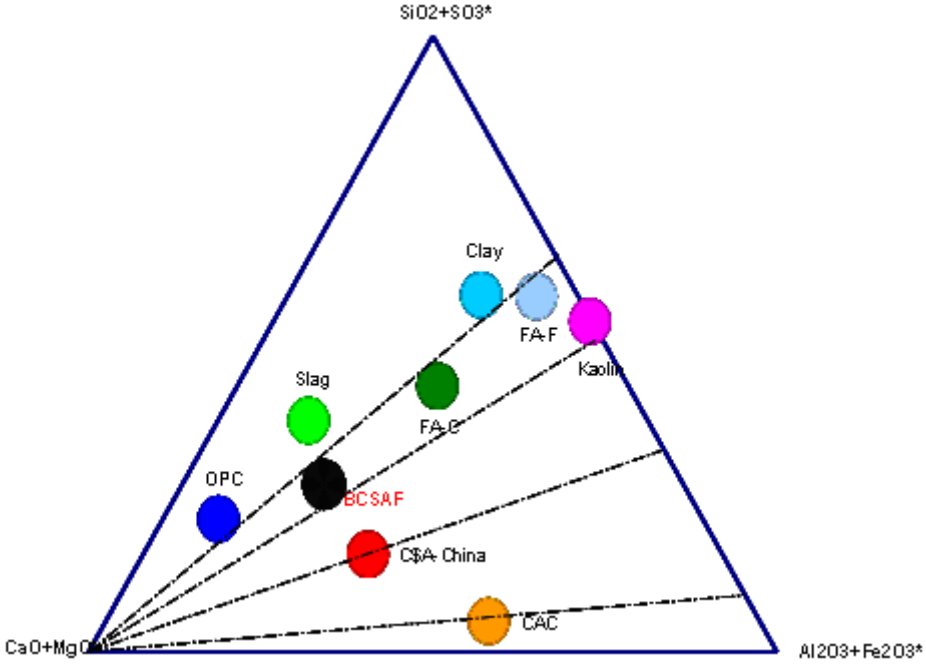

Figure 1-3: The position of different cements in the CSA system

1.4 Bibliography study

In Table 1-3, we can notice that belite and ferrite present around 70% by mass in BCSAF clinker. However, these two phases hydrate more slowly than alite and tricalcium aluminate in OPC and than ye'elimite in CSA. Therefore, the reactivity of these two phases and their interaction with other phases, which is often neglected in OPC and CSA due to the low content, should be asked in detail in the case of BCSAF. Therefore we must know how to accelerate their hydration before this new type of cement can go into production. Thus the mechanism of its hydration needs to be understood in depth so that the concrete will have predictable long-term performance. Both the kinetics of the hydration reactions and the nature of hydration products need to be understood in order to allow us to better formulate cements based on BCSAF clinkers. In addition, the stability of the hydration products under various conditions needs to be well understood in order to be able to make realistic predictions of concrete durability.

Much experience has been accumulated over many years on the hydration of Portland cements. However, the experience of OPC hydration cannot be applied directly to BCSAF cements, which have completely different phase compositions. Numerous studies were done on Chinese CSAs, which could give us some ideas. However, care should be taken when we

compare experimental results, because CSA clinkers that are prepared under different conditions have a wide range of compositions.

1.4.1 Reactivity of principal constituents of BCSAF cement and their hydration

In the clinker, all the anhydrous phases do not have the same reactivity.

$C_4A_3\$$ (Ye'elimite)

In Chinese industrial CSAs, $C_4A_3\$$ crystallizes in the form of very thin hexagonal or pseudo-hexagonal plates (5-10 μm) [9], which is considered as the most reactive phase [10,11,12,13], especially in the presence of lime or calcium sulphate [14,15,16]. In CSA products, calcium sulphate, in form of anhydrite or gypsum, is added into the clinker to govern the initial reactions and to give the early strength [17]. The reaction between $C_4A_3\$$ and anhydrite was studied [14,15,16]. It was shown that the nature and quantity of hydration products depends on the availability of anhydrite (C$) compared to $C_4A_3\$$:

- Without calcium sulphate, the final hydrates of ye'elimite are calcium monosulfoaluminate hydrate and aluminate hydroxide. Reaction equation can be written as:

$$C_4A_3\$ + 18H \Rightarrow C_4A\$H_{12} + 2AH_3 \quad (1.1)$$

- If the molar ratio between C$ and ye'elimite equals or higher than 2, the final hydrates are ettringite and aluminate hydroxide. Reaction equation can be written as:

$$C_4A_3\$ + 2C\$ + 38H \Rightarrow C_6A\$_3H_{32} + 2AH_3 \quad (1.2)$$

- If 0< (molar ratio between C$ and ye'elimite)<2, the final hydrates are a mixture of calcium monosulfoaluminate hydrate, ettringite and aluminate hydroxide. Reaction equation can be written as:

$$2C_4A_3\$ + 2C\$ + 38H \Rightarrow C_6A\$_3H_{32} + C_4A\$H_{12} + 4AH_3 \quad (1.3)$$

Belite

The majority of belite crystals in Chinese CSA are α' crystallographic form with a low proportion of β form. The crystals are very fine, usually less than 2-5 μm and intimately mixed with the crystals of $C_4A_3\$$ [18]. α'-C_2S is considered more reactive than β-C_2S [19]. Nevertheless, it should be noted that even in the form β-C_2S, belite might present a high level of activity with its large specific surface [20] or the presence of sulphate in its structure [21, 22]. Therefore, the belite in CSA could be 'more reactive' than that in OPC. The hydration of belite was also studied by lots of authors, and its hydration was found much lower than that of $C_4A_3\$$ [23,24]. C-S-H was identified as hydrates by some authors [25], ([3] P.159), while strätlingite by some others [26]. According to the different hydrates, different equations were proposed:

$$C_2S + 2.8H \Rightarrow CxSH(x+0.8) + (2-x)\ CH \quad (1.4)$$

$$C_2S + AH_3 + 5H \Rightarrow C_2AH_8 \quad (1.5)$$

Considering OPC, the studies on belite hydration are relatively fewer than those on alite. However, hydration of belite is much slower, but similar to that of alite in order to form both C-S-H and portlandite. Therefore, we can expect that the parameters that modify alite will also influence belite hydration. Three parameters known on alite may thus be useful to consider for belite hydration in the case of CSA:

- Hydration of alite seems to be strongly delayed by aluminium in the solution [27,28].
- Calcium sulphate in form of anhydrite or gypsum, but mainly limestone can accelerate the hydration of C_3S [29].

Ferrite

Ferrite phases in sulfoaluminate cements have very different compositions compared to those present in Portland cement, with the concentrations Si, Ti and Mg that can not be negligible [30]. In high ferrite CSAs, the composition of ferrite is found close to C_6AF_2, while in low ferrite CSAs, ferrite is found close to C_4AF [31]. C_4AF were found "more reactive" than those present in the OPC [32], perhaps due to the low sintering temperature. However, the hydration of ferrite in CSAs was found much slower than $C_4A_3\$$ [23]. Perhaps that is why in industrial CSAs products, calcium sulphate addition is defined only in terms of the content of $C_4A_3\$$ in the clinker [33], without taking consideration of reaction of ferrite and calcium sulphate. The hydrate phases of ferrite were identified as AFt, AFm and ion gel (FH_3), which contribute to later strength development [34].

Ferrite hydration in OPC cement is found much slower than that of alite ([21] P.187). Its hydrate phases were found as AFt, AFm and hydrogarnet ([21] P.207). Its hydration was found mainly delayed by the presence of gypsum or other form of calcium sulphate [35]

Limestone

Limestone is commonly interground with OPC [36] and CSA [9]. The effects of the limestone are partly physical and partly chemical. First, calcite surface can play as nucleation sites for C-S-H and thus enables C_3S hydration to reach greater percentage of reaction before becoming slow but this also reduces the induction period. Second, carbonate ions help to stabilize ettringite at the expense of calcium monosulfoaluminate hydrate when the sulphate concentration becomes low. Also at longer ages, calcium monosulfoaluminate hydrate can react to form some carbonated AFm phases:

$$3C_3A.C\$.H_{12}+2Ca^{2+}+[CO_3]^{2-}+2[OH]^{-}+17H \rightarrow C_3A.3C\$.H_{32} + 2C_3A.\tfrac{1}{2}C\overline{C}.\tfrac{1}{2}CH.H_{11} \quad (1.6)$$

Further reaction with $[CO_3]^{2-}$, calcium monocarbonate aluminate hydrate can replace calcium hemicarbonate aluminate hydrate. This is reported both in the literature of OPC [37] and CSA [3, P. 165]. But, in CSA experiments, WANG and SU [3, P.165] considered that the limestone is a more chemically reactive constituent in CSA compared to OPC.

1.4.2 Potential interaction between BCSAF cement constituents

In BCSAF cement, anhydrite is added as calcium sulphate source. Limestone was also added as admixture. Figure 1-4 and Figure 1-5 could help us to synthesize the potential interactions between the constituents in order to assess the complexity of the hydration.

.

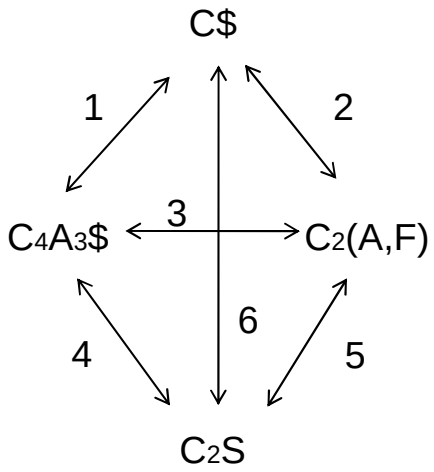

Figure 1-4: Potential interactions between the main constituents of BCSAF cement without limestone

From the literature, one can have a first guess of the relative intensity of the potential interactions knowing that all the interactions will of course do not arise at the same time:

Interaction 1 (C_4A_3\$/C\$):
Hydration of ye'elimite is expected to be accelerated by the presence of anhydrite.

Interaction 2 (Ferrite/C\$):
Ferrite hydration should be strongly delayed by the presence of anhydrite.

Interaction 3 (ye'elimite/ferrite):
No direct interaction between these phases is reported. However, we can imagine that dissolution of ferrite could liberate more calcium and aluminium ions to participate to the hydation of ye'elimite in equation (1.1, 1.2, 1.3).

Interaction 4 (C_2S/ C_4A_3\$):
No direct interaction between these phases is reported. However, we can imagine that the calcium ions liberated by belite can accelerate the hydration of ye'elimite. Also, if ye'elimite dissolves very faster in the solution, aluminium concentration would delay C-S-H nucleation and thus may be belite hydration.

Interaction 5 (ferrite/C_2S):
Both C_2S and ferrite hydrate slowly in CSAs and OPC. We can imagine that the dissolution of each phase can accelerate the hydration of each other.

Interaction 6 (anhydrite/belite):
Sulphate can accelerate the hydration of C_3S. This acceleration effect can be expected to be reproduced in the hydration of C_2S for OPC. However, this effect is not well reported in the hydration of CSAs.

The addition of limestone, will add three main potential additional interactions:

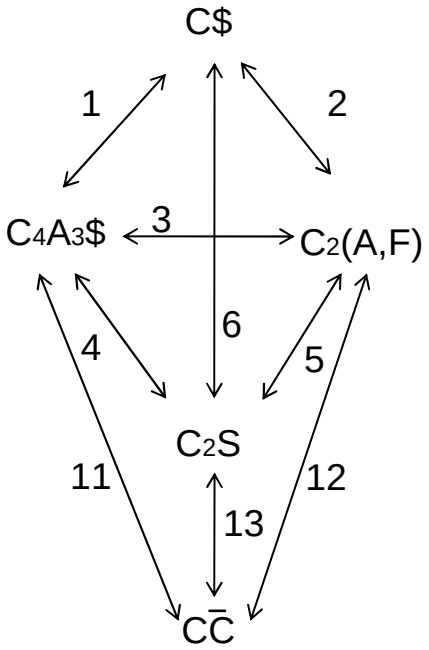

Figure 1-5: Potential interactions between the main composite of BCSAF cement containing limestone

Interaction 11 (ye'elimite/limestone):
Limestone may accelerate the hydration of ye'elimite considering equation (1.1). In equation (1.2), calcium monocarbo aluminate hydrate can be formed instead of calcium monosulfo aluminate hydrate.

Interaction 12 (ferrite/limestone):
Limestone may accelerate the hydration of ferrite but here we have to consider the presence or not of sulphate ions that changes the interaction.

Interaction 13: (belite/limestone):
Limestone may accelerate the hydration of C_2S if its rate depends on C-S-H nucleation.

Here, it is important to note that the hydration of anhydrous and their interactions are not necessarily simultaneous, neither consecutive. Also, in reality, some additional interactions will be possible as the hydrates may also interact with the anhydrous phases. This makes the system even more complicated.

1.5 Organization of the thesis

Face to the adventure of a new hydration world, the most urgent and difficult mission of this study was to adapt the experimental methods generally applied to OPC to our cement. This work was partly done during my initial 6 months internship at LCR [38] and has been continuously refined over the three years of my PhD thesis. For example, the paste studies were initially planned to cover only one month but this was finally prolonged to one year since the hydration of BCSAF cement was proved still quite 'active' after one month. As well, the crystallographic databases used for Rietveld estimates and the thermodynamic database used for CHESS calculations have been continuously updated.

Based on the first results of my internship [38], the objective of the thesis was defined to focus on the understanding the hydration mechanisms of cement BCSAF in order to develop simple mechanistic models which can help us to optimise mixtures of BCSAF clinker and other compounds for specific applications [39]. In particular, five key scientific questions were raised at the beginning of the thesis:

1) confirm the that major initial reaction for BCSAF cements is: $C_4A_3\$ + 2C\$ + 38H \Rightarrow C_6A\$_3H_{32} + 2AH_3$,
2) assess how the quantity of the initial soluble sulfates influence the later hydration,
3) determine the parameters that control ferrite phase hydration,
4) determine the factors that control belite hydration and induce a retardation of its start,
5) check if limestone has an accelerator effect on belite hydration such as in OPC,

In order to progressively answer the questions raised, the following methodology was followed:

- The description of k165 clinker and of the method to produce the cement from k165 clinker (chapter 2) but also of the experimental strategy to study hydration, were reported.
- The hydration of a cement containing 95% of clinker k165 with 5% anhydrite addition by mass was deeply investigated both in paste and suspension and some additional experiments on pure phases were performed (chapter 3)
- The hydration of clinker k165 blended with different quantities of anhydrite (0, 5 (done at chapter 3), 10 and 20 weight %) was investigated in chapter 4 following the same methodology as in chapter 3
- The effect of 15% limestone on a cement containing 95% of clinker k165 with 5% anhydrite addition was studied and also some pure phase systems were studied to check some hypothesis (chapter 5)

During the three years of my PhD thesis, most work was done in the CO_2 project team in LCR (Lafarge Research Centre) under the supervision of the project manager, Günther WALENTA and the principal scientist, Ellis Gartner. Denis Damidot of Civil Engineering department at Ecole des Mines de Douai was my PhD supervisor. Also, in order to facilitate the experience learning of Chinese CSA, the vice-president of CBMA, Sui Tongbo, was also involved in the thesis as one of my supervisors.

Chapter II

Materials and Methods

2 Materials and Methods

A specific BCSAF clinker, named k165, was used to produce the cement studied in the thesis. Thus this chapter first describes k165 clinker and the cement made from it. Then the methodology used to study hydration during the following chapter is detailed.

2.1 Materials

2.1.1 BCSAF Clinker k165

2.1.1.1 Mineralogical analysis

The clinker (named "k165") was made at ≈1300°C in a 1.25m diameter and 16m long oil-fired rotary kiln equipped with a rotary cooler, using a pre-nodulized raw mix made from limestone, kaolinite, gypsum and borax ($Na_2B_4O_7.10H_2O$) [7]. The elemental composition of the clinker (Table 2-1) was determined by X-ray fluorescence on a pressed powder pellet (Annex 2-1), coupled with ICP analysis (Annex 2-2) for boron and loss of ignition (LOI) measurement at 950°C.

Oxide:	SiO_2	Al_2O_3	Fe_2O_3	CaO	MgO	K_2O	Na_2O	SO_3	B_2O_3	TiO_2	LOI
mass %	16.21	17.14	6.58	50.62	0.65	0.76	0.66	5.29	1.32	0.31	0.21

Table 2-1: Elemental composition of clinker k165 expressed as oxides

The major clinker phase composition estimated by Rietveld-XRD method (Annex 2-3) is shown in Table 2-2. One can notice that the belite phase was mostly present as α' crystalline form.

Phase	Ye'elimite	β-C_2S	α'-C_2S	ferrite	Total
Mass (%)	33	3	49	14	99

Table 2-2: Estimated major phase composition of clinker k165

Figure 2-1 shows a backscattered electron image of a polished section of clinker k165 obtained using a FEG-SEM (Annex 2-4). Porosity (mostly epoxy-filled) appears black. Belites (light grey) are typically in the range 1-10µm and ye'elimite crystals (dark grey) are generally somewhat smaller (1-5µm). Compared with the same minerals in industrial CSAs, the belite and ye'elimite in BCSAF have larger crystal size [18, 9]. The ferrite phase (white) is present as a matrix between the other phases, indicated that it was liquid at clinkering temperatures, as expected [40].

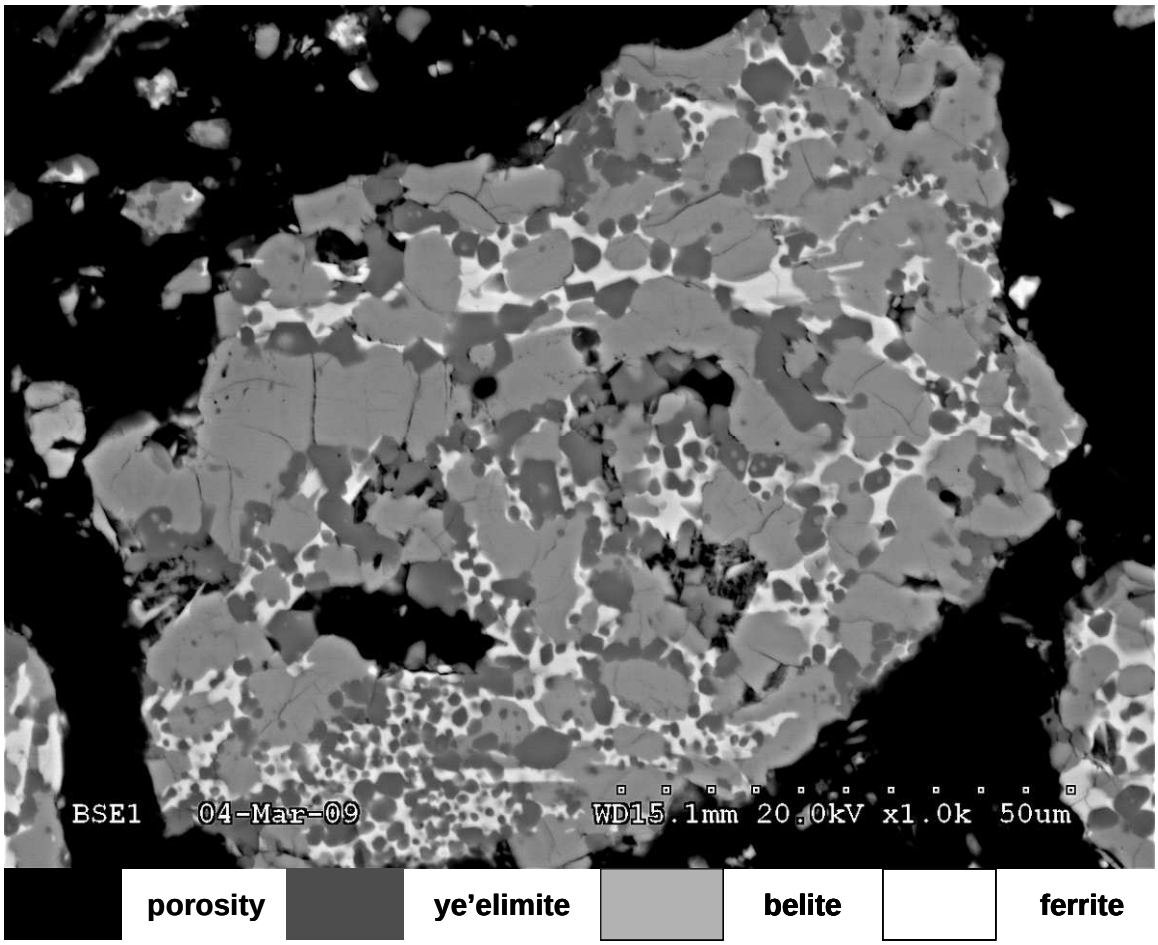

Figure 2-1: Typical FEG-SEM BSE image of clinker k165

2.1.1.2 Content of foreign ions in C_2S

In an industrial OPC clinker, C_2S can incorporate up to 4-6% (wt) foreign ions, such as Al^{3+}, Fe^{3+}, S^{6+}, Mg^{2+}, K^{+}, Na^{+}, P^{5+}, B^{3+}, etc([19], P.18). These ions can promote chemical combination at high temperature based on the effect of stabilizing the crystalline form of certain mineralogical phases present in the clinker.

Chemical composition of C_2S in k165 clinker was investigated. Selective dissolution with KOH and sucrose was used to remove the other phases from powdered clinker (Annex 2-5). Then the elemental composition of the residues was determined by X-ray fluorescence on a pressed powder pellet, coupled with ICP analysis for boron and loss of ignition measurement at 950°C (Table 2-3).

Oxide:	Al_2O_3	CaO	Fe_2O_3	K_2O	MgO	Na_2O	P_2O_5	SiO_2	SO_3	TiO_2	B_2O_3	LOI	Total
%	1.52	61.82	1.41	0.38	0.92	0.76	0.09	29.18	0.40	0.20	2.42	1.28	100.38

Table 2-3: Elemental composition of C_2S expressed as oxides in clinker k165

From Table 2-3, we see that the C_2S contains about 0.76% (2.42%*22/70) of elemental boron. Given that there is about 52% C_2S in this clinker, the B in C_2S represents 0.76%*52% = 0.39% by mass of clinker. Since the total B in this clinker was 0.41% (Table 2-1), we estimate that 0.39%/0.41%= 95% of the boron in this clinker is contained in the C_2S and that there is therefore only about 5% in the other phases.

Table 2-3 also shows that the minor elements in C_2S presents in total 7.44% in form of oxides, which probably explains why C_2S is mostly in the α' form. To verify the Ca/Si ratio, we suppose that 2 atoms of K^+ or 2 atoms of Na^+ or 1 atom of Mg^{2+} can replace 1 atom of Ca^{2+}, and that 4 atoms of B^{3+} or 4 atoms of Al^{3+} or 4 atoms of Fe^{3+} or 2 atoms of S^{6+} can replace 3 atoms of Si^{4+}. Based on the chemical analysis, we get a base/acid ratio very close to 2:

(Ca, Mg, Na, K)/(Si, Al, Fe, S, B)
= (61.82/56 + 0.92/40 + 0.76/62 + 0.38/94)/(29.18/60 + 1.52/102/4*3*2 + 1.41/160/4*3*2 + 0.4/80/2*3 + 2.42/70/4*3*2) = 1.967

This suggests a good precision of the chemical analysis and of the selective dissolution method.

2.1.1.3 Ferrite phases – solid solution between C_6AF_2 and C_4AF

Ferrite is mainly considered as solid solution which can be written as $Ca_2(Al_xFe_{1-x})_2O_5$, where $0<x<0.7$. Possible foreign ions in the structure include Mg^{2+} and Si^{4+} [41], Mn^{3+} [42], Ti^{4+} [43] and small amounts of SO_3 [44],[45].

Some Chinese literature [31] shows a method which permit getting pure ferrite phases in CSA clinker by removing the silicate phases with methanol – salicylic acid solution (10g clinker / 60g salicylic acid, 300ml methanol) and then by removing $C_4A_3\$$ with 5% Na_2CO_3 solution.

In our case, silicate phases were completely removed by methanol – salicylic acid solution without forming hydrate phases. However, the second step was not successful. $C_4A_3\$$ did disappear, but with the precipitation of $CaCO_3$. In order to remove this $CaCO_3$ we heated the sample to 1000°C and then dissolved the CaO with ethylene glycol at 110°C (Annex 2-6).

After this complex selective dissolution process, the elemental composition of the residual "ferrite concentrate" was determined by X-ray fluorescence on a pressed powder pellet, coupled with ICP analysis for boron and an loss of ignition measurement at 950°C (Table 2-4).

Oxide:	SiO_2	Al_2O_3	Fe_2O_3	CaO	MgO	K_2O	Na_2O	SO_3	TiO_2	LOI
mass %	4.52	13.29	29.33	46.88	1.29	0.01	2.98	0.44	0.99	0.26

Table 2-4: Elemental composition of ferrite concentrate expressed as oxides

The Na_2O content of this ferrite concentrate is evidently high due to the use of Na_2CO_3 during the extraction method, but we can assume that the other elements represent essentially the mean clinker ferrite phase. Thus the elemental composition of this ferrite can be estimated relatively to Al (Table 2-5).

Element	Al	Fe	Ca	Si	Mg	Ti	S
Atoms	1.00	1.41	3.21	0.29	0.12	0.05	0.02

Table 2-5: Atom ratios of ferrite phase components relative to Al

Therefore, this ferrite phase is close to $C_2A_xF_{(1-x)}$ with x = 0.41, but it is also necessary that Si and perhaps other atoms substitute for Al and Fe in order to maintain the usual acid:base ratio. We might also have to assume that there is still a little quantity of C_2S trapped in this residue.

2.1.2 Anhydrite

The anhydrite used in this work was a natural mineral from Le Pin in France. Its elemental composition was analyzed by X-ray fluorescence and is given in Table 2-6.

Oxide:	SiO_2	Al_2O_3	Fe_2O_3	CaO	MgO	K_2O	Na_2O	SO_3	LOI
mass %	1.93	0.27	0.12	40.05	1.01	0.06	0.02	51.12	4.65

Table 2-6: Elemental composition of anhydrite expressed as oxides

Its particle size distribution measured by the method given in Annex 2-7, is shown in Figure 2-2.

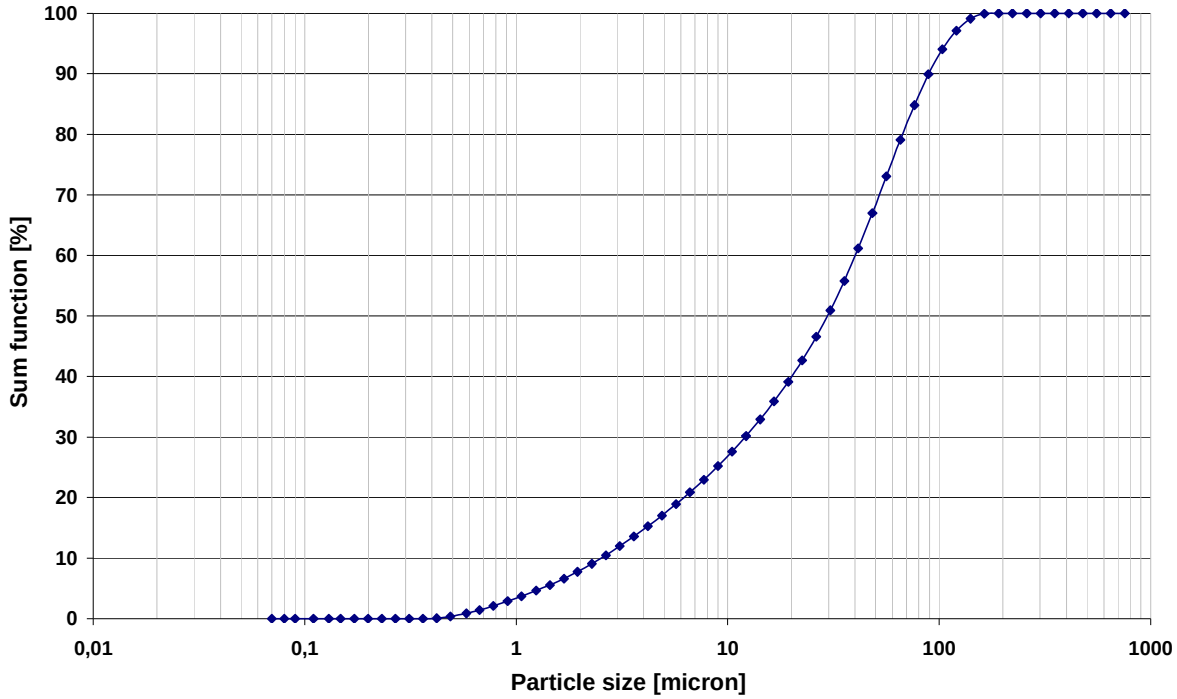

Figure 2-2: Particle size distribution of anhydrite expressed as sum function

2.1.3 Limestone

Limestone used in this work was also a natural mineral from Le Pin in France. It was crushed to a Blaine specific surface of 400m²/kg (Annex 2-8). Its elemental composition was analyzed by X-ray fluorescence and is given in Table 2-7. The particle size distribution composition is measured by the method given in Annex 2-7 and presented in the Figure 2-3.

SiO_2	Al_2O_3	Fe_2O_3	CaO	MgO	K_2O	Na_2O	SO_3	P_2O_5	PAF	Total
1.37	0.48	0.16	53.55	1.03	0.05	0.01	0.14	0.02	42.39	99.18

Table 2-7: Elemental composition of anhydrite expressed as oxides

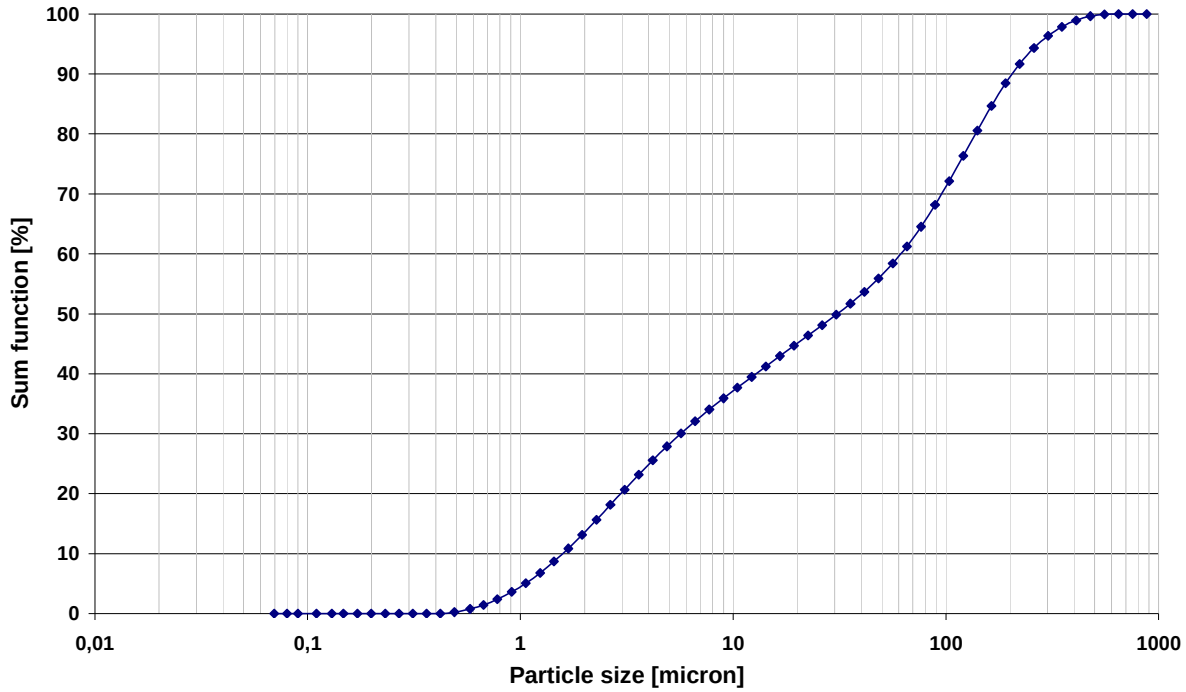

Figure 2-3: Particle size distribution of limestone expressed as sum function

2.1.4 BCSAF Cements made from k165 clinker

To make several BCSAF cements, clinker k165 and anhydrite were ground separately to about 400m²/kg Blaine specific surface area in a laboratory ball mill (see Annex 2-9). Then mixtures were made according the desired mass proportions, using a Turbula blender during 30 minutes to obtain a good homogeneity.

In order to facilitate the identification of cement samples, the following coding is used in this thesis: clinker name- Blaine specific surface area-% of constituents with A for anhydrite and L for limestone. For example, k165-400B-5A means that clinker k165 and anhydrite were ground separately to about 400m²/kg Blaine specific surface area in a laboratory ball mill, and then mixed in the ratio 95:5 by mass.

Table 2-8 summarizes the cement used for the thesis.

Chapter	Cement used
3	k165-400B-5A
4	k165-400B-0A, k165-400B-10A, k165-400B-20A
5	k165-400B-5A-15L

Table 2-8: Name of the cement used in the thesis

2.2 Method to study hydration

Cement hydration studies were done both on stirred suspensions (at W/C = 5) and on pastes (at W/C = 0.5). The laboratory temperature was maintained at 20±2°C.

Suspension experiments were carried out in a closed reactor containing 1-litre of solution that was maintained at 20°C by a water-jacket cooled by a thermoregulated circulator. Suspension uniformity was ensured by a stirrer operating at 350 rpm. Conductivity and pH (Annex 2-10) were measured continuously and recorded using the "AMANDINE 421" software developed by Lafarge. Samplings of the suspension for analysis were made at given times or at specific features of the conductivity curve. The recovered samples were filtered with a Pyrex support and cellulose membrane (HAWP Millipore). The wet filtercake was rinsed on a Whatman system (90mm diameter Whatman filter with Teflon support) twice in acetone and one time in ether to stop hydration, followed by storage in a desiccator under vacuum in order to avoid humidity and carbonation. Then, the powders were mainly analyzed by XRD to identify and quantify the crystallized and amorphous phases with Rietveld analysis (Annex 2-11). The liquid phases were acidified with HCl and diluted ten times for elemental analysis by ICP (Annex 2-2). CHESS, thermodynamic software [46], was used to estimate the saturation index of the solids using the results of ICP (Annex 2-12).

Paste experiments were performed with 60g cement and 30g water hand stirred for 30 seconds in a plastic mortar, using a spoon. The paste was then poured into hermetically closed Teflon tubes in the form of cylinder Φ3cm * 7cm until 1 day. Then, the samples were taken out and stored in demineralised water at 20°C. Small pieces were crushed by a hammer and taken out at age of 1, 2, 3 and 6 hours, 1, 2, 3, 7, 14 days, 1, 3, 8 months and 1 year. The pieces were ground in a porcelain mortar until all the powder passed through a 100-micron sieve. The resulting powder was treated by the acetone/ether rinse as described for the suspension experiments and then analyzed by XRD with a subsequent Rietveld analysis. Other techniques, such as NMR (Annex 2-13), SEM (Annex 2-4) and DTA (Annex 2-14), were used to supply additional results.

2.2.1 Temperature variation

As hydration is very sensitive to temperature, this parameter was followed in both systems knowing that only small variations from room temperature are expected thanks to the thermal regulation in stirred suspension and the small size of the samples in paste. A thermal sensor was introduced in the centre of paste sample. Temperature was registered every three minutes in the first hour and then every 5 minutes. In suspension, the temperature was measured directly by a thermometer every five minutes in the first half hour, the every fifteen minutes up to 4 hours and then every thirty minutes up to 8 hours.

For example, figure 2-4 shows that the temperature reached a maximum of about 30°C between 2 and 4 hours during K165-400B-5A hydration in paste (about 9°C above ambient temperature) but that by 12 hours it had effectively fallen back to ambient. On the other hand, the temperature never went above 23°C in suspension experiments (Figure 2.5).

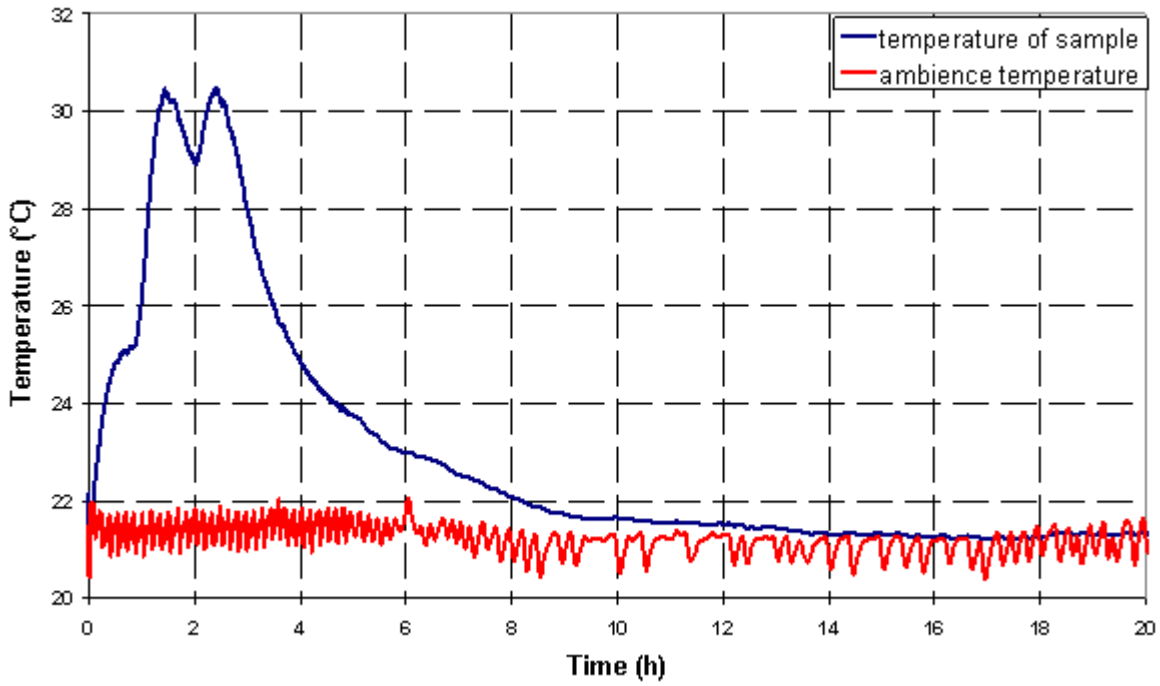

Figure 2-4: Variation of temperature of k165-400B-5A in paste over the first 20 hours

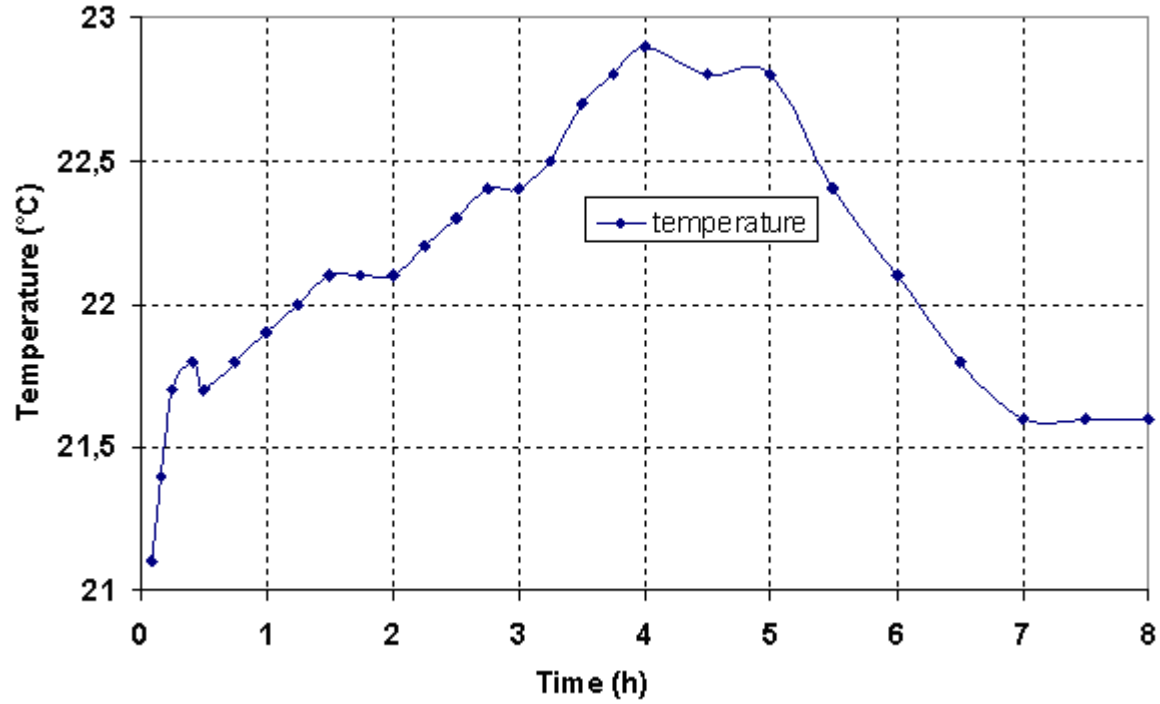

Figure 2-5: Variation of temperature of k165-400B-5A- in suspension over the first 8 hours

The impact of temperature on the stability of phases has been investigated in the system CaO-Al_2O_3-$CaSO_4$-H_2O with and without the presence of Na_2O and K_2O [47,48]. At 25°C, it was shown that AH_3, C_3AH_6, CH, ettringite and gypsum are all stable phases while calcium monosulfoaluminate hydrate is metastable relative to ettringite. However, if the temperature

exceeds 45°C, calcium monosulfoaluminate hydrate becomes stable at the expense of ettringite [49]. Similar conclusions can be made considering the $CaO\text{-}SiO_2\text{-}Al_2O_3\text{-}H_2O$ system. Indeed temperatures lower than 50°C are not expected to modify markedly the stability domains of strätlingite (C_2ASH_8) relative to hydrogarnet ($C_3AS_xH_{6-2x}$) [50].

Therefore, apart from a small increase of the initial kinetics in pastes, we can consider that the experiments in suspension and in paste should be reasonably similar in terms of the effect of temperature on the equilibria and thus the hydrates that are precipitated. However, special attention should be paid if BCSAF cement would be used in mass concrete where the temperature may rise much higher due to the larger volume/surface ratio.

2.2.2 Normalisation of Rietveld analysis to the initial mass of solid

The results of Rietveld estimation are given by mass fraction of each phase relative to the mass of hydrated cement. However, the mass of solid in the cement paste is higher than the initial mass of cement and is also increasing with the time. This corresponds to the mass gain due to the water in the hydrates for a given fraction of reaction (Mcw) but also to the mass loss, mostly in suspension, due to the amount of dissolved cement into the solution (Mad).

In order to be able to compare the amounts of the different phases during hydration, it is thus necessary to normalise the mass percentage given by Rietveld analysis to the mass of the initial anhydrous cement (Minitial, 200g for suspension experiments, 60g for paste experiments).

At time (t), we know from Rietveld analysis, the fraction of phase Y ($Y_h(t)$) by mass of cement paste M(t). Thus the mass of phase Y, $M_y(t)$, can be calculated as:

$$M_y(t) = Y_h(t) * M(t) \qquad (2.1)$$

At time (t), the relation between M(t), Mcw(t), Mad(t) and Minitial can be expressed as:

$$\text{Minitial} - \text{Mad}(t) = M(t) - \text{Mcw}(t) \qquad (2.2)$$

Mcw(t) which is the combined water in the hydrates, can be estimated by the ignition loss of the cement paste at 600°C, $M_{il}(t)$, which is generally expressed in fraction by mass of M(t).

Therefore, equation (2.2) can be changed into (2.3):

$$\text{Minitial} - \text{Mad}(t) = \frac{[100 - \text{Mil}(t)]}{100} * M(t) \qquad (2.3)$$

Equation (2.1) can be changed into (2.4):

$$\text{Minitial} - \text{Mad}(t) = \text{Yh}(t) * \frac{[\text{Minitial} - \text{Mad}(t)]}{[100 - \text{Mil}(t)]} * 100 \qquad (2.4)$$

Finally, the fraction of phase Y at time (t) by mass of the initial anhydrous cement can be expressed as equation (2.5):

$$\frac{\text{My}(t)}{\text{Minitial}} = \text{Yh}(t) * [1 - \frac{\text{Mad}(t)}{\text{Minitial}}] * \frac{100}{[100 - \text{Mil}(t)]} \qquad (2.5)$$

For suspension experiments, anhydrous dissolved into the solution Mad(t) can be estimated by adding up the mass of total ions in the solution (supposing the solution volume remains constant at 1L).

Table 2-9 shows the calculated value of Mad(t) in gram for the hydration of K165-400B-5A in suspension. For paste experiments, Mad (t) is negligible compared to Minitial due to the small volume of water. Thus is not accounted for knowing that also we do not have the chemical analysis of the aqueous phase in paste experiments. For suspension experiments, anhydrous dissolved into the solution Mad(t) can be estimated by adding up the mass of total ions in the solution (supposing the solution volume remains constant at 1L).

Time (h)	0	0.083h	0.16h	0.25h	0.32h	0.5h	1h	1.8h	2h	2.1h	3h
Mass (g)	0	4.48	4.42	4.39	4.28	4.09	3.94	3.74	3.75	3.56	3.49
Time (h)	4h	5h	5.7h	6.25h	8h	18.5h	22.8h	24h	31h	42.5h	47h
Mass (g)	3.38	3.46	3.48	3.59	3.47	3.42	2.40	2.31	2.22	2.31	2.40

Table 2-9: Amounts of cement (in g) dissolved in the solution during K165-400B-5A suspension experiment

Table 2-10 and table 2-11 show the ignition loss in fraction by mass of the cement paste at 600°C, respectively in suspension and paste experiments for cement K165-400B-5A. These experiments have been carried out by TGA and the loss of ignition is calculated until 600°C. This temperature is lower than usually performed for Ordinary Portland Cement paste but was chosen to avoid mass loss due to the decarbonation of limestone when present in our cements.

Time (h)	0	0.083h	0.16h	0.25h	0.32h	0.5h	1h	1.8h	2h	2.1h	3h
Loss (%)	0.32	1.42	1.56	1.78	2.05	2.36	3.12	4.31	4.58	4.67	9.26
Time (h)	4h	5h	5.7h	6.25h	8h	18.5h	22.8h	24h	31h	42.5h	47h
Loss (%)	15.94	16.5	17.8	18.23	21.08	21.85	23.87	23.98	28.1	29.35	28.75

Table 2-10: Loss of ignition obtained by TGA until 600°C on the solid recovered during K165-400B-5A hydration in suspension until 600°C

Time	0	1h	2h	3h	6h	1d	2d	3d	7d	14d	28d	3m	8m	1y
Loss (%)	0	13.1	15.8	15.2	17.8	17.9	18.7	20	21.2	26.5	27.8	28.5	28.9	29.6

Table 2-11: Loss of ignition obtained by TGA until 600°C on the solid recovered during K165-400B-5A cement hydration in paste until 600°C

We can also normalise the results to 100g of initial cement if needed as for example to calculate some volume changes during hydration and to compare them with other cements like OPC.

Chapter III

Detailed investigation of the hydration of cement K165-400B-5A

3. Detailed investigation of the hydration of cement k165-400B-5A

The cement K165-400B-5A was chosen first. The objective was to establish the basic hydration mechanisms of hydration with the methodology described in chapter 2. Precision of each technique is discussed in the text or in the annexes.

In order to facilitate the reading and to enable a direct comparison of the results, the major figures and tables have been grouped at the end of the chapter. Tables 3-1 and 3-2 summary the figures and tables giving the major results in suspension (W/C=5) and paste (W/C=0.5) respectively.

K165-400B-5A (W/C=5)						
Conductivity pH	Liquid phases		Solid phases			CHESS calculation
	Major	Minor	anhydrous	major hydrate	minor hydrate	
Figure 3-1	Figure 3-2	Figure 3-3	Figure 3-4	Figure 3-5	Table 3-3	Table 3-4, 3-5

Table 3-1: Summary of figures and tables for the major results of k165-400B-5A in suspension

W/C=0.5	Solid phases		
	Anhydrous	major hydrate	minor hydrate
K165-400B-5A	Figure 3-6	Figure 3-7	Table 3-6

Table 3-2: Summary of figures and tables for the major results of k165-400B-5A in paste

3.1 Suspension experiments

Figure 3-4 shows the mass percentage of the anhydrous phases hydrating in suspension up to 2 days, relative to the mass of original anhydrous cement. It is evident that all the anhydrous phases do not hydrate simultaneously.

The amount of anhydrite declines slowly in the first two hours with a sudden drop later. After 4 hours, no anhydrite can be detected by XRD. The consumption of $C_4A_3\$$ seems to be parallel with anhydrite; slower in the first two hours (its amount passes from 35% to 30%) and much faster between 2 hours to 4 hours (its amount passes from 30% to 10%). Only about 5% relative to the mass of original anhydrous mass remains after 4 hours, but its rate of consumption slows down until ye'elimite cannot be detected by XRD at 8 hours.

The consumption of belite phase seems very slow before 6.25 hours, and then accelerates in a two stages process. Around 5% of belite is consumed from 6.25 hours to 8 hours and then around 14% from 18 hours to 23 hours. Interestingly, the consumption of ferrite seems to be coupled and proportional with the consumption of belite.

The major hydration products formed are shown in Figure 3-5. We can find that the only crystalline hydrate formed during the first four hours, is ettringite, and its rate of increase is directly related to the consumption of ye'elimite and anhydrite (from 0 to 8.3% in the first hours, then 8.3% to 48% in the following two hours).

Figure 3-2 shows the concentrations of the major chemical elements of the aqueous phase up to 2 days. We can notice that during the first minutes, the concentrations of sulphate, calcium

and aluminate reach 23mM, 14mM and 5mM respectively, which suggests a strong dissolution of anhydrite and ye'elimite once mixed with water. Also the concentrations of the alkali ions also arrive around 16.6mM after the first minutes, which suggests a rapidly soluble form (e.g. as sulphates) in our clinker.

The concentration of sulphate decreases almost to zero by 5 hours. This sulphate consumption does not appear to increase the hydroxide ion concentration as pH drops in this period while aluminate ion concentration increases (Figure 3-1). In this initial period of K165-400B-5A hydration, when the $C_4A_3\$$ and anhydrite are dissolving in the solution, some of the released sulphate, calcium and aluminate ions combine to form ettringite. Ettringite consumes less Al than that are freed by $C_4A_3\$$. For this reason, the concentrations of calcium and sulphate declines, and that of the aluminium increases. However, no other crystallized phases are identified in XRD pattern but a very small quantity of amorphous phase is estimated by Rietveld: 0.7%, 0.3%, 2.2% at 1h, 3h and in 5h respectively (Table 3-3). Therefore, the reaction of ye'elimite and anhydrite to form ettringite can be expressed by equation (3.1).

$$C_4A_3\$ + 2C\$ + 32H \rightarrow C_3A.3C\$.H_{32} + \text{Al in aq. phase} \quad (3.1)$$

A simple mass balance can be made at 2 and 4 hours to verify equation (3.1). To simplify the calculation, some hypothesis was made:

- All of the 16.6 mmol/litre of alkalis (K_2O and Na_2O) which were dissolved in the solution at the time of the first measurement were in the form of alkali sulfate.
- The quantity of C_2S and ferrite dissolving in the solution is negligible and thus considered to be 0,
- Ye'elimite, anhydrite and ettringite are pure phases
- The volume of solution phase in the reactor stays constant (1L)

Three equations can be made for the mass balance with respect to SO_3, CaO and Al_2O_3 at time t:

- $\Delta(C_4A_3\$) + \Delta(C\$) + \Delta(R_2SO_4) = 3*\Delta(\text{ettringite}) + [SO_3]_t$ (I)
- $4*\Delta(C_4A_3\$) + \Delta(C\$) = 6*\Delta(\text{ettringite}) + [CaO]_t$ (II)
- $3*\Delta(C_4A_3\$) = \Delta(\text{ettringite}) + [Al_2O_3]_t$ (III)

Here, $\Delta(C_4A_3\$)$, $\Delta(C\$)$, $\Delta(\text{ettringite})$ mean respectively the changes in the number of moles of ye'elimite, anhydrite and ettringite ($\Delta(C_4A_3\$) = \Delta(C_4A_3\$)_0 - \Delta(C_4A_3\$)_t$, $\Delta(C\$) = \Delta(C\$)_0 - \Delta(C\$)_t$, $\Delta(\text{ettringite}) = \Delta(\text{ettringite})_t - \Delta(\text{ettringite})_0$) per litre of solution (i.e. per 200g of initial solids). $[SO_3]t$, $[Al_2O_3]_t$, $[CaO]_t$ mean respectively the molarity of sulfate, Al_2O_3 and calcium in the solution at time t. And $\Delta(R_2SO_4)$ means the molarity of solid alkali sulfate, which, as we said above, equals 16.6 mM.

If we use the ICP analysis data in the equation (I), (II), (III), we have only $\Delta(C_4A_3\$)$, $\Delta(C\$)$, and $\Delta(\text{ettringite})$ as unknown values. Therefore, we can calculate these values by changing the equations into following form:

- $\Delta(C_4A_3\$)=[Al_2O_3]/2-(R_2SO_4)/6+[SO_3]/6-[CaO]/6$ (I')
- $\Delta(C\$)=[Al_2O_3]-(R_2SO_4)*7/3+[SO_3]*7/3-[CaO]*4/3$ (II')
- $\Delta(\text{ettringite})=[Al_2O_3]/2-(R_2SO_4)/2+[SO_3]/2-[CaO]/2$ (III')

The calculated values at 2 and 4 hours are shown in Table 3-7:

Time	$\Delta(C_4A_3\$)$	$\Delta(C\$)$	Δ(ettringite)
0-2h	2.2	-14.4	-2.0
0-4h	3.6	-32.4	-3.3

Table 3-7: Ye'elimite, ettringite and anhydrite molar calculated change (mmol)

The results mean that after 2 or 4 hours, we should have more anhydrite than at the beginning, which is obviously absurd. This suggests that some important hydrate phases are not quantified by the Rietveld estimate. On the other hand, we are confident that no significant quantity of some other crystalline phases appears in the XRD pattern. So the only explanation seems to be that an amorphous hydrate phase is present but is under-estimated by the Rietveld estimate

DTA analysis of the solids at 4 hours (Figure 3-8) shows indeed that, besides the peak around 140°C which is characteristic of ettringite, another peak is present around 275°C which fits well with alumina gel (AH_3). More evidence can be found in the evolution of the supersaturation of the solution with respect to the hydrates as calculated by CHESS in tables 3-4 and 3-5. If the value is greater than 0, it means that this phase could precipitate. If the value is less than 0, this phase should dissolve if present or if not present, should not precipitate. According to these calculations, gibbsite is supersaturated until 30 hours, which means that AH_3 could precipitate at the beginning of hydration, but after 30 hours it should redissolve into the solution. CAH_{10} is also slightly supersaturated. This hydrate is sometimes observed in some CSA cements generally rich in $C_4A_3\$$ and other calcium aluminate phase such as $C_{12}A_7$ [51]. However, its expected dehydration peak at 130°C is not obvious in the DTA curve perhaps because of the overlap with the peak of ettringite (around 140°C). So, we can't rule out the possibility of some CAH_{10} in the hydrates, but its quantitie should be small compared to AH_3. Thus, it is reasonable to suppose that the quantity of amorphous phase that would correspond to AH_3 is underestimated by XRD measurement.

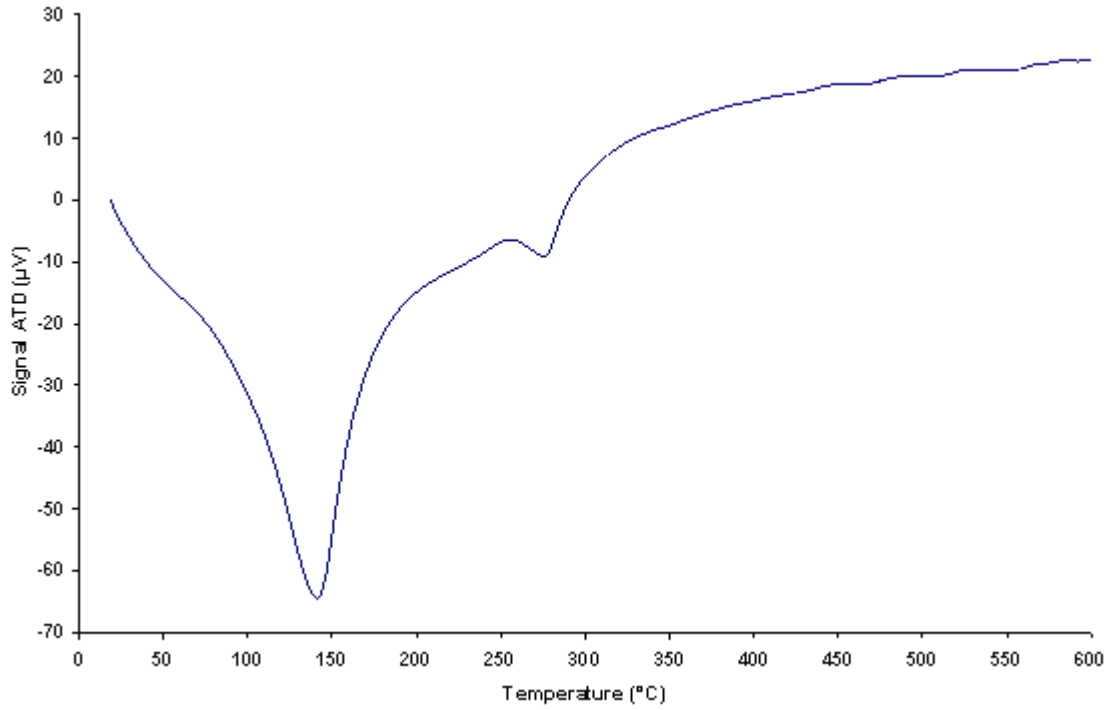

Figure 3-8: DTA of solid phases recovered after 4 hours of hydration of cement k165-400B-5A

Thus equation (3.1) can be rewritten to account for AH_3 precipitation:

$$C_4A_3\$ + 2C\$ + 38H \rightarrow C_3A.3C\$.H_{32} + 2AH_3 \quad \text{(3.2)}$$

Now the mass balance of the previous equations becomes:

- $\Delta(C_4A_3\$) + \Delta(C\$) + \Delta(R_2SO_4) = 3*\Delta(\text{ettringite}) + [SO_3]_t$ (I'')
- $4*\Delta(C_4A_3\$) + \Delta(C\$) = 6*\Delta(\text{ettringite}) + [CaO]_t$ (II'')
- $3*\Delta(C_4A_3\$) = \Delta(\text{ettringite}) + [Al_2O_3]_t + \Delta(AH_3)$ (III'')

Unfortunately there are four variables in these three equations. However, anhydrite is no longer detectable by 4 hours. Therefore, $\Delta(C\$)$ can be calculated at that time, as we are sure of the quantity introduced into the cement (5% of anhydrite compared to clinker is equivalent to 70 mmol in 200g cement). Then, $\Delta(C_4A_3\$)$, $\Delta(\text{ettringite})$, $\Delta(AH_3)$ can be calculated as shown in Table 3-8. Also, the changes in molar contents of each phase according to XRD are presented.

Time	$\Delta(C_4A_3\$)$ M	$\Delta(C\$)$ M	Δ(ettringite) M	$\Delta(AH_3)$ M
0-4h	85.4	55.7	76.5	0.00
Time	$\Delta(C_4A_3\$)$ C	$\Delta(C\$)$ R*	Δ(ettringite) C	$\Delta(AH_3)$ C
0-4h	54.8	70.0	47.9	108.8

Table 3-8: Comparison of measured and calculated molar changes relative to 200g of cement (C: calculated, M: measured, R: real) in suspension experiment between 0-4h

* "real" value is different from the measured one due to the precision of Rietveld estimate for clinker phases

If we change these values into the percentage by mass compared to original anhydrous cement in Table 3-9, this also enables us to estimate the precision of XRD with the Rietveld estimation.

Time	$C_4A_3\$$ M	C$ M	Ettringite M	AH_3 M
4h	9.4	0	48.0	0.00
Time	$C_4A_3\$$ C	C$ C	Ettringite C	AH_3 C
4h	18.7	0	30.0	8.5

Table 3-9: Comparison of measure and calculated % of phases relative to the initial mass of cement during a suspension experiment after 4h(C: calculated, M: measured)

Based on these hypotheses, and comparing the differences between the measured values and the values calculated by mass balance, we can conclude that, in the Rietveld estimate:

- The quantity of amorphous in the solid phase at four hours is largely underestimated
- The quantity of ettringite in the solid phase at four hours is slightly overestimated
- The quantity of ye'elimite in the solid phase at four hours is strongly underestimated.
- The quantity of anhydrite in the unhydrated cement is slightly underestimated

These calculations tend to indicate that the accuracy of the results of XRD based on a quantification using the Rietveld method is not very good. However the calculations are simplified and may also be different from reality. Indeed the results of the thesis mainly rely on the quantification of the phases by XRD and the reader will see that this method provides

reliable results when comparing experiments done in the same conditions and with the same cements.

After 4 hours, no solid anhydrite is detectable by XRD (Figure 3-4). However, there is still around 5mmol/L of SO_4^{2-} available in the solution, although this concentration decreases to zero by 5 hours (Figure 3-2). Therefore, we might suppose that the reaction between 4 and 5 hours could be expressed by the following equation:

$$C_4A_3\$ + 2[Ca^{2+}] + 2[SO_4^{2-}] + 38H \rightarrow C_3A.3C\$.H_{32} + 2AH_3 \ldots\ldots\ldots\ldots\ldots\ldots (3.3)$$

However, between 4 and 5 hours, the aqueous calcium concentration also increases by around 1.3 mM which suggests that at least one other calcium source, e.g., C_2S or ferrite, may also be dissolving in the solution. During the same period, the aluminium concentration increases by around 4.2 mM, but begins to decrease after 8 hours (Figure 3-2), when no more $C_4A_3\$$ can be detected by XRD (Figure 3-4). This suggests that the main aluminium source is $C_4A_3\$$ over this whole time period.

Meanwhile, only a very small amount of calcium monosulfoaluminate hydrate (<1%) could be detected (at 6.25h). As ferrite phase is quasi not reacting, this hydrate could be due to the final $C_4A_3\$$ hydration when sulphate concentration becomes very low:

$$C_4A_3\$ + 18H \rightarrow C_3A.C\$.H_{12} + 2AH_3 \ldots\ldots\ldots\ldots\ldots\ldots\ldots\ldots (4)$$

Small amounts (<3%) of carbonated AFm phases were also detected after 8h due to external contamination by atmospheric CO_2.

Hydration of C_2S seems linked with the concentration of aluminate and thus indirectly with the presence of $C_4A_3\$$ that maintains high concentrations of aluminate. After 8 hours, when aluminium concentration is decreasing as $C_4A_3\$$ is almost totally consumed, we can see that the quantity of C_2S is decreasing by around 5% (Figure 3-4). At the same time, strätlingite (C_2ASH_8) starts to form (Figure 3-5) and confirms the consumption of C_2S. Also, it is interesting to notice that boron also starts to accumulate into the solution at about this time (Figure 3-3). As discussed in Chapter 2, almost all of the boron in the clinker is contained in the belite phase and almost no boron is in ferrite. Therefore, the concentration of boron in solution would be expected to increase when the belite starts to hydrate.

After 12 hours, when the aluminium concentration decreases lower to around 5mmol/L, the quantity of C_2S decreases to around 30% (leading to a consumption of about 15% in this period, Figure 3-4) linked with an obvious consumption of ferrite phase (around 8%) between 18h30 to 23h. An increase of around 23% of strätlingite occurs at the same time (Figure 3-5). After 23 hours, the quantity of strätlingite continues to increase until a maximum value (70%) at 42 hours. Also, the concentration of boron continues increasing until 30h with a maximum value around 0.85mmol (Figure 3-3). These observations confirm that the C_2S probably starts to react quickly at about 12 hours.

The very interesting point reported here, is that C_2S hydrates to form C_2ASH_8 instead of C-S-H as usual either hydrated alone or in OPC. This needs a source of alumina that is expected to come mostly from the previously precipitated AH_3:

$$C_2S + AH_3 + 5H \rightarrow C_2ASH_8 \ldots\ldots\ldots\ldots\ldots\ldots (3.5)$$

The formation of C_2ASH_8 instead of C-S-H can be due to the poisoning effect of aluminate on the nucleation of C-S-H that has been reported in the literature from experiments carried out on C_3S with different aluminate sources such as mixtures of C_3S and CA [52,53,54]. Moreover C-S-H seems to be very slightly undersaturated as reported in Table 3-5 while C_2ASH_8 is always supersaturated (Table 3-4). Here, it is important to note that the CHESS calculation (Annex 2-11) for C-S-H is not taken into consideration the substitution of foreign ions. In the work of BEGARIN [54] shows that in hydration of alite in solution aluminates ions, a small quantity of calcium alumino-silicate hydrates noted as C-A-S-H could precipitate before strätlingite, and the later work of CHEN [55] showed that the pure phase C-A-S-H can be obtained when the concentration of calcium is less than 4.5mmol/L. In our case, with the low sulphate, calcium and high aluminium concentration, C-A-S-H may also be formed in very small amounts at the hydration beginning. However, the large quantity of strätlingite formed when belite reacts fast, suggests that the nucleation of C_2ASH_8 governs the hydration of belite during this step.

Ferrite phase can also provide some alumina and is also expected to participate to the formation of an iron substituted strätlingite as no AFm phases are detected by XRD:

$$C_2S + C_2(A,F) + 10H \rightarrow C_2(A,F)SH_8 + [Ca^{2+}] \text{ and } [OH^-] \text{ in solution}\ldots\ldots(3.6)$$

Indeed after 12 hours, the consumption of ferrite induces a rapid increase of conductivity and of pH that are mainly due to an increase in $[OH^-]$.

After 12 hours, the quantity of ettringite shows a strange behavior, decreasing by around 10% and then increasing by 10% (Figure 3-5). Ettringite, (even including Fe-ettringite), is not saturated after 18.5 hours, which means that the quantity of ettringite shouldn't increase after that time. One explanation could be the formation of a borate-substituted ettringite whose solubility is much lower than that of sulphate ettringite at 25°C[56], since the concentration of boron decreases after 30 hours. But the apparent increase in ettringite content from 44 hours to 48 hours is too much to be explained by that mechanism, so it seems that the Rietveld estimates are in cause may be due to the presence of badly crystallized phases that may also be ettringite.

Besides, some small amount of $Ca_3AlFeSiO_4(OH)_8$ can be detected at 47h after the quantity of $C_2(A,F)SH_8$ reaches its maximum value. The formation of $Ca_3AlFeSiO_4(OH)_8$ at the expense of $C_2(A,F)SH_8$ could be the consequence of the destabilisation of $C_2(A,F)SH_8$ due to the progressive increase of pH and $[Ca^{2+}]$ in the aqueous phase. This point is known from the stability domains of these hydrates in the $CaO\text{-}Al_2O_3\text{-}SiO_2\text{-}H_2O$ system [57]. Thus $C_2(A,F)SH_8$ would progressively dissolve and the released ions would react with ions liberated with C_2S and ferrite phase to form $C_3(A,F)SH_4$.

Also, carbonate-AFm phases are present as trace and stay stable at this time, while calcium monosulfoaluminate hydrate is hardly detectable. It seems that carbonate-AFm is more stable than calcium monosulfoaluminate hydrate in this system, although it can only be formed as a result of the leakage of some atmospheric CO_2 into the system.

3.2 Paste experiments

Paste experiment do not allow us to know the evolution of the aqueous phase but as the volume of liquid is less, smaller quantities of anhydrous phases are required to reach similar concentrations of the aqueous phase. Thus usually, the same period of the hydration is reached at lower percentage of reaction in paste than in suspension: this is all the more true that the W/C of the suspension is higher. As a consequence the latter steps observed in paste may not be observed in suspension as the system has already completely reacted or the duration of the experiment is not long enough.

The paste experiment will thus be used, first to confirm the initial steps found in suspension and also assess if other steps may arise at longer ages.

The mass percentages of the major anhydrous phases in the cement paste, relative to the mass of original anhydrous cement, are given in Figure 3-6 for one year of hydration. It demonstrates again that the anhydrite was consumed first – it had become essentially undetectable by XRD by the second measurement, made after one hour. Ye'elimite consumption is also very rapid, about half of that initially present having been consumed within the first hour. Its rate of consumption slows down with time but only about 2% (relative to the mass of the original cement) remains after 2 days. On the other hand, the ferrite phase is consumed much more slowly – only about 1-2% (relative to the mass of the original cement) is consumed by 7 days, although the rate of consumption appears to increase after that time (but bear in mind that the time axis in Figure 3-6 is logarithmic, which exaggerates the apparent rate). Interestingly, the belite phase and the ferrite phase appear to be consumed in an almost constant proportion from one day onwards, which suggests that their hydration reactions are somehow coupled. These observations were similar in the suspension, except that the time scale was different.

The major hydration products formed are shown in Figure 3-7 using exactly same scales as in Figure 3-6. On comparing the two, it is evident that the main crystalline hydrate formed in the first hour is ettringite, but that a significant amount (higher than 17wt% at 6 hours, 1day and 2 days) of a X-ray-amorphous phase is formed at the same time. Since the C_2S and ferrite do not participate yet the hydration, no silicate source or iron source can be supplied to form C-S-H gel or $Fe(OH)_3$ gel. The amorphous phases could be aluminate gel. This is entirely consistent with the expected reaction between ye'elimite, anhydrite and water to give ettringite plus amorphous aluminium hydroxide as already discussed in suspension experiments:

$$C_4A_3\$ + 2C\$ + 38H \rightarrow C_3A.3C\$.H_{32} + 2AH_3 \quad \text{(3.2)}$$

In order to confirm the presence of $Al(OH)_3$, the solid recovered at 1 hour of hydration was analyzed by solid state NMR for ^{27}Al at E.S.P.C.I. (Ecole Supérieure de Physique et de Chimie Industrielles de la Ville de Paris). The solid state ^{27}Al nuclear magnetic resonance spectra were recorded on a Bruker DRX spectrometer in 4mm zirconia rotors rotating at 14.1 kHz for about 5 hours. (Figure 3-9) The ^{27}Al NMR signal clearly separates the tetrahedrally-coordinated Al nuclei (with peaks around 50-100 ppm) and octahedrally-coordinated Al nuclei (with peaks at 10-20 ppm). In ye'elimite, all the Al is in tetrahedral sites [3, P.37], but in the ferrite phase, aluminium atoms are distributed between octahedral and tetrahedral sites ([19], P.25-26). Skibsted *et al* studied different aluminate and iron content of calcium aluminoferrites phases $Ca_2Al_xFe_{2-x}O_5$ (with x values of 0.93, 1 and 1.33) with MAS NMR [58]. Only with the lowest iron content ferrite (x=1.33), could a clear peak (at 8 ppm) be

detected for a small quantity of octahedally coordinated Al. However, in our NMR pattern, we cannot observe the huge peak in 71 ppm. As mentioned in 2.1, the ferrite phase is close to $C_2A_xF_{(1-x)}$ with x = 0.41, which is higher than the highest irons content of Skibsted's studies. Therefore, we can suppose that the influence of octahedral Al from ferrite phases in our cement cannot be neglected. In octahedral sites, ettringite shows its peaks around 13 ppm [59], calcium monosulfoaluminate hydrate around 9 ppm [59], a non-assigned peak around 3.5 ppm [60] and gibbsite around 8.3 ppm [61]. In our system, AFm was not detected by XRD. Therefore the peak around 9 ppm can probably be gibbsite. However, the peak of ettringite seems too weak, perhaps due to limited time of detection. Some more 27Al NMR experiences, including some pure phase's studies such as ferrite, ye'elimite, should be done to get quantified results and show the influence of substitution of foreign ions in AFt, gibbsite structures.

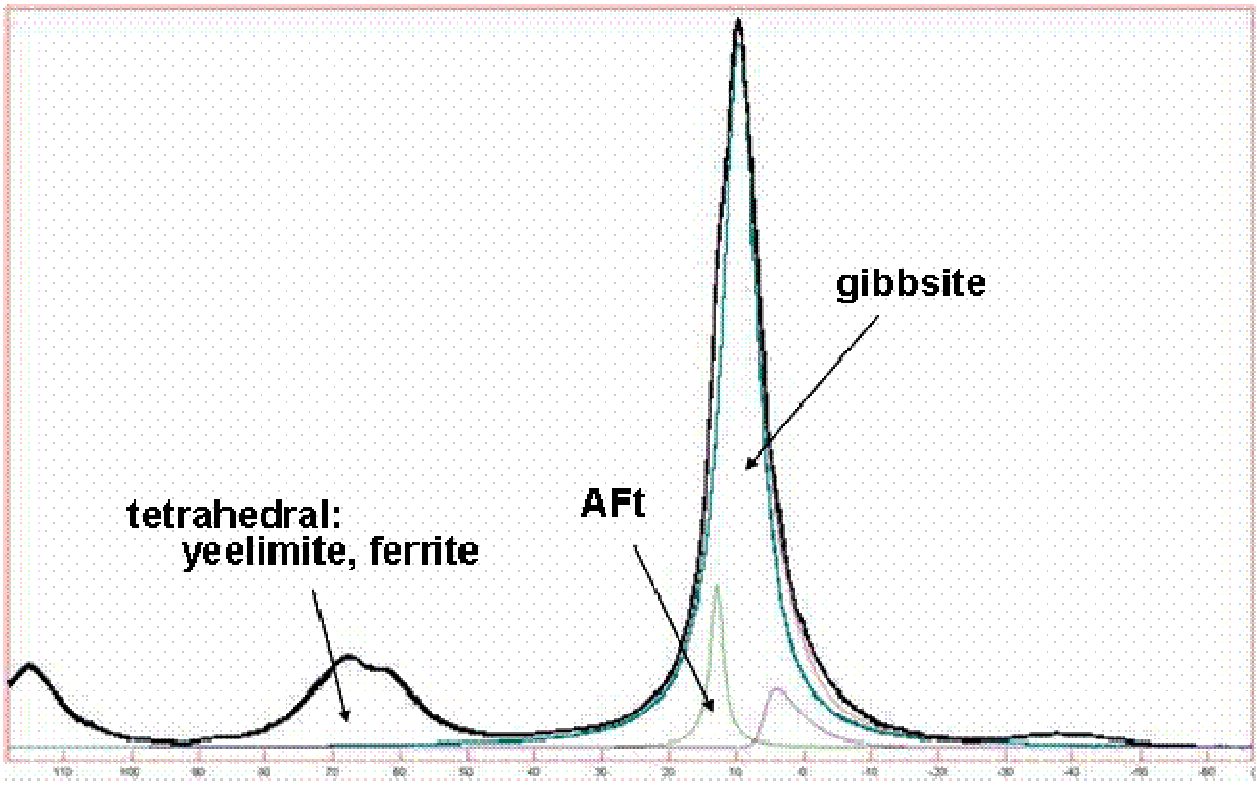

Figure 3-9: 27Al NMR results of solid recovered during k165-400B-5A hydration in paste after 1 hour

Another interesting feature of the results is that the rate of ye'elimite consumption appears to decrease after all of the anhydrite has been consumed. Some ye'elimite is still detectable at one week, although it has disappeared by two weeks. The amount of ettringite also follows a similar but inverse trend, reaching a maximum at about the same time that the ye'elimite disappears completely (i.e. by the measurement at two weeks). If we assume, however, that the anhydrite has all been consumed by 1 hour, the mechanism for ettringite formation after the first hour must be different to that shown in eq.(2). First of all, if sulfate ions from solution (i.e. mainly balanced by alkalis) are consumed, there must also be another source of soluble calcium in order to be able to make ettringite:

$$C_4A_3\$ + 2[Ca^{2+}] + 2[SO_4^{2-}] + 38H \rightarrow C_3A.3C\$.H_{32} + 2AH_3 \ldots\ldots\ldots\ldots\ldots\ldots (3.3)$$

However, the only potential sources of sufficient quantities of calcium ions are the other two main clinker phases, belite and ferrite. The Rietveld estimates in Figure 3-6 seem to show a small decrease in the amount of ferrite between 1 hour and 1 week, but the amount of belite actually appears to increase slightly, although this change is probably well within the range of experimental error. It is thus hard to say which of these two phases is more involved but the amount of calcium required is small, so it is quite possible that it mainly comes from ferrite phase hydration. Note that one might also consider that ye'elimite hydration could in principle continue to give some ettringite after the disappearance of all other sources of sulphate, by a reaction such as:

$$3C_4A_3\$ + 38H \rightarrow C_3A.3C\$.H_{32} + 2C_3AH_6 + 6AH_3 \ldots\ldots\ldots\ldots\ldots\ldots (3.4')$$

However, the XRD data in Figure 3-7 also show the appearance of calcium monosulfoaluminate hydrate at ages as early as two days, at a time when ettringite also still appears to be forming, and there is as yet no sign of any hydrogarnet formation. It is therefore more logical to assume that the formation of this phase is also mostly a direct result of ye'elimite hydration knowing that small amount of ferrite phase may also form additional amounts of this phase:

$$C_4A_3\$ + 18H \rightarrow C_3A.C\$.H_{12} + 2AH_3 \ldots\ldots\ldots\ldots\ldots\ldots\ldots\ldots (3.4)$$

An additional parameter that may partly explain the variation of ettringite content, relies on the fact that ettringite may be ill-crystallized at the hydration beginning and then progressively better crystallizes.

It is interesting to note that the amount of "amorphous phase", expected to be mostly AH_3, decreases rapidly after reaching a first maximum at about two days, while, simultaneously, the amount of belite decreases rapidly and the amount of strätlingite formed increases rapidly. The reaction of amorphous alumina gel with hydrating belite to give strätlingite can readily explain this change as observed in suspension experiment:

$$C_2S + AH_3 + 5H \rightarrow C_2ASH_8 \ldots\ldots\ldots\ldots\ldots\ldots\ldots\ldots\ldots\ldots\ldots\ldots (3.5)$$

As in suspension, ferrite phase certainly also participate to strätlingite precipitation:

$$C_2S + C_2(A,F) + 10H \rightarrow C_2(A,F)SH_8 + [Ca^{2+}] \text{ and } [OH^-] \text{ in solution} \ldots \ldots (3.6)$$

The amount of AH_3 in the paste reaches a minimum (effectively zero) by two weeks, which coincides roughly with the maximum amount of strätlingite (about 50% by mass of anhydrous cement). At the same time, we begin to see a significant amount of an iron-containing siliceous hydrogarnet that coincides with further hydration of both belite and ferrite phases. The formation of siliceous hydrogarnet is like in suspension experiment, the consequence of the C_2ASH_8 destabilisation once pH and calcium ion concentration increase.

$$C_2S + C_2(A,F) + C_2(A,F)SH_8 \rightarrow 2\ C_3(A,F)SH_4 \ldots\ldots\ldots (3.7)$$

Alternatively as pH and calcium concentration is still expected to increase, siliceous hydrogarnet may be formed directly from C_2S and $C_2(A,F)$ hydration:

$$C_2S + C_2(A,F) + 5H \rightarrow C_3(A,F)SH_4 + [Ca^{2+}] \text{ and } [OH^-] \text{ in solution} \ldots\ldots\ldots (3.8)$$

Note also that katoite formed in the above reaction does not necessarily have exactly the composition shown [$C_3(A,F)SH_4$]. A more general formula, $Ca_3(Al,Fe)_2(SiO_4)_x(OH)_{(12-4x)}$ [$C_3(A,F)S_xH_{6-2x}$] is preferable, because we are not currently able to determine either the Al/Fe ratio or the value of x with any certainty. Likewise, we are not currently certain of the exact composition of the ferrite phase in our clinker, which is why we call it "$C_2(A,F)$," although there are good indications that it has an Al/Fe ratio of <1.

Equations 3.7 and 3.8 explain why C_2S and ferrite phase hydrations are linked and thus that their consumption is quasi proportional during this period.

After two weeks, the amount of amorphous phase begins again to increase, while strätlingite and belite decrease although the ferrite phase is consumed more slowly. At the same time, some peaks that can attributed to C-S-H [62] appear in the X-ray diffraction pattern. In order to confirm the presence of C-S-H, the sample at 8 months (19.3% amorphous phases according to XRD with Rietveld) was also analyzed by solid state NMR for Si at E.S.P.C.I. The solid state ^{29}Si nuclear magnetic resonance spectra were recorded on a Bruker DRX spectrometer in 4mm zirconia rotors at 5 kHz for about 17 hours. The work of Kwan *et al* shows that the silicon atoms in strätlingite exist predominantly in Q_2, Q_{2p}, and $Q_{2(2Al)}$ environments [63]. Other studies [64] show that the chemical shift of Si in hydrogarnet is around -89 ppm, the tetrahedral SiO_4 in C_2S gives its signal around -70ppm (Q_0), while in the structure of C-S-H, the main ^{29}Si peaks can be found around -78 ppm (Q_1), -81 ppm(Q_2) and -84 ppm(Q_{2p}) which correspond to different degrees of silicate anion polymerization. In our spectrum (Figure 3-10), we see four main peaks: -70ppm (Q_0), - 78ppm(Q_1), -81ppm(Q_2) and -84ppm(Q_{2p}). This implies that some amount of C_2S has not yet hydrated after 8 months, and some C-S-H can be found as hydrated phases, which fits well the results of XRD. However, our results can only be used for identifying the hydrates. More experiments would be needed to quantify the results and estimate the distribution of Si in the hydrates, for example, hydrogarnet or C-S-H.

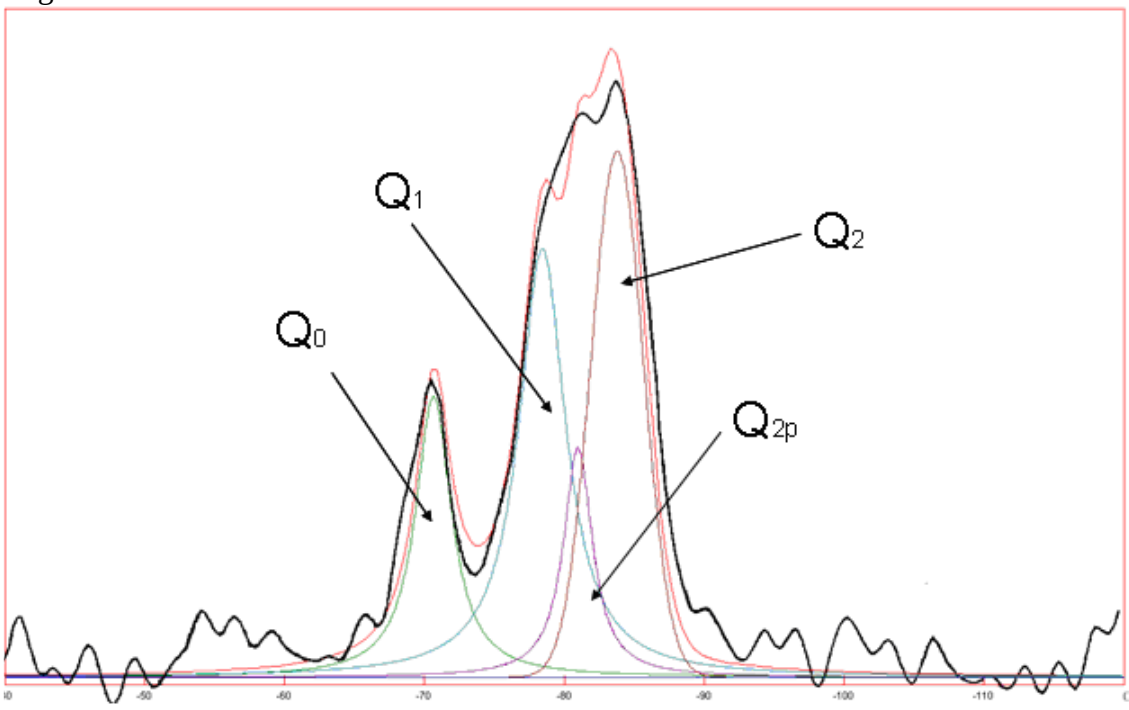

Figure 3-10: 29Si NMR results of solid recovered during k165-400B-5A hydration in paste after 8 months

We therefore assume that the new amorphous phase is C-S-H (here considered to have a C/S ratio of 1), produced by reaction of belite and strätlingite, perhaps as suggested below:

$$C_2S + C_2ASH_8 \rightarrow C_3ASH_4 + C\text{-}S\text{-}Hx + (4\text{-}x)H \quad (3.9)$$

About at the same time, the amount of calcium monosulfoaluminate hydrate, also begins to increase significantly. However there is no additional source of sulphate ions and we do no see a significant decrease in ettringite at this time. Once again this may be the influence of the increase of pH and of calcium concentration that would free some sulphate by two potential mechanisms: first, a greater substitution of sulphate ions by hydroxide ions both in ettringite and calcium monosulfoaluminate hydrate. Second, a further decrease of the sulphate concentration to stabilize these phases as demonstrated by the sulphate concentration at the invariant points of the $CaO\text{-}Al_2O_3\text{-}CaSO_4\text{-}H_2O$ system containing AH_3 compared to those that contains portlandite (CH). Additionally if some alkalis are incorporated into the interlayer of C-S-H, the equilibrium sulphate concentration would also markedly decrease. Thus calcium monosulfoaluminate hydrate may be formed accordingly to the following reaction:

$$2C_2S + C_2(A,F) + [SO_4^{2-}] \text{ in solution} + xH \rightarrow C_3(A,F).C\$.H_{12} + 2\ C\text{-}S\text{-}H_x \quad (3.10)$$

3.3 Interpretations and discussions

Comparing the results both in suspension and in paste, we find that the equivalent reaction steps occur at the beginning of hydration but at higher percentage of reaction for the hydration in suspension. As a consequence, the hydration rate in suspension looks slower. As a consequence, if we consider the difference of time, 2 days in suspension and 1 year in paste, the final steps are likely not to be reached in suspension experiment. However, the hydration path can be described by similar chemical equations that can be divided into five steps.

Step 1

W/C=5	W/C=0.5	Present phases
0-4H	0-1H	ye'elimite, anhydrite, ettringite, AH_3, belite, ferrite

During this step, ye'elimite and anhydrite reacts quickly to form ettringite and aluminate gel (AH_3), while the hydration of belite and ferrite is very slow. Equation can be written as:

Ye'elimite with anhydrite:

$$C_4A_3\$ + 2C\$ + 38H \rightarrow C_3A.3C\$.H_{32} + 2AH_3 \text{ (amorphous)} \quad (3.2)$$

Also, alkali sulphate is also a sulphate source for ye'elimite. Their reaction can be written as (3.3).

$$C_4A_3\$ + 2[Ca^{2+}] + 2[SO_4^{2-}] + 38H \rightarrow C_3A.3C\$.H_{32} + 2AH_3 \quad (3.3)$$

Belite or ferrite or both could be the calcium source, but the quantity is expected to be very small.

The interactions summarized in Figure 3-11 can help us to explain this phenomenon:

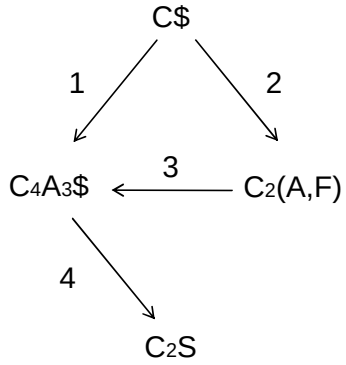

Figure 3-11: Interaction of involved phases in step 1

Interaction 1: hydration of ye'elimite is accelerated by the presence of anhydrite (equation 3.2), as found in the literature.

Interaction 2: ferrite hydration is strongly retarded by the effect of sulphate ions in the solution which is given by anhydrite, alkali sulphate and to a lesser extent ye'elimite. This is like if C_4AF would hydrate in the presence of sulphate.

Interaction 3: ferrite could supply calcium ions to facilitate the equation (3.3). However, since the ferrite hydration is slow, this interaction is very small.

Interaction 4: hydration of C_2S is very slow in this step because even if it should rapidly reach its solubility, no Si containing hydrates can be precipitated: due to high aluminate concentration which is freed by the strong ye'elimite dissolution, the nucleation of C-S-H is inhibited. Also due to the high concentration of sulphate, strätlingite and hydrogarnet are not stable. Therefore, hydration of C_2S is blocked waiting for the hydrates to precipitate once the conditions will enable it.

Step 1 ends when anhydrite is no more available in the system.

Step 2

W/C=5	W/C=0.5	Present phases
4-6.25H	1H-3D	ye'elimite, ettringite, AH_3, monosulfoaluminate, belite, ferrite, Carbonated AFm

When anhydrite is totally consumed, the concentration of aluminate and sulphate still stays very high. However, the hydration of ye'elimite without anhydrite as equation (3.3), (3.4) will drive down the concentration of aluminium and sulphate. At this time, the hydration of C_2S and ferrite is still slow.

When sulphate is still available in the solution:

$$C_4A_3\$ + 2(Ca^{2+}) + 2(SO_4^{2-}) + 38H \rightarrow C_3A.3C\$.H_{32} + 2AH_3 \quad (3.3)$$

When sulphate is close to zero:

$$C_4A_3\$ + 18H \rightarrow C_3A.C\$.H_{12} + 2AH_3 \quad (3.4)$$

The interactions summarized in Figure 3-12 can help us to explain these phenomena:

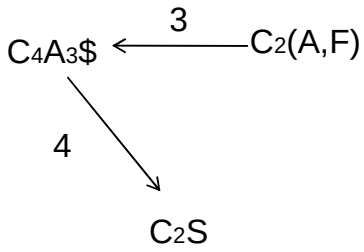

Figure 3-12: Interaction of involved phases in step 2

In this step, the interactions are similar to those in step 1, except that the aluminate and sulphate concentrations continue to decrease. When ye'elimite is completely consumed, sulphate becomes too low to inhibit ferrite hydration (interaction 3) and to avoid strätlingite nucleation (interaction 4). However, in reality, a little amount of ye'elimite may stay in bigger clinker grains without being in contact with the aqueous phase and stay in the solid phases as it can be shown in a backscattered electron image of a polished section of the hydrate cement of k165-400B-5A after 7 days obtained using a FEG-SEM, Figure 3-13).

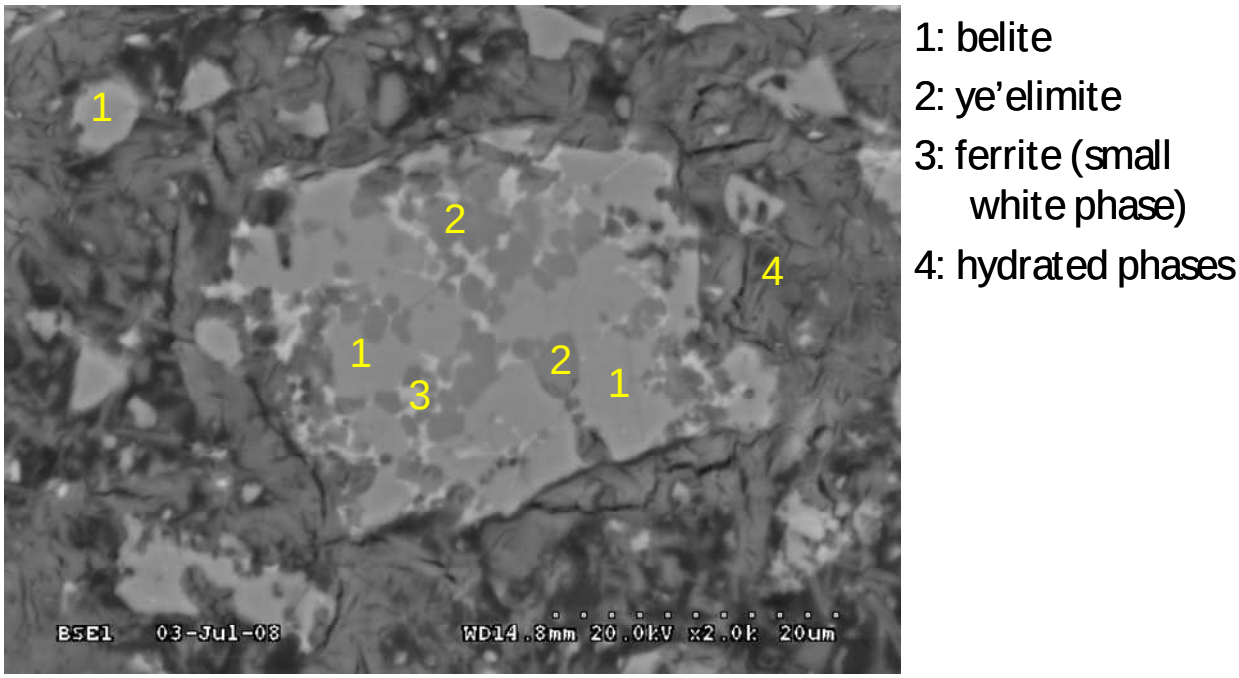

Figure 3-13: SEM micrography of cement of k165-400B-5A hydrated in paste for 7 days

On the other hand, aluminate concentration that is mainly governed by AH_3 solubility is still too high to enable C-S-H nucleation (interaction 4). Step 2 ends when $C_4A_3\$$ is totally consumed (in fact, quasi consumed as some ye'elimite may not be in contact of water for longer times).

Also, it is also important to indicate that the carbonation phenomena seem to play an important role in this step, especially in suspension, which probably facilitates carbonation. At the same time, the quantity of calcium monosulfoaluminate hydrate in suspension is much less than that in paste, which probably suggests a competition of carbonate ions and sulphate ions to combine with calcium and aluminium sources. Indeed calcium monosulfoaluminate hydrate, calcium moncarboaluminate hydrate and calcium hemicarboaluminate hydrate are AFm phases [65] that can exchange anions but also have different stability domains

[66,67,68]. The extent of reaction depends on the activity of CO_2 and the environmental condition [68]. Nevertheless AFm phases are just detected as trace in the suspension experiment.

Step 3

W/C=5	W/C=0.5	Present phases
6.25-44H	7D-28D	ettringite, AH_3, monosulfoaluminate, monocarbonaluminate, belite, ferrite, strätlingite

During this step, C_2S starts to react with AH_3 to form strätlingite as in equation (3.5).

$$C_2S + AH_3 + 5H \rightarrow C_2ASH_8 \quad (3.5)$$

Ferrite also reacts with C_2S to form an iron substituted strätlingite (3.6):

$$C_2S + C_2(A,F) + 10H \rightarrow C_2(A,F)SH_8 + [Ca^{2+}] \text{ and } [OH^-] \text{ in solution} \quad (3.6)$$

The interactions summarized in Figure 3-14 can help us to explain this phenomenon:

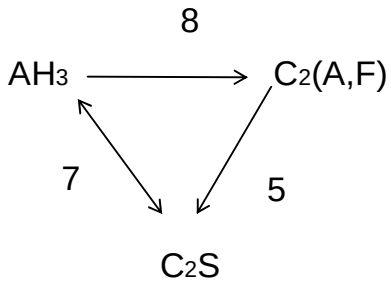

Figure 3-14: Interaction of involved phases in step 3

Interaction 7: C_2S reacts with the aluminate ions in the solution to form strätlingite, which decreases its concentration. This drives AH_3 dissolves into the solution to oppose it: thus the amount of AH_3 decreases. On the other hand, the aluminate concentration mostly determined by AH_3, still unables the nucleation of C-S-H. This effect could be confirmed by the hydration of belite extracted by k165 clinker (Annex 2-5) in Figure 3-15.

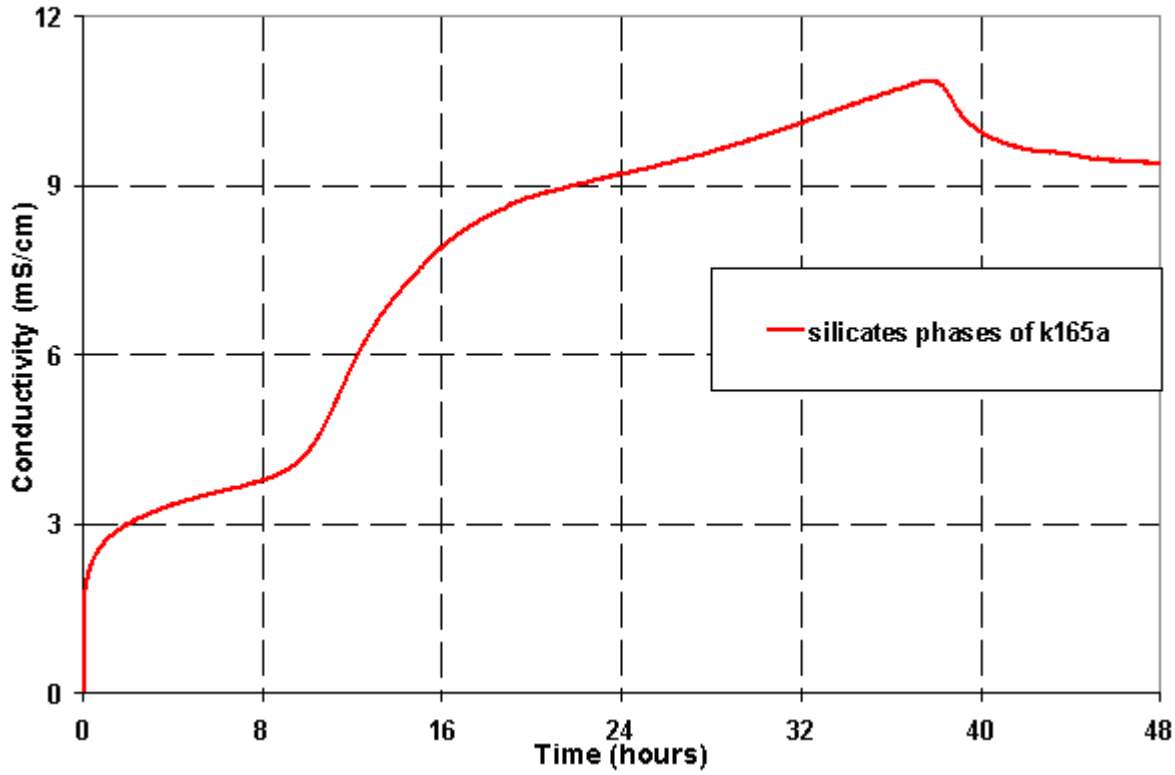

Figure 3-15: Conductivity trace of silicate phase of k165 in suspension (W/C=5)

Belite from clinker k165 shows similar hydration kinetics to those described in the literature for other belites ([19], P.155-156). Thus belite in k165 clinker is reactive when placed in adequate conditions but during the initial hydration of k165-400B-5A cement, belite hydrates with a different route due to the interaction 7.

Interaction 8: ferrite starts to dissolve into the solution, but it exists a competition with AH_3 to react with C_2S and as a consequence, its dissolution is delayed by the dissolution of AH_3.

Interaction 5: Despite that AH_3 will react mostly with belite, this interaction enables the aqueous phase to reach higher pH and higher calcium concentration leading to a further destabilisation of AH_3.

The concentration of boron can be used as a tracer of C_2S hydration: it is interesting to note that boron accumulate into the aqueous phase at the beginning of C_2S reaction and then decreases that suggests the precipitation of boron-ettrinigite or the absorption on some phases.

This step will continue until AH_3 is totally consumed.

Step 4

W/C=5	W/C=0.5	Present phases
44-48H*	7D-28D	ettringite, monosulfoaluminate, monocarboaluminate, belite, ferrite, strätlingite, hydrogarnet

* Suspension experiments of k165-400B-5A ended at 48 hours.

As both pH and calcium concentration increases, strätlingite is no longer stable are expected to be released by mostly anions exchange between sulphate and hydroxide in ettringite. This will provide ions that may react with C_2S and ferrite phase. Thus in this step C_2S and ferrite hydration are strongly connected to form mainly hydrogarnet:

$$C_2S + C_2(A,F) + C_2(A,F)SH_8 \rightarrow 2\ C_3(A,F)SH_4 \quad (3.7)$$

$$C_2S + C_2(A,F) + 5H \rightarrow C_3(A,F)SH_4 + [Ca^{2+}] \text{ and } [OH^-] \text{ in solution} \quad (3.8)$$

The interactions summarized in Figure 3-16 can help us to explain this phenomenon:

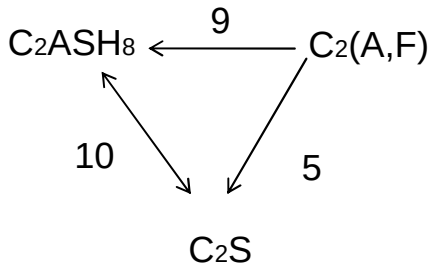

Figure 3-16: Interaction of involved phases in step 4

Interaction 10: the aluminate concentration mostly determined by C_2ASH_8 still unables the nucleation of C-S-H but C_2S hydration consume C_2ASH_8 and now forms hydrogarnet instead of C_2ASH_8 but it needs additional calcium that is provided by ferrite phase.

Interaction 5, 9: Dissolution of ferrite is strongly linked with C_2S hydration as both are associated to form hydrogarnet.

This step ends when C-S-H appears that is linked with the disappearance of C_2ASH_8 in contact with the aqueous phase.

Step 5

W/C=5	W/C=0.5	Present phases
-	> 1M	ettringite, monosulfoaluminate, monocarboaluminate, belite, ferrite, (strätlingite), hydrogarnet, C-S-H

The aluminate concentration in equilibrium with hydrogarnet can be far less than the one in equilibrium with strätlingite. Thus the inhibition of C-S-H nucleation is no longer active and then C-S-H may form along with hydrogarnet and calcium monosulfoaluminate hydrate.

This step that occurs after several months in paste, is missing in suspension as the duration of the experiment was only two days.

Equations can be given as follows:

$$C_2S + C_2ASH_8 \rightarrow C_3ASH_4 + C\text{-}S\text{-}Hx + (4\text{-}x)H \ldots\ldots\ldots\ldots\ldots\ldots\ldots\ldots (3.9)$$

$$2C_2S + C_2(A,F) + [SO_4^{2-}] \text{ in solution} + xH \rightarrow C_3(A,F).C\$.H_{12} + 2\ C\text{-}S\text{-}H_x \quad (3.10)$$

The interactions summarized in Figure 3-17 can help us to explain this phenomenon:

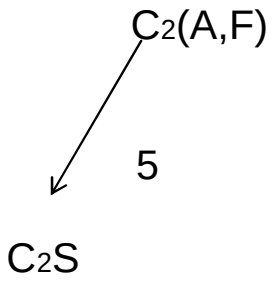

Figure 3-17: Interaction of involved phases in step 5

Interaction 5: Identical to step 4, C_2S and ferrite hydration are linked to be able to produce hydrates having more calcium ions than the dissolving solids.

This step ends when C_4AF is totally consumed. We could have then considered another step during which C_2S hydrates alone to form C-S-H

Phase composition evolution during hydration

We can conclude that compared to OPC, hydration of BCSAF stays quite active even up to 1 year. This might have some consequence on the macroscopic properties of the cement paste, such as the macroscopic porosity that is related to the mechanical strength of the cement paste or the concrete made from it.

The densities of the known anhydrous and hydrate phases can be found in the literature [69,70]. Given the mass of anhydrous and hydrate phases by 100g of initial anhydrous cement, we can easily obtain the total volume of anhydrous and hydrate phases in paste and thus the volume changes during hydration (Figure 3-18). We can see that the hydration reactions at long ages (steps 3 and 4) do not lead to much change in the solid volume, which suggests that the macroscopic properties should not be changed too markedly. Nevertheless experiments in order to record the volume changes should be made to confirm that point.

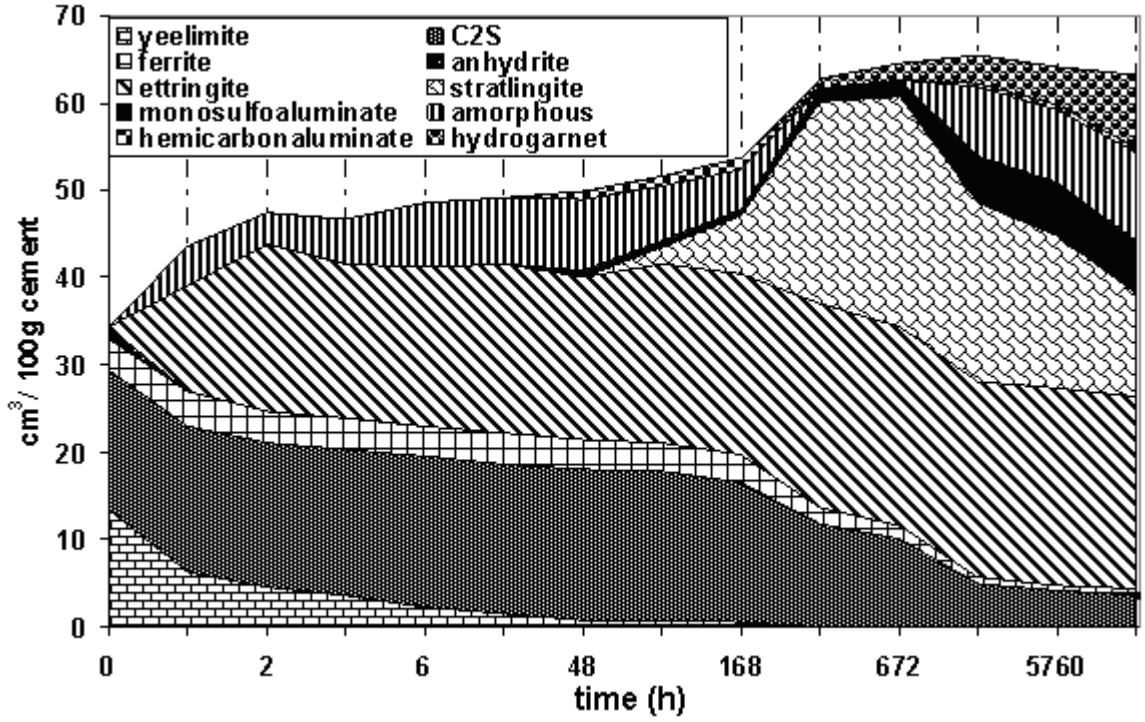

Figure 3-18: Volume evolution of a cement paste of k165-400B-5A during 1 year, in cm^3 by 100g of initial cement

3.4 First conclusions on the mechanism of hydration and points needed for further improvements

The study of a new chemical system is always not so obvious even if a lot is known on OPC. The hydration of K165-400B-5A cement leads to a very specific mechanism of hydration that is complex (at least 5 steps) and lasts over several months. Moreover usual and proven techniques developed on OPC such as Rietveld refinement needed to be adapted to these new chemical systems.

The steps of K165-400B-5A cement have been summarised on figures 3-19 and 3-20 knowing that the last step of the paste experiment is missing in the suspension experiment.

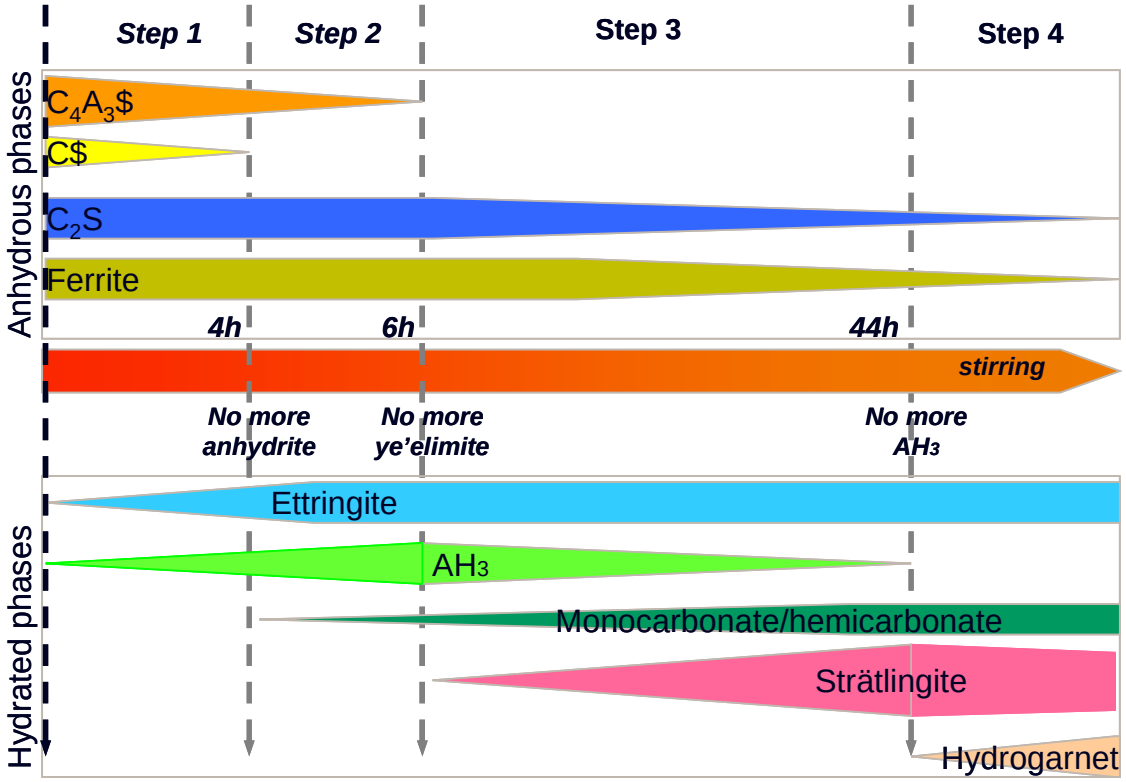

Figure 3-19: Steps observed during the hydration of k165-400B-5A in suspension up to two days

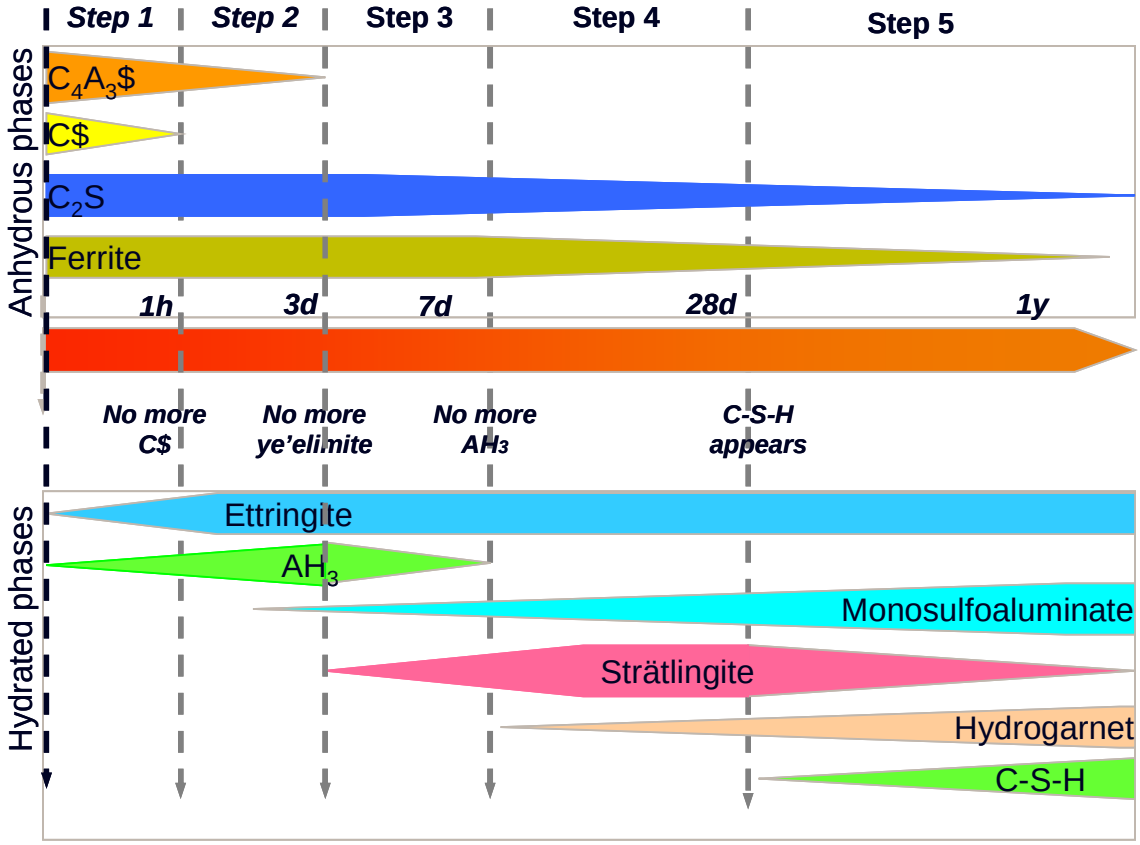

Figure 3-20: Steps observed during the hydration of k165-400B-5A in paste during the first year

It appears that K165-400B-5A cement has two main successive mechanisms of hydration: the beginning of hydration is controlled by $C_4A_3\$$ and C\$, while the remaining of hydration is governed by C_2S and the ferrite phase that react with some of the hydrates formed during the first period.

We have made some hypothesis to explain the parameters that control these steps and especially why the C_2S and the ferrite phase do not hydrate till the beginning. Nevertheless a careful observation of the microstructure obtained shows some important heterogeneities and thus the presence of local equilibria. As a consequence the time at which the steps occur may vary from a place to another of the microstructure and thus we may have less defined boundaries between the steps than schematically described.

Nevertheless with the given results, we can start to answer the five key questions given in section 1.4:

Question 1: confirm the that major initial reaction is: $C_4A_3\$ + 2C\$ + 38H \Rightarrow C_6A\$_3H_{32} + 2AH_3$

➔ It is confirmed both in suspension and paste.

Question 2: assess how the form and quantity of the initial soluble sulphates influence the later hydration

➔ This question cannot answer yet; this is the purpose of the next chapter.

Question 3: determine the parameters that control ferrite phase hydration,

➔ Anhydrite control ferrite hydration by blocking it at very beginning. Ferrite hydration will only start when sulphate concentration becomes very low and when it will become coupled with C_2S hydration.

Question 4: determine the factors that control belite hydration and induce a retardation of its start

➔ It is C_2ASH_8 nucleation rate that governs the beginning of the hydration of C_2S. The main parameter that governs the nucleation rate of C_2ASH_8 is $[SO_4]^{2-}$ that has to be low. C-S-H does not form as the initial hydrate for belite hydration because it is not saturated in the beginning due to low calcium and silicon concentration and its formation is further delayed later by the inhibition effect of high aluminate concentration on C-S-H nucleation. As a consequence, this is indirectly the sulphate concentration that controls the beginning of C_2S hydration and thus the reactions leading to its reduction, mainly the hydration of $C_4A_3\$$. Globally it is once $C_4A_3\$$ has been completely reacted that C_2ASH_8 may nucleate.

Question 5: check if limestone has an accelerator effect on belite hydration such in OPC

➔ Unknown yet: it will be answered in chapter 5.

The robustness of these hypotheses and the answer to question will now be assessed by studying the hydration of cements made with k165 clinker and different quantities of anhydrite with the same experimental conditions.

Figures and Tables of experimental results of k165-400B-5A in paste and in suspension

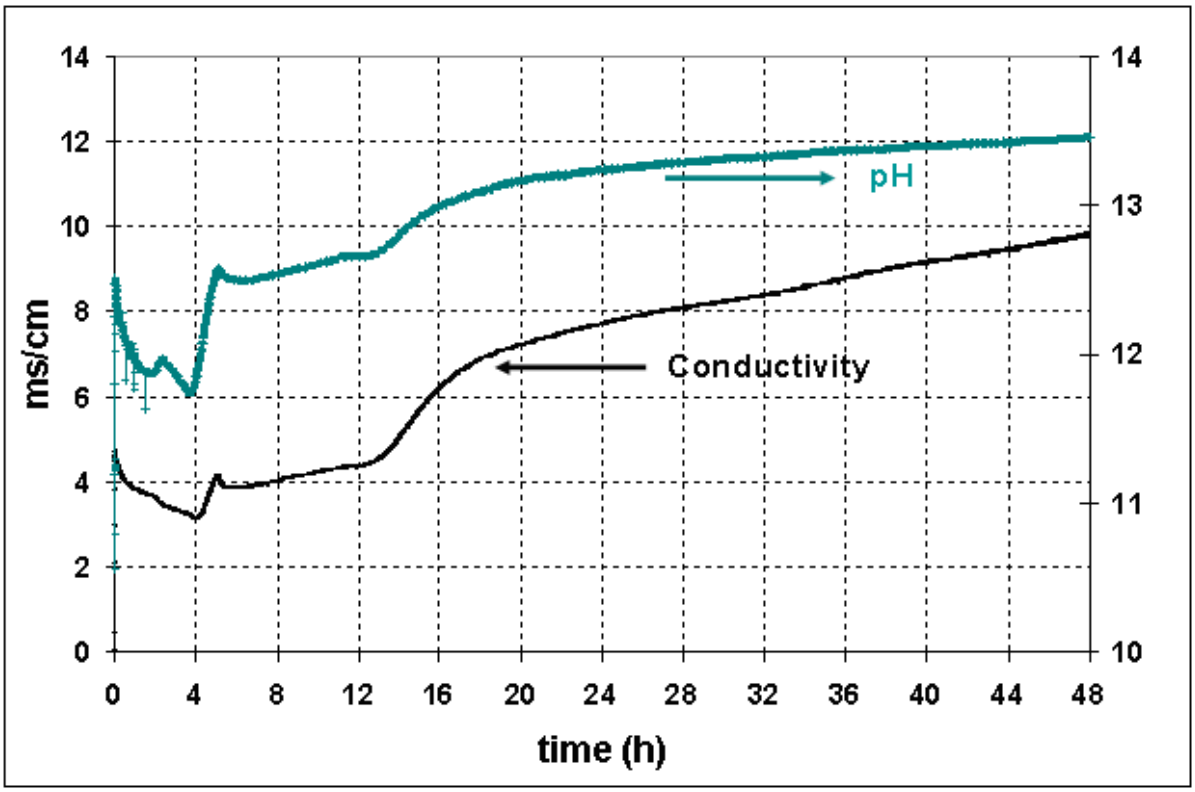

Figure 3-1: Electrical Conductivity and pH of k165-400B-5A hydrated in suspension at w/c =5

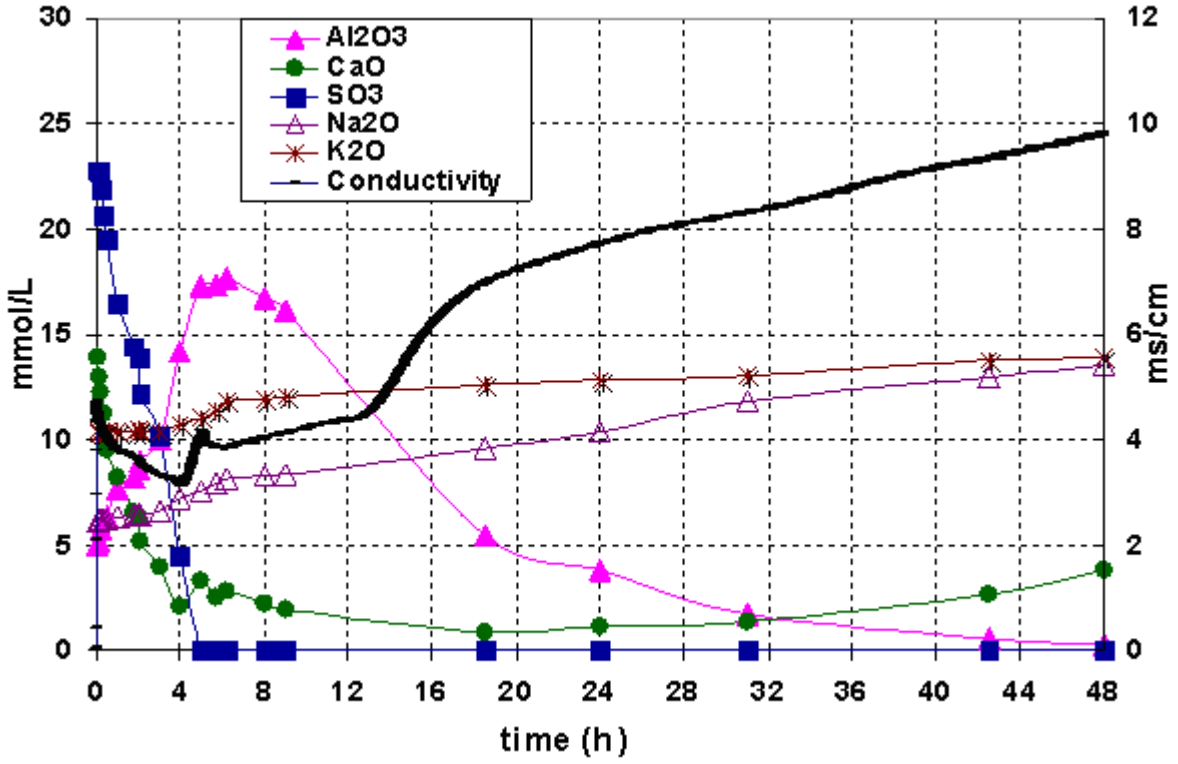

Figure 3-2: Electrical conductivity and major chemical elements of the liquid phase recovered during k165-400B-5A hydration in suspension (w/c = 5) during two days

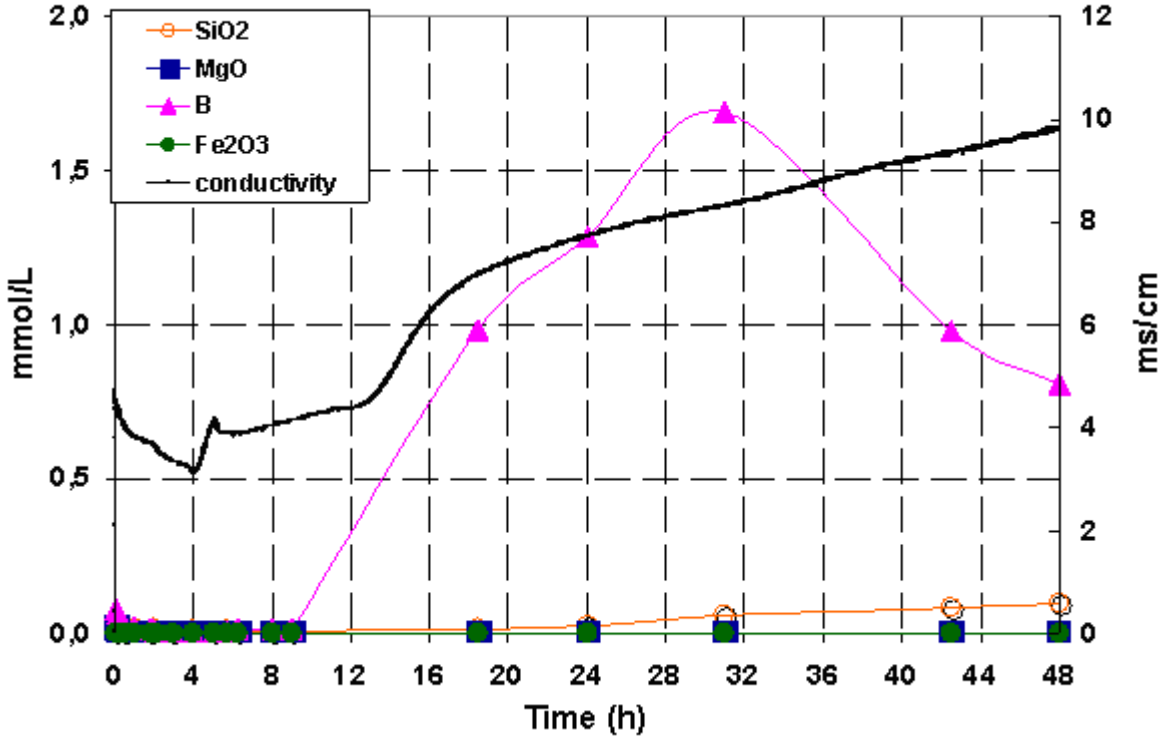

Figure 3-3: Minor chemical elements of the liquid phase recovered during k165-400B-5A hydration in suspension (w/c = 5) during two days

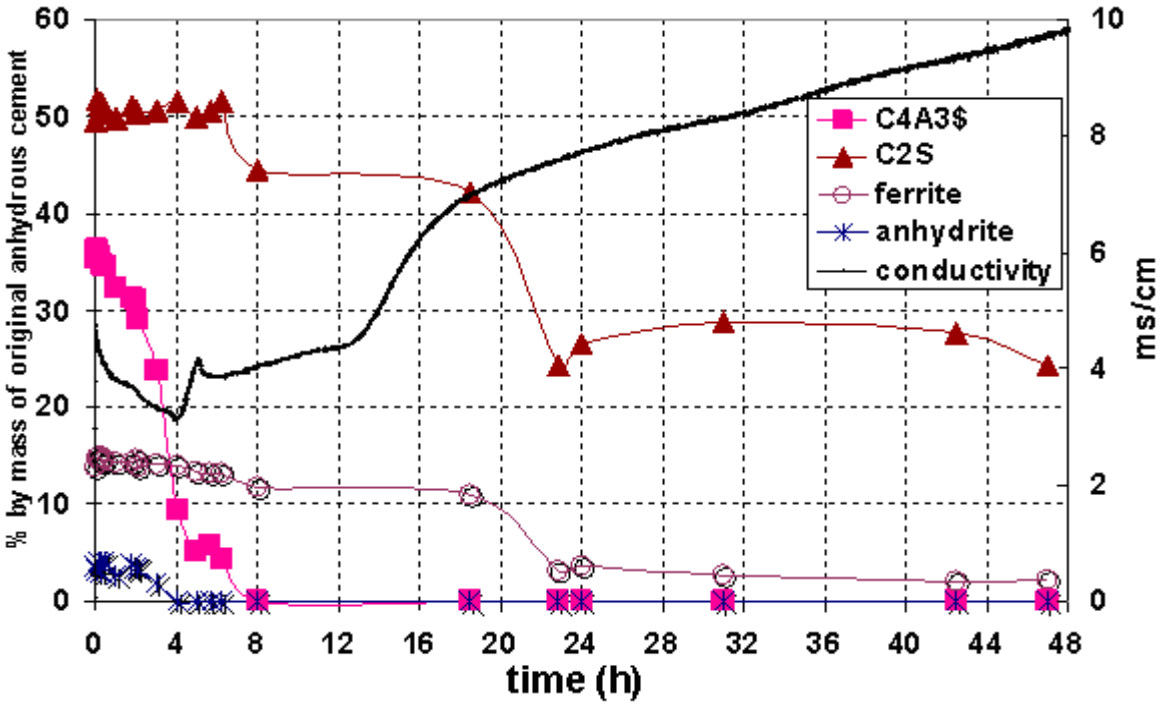

Figure 3-4: Electrical conductivity and normalised Rietveld estimates of anhydrous phases of cement k165-400B-5A hydrated in suspension during two days, in % by mass of original anhydrous cement

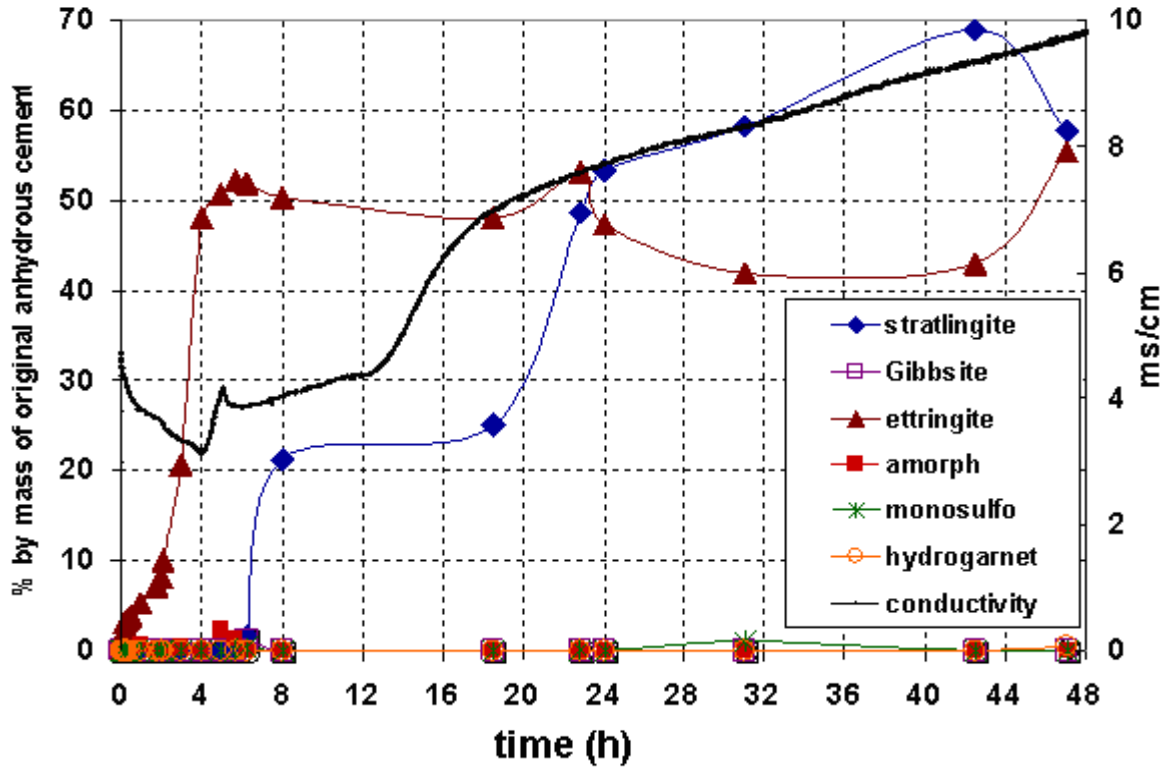

Figure 3-5: Electrical conductivity and normalised Rietveld estimates of major hydrate phases of k165-400B-5A hydrated in suspension during two days, in % by mass of original anhydrous cement

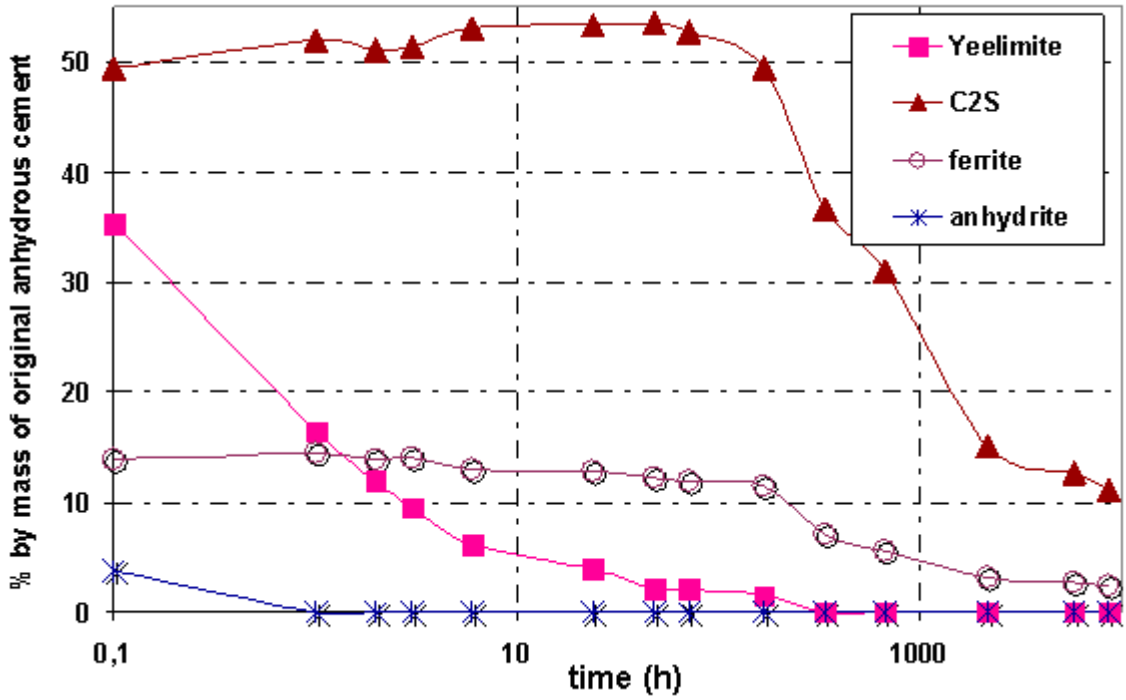

Figure 3-6: Normalised Rietveld estimates of anhydrous phases of k165-400B-5A hydrated in paste during 1 year, in % by mass of original anhydrous cement

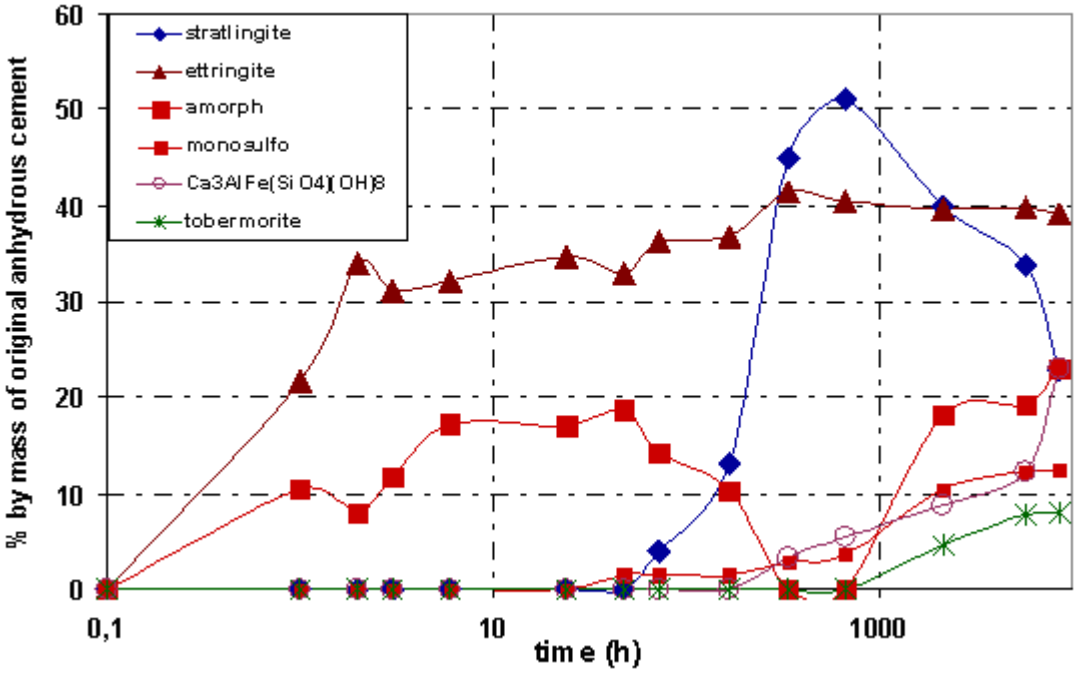

Figure 3-7: Normalised Rietveld estimates of major hydrate phases of cement k165-400B-5A hydrated in pasted during 1 year, in % by mass of original anhydrous cement

	Minor hydrate phases				
Time (h)	monosulfo	Amorphous	Gibbsit	Hydrogarnet	Carbonate
0.00	0	0	0	0	0
0.08	0	0	0	0	0
0.17	0	0	0	0	0
0.25	0	0	0	0	0
0.33	0	0	0	0	0
0.50	0	0	0	0	0
1.00	0	0.7	0	0	0
1.80	0	0	0	0	0
2.00	0	0	0	0	0
2.10	0	0	0	0	0
3.00	0	0.3	0	0	0
4.00	0	0	0	0	0
5.00	0	2.2	0	0	0
5.70	0	1.4	0	0	0
6.25	0.3	0	1.3	0	0
8.00	0	0	0	0	2.4
18.50	0	0	0	0	3.4
22.80	0	0	0	0	3.3
24.00	0	0	0	0	1.8
31.00	1.0	0	0	0	6.6
42.50	0	0	0	0	1.0
47.00	0	0	0	0.5	1.2

Table 3-3: Normalised Rietveld estimates of minor hydrates during k165-400B-5A hydration in suspension for two days, in % by mass of original anhydrous cement

Time	Strätlingite	Gibbsite	Monosulfo	C_3AH_6	Ettringite	Portlandite	Gypsum	CAH_{10}	C_2AH_8	C_4AH_{13}	C_2S
5m	2.87	1.44	3.57	-0.25	10.01	-2.08	-0,12	0.88	-0.29	<-3	<-3
10m	2.93	1.68	2.56	-1.24	8.95	-2.58	-0,14	0.88	-0.79	<-3	<-3
15m	2.87	1.91	1.85	-1.92	8.19	-2.96	-0,17	0.96	-1.09	<-3	<-3
20m	3.01	1.91	1.92	-1.18	8.17	-2.92	-0,22	0.99	-1.02	<-3	<-3
30m	1.67	2.45	-0.43	-3.00	5.68	<-3	-0,29	0.95	-2.18	<-3	<-3
1h	2.64	2.25	0.69	-2.86	6.60	<-3	-0,39	1.09	-1.49	<-3	<-3
1.9h	2.34	2.15	0.87	-2.57	6.54	<-3	-0,51	1.06	-1.36	<-3	<-3
2h	2.61	2.21	0.72	-2.68	6.35	<-3	-0,53	1.10	-1.40	<-3	<-3
2.15h	2.46	2.23	0.43	-2.86	5.83	<-3	-0,65	1.07	-1.51	<-3	<-3
3h	2.09	2.22	0.32	-2.82	5.40	<-3	-0,80	1.72	-1.49	<-3	<-3
4h	2.53	2.17	0.30	-2.30	4.31	<-3	-1,34	1.18	-1.17	<-3	<-3
5h	3.46	1.72	1.57	0.76	2.00	-1.94	<-3	1.59	0.57	-1.77	<-3
5.8h	3.59	1.74	1.07	0.34	1.36	-2.05	<-3	1.48	0.30	-2.34	<-3
6.25h	3.51	1.69	1.56	0.68	2.14	-2.45	<-3	1.52	0.49	-1.85	<-3
8h	3.28	1.61	1.23	0.53	1.43	-1.94	<-3	1.38	0.35	-2.00	<-3
9h	3.20	1.55	1.18	0.54	1.27	-1.90	<-3	1.29	0.31	-1.94	<-3
18.5h	2.31	0.64	0.18	0.08	-0.80	-1.44	<-3	-0.07	-0.61	-1.95	<-3
24h	2.38	0.41	0.18	0.27	-1.18	-1.23	<-3	-0.31	-0.63	-1.55	<-3
31h	2.14	0.00	-0.02	0.05	-1.33	-1.03	<-3	-0.94	-1.06	-1.57	<-3
42.5h	1.68	-0.57	0.06	0.13	-1.27	-0.62	<-3	-1.67	-1.38	-1.09	<-3
48h	1.50	-0.84	0.24	0.18	-0.84	-0.43	<-3	-2.01	-1.52	-0.84	<-3

Table 3-4: Saturation indexes with respect to hydrate phases from the aqueous phase composition recovered during K165-400B-5A hydration in suspension (w/c = 5)

Time	CSH09	CSH10	CSH11	CSH12	CSH13	CSH14	CSH15	CSH16	CSH17	CSH18
5min	-2.08	-2.11	-2.07	-2.02	-2.07	-2.17	-2.36	-2.57	-2.81	<-3
10min	-1.98	-2.05	-2.06	-2.07	-2.16	-2.31	-2.56	-2.81	<-3	<-3
15min	-2.07	-2.19	-2.24	-2.28	-2.41	-2.60	-2.88	<-3	<-3	<-3
20min	-1.97	-2.07	-2.12	-2.16	-2.28	-2.47	-2.75	<-3	<-3	<-3
30min	<-3	<-3	<-3	<-3	<-3	<-3	<-3	<-3	<-3	<-3
1h	-2.38	-2.54	-2.65	-2.74	-2.93	<-3	<-3	<-3	<-3	<-3
1h50	-2.67	-2.82	-2.91	-2.99	<-3	<-3	<-3	<-3	<-3	<-3
2h	-2.44	-2.59	-2.69	-2.78	-2.95	<-3	<-3	<-3	<-3	<-3
2h10	-2.55	-2.71	-2.81	-2.91	<-3	<-3	<-3	<-3	<-3	<-3
3h	-2.92	<-3	<-3	<-3	<-3	<-3	<-3	<-3	<-3	<-3
4h	-2.61	-2.75	-2.83	-2.90	<-3	<-3	<-3	<-3	<-3	<-3
5h	-2.22	-2.23	-2.18	-2.12	-2.15	-2.23	-2.41	-2.60	-2.83	<-3
5h40	-1.96	-1.98	-1.95	-1.90	-1.95	-2.05	-2.24	-2.45	-2.69	-2.90
6h15	-2.10	-2.11	-2.06	-2.00	-2.03	-2.12	-2.30	-2.49	-2.72	-2.91
8h	-2.19	-2.20	-2.15	-2.09	-2.11	-2.20	-2.38	-2.57	-2.80	-2.99
9h	-2.18	-2.19	-2.13	-2.07	-2.09	-2.18	-2.35	-2.54	-2.76	-2.94
18h30	-1.75	-1.71	-1.61	-1.50	-1.48	-1.52	-1.65	-1.79	-1.97	-2.11
24h	-1.47	-1.41	-1.29	-1.15	-1.11	-1.13	-1.24	-1.35	-1.51	-1.63
31h	-1.10	-1.02	-0.87	-0.72	-0.66	-0.66	-0.75	-0.84	-0.98	-1.08
42h30	-0.88	-0.76	-0.57	-0.38	-0.28	-0.23	-0.28	-0.34	-0.44	-0.49
48h	-0.78	-0.64	-0.44	-0.23	-0.10	-0.04	-0.07	-0.11	-0.18	-0.22

Table 3-5: Saturation indexes with respect to C-S-H from the aqueous phase composition recovered during K165-400B-5A hydration in suspension (w/c = 5)

*notion of different C-S-H can be found in Annex 2-11

	Minor hydrate phases					
Time	Monosulphate	Hydrogarnet	Gibbsite	Hemicarbonate	Tobermorite	Amorph [%]
0	0	0	0	0	0	0
1h	0	0	0	0	0	10.5
2h	0	0	0	0	0	8.0
3h	0	0	0	0	0	11.8
6h	0	0	0	0	0	17.2
1d	0	0	0	0	0	17.1
2d	1.4	0	0	1.9	0	18.8
3d	1.5	0	0	2.3	0	14.2
7d	1.4	0	0	2.8	0	10.3
14d	2.8	3.3	0	0	0	0
28d	3.7	5.5	0	0	0	0
3m	10.5	8.8	0	Presence	4.6	18.3
8m	12.3	12.2	0	Presence	7.9	19.3
1y	12.4	23.1	0	Presence	7.9	23.0

Table 3-6: Normalised Rietveld estimates of minor hydrate phases for cement k165-400B-5A hydration in paste during 1 year, in % by mass of original anhydrous cement

Chapter IV

Hydration of k165 clinker with different quantities of anhydrite

4. Hydration of BCSAF cement with different quantity of anhydrite addition

The objective of this chapter is to confirm the hypothesis of five steps of hydration and to estimate the influence of quantity of anhydrite addition. In order to better compare the results, all the experiments were done under the same condition and the used calculation methods were the same.

4.1 Choice of quantity of anhydrite

As discussed in chapter 3, anhydrite mainly participates in the first step of hydration with ye'elimite to form ettringite and AH_3, as described by equation (3.2). With given percentage (33%) of ye'elimite by mass in the clinker k165, the percentage of anhydrite needed by mass compared to clinker can be calculated as 12.8% to consume all ye'elimite during the first step:

$$\underset{610.25}{C_4A_3\$} + \underset{2*136.14}{2C\$} + 38H \rightarrow C_3A.3C\$.H_{32} + 2AH_3\ (\text{amorphous}) \quad \text{g/molar} \qquad (3.2)$$

Knowing that soluble sulphates from the clinker (e.g. alkali sulphates) can also react with ye'elimite, we choose 0, 10% and 20% anhydrite additions by mass compared to clinker.

With 0% anhydrite and 10% anhydrite, we can expect strong influence on the duration of step 1 while the following steps should come successively. Therefore, all the five steps should be confirmed. These corresponding results are presented in 4.2.1.

On the other hand, with 20% anhydrite, we expect that some anhydrite will remain after ye'elimite is totally consumed. In this case, the hydration of C_2S and ferrite are expected to occur in a quite different composition of the aqueous phase that will be strongly concentrated in sulphate ions instead of having very low concentrations of sulphate. Then we can suppose that ferrite will hydrate with the presence of anhydrite in order to form greater amounts of ettringite as written by equation (4.1):

$$\underset{486}{C_4AF} + \underset{6*136.14}{6C\$} + 2Ca^{2+} \rightarrow 2C_3(A,F).3C\$.H_{32} \quad \text{g/molar} \qquad (4.1)$$

With given 14% of ferrite (considered as C_4AF to simplify) by mass in the clinker k165, the percentage of anhydrite needed by mass compared to clinker to satisfy equations 3.2 and 4.1, can be calculated as 23.5%. Here we should mention that it still exists some other aluminate sources, such as amorphous AH_3 brought by equation (3.2) that can consume anhydrite to form ettringite if an additional calcium source is present. Therefore, 20% anhydrite is not enough to form the maximum ettringite with k165 clinker. As K165-400B-20A is expected to be quite different than the other cements, the results of this cement are presented separately in 4.2.2.

4.2 Interpretation and discussion

In order to facilitate reading, the major tables and figures of the results of k165-400B-0A, k165-400B-10A and k165-400B-20A in suspension and in paste are shown at the end of this chapter. Tables 4-1 and 4-2 report the corresponding tables and figures the results in suspension and in paste.

W/C=5	Liquid phases		Solid phases		
	Major	Minor	anhydrous	major hydrate	minor hydrate
0A	Figure 4-1	Figure 4-2	Figure 4-3	Figure 4-4	Table 4-3
5A	Figure 3-2	Figure 3-3	Figure 3-4	Figure 3-5	Table 3-3
10A	Figure 4-5	Figure 4-6	Figure 4-7	Figure 4-8	Table 4-4
20A	Figure 4-9	Figure 4-10	Figure 4-11	Figure 4-12	Table 4-5

Table 4-1: Figures and tables for the results of k165 with different anhydrite levels in suspension

W/C=0.5	Solid phases		
	Anhydrous	major hydrate	minor hydrate
0A	Figure 4-13	Figure 4-14	Table 4-6
5A	Figure 3-6	Figure 3-7	Table 3-6
10A	Figure 4-15	Figure 4-16	Table 4-7
20A	Figure 4-17	Figure 4-18	Table 4-8

Table 4-2: Figures and tables for the results of k165 with different anhydrite levels in paste

4.2.1 Confirmation of fives steps with the results of k165-400B-0A and k165-400B-10A

Step 1

Till the beginning of hydration, the amounts of ye'elimite (Figures 4-19 & 4-20) and anhydrite (Figures 4-21 & 4-22) decrease. At the same time, the quantity of ettringite (Figures 4-23 & 4-24) increases. The quantity of amorphous phases, considered as AH_3, also increases in paste (Figure 4-25) but in suspension, significant amounts of amorphous phases are only detected for k165-400B-0A (Figure 4-26). It is not easy to explain these differences mainly in paste or suspension but two remarks can be made. First, as said before, a part of the amorphous phase may be ettringite and also during the suspension experiment, a part of hydrates precipitate on the wall of the vessel and thus are not recovered for the analysis thereafter.

Before anhydrite is consumed, the rates of hydration of both belite (Figures 4-27 & 4-28) and ferrite phase (Figures 4-29 & 4-30) stay very slow.

Therefore, step 1 is confirmed. However, the duration of this step is increased as a function of anhydrite content (Table 4-9).

With 0% anhydrite in the cement, the sulphate coming from alkali sulphate and ye'elimite dissolution passes rapidly through a maximum (25mmol/L) after 5 minutes of hydration (Figure 4-1). Also, the quick dissolution of ye'elimite drives aluminium concentration to about 4mmol/L in 5 minutes (Figure 4-1).

W/C=5	Starting time	Ending time	Duration	W/C=0.5	Starting time	Ending time	Duration
0A*	-	-	-	0A	-	-	-
5A	0H	4H	4H	5A	0H	2H	2H
10A	0H	4H	4H	10A	0H	3H	3H

Table 4-9: Summary of the starting, ending time and the duration of step 1

* Particular case: no step 1 in k165-400B-0A

The equations proposed in 3.3 are still valid:

Ye'elimite reacts with anhydrite:

$$C_4A_3\$ + 2C\$ + 38H \rightarrow C_3A.3C\$.H_{32} + 2AH_3 \text{ (amorphous)} \quad (3.2)$$

Also, alkali sulphate is also a sulphate source to react with ye'elimite. Their reaction can be written as (2) considering an additional supply of calcium ions:

$$C_4A_3\$ + 2[Ca^{2+}] + 2[SO_4^{2-}] + 38H \rightarrow C_3A.3C\$.H_{32} + 2AH_3 \quad (3.3)$$

Belite or ferrite or both could be the calcium source, but the quantity is expected to be very small as these phases just hydrate very slowly at the hydration beginning.

The interactions between the constituents are the same than those reported previously in Figure 3-11.

Interaction 1: Without anhydrite, ye'elimite takes almost 9 hours and 3 days to be consumed relatively in suspension (Figure 4-3) and in paste (Figure 4-13) respectively. Compared to other two cements containing 5 and 10% anhydrite, we can observe the obvious acceleration effect of anhydrite on the hydration of ye'elimite.

Moreover, the more anhydrite is added, the more ettringite is formed (Figure 4-23, 4-24). This is consistent with the literature [71].

The main interactions between the constituents are similar to those described in the previous chapter for cement k165-400B-5A:

Interaction 2: Similar as step 1 reported for the hydration of k165-400B-5A. Ferrite hydration is retarded by the effect of sulphate ions in the solution as expected (Figure 4-31).

Interaction 3: Similar as step 1 reported for the hydration of k165-400B-5A. Ferrite could supply calcium ions to facilitate the equation (3.3). However, since the ferrite hydration is slow, this interaction is very small.

Interaction 4: Similar as step 1 reported for the hydration of k165-400B-5A. Hydration of belite is blocked by the high concentration of aluminium (Figure 4-32) and sulphate in the solution (Figure 4-31).

Therefore, we can see that all the interactions are similar to that of k165-400B-5A, except the interaction 1, which finally controls to the duration of step 1. Step 1 ends when anhydrite is totally consumed.

Step 2

After anydrite (Figure 4-21) is totally consumed, sulphate is still available in the solution (Figure 4-31). Ye'elimite continues to react and its content decreases (Figures 4-19 & 4-20) while the amount of ettringite is increasing (Figures 4-23 & 4-24).

Then, when the amount of ye'elimite is decreasing slowly to reach zero (Figures 4-19 & 4-20), calcium monocarbo-aluminate hydrate and calcium hemicarbo-aluminate hydrate (Tables 4-3 & 4-4) could be found as traces in all suspension experiments. On the other hand, calcium monosulfo-aluminate hydrate was the only AFm phase observed in paste samples (Tables 4-6 & 4-7). This tends to confirm the occurrence of additional carbonation in suspension experiments. As said before, the presence of CO_3^{2-} coming from air, calcium monocarbonate hydrate or calcium hemicarbonate hydrate can stabilize ettringte at the expense of calcium monosulfoaliminate hydrate.

At the same time, the hydration of ferrite (Figures 4-29 & 4-30) and C_2S (Figure 4-27 & 4-28) is always slow.

Therefore, step 2 is also confirmed and the main chemical equations proposed in 3.3 are still valid.

The impact of quantity of anhydrite addition seems indirect on this step. Step 2 ends successively after step 1, when ye'elimite is totally consumed, thus it appends later with greater amounts of anhydrite (Table 4-10). The duration of this step is quite different in suspension or in paste: it seems more rapid with higher anhydrite contents in suspension while its duration increases markedly in paste.

Table 4-10 summarizes the starting time, ending time and duration of this step:

W/C=5	Starting time	Ending time	Duration	W/C=0.5	Starting time	Ending time	Duration
0A	0H	18.5H	18.5H	0A	0H	1D	1D
5A	4H	6.25H	2.25H	5A	1H	3D	3D
10A	4H	6H	2H	10A	3H	7D	7D

Table 4-10: Starting and ending times and of the duration of step 2

The main interactions between the constituents are similar to those described in the previous chapter for cement k165-400B-5A (Figure 3-12).

The explanation is similar as in 3.3: when anhydrite is consumed, the sulphate (Figure 4-31) and aluminium concentrations (Figure 4-32) stay high. Therefore, the hydration of ferrite is slow and the hydration of belite almost inhibited.

Step 3

After the total consumption of ye'elimite (Figures 4-19 & 4-20) the amount of belite starts to decrease (Figures 4-27 & 4-28). This is confirmed by the increase of boron concentration in the aqueous phase during the suspension experiments (Figure 4-33). At the same time, strätlingite starts to precipitate (Figures 4-34 & 4-35).

The amount of ferrite is also slight decreasing (Figures 4-29 & 4-30). The amorphous phases, considered as to be mostly AH_3, is thus decreasing for the experiment where amorphous phases are determined by XRD: in all paste experiments (Figure 4-25), and only during of k165-400B-0A hydration in suspension (Figure 4-26). Therefore, step 3 is also confirmed for all cements.

This step that follows steps 1 and 2 starts of course at longer ages with higher anhydrite contents but its duration varies quite differently in paste experiments compared to suspension ones (Table 4-11). Especially the duration of step 3 is very long in paste with 10% of anhydrite.

Table 4-11 summarizes the starting time, ending time and duration of this step:

W/C=5	Starting time	Ending time	Duration	W/C=0.5	Starting time	Ending time	Duration
0A	18.5H	44H	29.5H	0A	1D	2D	1D
5A	6.25H	48H	37.75H	5A	3D	7D	4D
10A	6H	38H	32H	10A	7D	28D	21D

Table 4-11: Starting and ending times and of the duration of step 3

During this step, C_2S starts to react with AH_3 to form strätlingite as in equation (3.5).

$$C_2S + AH_3 + 5H \rightarrow C_2ASH_8 \qquad (3.5)$$

Ferrite also reacts with C_2S to form an iron substituted strätlingite (3.6):

$$C_2S + C_2(A,F) + 10H \rightarrow C_2(A,F)SH_8 + [Ca^{2+}] \text{ and } [OH^-] \text{ in solution} \qquad (3.6)$$

The main interactions between the constituents are similar to those described in the previous chapter for cement k165-400B-5A in Figure 3-14.

Interaction 7: The hydration of C_2S to form strätlingite consumes the amount of AH_3. On the other hand, the aluminate concentration mostly determined by AH_3 still disables the nucleation of C-S-H.

Interaction 8: The strong dissolution of AH_3 competes with ferrite dissolution and delays it.

Interaction 5: Ferrite will enhance the formation of strätlingite by reacting with belite. Reaction (3.6) leads to a further destabilisation of AH_3.

Step 4

After the step 3, the calcium concentration increases as observed for the suspension experiment (Figure 4-36). The electrical conductivity also increases (Figure 4-37), which suggests more $[OH^-]$ passing in the solution. At the same time, the quantities of strätlingite (Figures 4-34 & 4-35), belite (Figures 4-27 & 4-28) and ferrite (Figures 4-29 & 4-30) decrease. Meanwhile, hydrogarnet (Figures 4-38 & 4-39) and some calcium monosulfoaluminate hydrate (Figures 4-40 & 4-41) are found. Only traces of carbonated AFm phases were observed in the suspensions (Table 4-3 & Table 4-4).

This step is the longest compared to the three previous ones: between 1 and 2 months depending on the amount of anhydrite (Table 4-12). Similarly to step 3, 10% of anhydrite induces a much longer duration than 0 or 5% addition.

Table 4-12 summarizes the starting time, ending time and the duration of 3rd step.

W/C=5	Starting time	Ending time	Duration	W/C=0.5	Starting time	Ending time	Duration
0A	44H	unknown*	-	0A	2D	28D	26D
5A	48H	unknown*	-	5A	7D	28D	21D
10A	38H	unknown*	-	10A	28D	3M	2M

Table 4-12: Starting and ending times and of the duration of step 4

***Note: suspension experiments with k165-400B-0A, k165-400B-5A and k165-400B-10A end at 48h so this step is not ended.

Therefore, the step 4 is also confirmed and the previous hypotheses relative to the interactions between the constituents (Figure 3-16) are still valid.

Interaction 10: the aluminate concentration mostly determined by C_2ASH_8 solubility, still does not allow the nucleation of C-S-H but C_2S hydrates and reacts with C_2ASH_8 to precipitate hydrogarnet instead of C_2ASH_8. However this requires additional calcium ions that may be provided by the ferrite phase.

Interaction 5, 9: Dissolution of ferrite is strongly linked with C_2S hydration as both are associated to form hydrogarnet and calcium monosulfoaluminate hydrate.

Step 5

After step 4, the quantity of strätlingite decreases (Figure 4-35), the amount of amorphous phase, in this case, C-S-H (Figure 4-25), increases, and calcium monosulfoaluminate hydrate also continues to increase in quantity (Figure 4-39). Therefore, the step 5 is also confirmed.

Equations and the interactions (Figure 3-17) proposed in 3.3 are still valid:

Interaction 5: Identically to step 4, C_2S and ferrite hydration are linked to be able to produce hydrates having more $[Ca^{2+}]$ than the dissolving solids.

This step ends when C_4AF or C_2S is totally consumed. Thus the end of this period is never reached in our experiments and it is thus not possible to determine if its duration is longer with higher amounts of anhydrite.

W/C=0.5	Starting time	Ending time	Duration
0A	1M	unknown	-
5A	1M	unknown	-
10A	3M	unknown	-

Table 4-13: Starting and ending times and of the duration of step 5 for paste experiments

*Note: paste experiments with k165-400B-0A, k165-400B-10A ended at 8 months.

4.2.2 Particular case: cement k165-400B-20A

Step 1 bis

From the results both from paste and suspension experiments of k165-400B-20A, we can observe a decrease of ye'elimite and anhydrite (Figures 4-11 & 4-17) in parallel with an increase of ettringite and certainly an amorphous phase being AH_3 (Figures 4-12 & 4-18). In this case, the amorphous phase is detected also in suspension but its quantity remains low even in paste. This reaction will continue until anhydrite is totally consumed at 1 day in paste and at around 11 hours in suspension but contrarily to the other cement containing less anhydrite, ye'elimite is totally consumed before anhydrite so step 2 does no longer exists.

Moreover, the quantity of C_2S is already decreasing after four hours in suspension (Figure 4-11) and after 1 day in paste (Figure 4-17). In suspension, boron starts to be accumulated into the solution after 8 hours, which confirms C_2S dissolution (Figure 4-10). Therefore, it seems that C_2S reacts before step 1 is ended contrarily to the other cements that contain less anhydrite.

However it is not easy to define the silicate containing hydrate that is formed. Indeed, no additional crystalline phase except ettringite is detected by XRD at that time. In Figure 4-9, we can observe that about 10mmol/L of sulphate is available in the aqueous phase of the suspension after 48 hours. This can probably explain the absence of strätlingite, and AFm phases. On the other hand, the aluminate concentration is rapidly very low and thus C-S-H nucleation may not be inhibited contrarily to the other cements having less anhydrite. Nevertheless the calculation of saturation index using CHESS shows that C-S-H is undersaturated until 64 hours (Table 4-15, see in the end of the chapter). This cannot completely rules out the precipitation of C-S-H as it is difficult to model thermodynamically C-S-H and saturation indexes are close to equilibrium.

Another possibility would be to form a silicate containing ettringite [72]. So the dissolved silicon ions might go initially into ettringite before 64 hours and could precipitate as C-S-H later.

Therefore, the reaction of hydration and the relative interaction should be modified compared to that for k165-400B-5A:

W/C=5	W/C=0.5	Present phases
0-11H	0-1D	ye'elimite, anhydrite, ettringite, AH_3, belite, ferrite

Equations can be proposed as:

Ye'elimite reacts with anhydrite:

$$C_4A_3\$ + 2C\$ + 38H \rightarrow C_3A.3C\$.H_{32} + 2AH_3 \text{ (amorphous)} \quad (3.2)$$

Also, the reaction of alkali sulphate with ye'elimite can be written as (3.3):

$$C_4A_3\$ + 2[Ca^{2+}] + 2[SO_4^{2-}] + 38H \rightarrow C_3A.3C\$.H_{32} + 2AH_3 \quad (3.3)$$

As belite reacts more intensely here, it could be an additional calcium source.

$$C_2S \rightarrow 2[Ca^{2+}] + [H_2SiO4]^{2-} \quad (4.2)$$

Silicate could either enter the structure of ettringite or form some C-S-H.

Thus the interaction in step 1 bis could be represented on Figure 4-41:

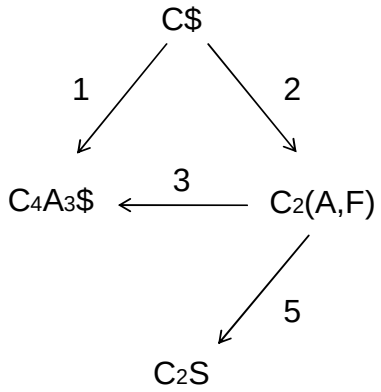

Figure 4-41: Interaction between the phases in step1 bis observed during the hydration of k165-400B-20A

Interaction 1: hydration of ye'elimite is accelerated by anhydrite as for k165-400b-5A et k165-400b-10A.

Interaction 2: similar to k165-400B-5A. Ferrite hydration is blocked by the sulphate liberated by anhydrite.

Interaction 3: similar to k165-400B-5A. Ferrite could supply calcium ions to facilitate the hydration of ye'elimite to form ettringite. However, since the ferrite hydration is slow, this interaction is very small.

Interaction 4: compared to k165-400B-5A, the interaction 4 between ye'elimite and belite is modified. Ye'elimite does dissolve in the system. However, the aluminium from ye'elimite is consumed quickly with high amount of calcium and sulphate liberated by anhydrite to form ettringite. This leads to a low aluminium concentration (Figure 4-9), which do not inhibit C-S-H nucleation any longer and thus C_2S hydrates already in this first step. However the amount of hydrated belite remains low and it is thus difficult to determine which hydrate is formed: it could be either C-S-H or a Si substituted ettringite.

Interaction 5: Ferrite could supply calcium ions to participate to the hydration of belite. However, since the ferrite hydration is slow, this interaction is very small.

This step will end when ye'elimite is total consumed. Also, if we compare the duration of the reaction (3.2) in this case with that of k165-400B-5A and k165-400B-10A (Table 4-14), we can confirm that the duration of this step increases with a greater anhydrite quantity.

W/C=5	Duration	W/C=0.5	Duration
5A	4H	5A	1H
10A	4H	10A	3H
20A	11H	20A	1D

Table 4-14: Duration of step 1 and 1bis (only case 20A)

Step 2 bis

After the consumption of ye'elimite, in suspension, anhydrite (Figure 4-11) decreases slowly. The rate of belite hydration is still slow, but it hydrates as this can be confirmed by the increasing boron concentration in the solution (Figure 4-10). At the same time, the amount of ettringite increases also slowly. In consideration of slow ferrite hydration, the aluminium source for ettringite could also be AH_3. Meanwhile, the saturation index of C-S-H, tends to indicate the aqueous phase is still undersaturated with respect to C-S-H (Table 4-15, see in the end of chapter).

In paste, anhydrite is totally consumed at 2 days. At the same time, the amount of belite obviously decreases, relatively from 45% to 35%, while the decrease of ferrite is much more modest from 12% to 10%, relative to the original mass of anhydrous cement (Figure 4-17). Meanwhile, the amount of ettringite increases more importantly from 52% to 70% (Figure 4-18). Additionally the increase of the ettringite content observed by XRD may also arise from an improved crystallization of ettringite over the time.

Therefore, the reaction of hydration and the relative interaction should be modified compared to that defined cements with lower anhydrite amounts:

W/C=5	W/C=0.5	Present phases
11-32H	1D-2D	anhydrite, ettringite, AH_3, belite, ferrite

The equation during this step can be proposed as:

$$C_2S \rightarrow 2[Ca^{2+}] + [H_2SiO_4]^{2--} \quad (4.2)$$

$$3C\$ + 3(Ca^{2+}) + AH_3 + 32H \rightarrow C_3A.3C\$.H_{32} \quad (4.3)$$

$$C_2(A,F) + 4(Ca^{2+}) + 3(SO_4)^{2-} + 32H \rightarrow C_3(AF).3C\$.H_{32} \quad (4.4)$$

where silicate ions could be used to precipitate either a Si containing ettringite or C-S-H.

The major interactions of this step can be schematized on Figure 4-42:

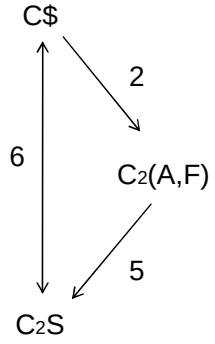

Figure 4-42: Interaction involved in step2 bis observed during the hdyration of k165-400B-20A

Interaction 2: with anhydrite available, sulphate in the solution stays still high (Figure 4-9), which drives the hydration of ferrite very slow. Therefore, the contribution of ettringite from ferrite (equation 4.4) shouldn't be significant.

Interaction 5: the calcium ions liberated from ferrite may accelerate the hydration of C_2S form C-S-H, however, the effect is small since the hydration of ferrite is slow.

Interaction 6: anhydrite dissolution keeps the concentration of sulphate high (Figure 4-9), which still inhibits the hydration of C_2S to form strätlingite or other "CASH" hydrates but C_2S reacts perhaps to precipitate C-S-H or a Si containing ettringite.

This step ends when anhydrite is totally consumed.

Step 3 bis

In suspension, after total consumption of anhydrite, the rate of belite consumption is still slow (Figure 4-11) but its hydration can be confirmed by the obvious increase of silicon concentration (Figure 4-10). However, CHESS calculation shows that C-S-H (Table 4-16) is still not saturated, which is mainly due to the low calcium concentration (Figure 4-9).

During this time, ettringite, the only identified hydrate phases, increases very slowly (Figure 4-12). This is probably due to the borate-ettringite formation, which can be seen by the decrease of boron concentration (Figure 4-10) and to slow ferrite hydration as equation (4.4), which can be proved by the decrease of sulphate concentration to 9 mM at 64 hours.

In paste, belite hydrates more quickly (Figure 4-17) and the small amount of amorphous phases identified after 3 months (Table 4-8) makes us consider that C-S-H is forming. At the same time, ferrite hydration is much more modest, while the amount of ettringite still shows a little increase. Thus in this case ferrite phase hydration is less linked with belite hydration than with the cements having less anhydrite.

The main interaction of step 3 bis can be presented on Figure 4-43:

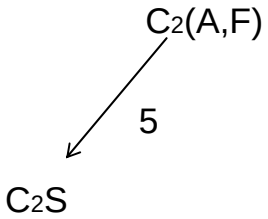

Figure 4-43: Main interaction involved in step 3 bis during k165-400B-20A hydration

Interaction 5: when anhydrite is totally consumed, the sulphate concentration is still high. Therefore, the hydration of ferrite is still very slow. Meanwhile, the formation of strätlingite by belite is still inhibited. Therefore in this condition, the hydration of belite leads to the formation of C-S-H. The calcium iron liberated from ferrite can accelerate this reaction; even its effect is very small due to the slow hydration of ferrite.

The following equations are proposed:

Hydration of belite:

$$C_2S + xH \rightarrow C\text{-}S\text{-}Hx + [Ca]^{2+} \quad (4.5)$$

When sulphate in the solution is almost consumed:

$$C_2S + C_2(A,F) + 5H \rightarrow C_2(A,F)SH_4 + [Ca^{2+}] \text{ and } [OH^-] \text{ in solution} \quad (3.6)$$

However, strätlingite is identified neither in suspension nor in paste samples. Therefore, step 3 bis observed during the hydration of k165-400B-20A must be not finished in our experiments even after 8 months of hydration in paste:

W/C=5	W/C=0.5	Present phases
32-64H*	2D-8M**	C-S-H, ettringite, belite, ferrite

*suspension experiments ended at 64 hours, and solid sample at 64 hours was lost
**paste experiments ended at 8 months, and solid sample at 28 days was lost

Expected Step 4 bis:

When sulphate concentration becomes low enough, ferrite hydration should start again to hydrate more rapidly. As the aqueous phase contains a moderate concentration of calcium ions and the pH is also moderate, but also AH_3 has been consumed, strätlingite is not expected to form. Instead hydrogarnet may be formed along with C-S-H by implying again a synergy between, belite and ferrite as discussed in step 4 of k165-400B-5A:

$$C_2S + C_2(A,F) + 5H \rightarrow C_3(A,F)SH_4 + [Ca^{2+}] \text{ and } [OH^-] \text{ in solution} \qquad (3.8)$$

However, this phenomenon is not observed neither in suspension and neither in paste. It is probably that the experiences were stopped too early.

4.3 Intermediate conclusions and points that will be assessed in the next chapter

The hydration of clinker k165 with different quantities of anhydrite was studied. It was found that according to the quantity of anhydrite, two hydration mechanisms will happen.

According to equation (3.2), if the quantity of anhydrite is less than that required to consume all ye'elimite to form ettringite, the same hydration steps as k165-400B-5A will happen successively (Figure 4-44). The quantity of sulphate will influence on:

1- step 1: a longer step 1 due to greater anhydrite contents will delay the other steps.
2- steps 3 and 4 that are expected to be longer with greater anhydrite amounts.

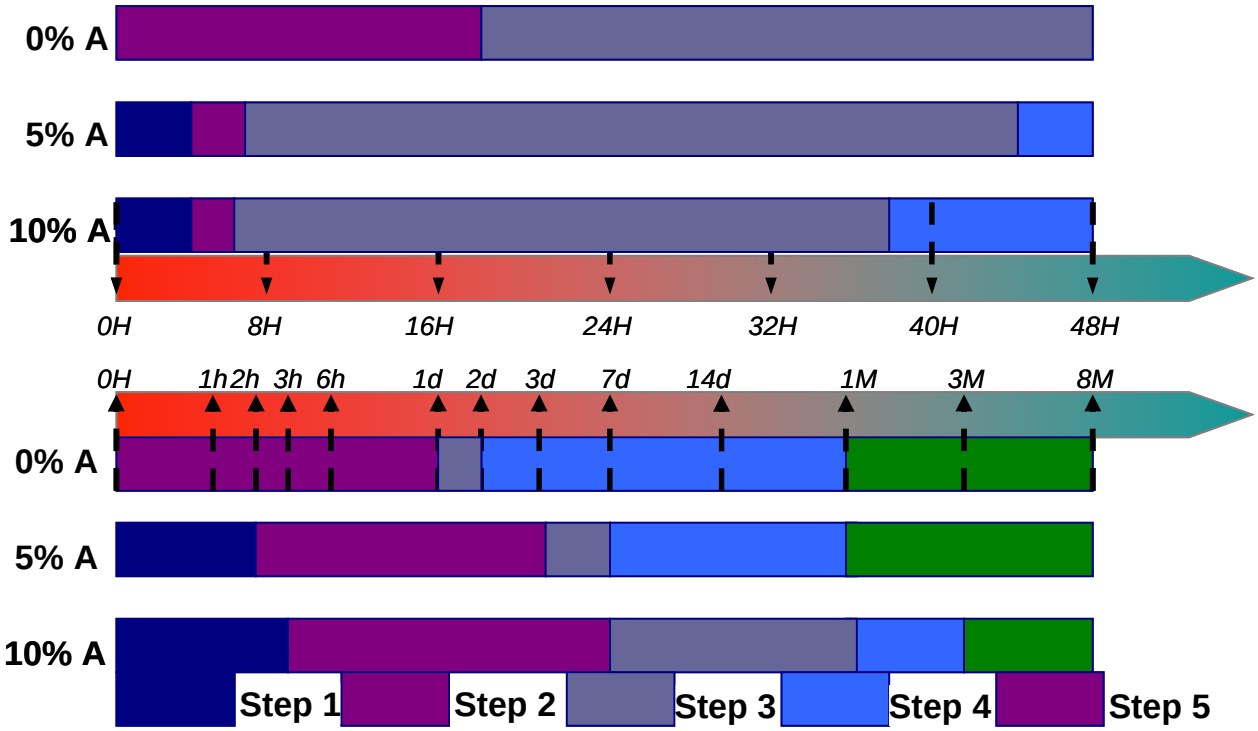

Figure 4-44: Influence of quantity of added anhydrite on the hydration of clinker k165 in suspension (up) and in paste (bottom)

If the quantity of anhydrite is more than that required to form ettringite from $C_4A_3\$$, the hydration mechanism will change markedly (Figure 4-45 for suspension and Figure 4-46 for paste).

In this case, belite hydration is no longer delayed but starts till the beginning in order to form either C-S-H or a Si substituted ettringite. Nevertheless, when belite is reacting in this more common pathway, its hydration is slower than when it reacts by precipitating first C_2ASH_8 and then especially hydrogarnet due to the synergy with the ferrite phase to form this latter hydrate.

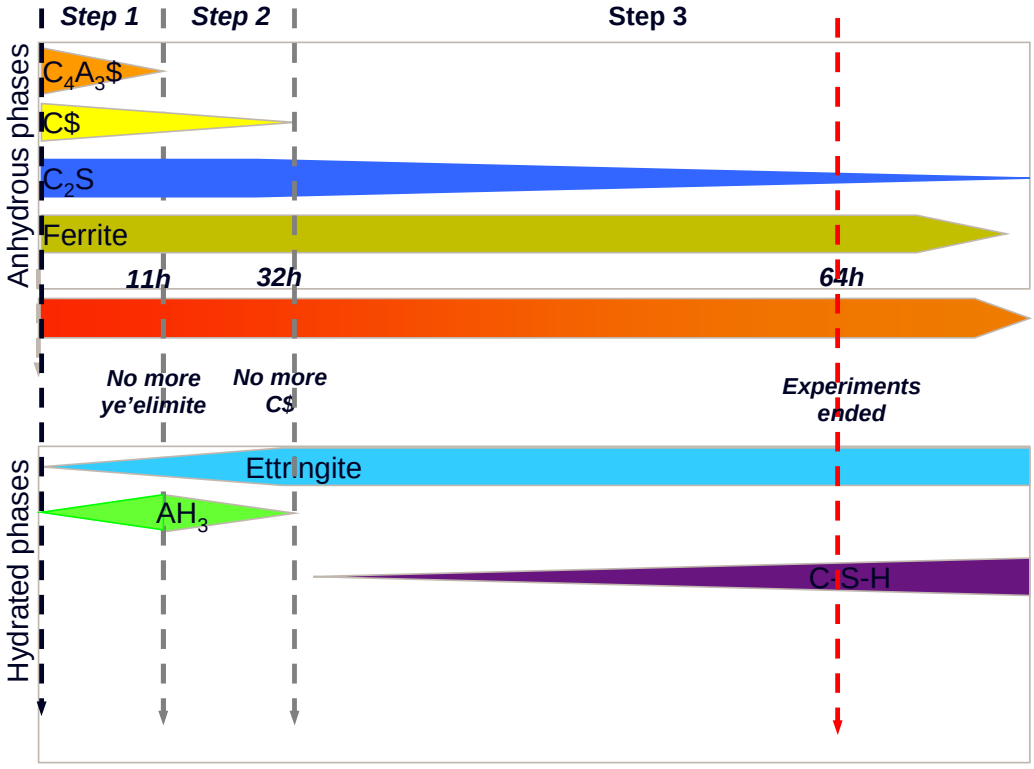

Figure 4-45: Steps observed during the hydration of k165-400B-20A in suspension during two days

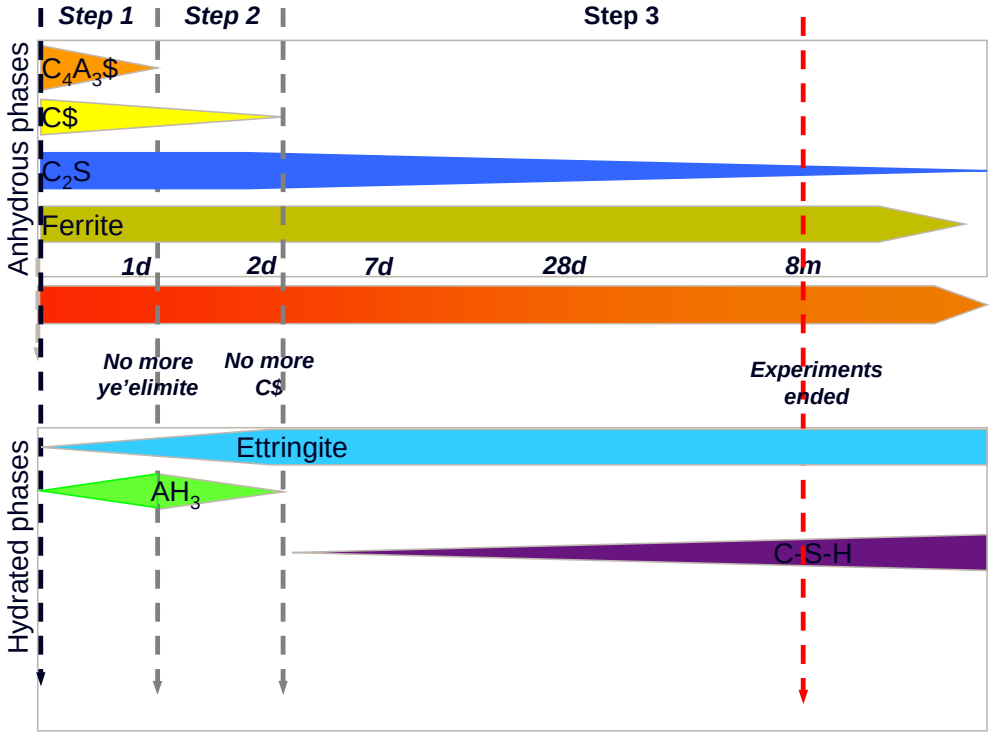

Figure 4-46: Steps observed during the hydration of k165-400B-20A in paste during the first eight months

With the given results, we can answer more precisely the five key questions raised in the introduction of the thesis:

Question 1: confirm the that major initial reaction is: $C_4A_3\$ + 2C\$ + 38H \Rightarrow C_6A\$_3H_{32} + 2AH_3$

- ➔ It is confirmed both for the hydration in suspension and paste of cements made with clinker k165 and different anhydrite additions. This step also occurs, even with 0% anhydrite, as k165 contains some alkali sulphate.

Question 2: assess how the form and quantity of the initial soluble sulfates influence the later hydration

- ➔ For anhydrite amounts less than the stoechiometry to form ettringite from $C_4A_3\$$, different quantities of anhydrite do not change the mechanism of hydration : it only makes steps 1 longer and thus it delays the other steps and especially step 3 corresponding to the beginning of belite hydration (step 3). Higher amounts of anhydrite also seem to slow down the rate of hydration in steps 3 and 4 and perhaps step 5.
- ➔ For anhydrite amounts higher than the stoechiometry to form ettringite from $C_4A_3\$$, the mechanism of hydration is changed: belite reacts till the beginning to form either a Si containing ettringite and / or C-S-H. Belite reacts till the beginning even if slowly.

Question 3: determine the parameters that control ferrite phase hydration,

- ➔ Anhydrite control ferrite hydration by blocking it at very beginning. Ferrite hydration will only start when sulphate concentration becomes very low then ferrite is strongly coupled with belite hydration especially for the cements containing less anhydrite than the quantity required to form ettringite with all $C_4A_3\$$

Question 4: determine the factors that control belite hydration and induce a retardation of its start

- ➔ The factors are different depending on the amount of anhydrite :
  - o For anhydrite amounts less than the stoechiometry to form ettringite from $C_4A_3\$$, It is C_2ASH_8 nucleation rate that governs the beginning of the hydration of belite. The main parameter that governs the nucleation rate of C_2ASH_8 is $[SO_4]^{2-}$ that has to be low. C-S-H does not form as the initial hydrate for belite hydration because it is not saturated in the beginning due to low calcium and silicon concentration and its formation is further delayed later by the inhibition effect of high aluminate concentration on C-S-H nucleation. As a consequence, this is indirectly the sulphate concentration that controls the beginning of belite hydration and thus the reactions leading to its reduction, mainly the hydration of $C_4A_3\$$. Globally it is once $C_4A_3\$$ has been completely reacted that C_2ASH_8 may nucleate.
  - o For anhydrite amounts higher than the stoechiometry to form ettringite from $C_4A_3\$$, it is more likely to be the nucleation rate of C-S-H, but may be also the precipitation rate of a Si containing ettringite that would govern the reaction rate of belite.

Question 5: check if limestone has an accelerator effect on belite hydration such in OPC

- ➔ Unknown yet: it will be answered in next chapter.

.

Figures and tables of experimental results of k165-400B-0A, k165-400B-10A and k165-400B-20A in paste and in suspension

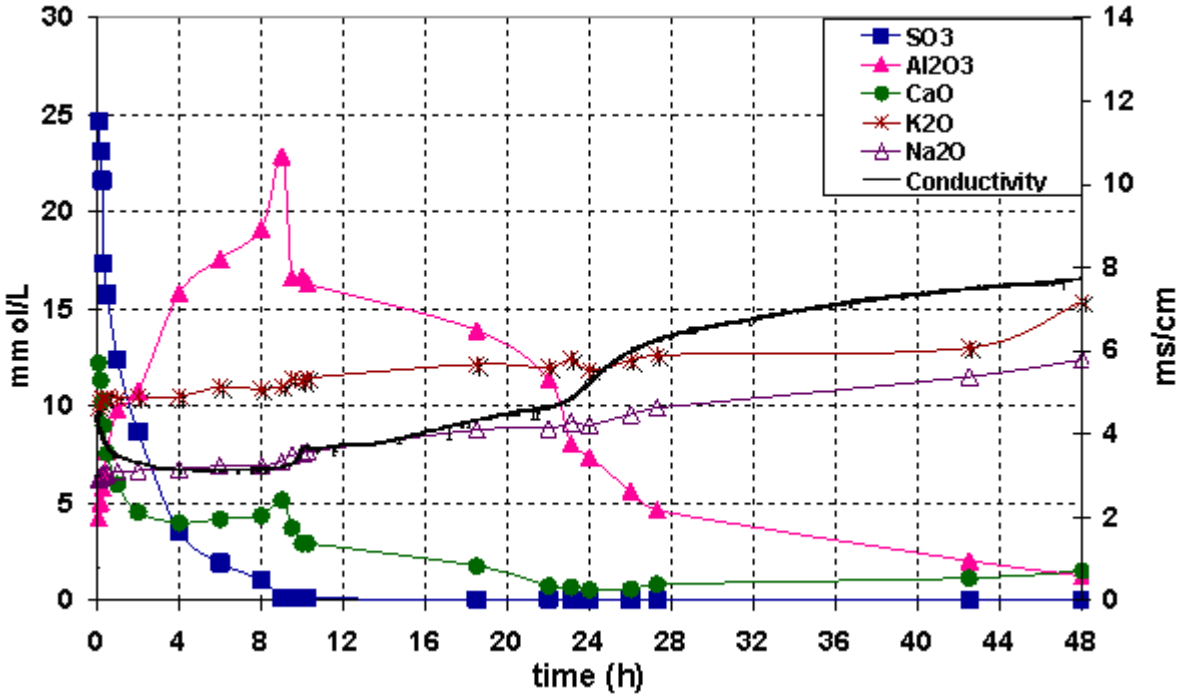

Figure 4-1: Electrical conductivity and major chemical elements of the liquid phase recovered during cement k165-400B-0A hydration in suspension (w/c = 5) during two days

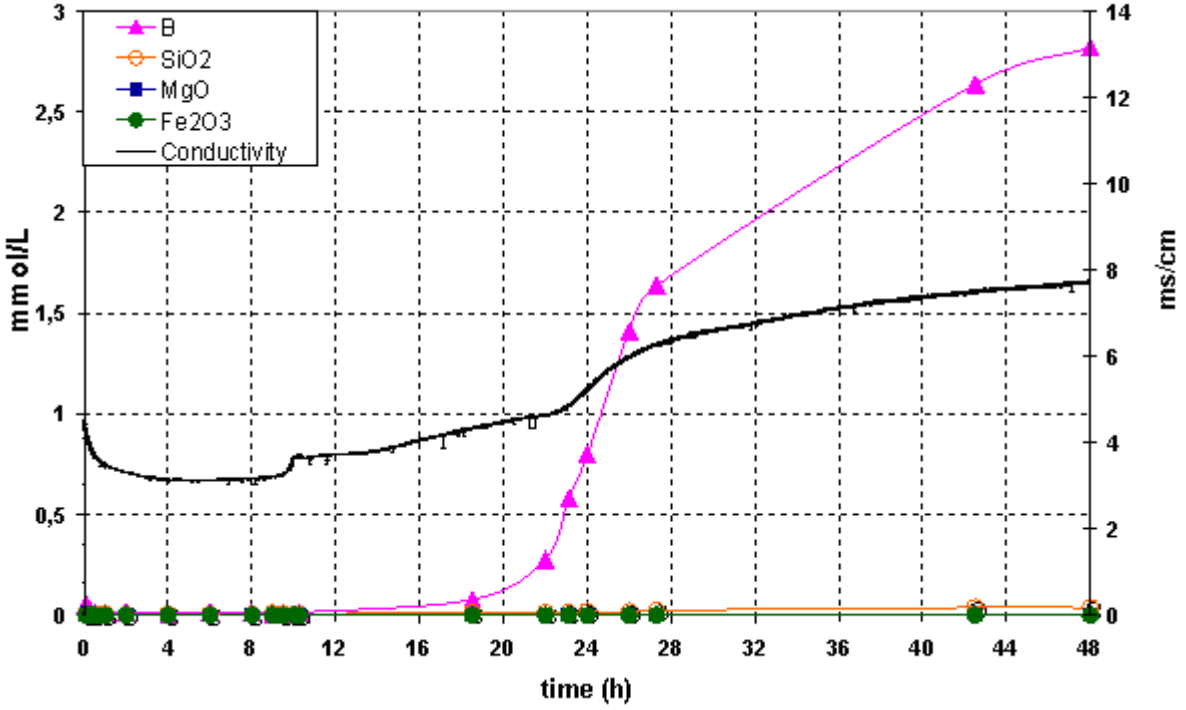

Figure 4-2: Electrical conductivity and minor chemical elements of the liquid phase recovered during cement k165-400B-0A hydration in suspension (w/c = 5) during two days

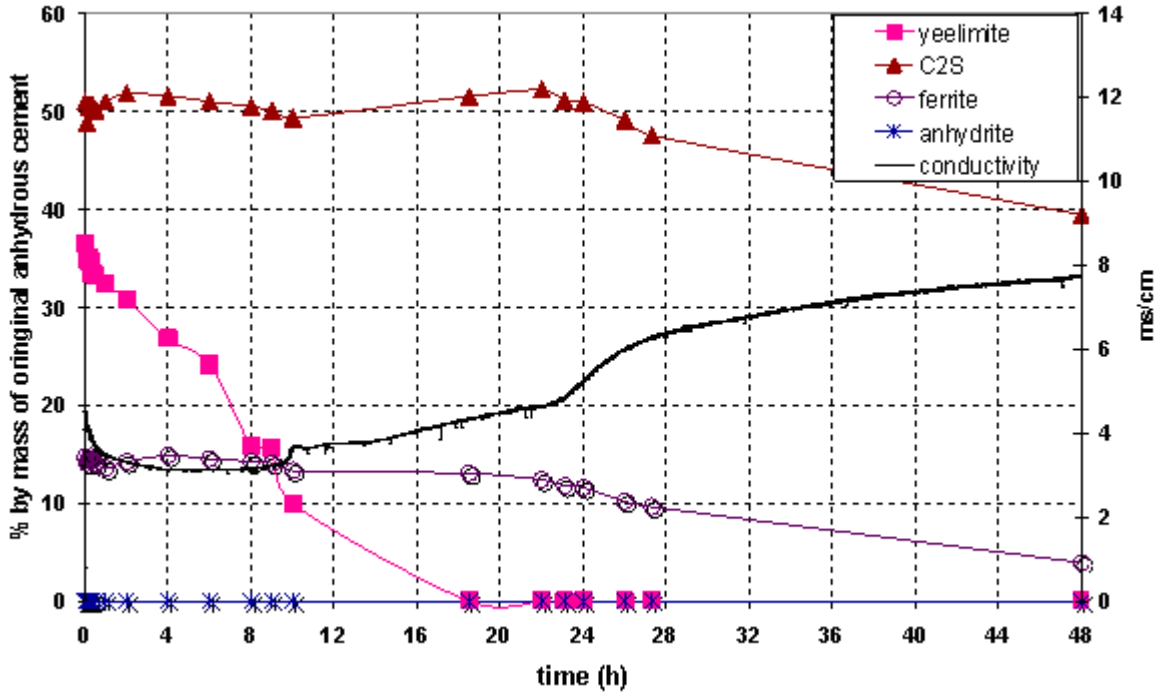

Figure 4-3: Electrical conductivity and normalised Rietveld estimates of anhydrous phases of cement k165-400B-0A hydrated in suspension (w/c=5) during two days, in % by mass of original anhydrous cement

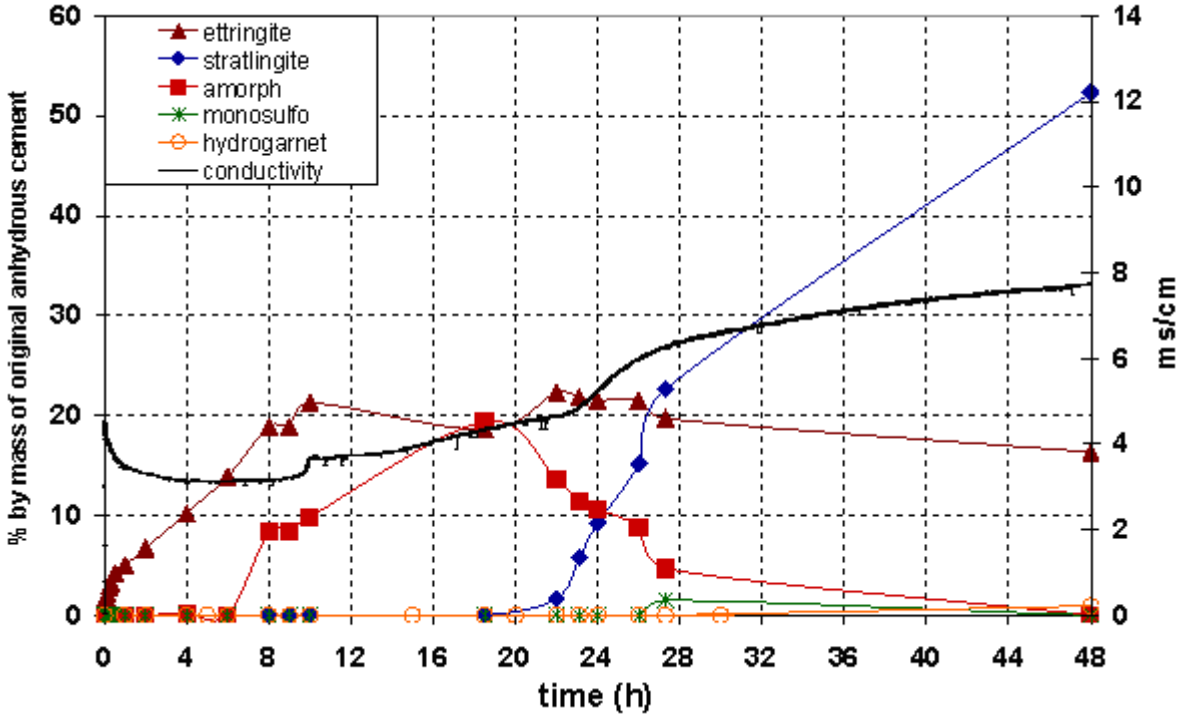

Figure 4-4: Electrical conductivity and normalised Rietveld estimates of major hydrate phases of cement k165-400B-0A hydrated in suspension (w/c=5) during two days, in % by mass of original anhydrous cement

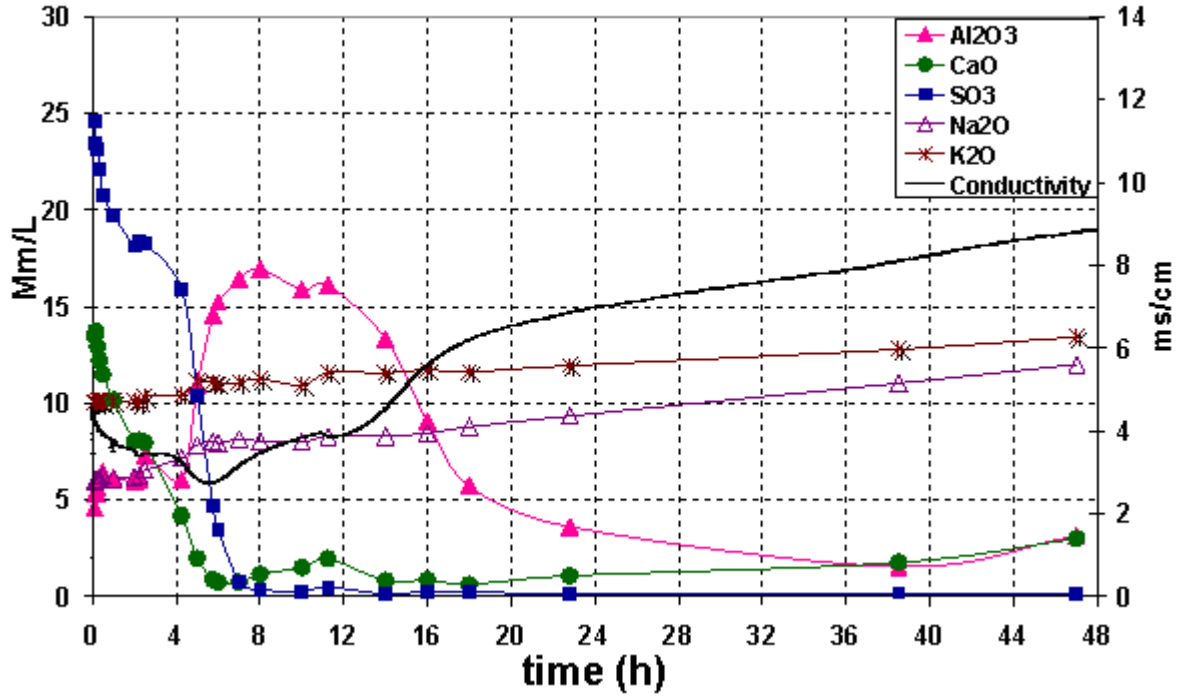

Figure 4-5: Electrical conductivity and major chemical elements of the liquid phase recovered during cement k165-400B-10A hydration in suspension (w/c = 5) during two days

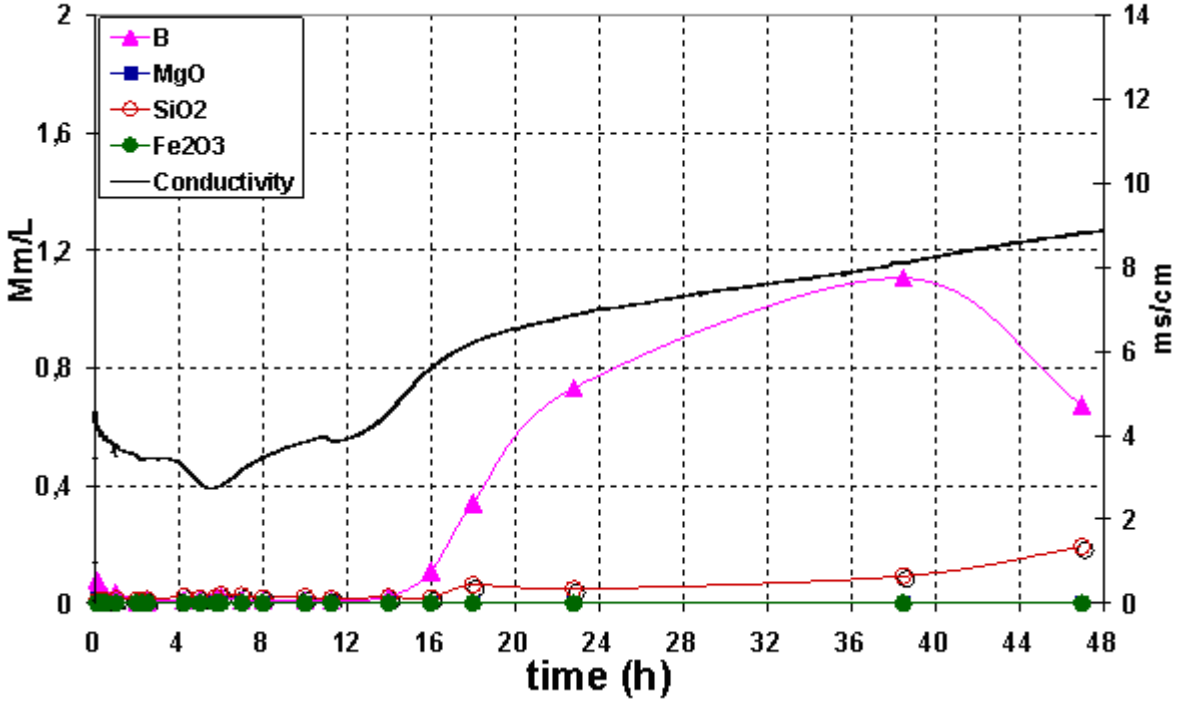

Figure 4-6: Electrical conductivity and minor chemical elements of the liquid phase recovered during cement k165-400B-10A hydration in suspension (w/c = 5) during two days

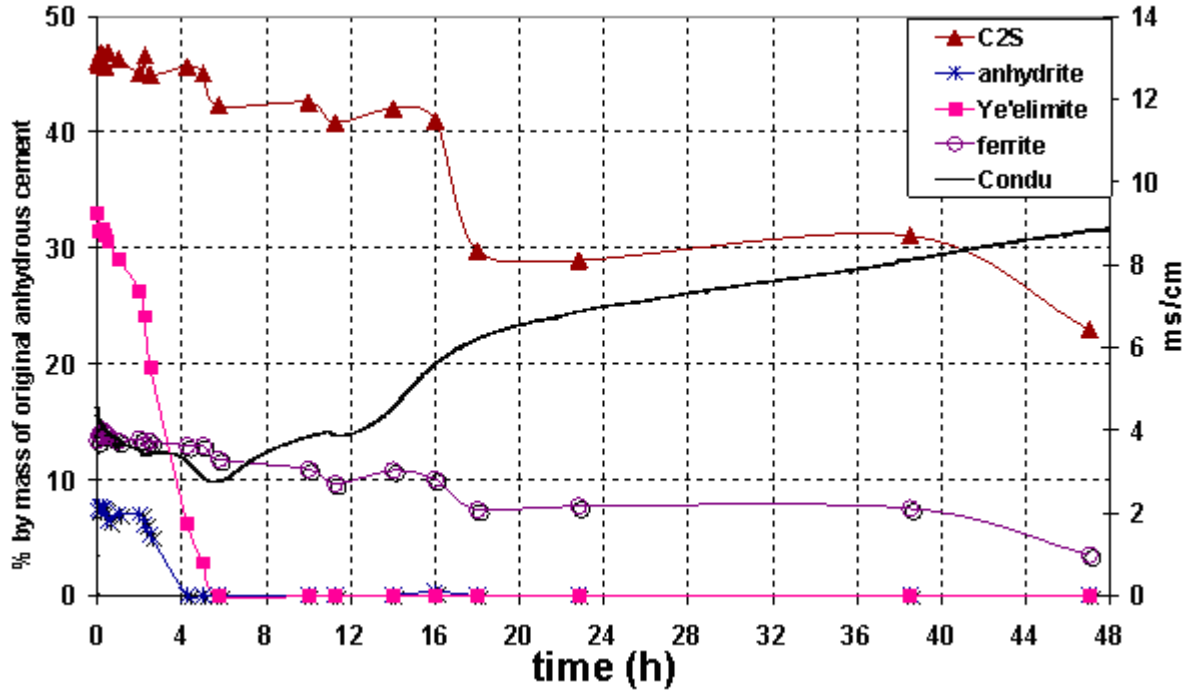

Figure 4-7: Electrical conductivity and normalised Rietveld estimates of anhydrous phases of cement k165-400B-10A hydrated in suspension (w/c=5) during two days, in % by mass of original anhydrous cement

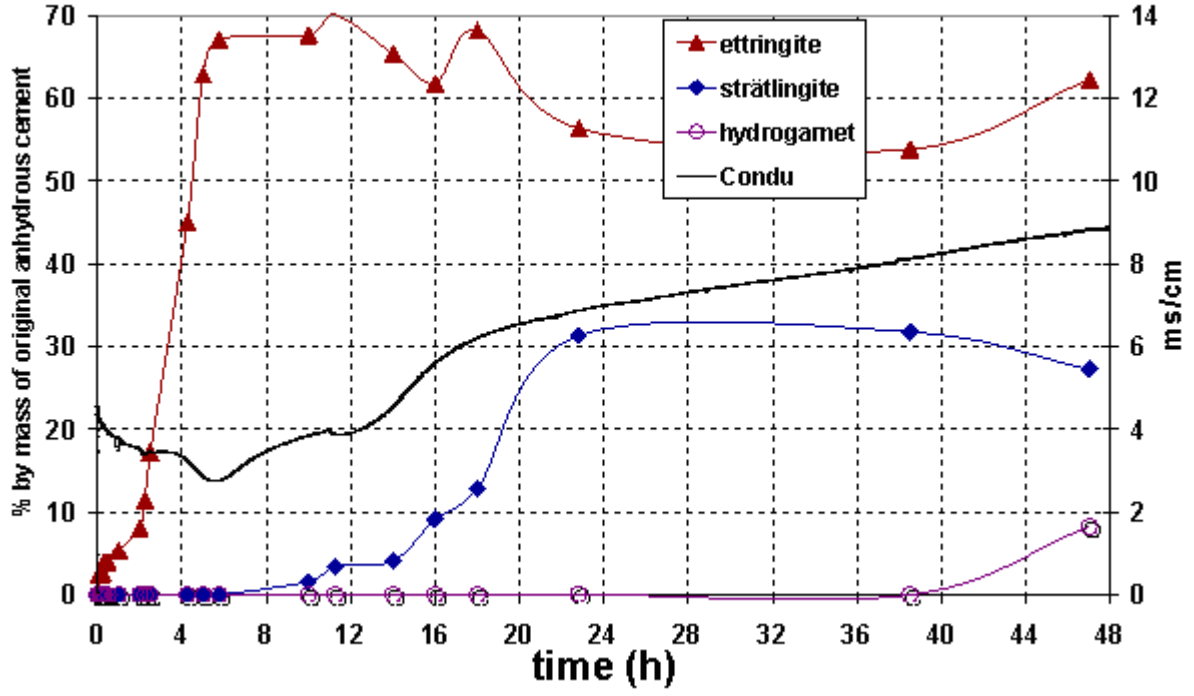

Figure 4-8: Electrical conductivity and normalised Rietveld estimates of major hydrate phases of cement k165-400B-10A hydrated in suspension (w/c=5) during two days, in % by mass of original anhydrous cement

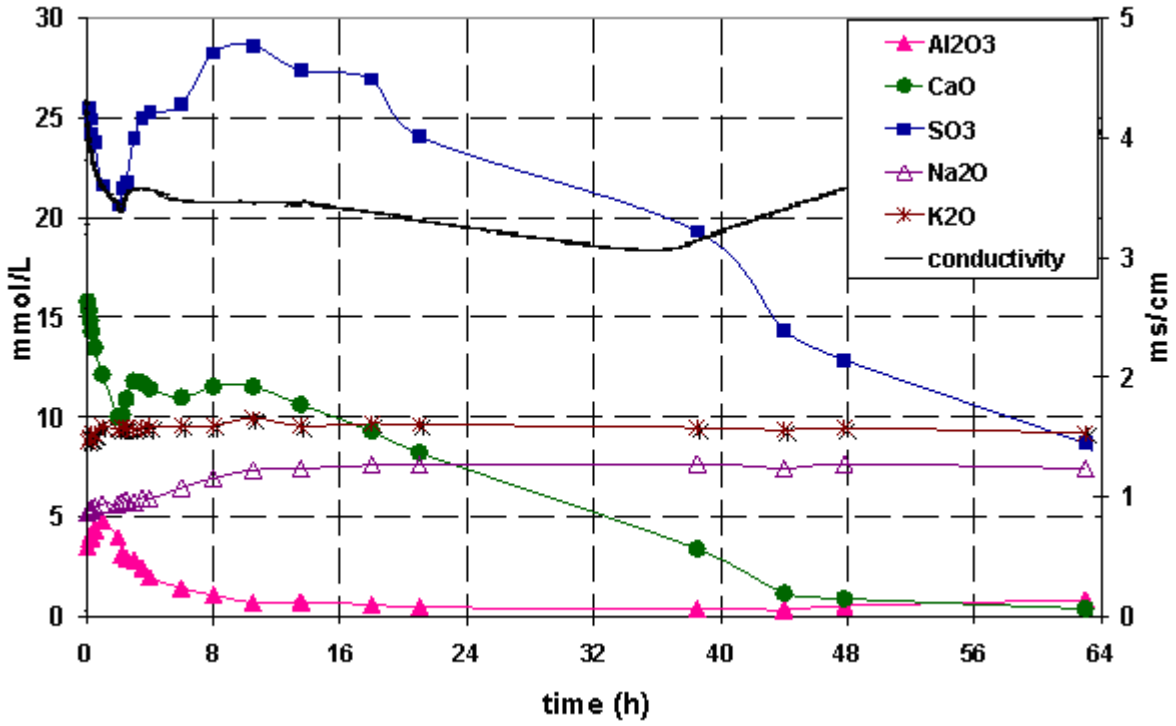

Figure 4-9: Electrical conductivity and major chemical elements of the liquid phase recovered during cement k165-400B-20A hydration in suspension (w/c = 5) during three days

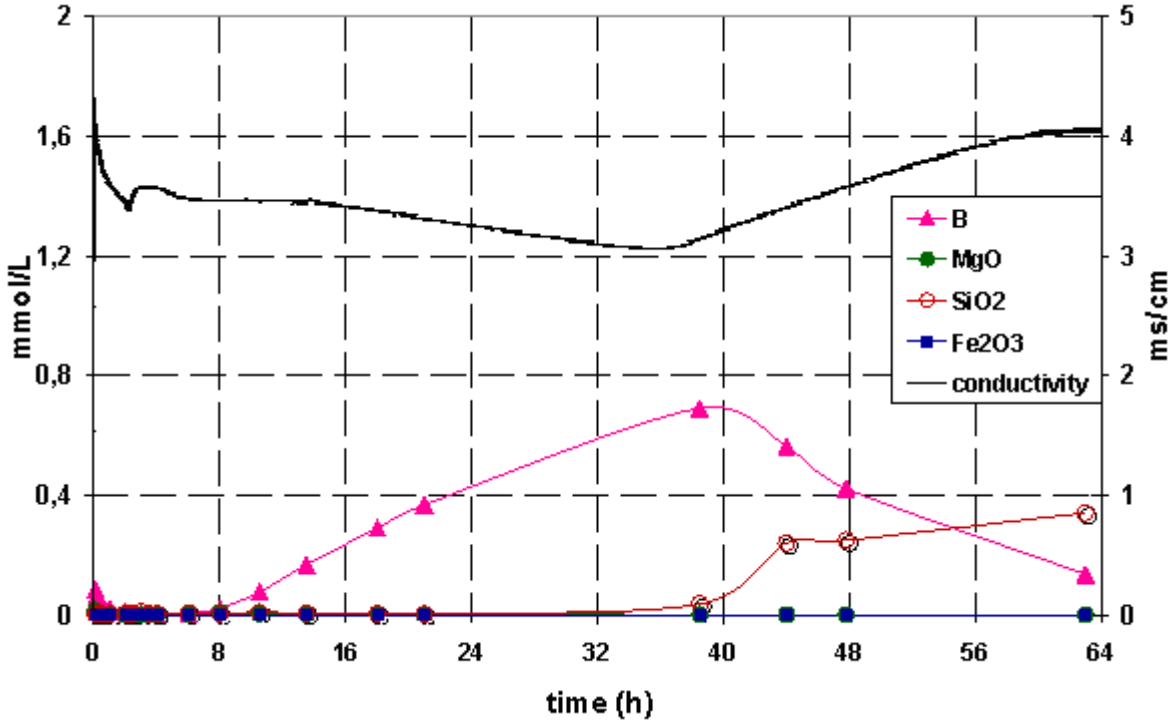

Figure 4-10: Electrical conductivity and minor chemical elements of the liquid phase recovered during cement k165-400B-20A hydration in suspension (w/c = 5) during three days

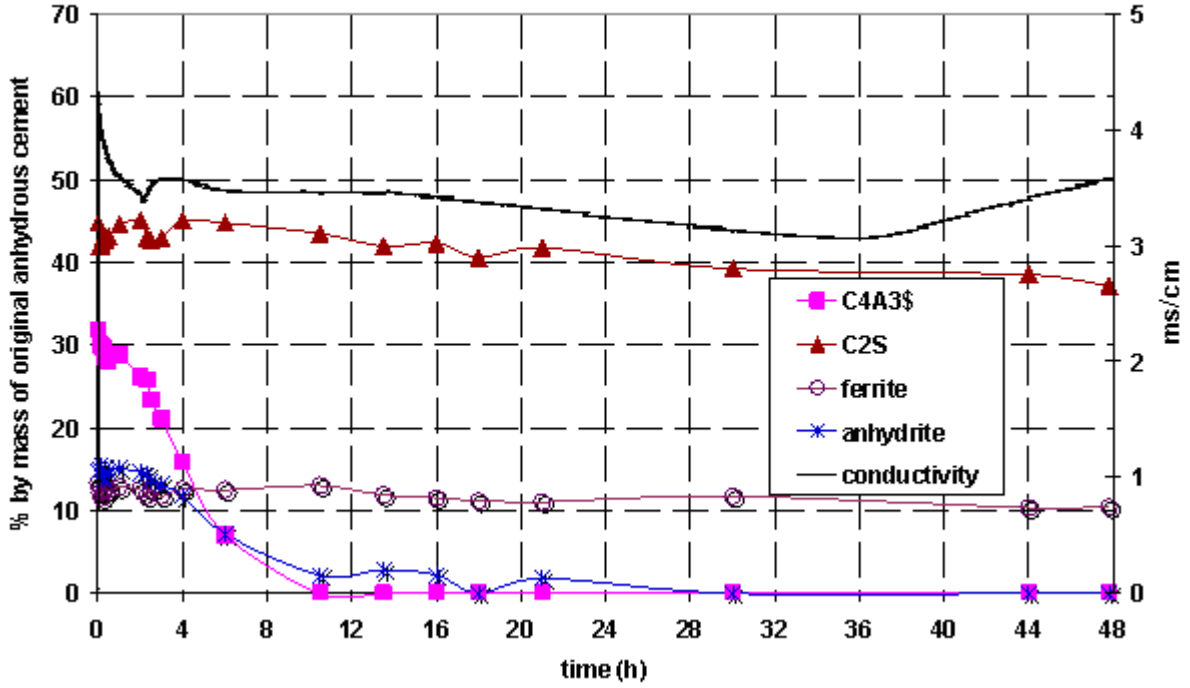

Figure 4-11: Electrical conductivity and normalised Rietveld estimates of anhydrous phases of cement k165-400B-20A hydrated in suspension (w/c=5) during two days, in % by mass of original anhydrous cement

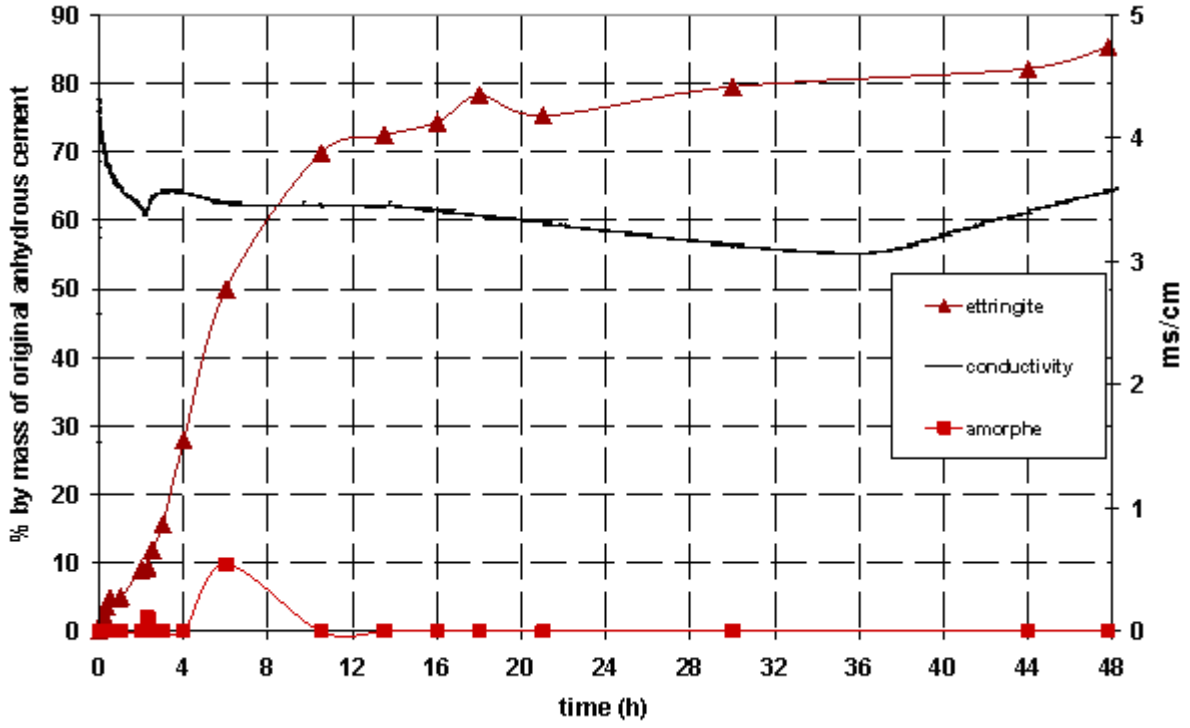

Figure 4-12: Electrical conductivity and normalised Rietveld estimates of major hydrate phases of cement k165-400B-20A hydrated in suspension (w/c=5) during two days, in % by mass of original anhydrous cement

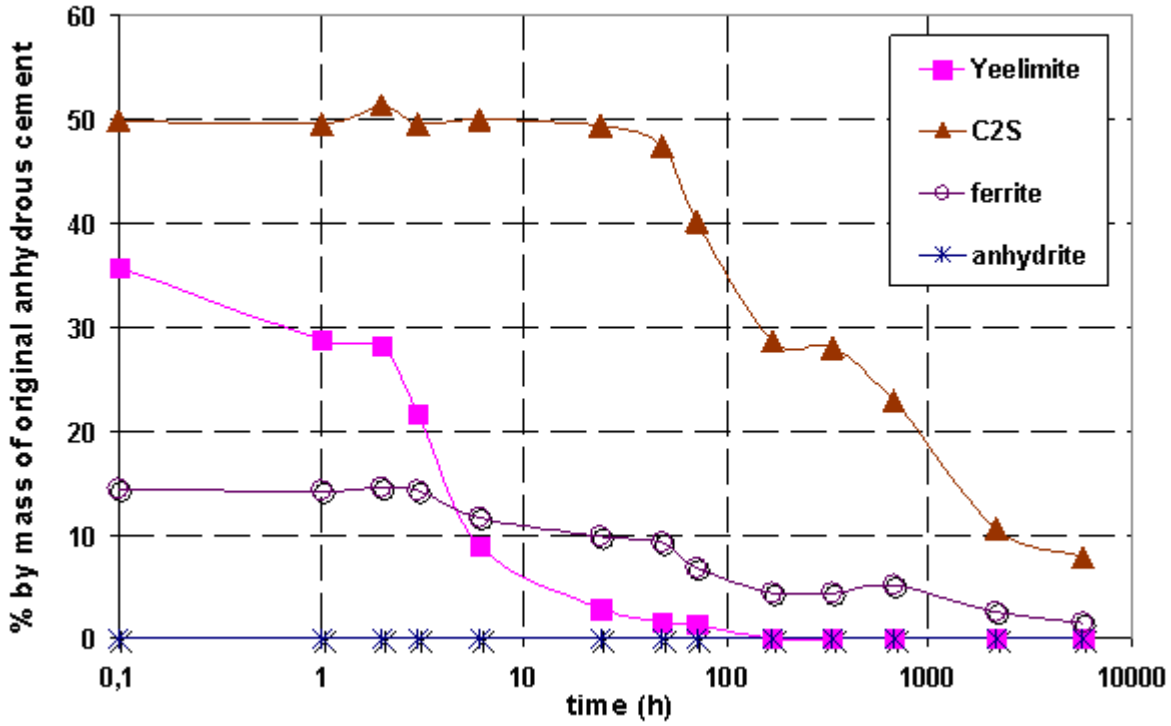

Figure 4-13: Normalised Rietveld estimates of anhydrous phases of cement k165-400B-0A hydrated in paste (w/c=0.5) during 1 year, in % by mass of original anhydrous cement

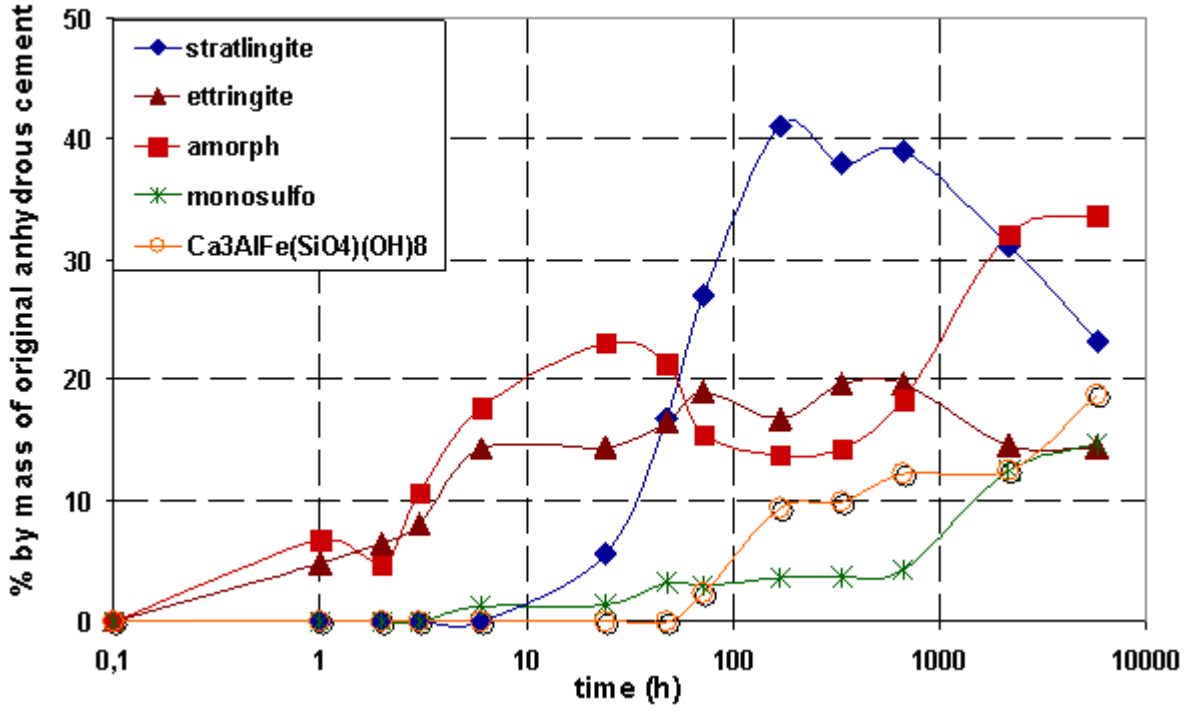

Figure 4-14: Normalised Rietveld estimates of major hydrate phases of cement k165-400B-0A hydrated in paste (w/c=0.5) during 1 year, in % by mass of original anhydrous cement

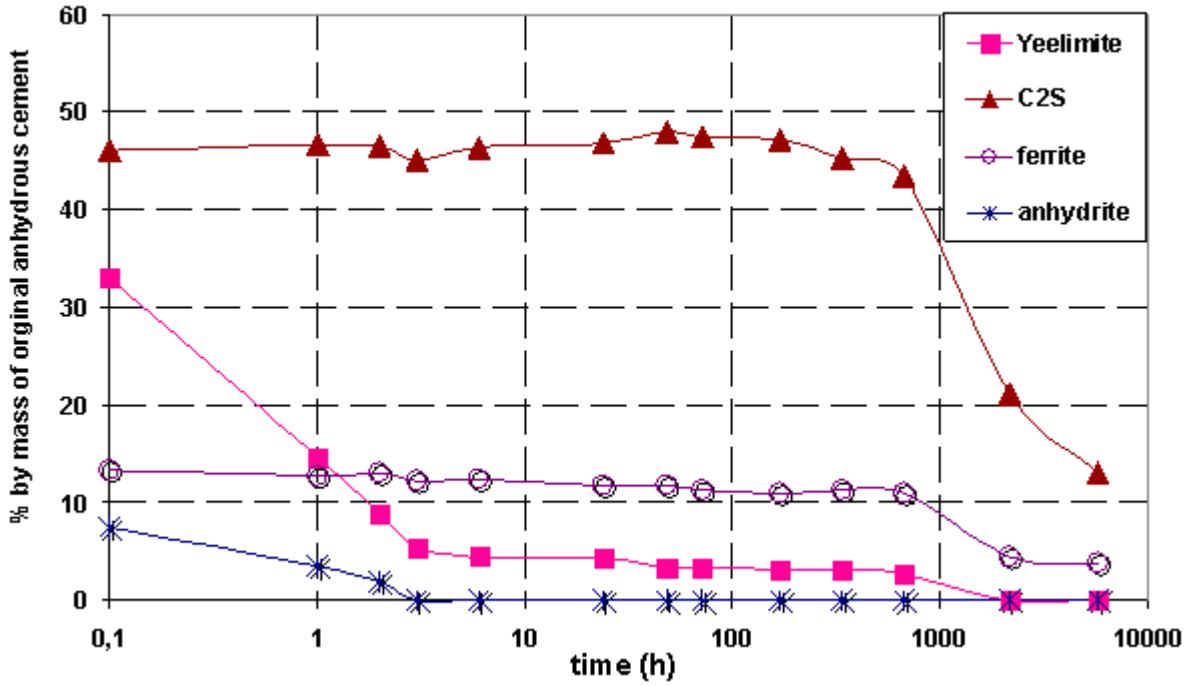

Figure 4-15: Normalised Rietveld estimates of anhydrous phases of cement k165-400B-10A hydrated in paste (w/c=0.5) during eight months, in % by mass of original anhydrous cement

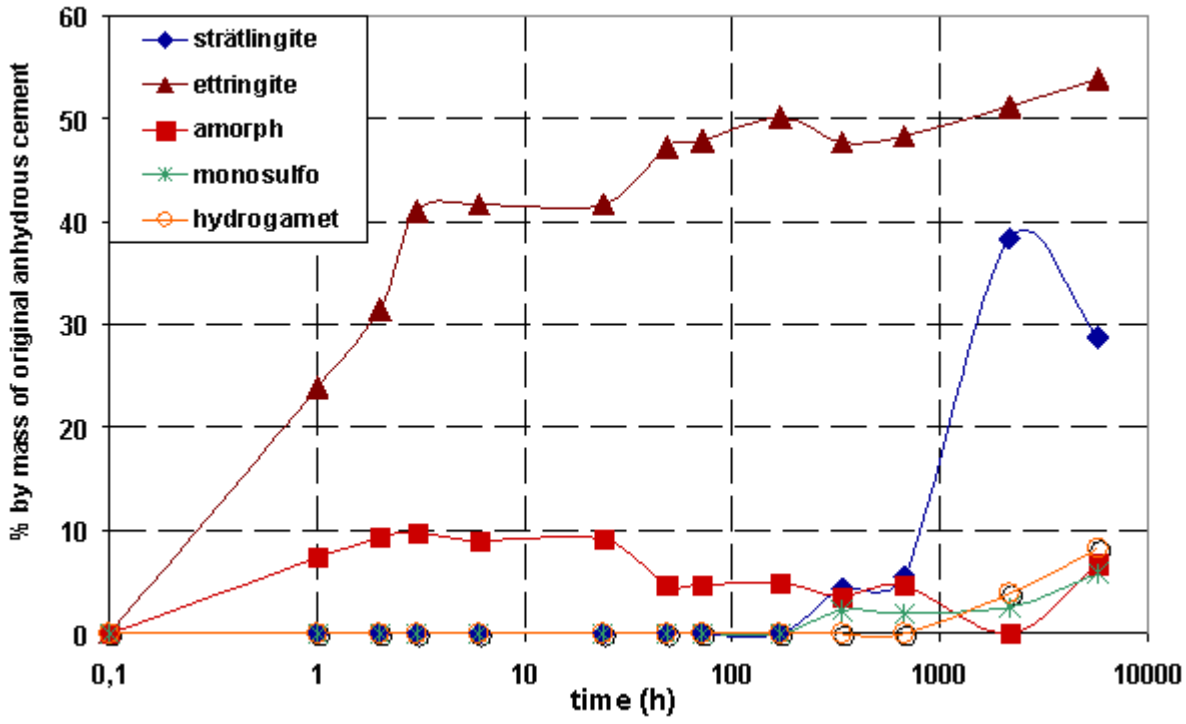

Figure 4-16: Normalised Rietveld estimates of major hydrate phases of cement k165-400B-10A hydrated in paste (w/c=0.5) during eight months, in % by mass of original anhydrous cement

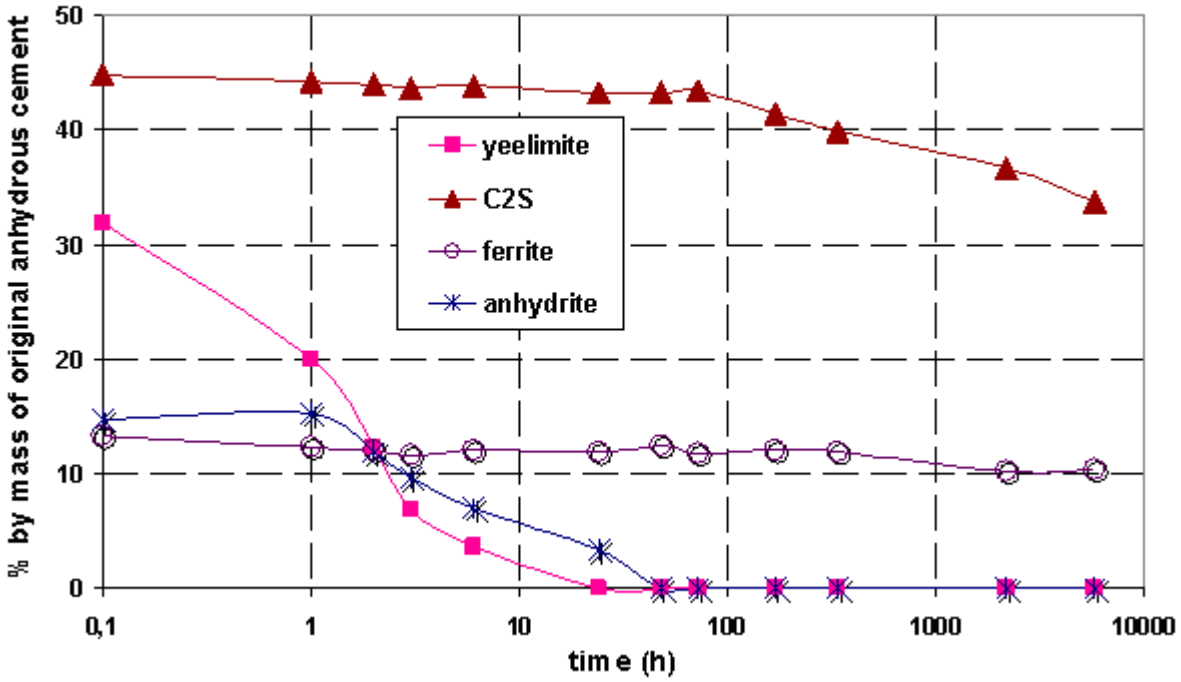

Figure 4-17: Normalised Rietveld estimates of anhydrous phases of cement k165-400B-20A hydrated in paste (w/c=0.5) during eight months, in % by mass of original anhydrous cement

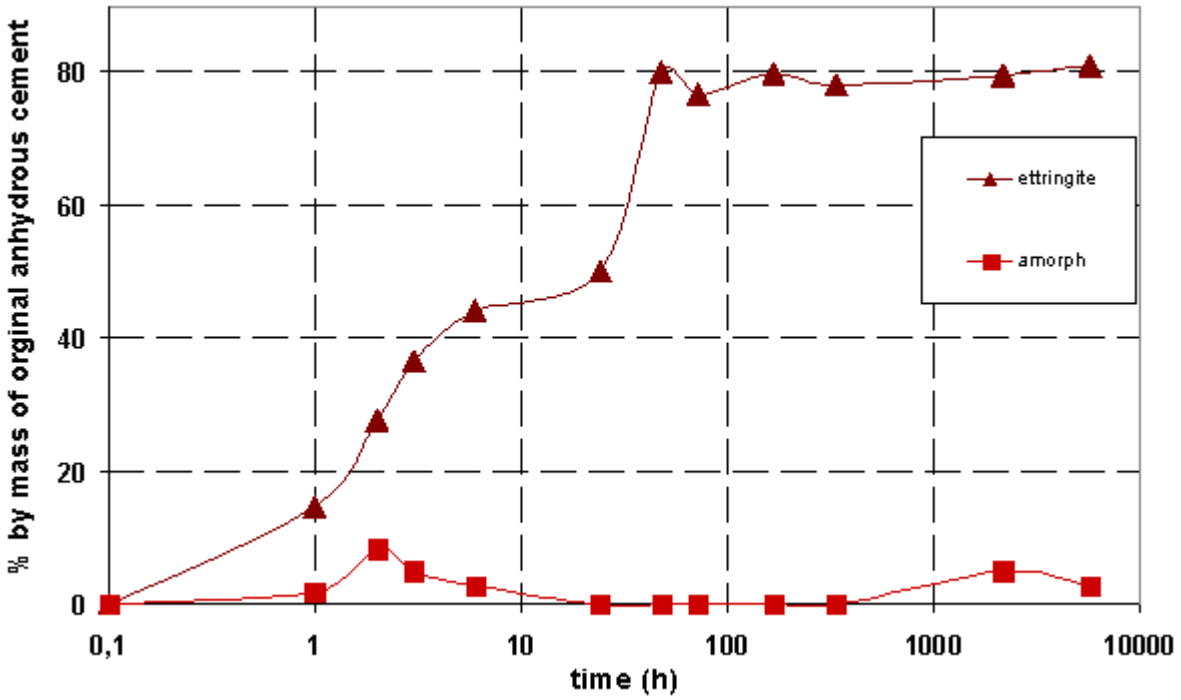

Figure 4-18: Normalised Rietveld estimates of major hydrate phases of cement k165-400B-20A hydrated in paste (w/c=0.5) during eight months, in % by mass of original anhydrous cement

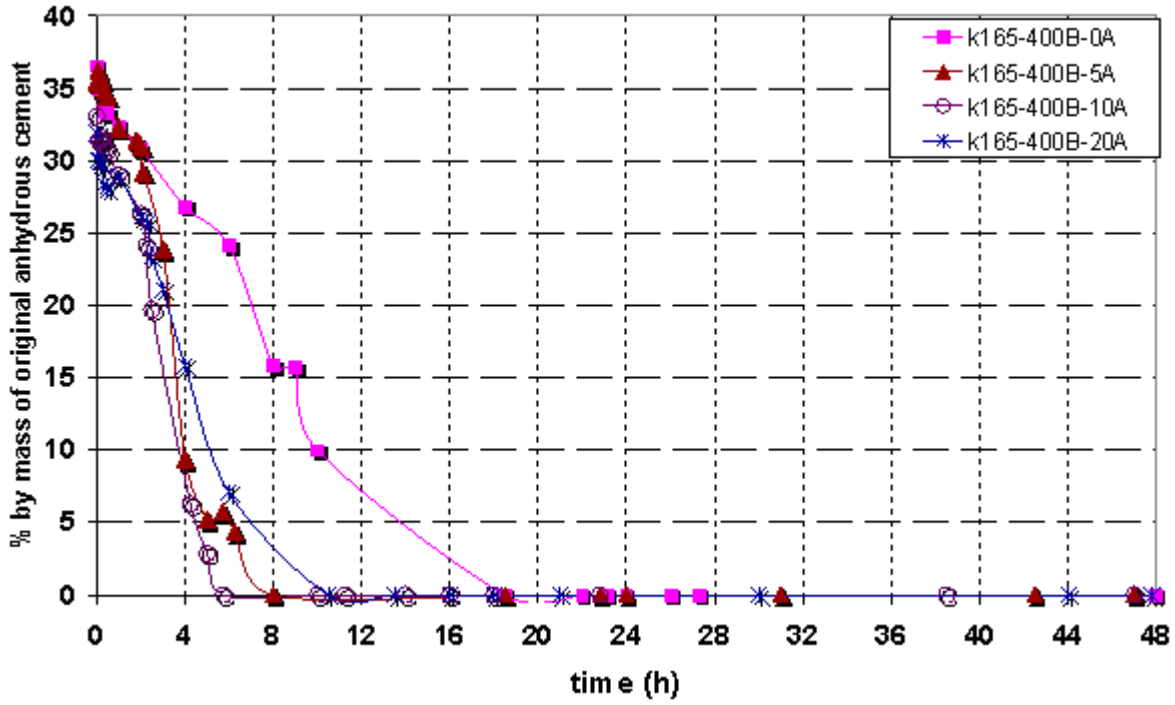

Figure 4-19: Comparison of ye'elimite evolution during the hydration of cement k165-400B-0A, k165-400B-5A, k165-400B-10A, k165-400B-20A in suspension (w/c=5), in % by mass of original anhydrous cement

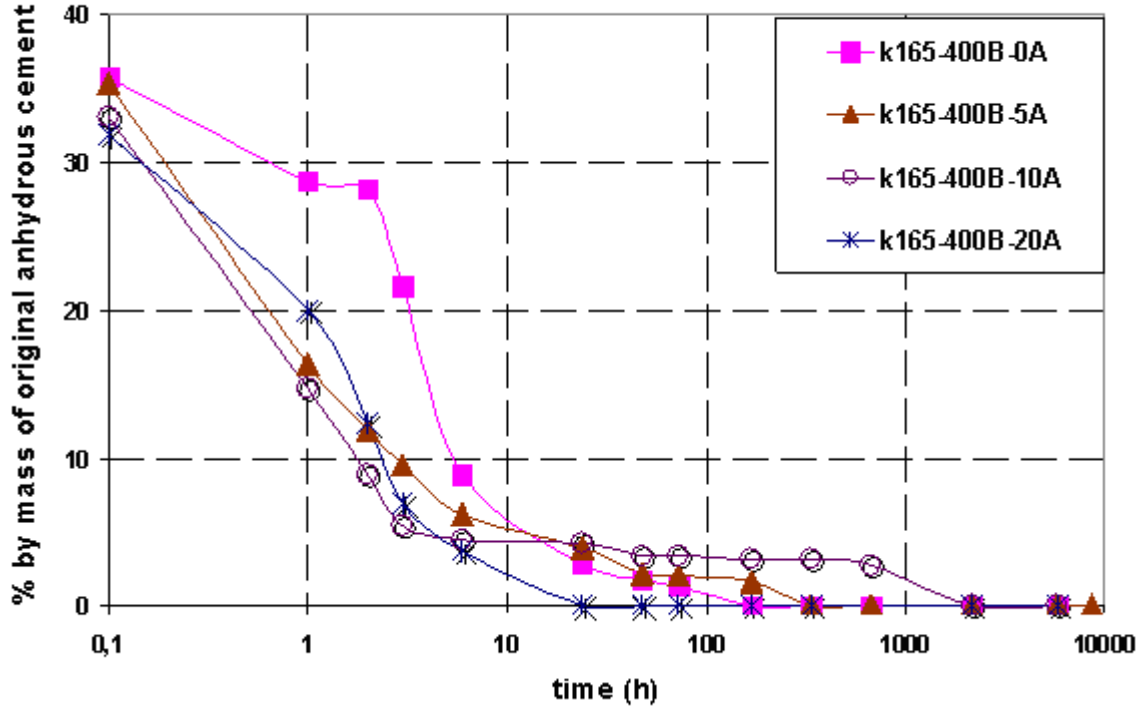

Figure 4-20: Comparison of ye'elimite evolution during the hydration of cement k165-400B-0A, k165-400B-5A, k165-400B-10A, k165-400B-20A in paste (w/c=0.5), in % by mass of original anhydrous cement

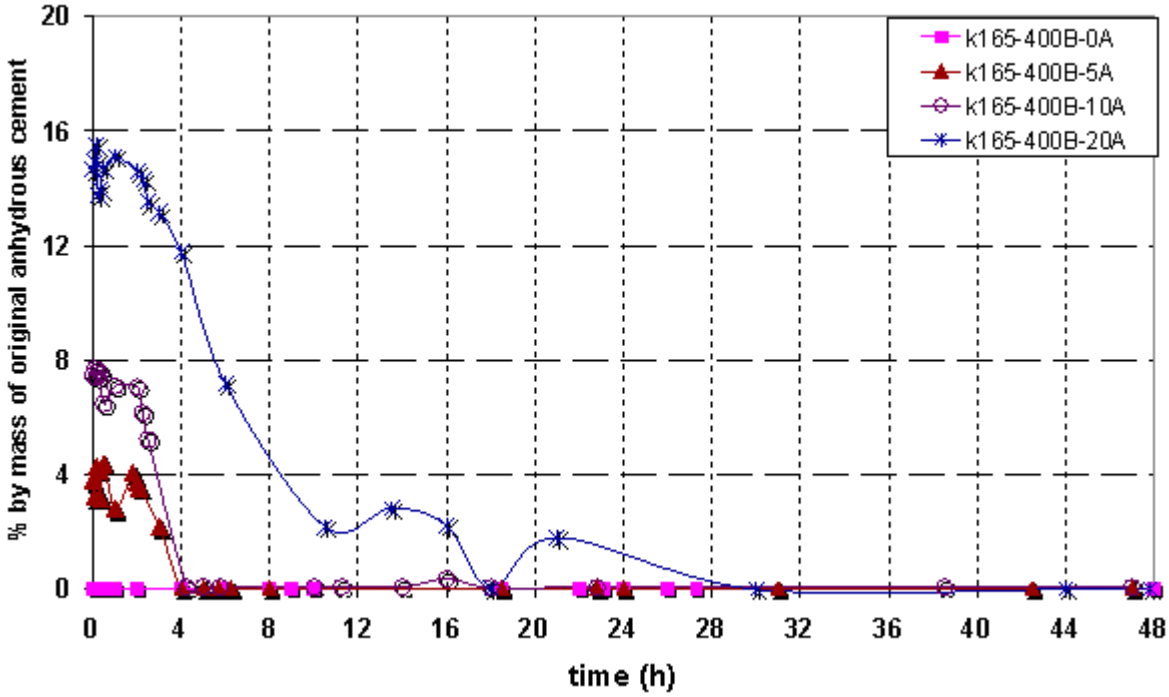

Figure 4-21: Comparison of anhydrite evolution during the hydration of cement k165-400B-0A, k165-400B-5A, k165-400B-10A, k165-400B-20A in suspension (w/c=5), in % by mass of original anhydrous cement

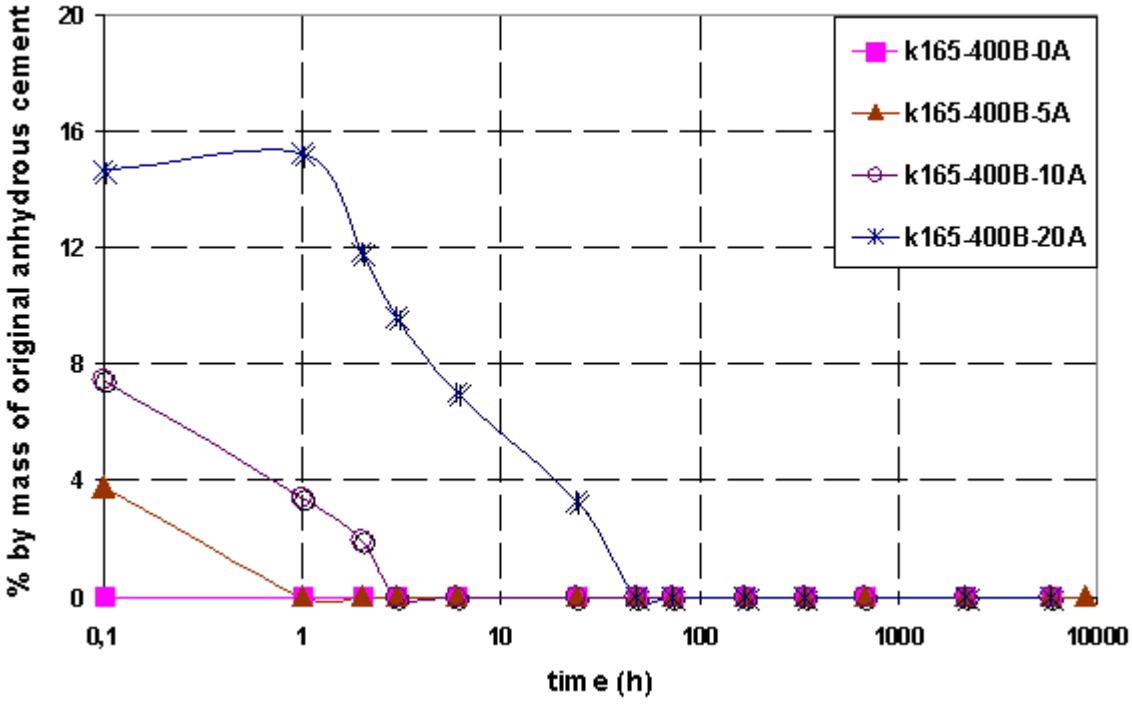

Figure 4-22: Comparison of anhydrite evolution during the hydration of cement k165-400B-0A, k165-400B-5A, k165-400B-10A, k165-400B-20A in paste (w/c=0.5), in % by mass of original anhydrous cement

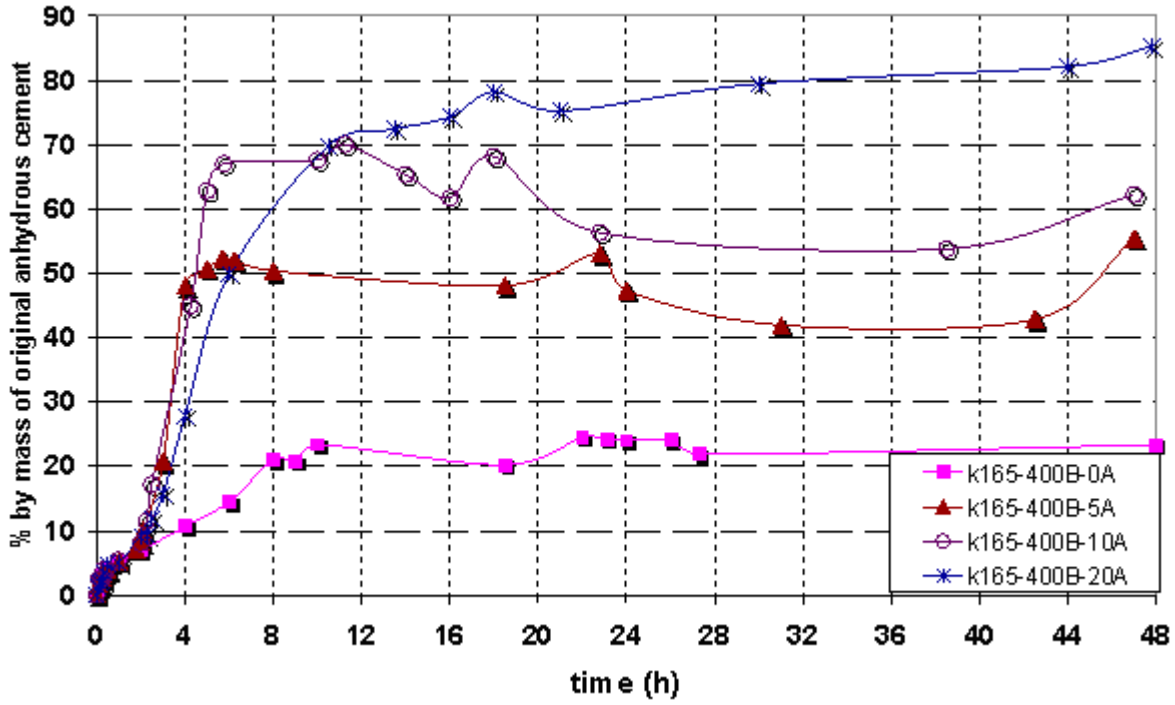

Figure 4-23: Comparison of ettringite evolution during the hydration of cement k165-400B-0A, k165-400B-5A, k165-400B-10A, k165-400B-20A in suspension (w/c=5), in % by mass of original anhydrous cement

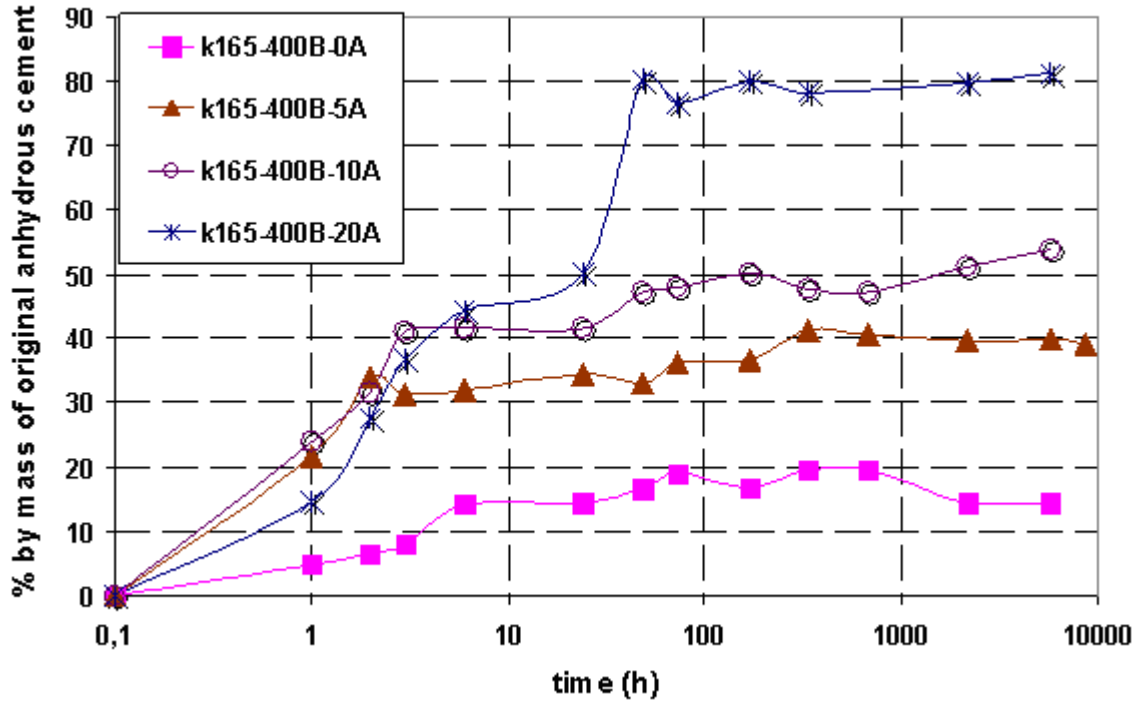

Figure 4-24: Comparison of ettringite evolution during the hydration of cement k165-400B-0A, k165-400B-5A, k165-400B-10A, k165-400B-20A in paste (w/c=0.5), in % by mass of original anhydrous cement

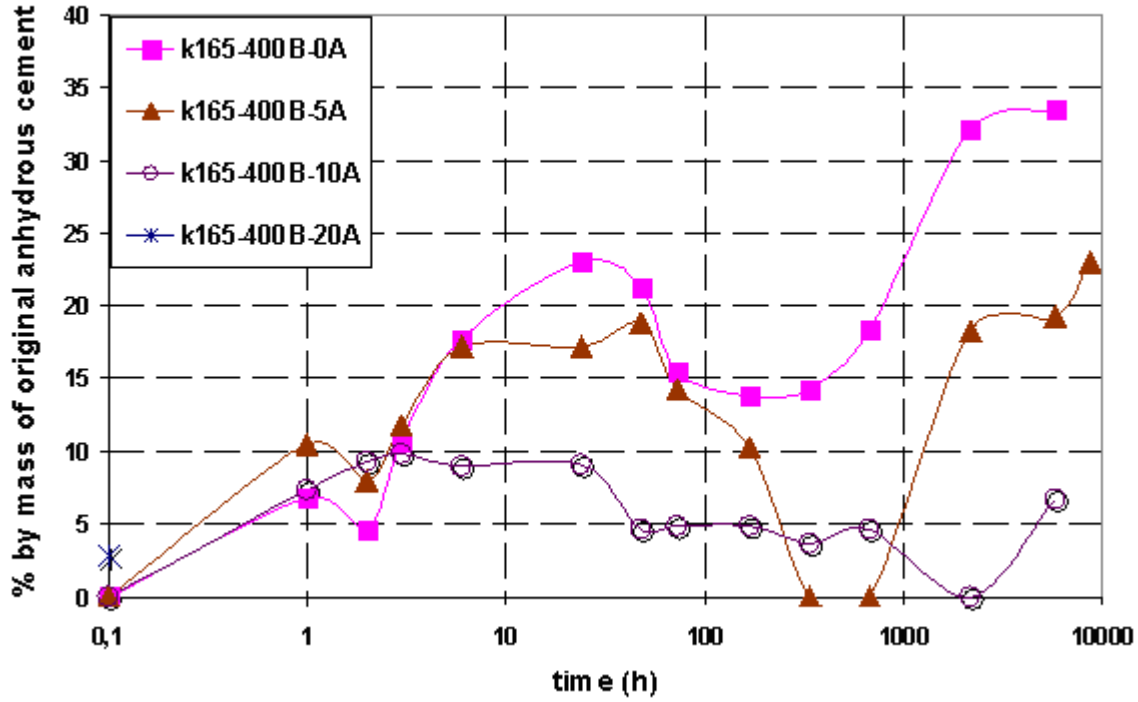

Figure 4-25: Comparison of amorphous phases' evolution during the hydration of cement k165-400B-0A, k165-400B-5A, k165-400B-10A, k165-400B-20A in paste (w/c=0.5), in % by mass of original anhydrous cement

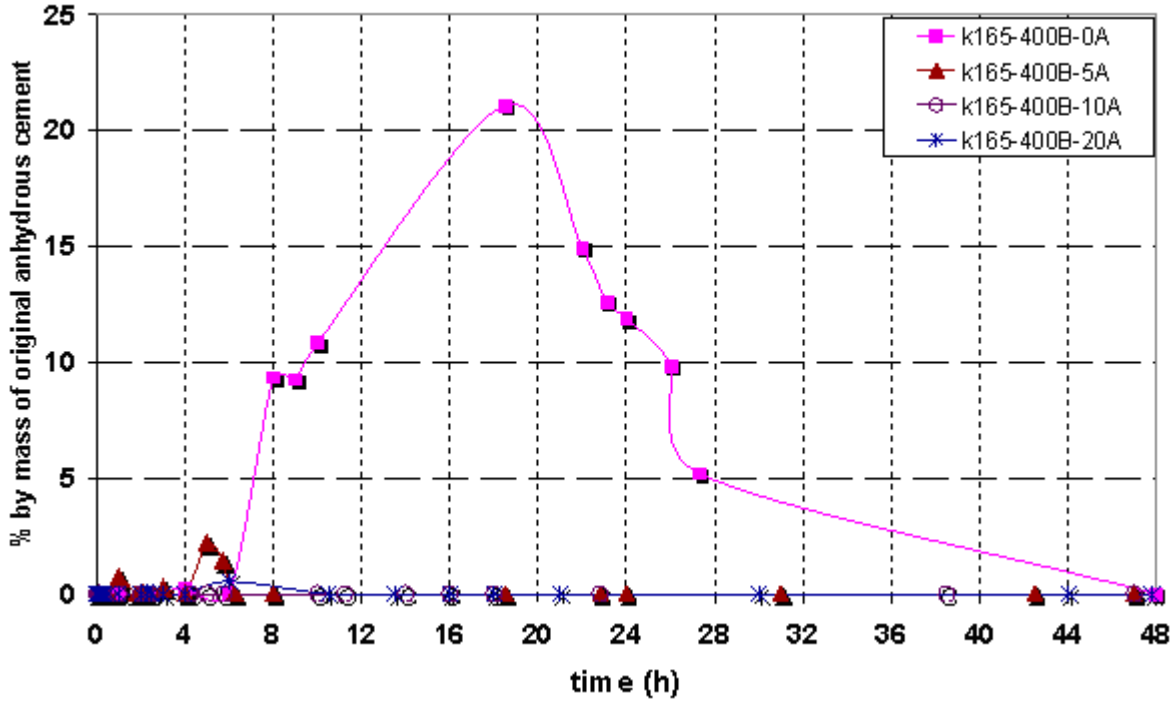

Figure 4-26: Comparison of amorphous phases' evolution during the hydration of cement k165-400B-0A, k165-400B-5A, k165-400B-10A, k165-400B-20A in suspension (w/c=5), in % by mass of original anhydrous cement

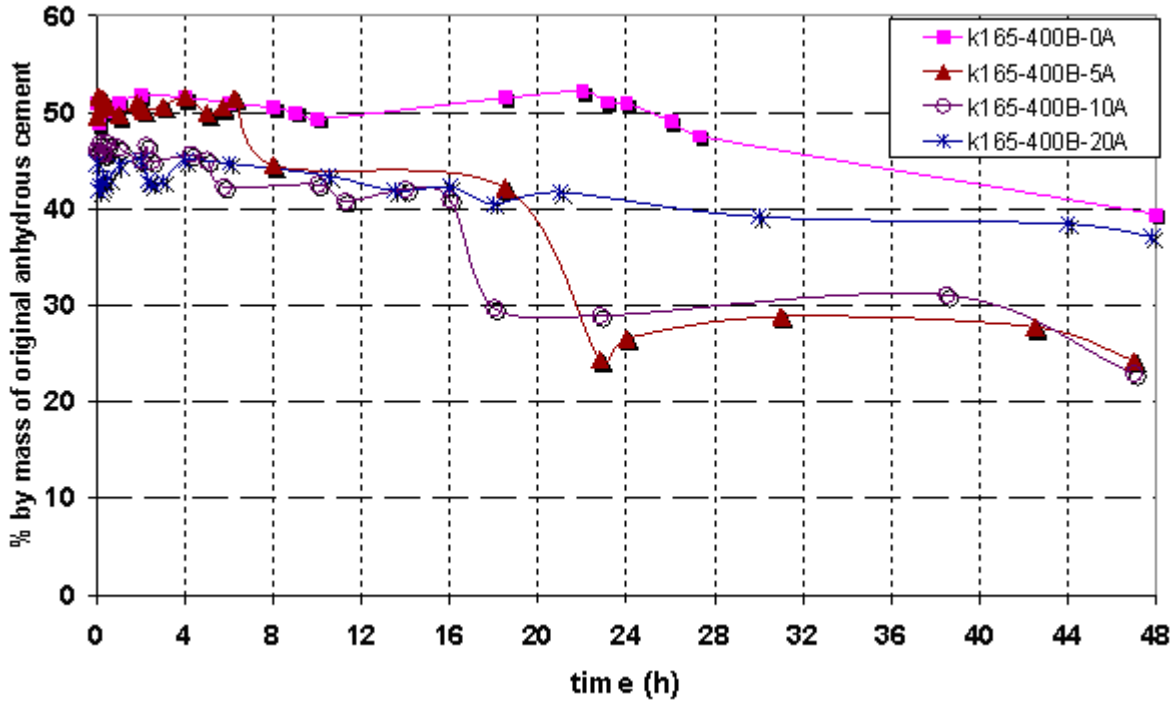

Figure 4-27: Comparison of belite evolution during the hydration of cement k165-400B-0A, k165-400B-5A, k165-400B-10A, k165-400B-20A in suspension (w/c=5), in % by mass of original anhydrous cement

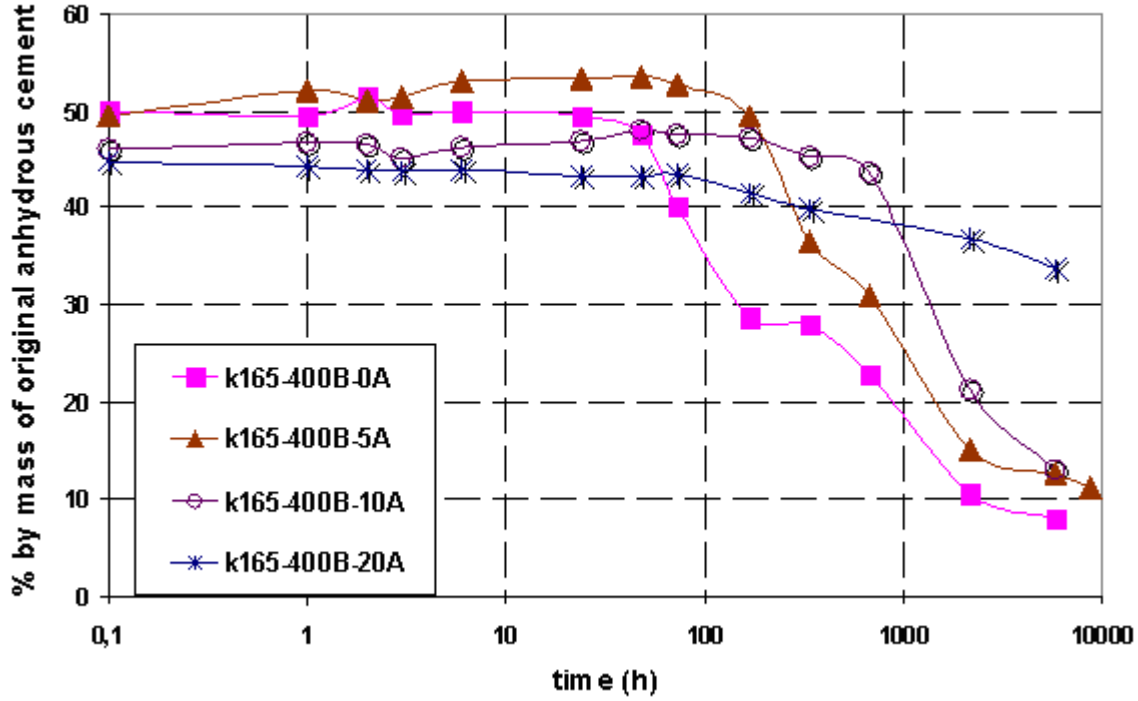

Figure 4-28: Comparison of belite evolution during the hydration of cement k165-400B-0A, k165-400B-5A, k165-400B-10A, k165-400B-20A in paste (w/c=0.5), in % by mass of original anhydrous cement

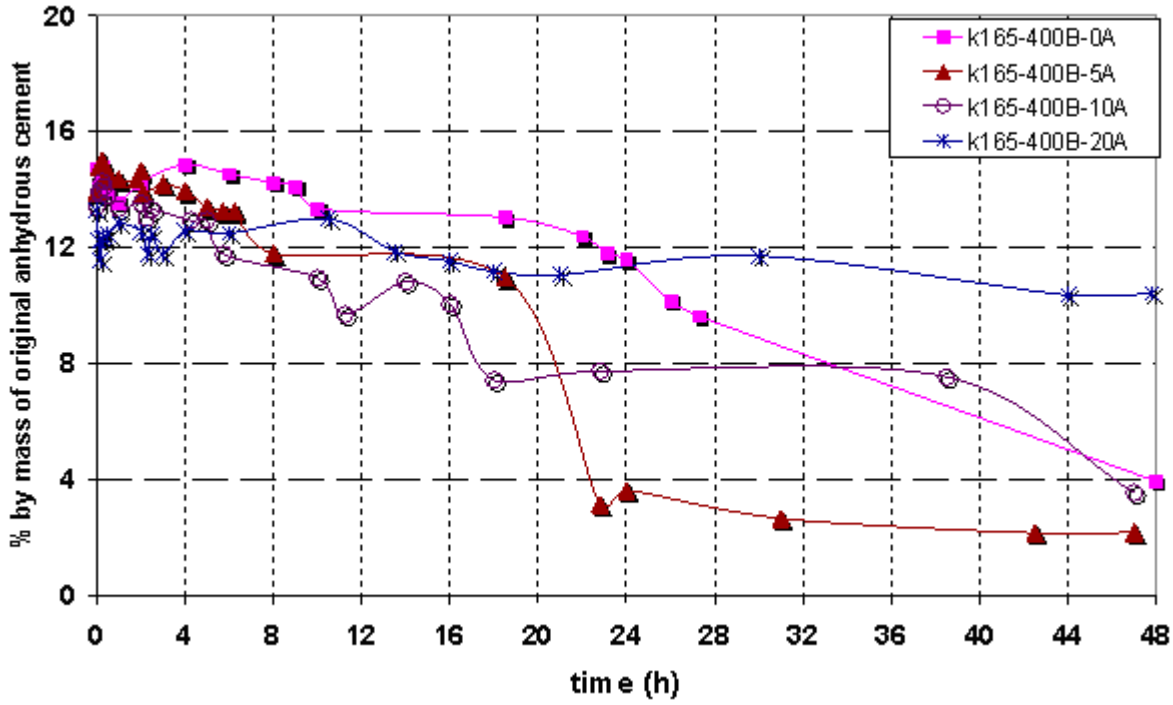

Figure 4-29: Comparison of ferrite evolution during the hydration of cement k165-400B-0A, k165-400B-5A, k165-400B-10A, k165-400B-20A in suspension (w/c=5), in % by mass of original anhydrous cement

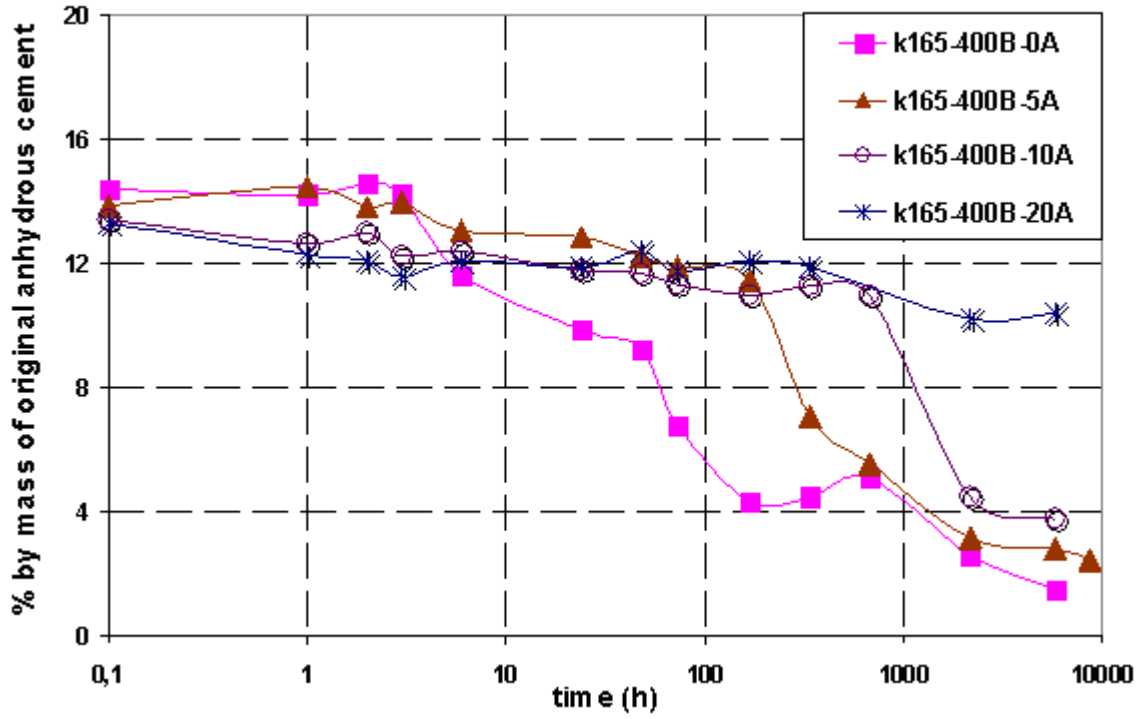

Figure 4-30: Comparison of ferrite evolution during the hydration of cement k165-400B-0A, k165-400B-5A, k165-400B-10A, k165-400B-20A in paste (w/c=0.5), in % by mass of original anhydrous cement

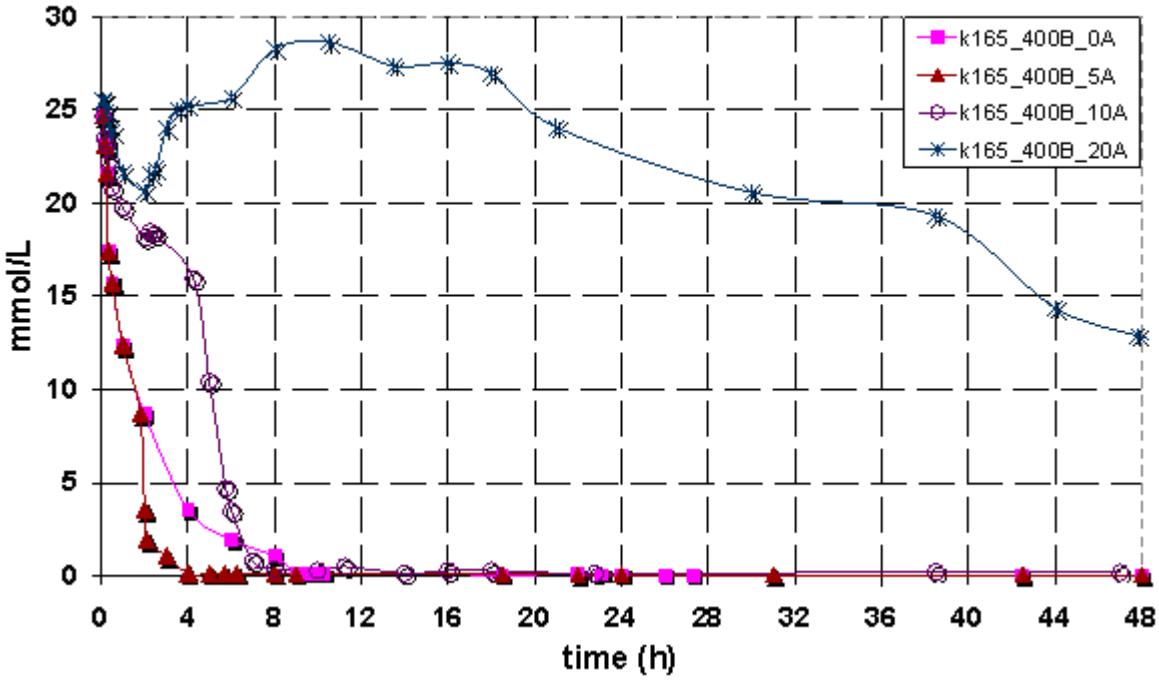

Figure 4-31: Comparison of sulphate element (SO_3) of the liquid phases recovered during the hydration of cement k165-400B-0A, k165-400B-5A, k165-400B-10A, k165-400B-20A in suspension (w/c=5) during two days

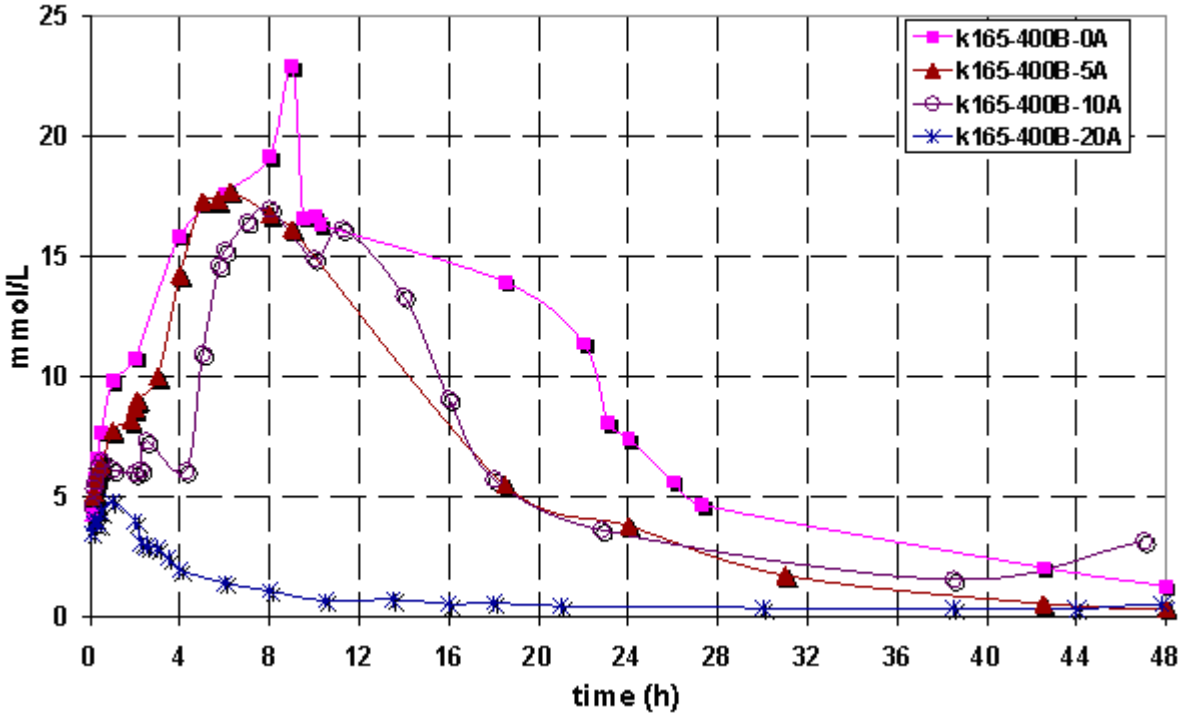

Figure 4-32: Comparison of aluminium element (Al_2O_3) of the liquid phases recovered during the hydration of cement k165-400B-0A, k165-400B-5A, k165-400B-10A, k165-400B-20A in suspension (w/c=5) during two days

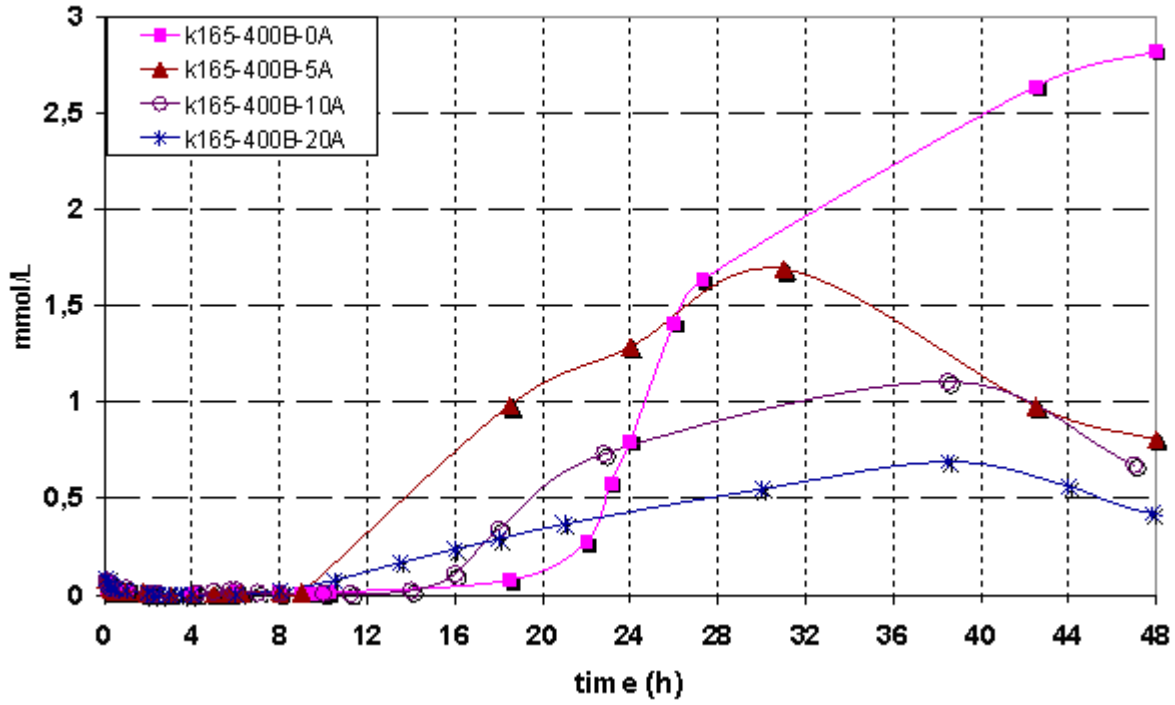

Figure 4-33: Comparison of boron element (B) of the liquid phases recovered during the hydration of cement k165-400B-0A, k165-400B-5A, k165-400B-10A, k165-400B-20A in suspension (w/c=5) during two days

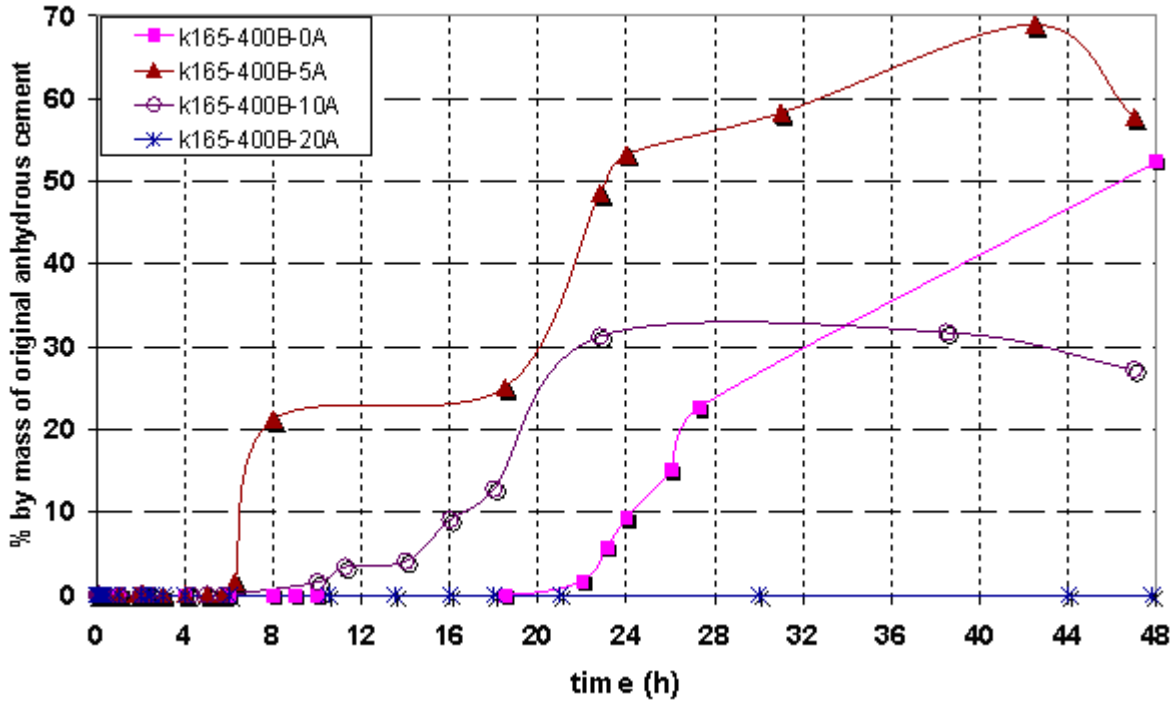

Figure 4-34: Comparison of strätlingite evolution during the hydration of cement k165-400B-0A, k165-400B-5A, k165-400B-10A, k165-400B-20A in suspension (w/c=5) during two days, in % by mass of original anhydrous cement

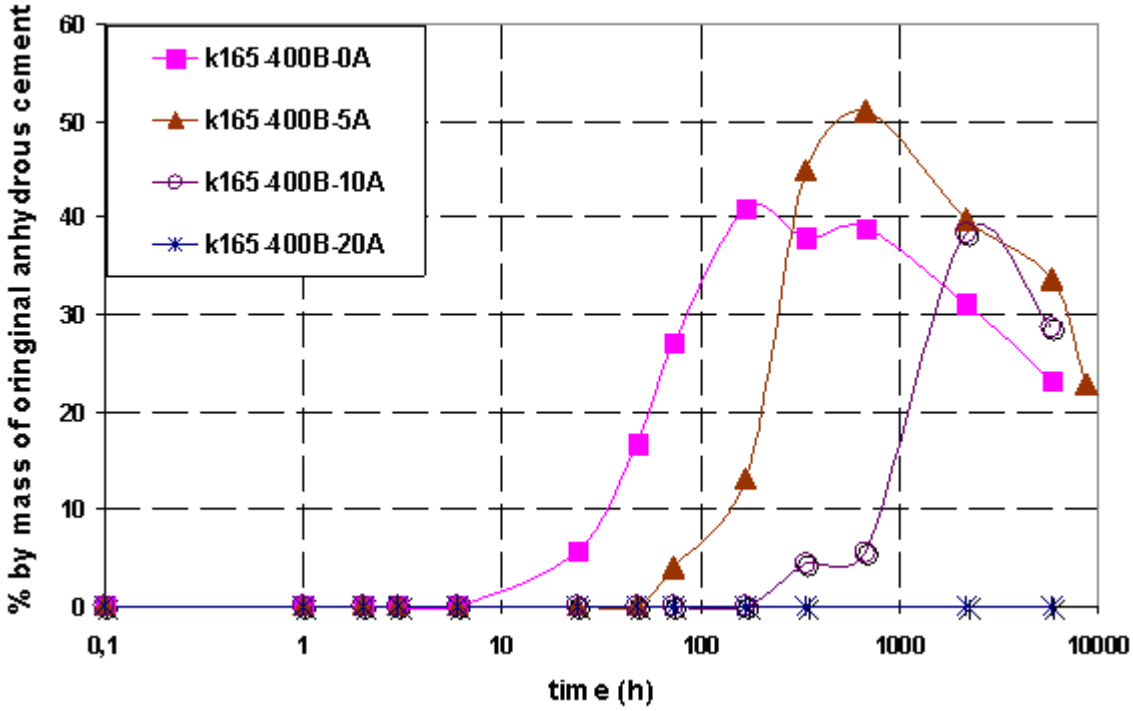

Figure 4-35: Comparison of strätlingite evolution during the hydration of cement k165-400B-0A, k165-400B-5A, k165-400B-10A, k165-400B-20A in paste (w/c=0.5) during one year, in % by mass of original anhydrous cement

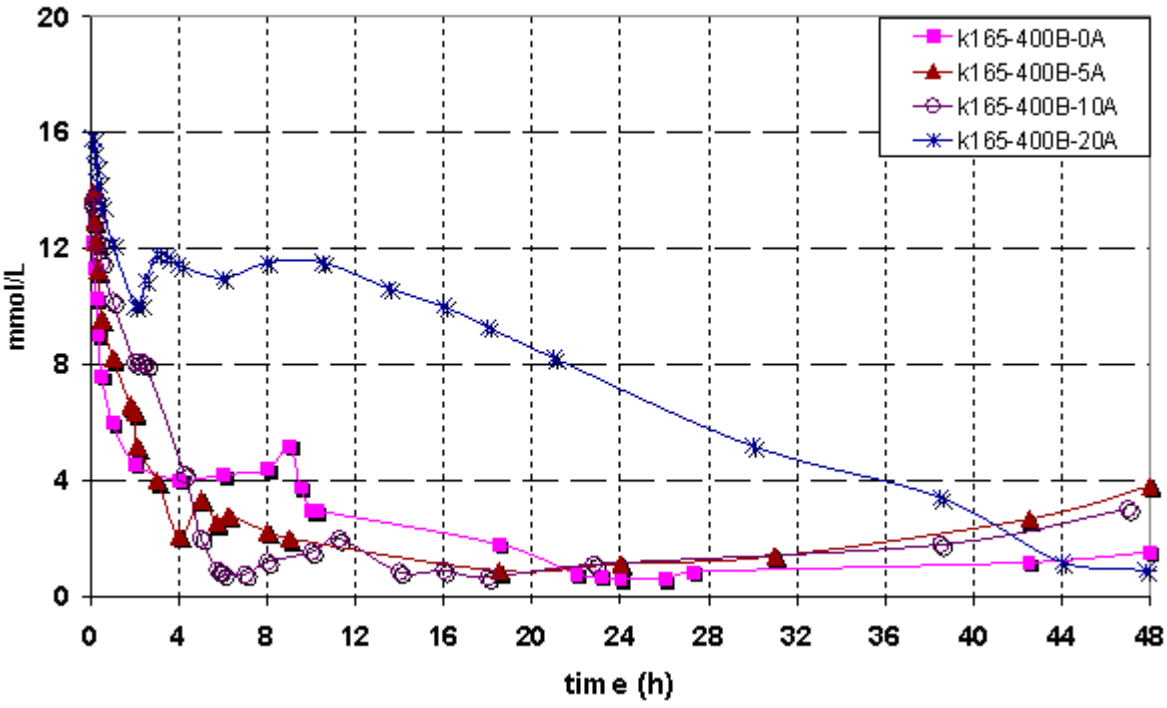

Figure 4-36: Comparison of calcium element (CaO) of the liquid phases recovered during the hydration of cement k165-400B-0A, k165-400B-5A, k165-400B-10A, k165-400B-20A in suspension (w/c=5)

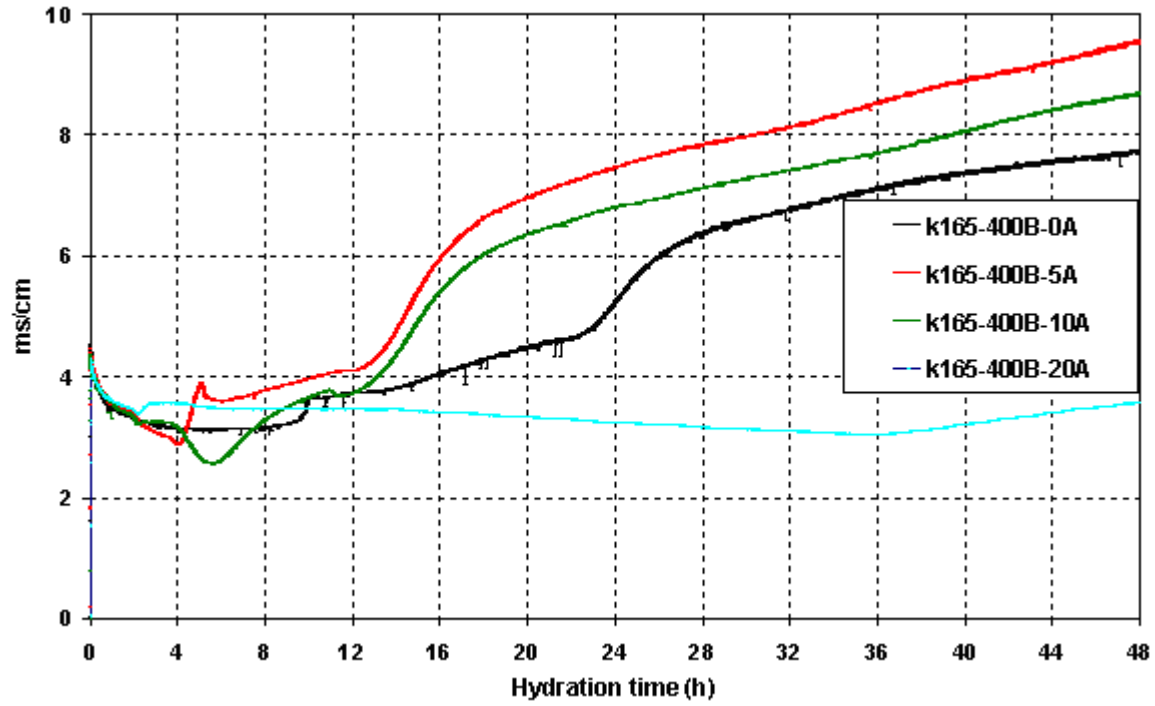

Figure 4-37: Change in electrical conductivity during the hydration of cement k165-400B-0A, k165-400B-5A, k165-400B-10A, k165-400B-20A in suspension (w/c=5) during two days

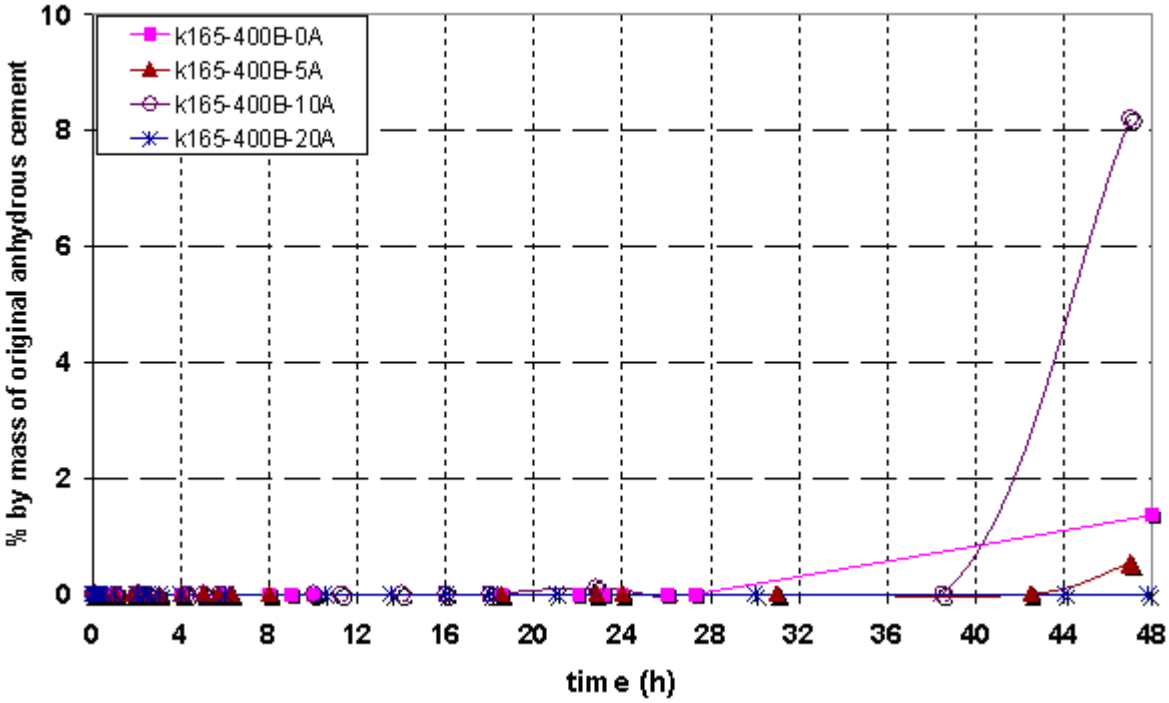

Figure 4-38: Comparison of hydrogarnet evolution during the hydration of cement k165-400B-0A, k165-400B-5A, k165-400B-10A, k165-400B-20A in suspension (w/c=5) during two days, in % by mass of original anhydrous cement

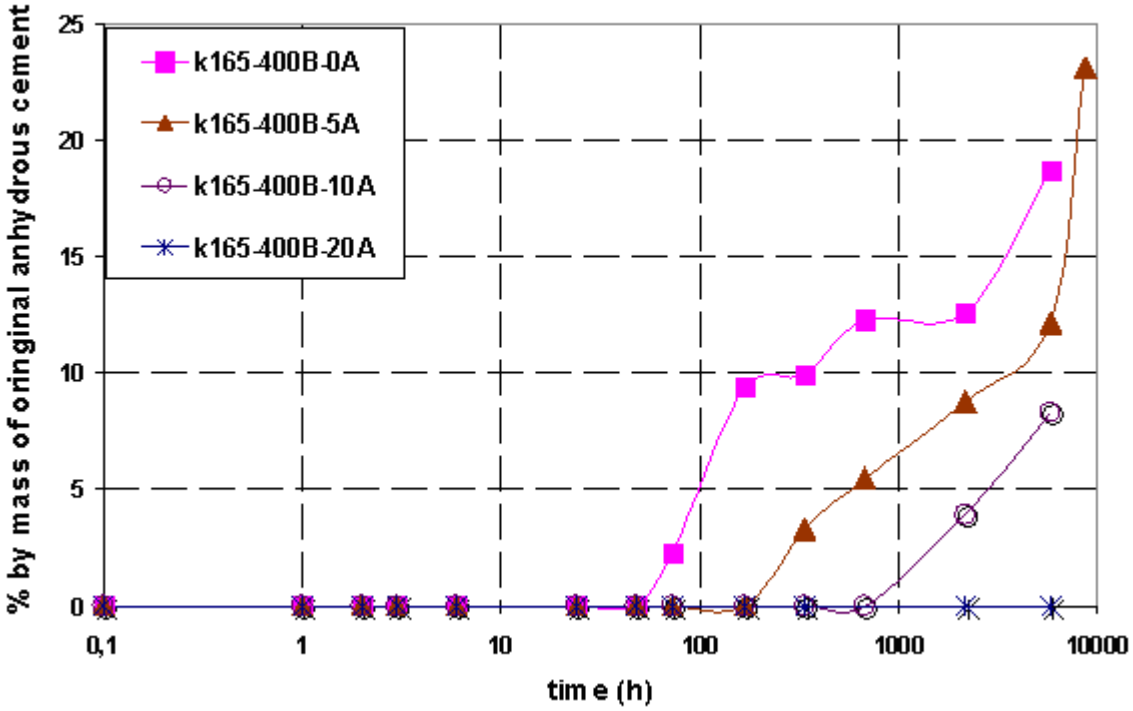

Figure 4-39: Comparison of hydrogarnet evolution during the hydration of cement k165-400B-0A, k165-400B-5A, k165-400B-10A, k165-400B-20A in paste (w/c=0.5) during one year, in % by mass of original anhydrous cement

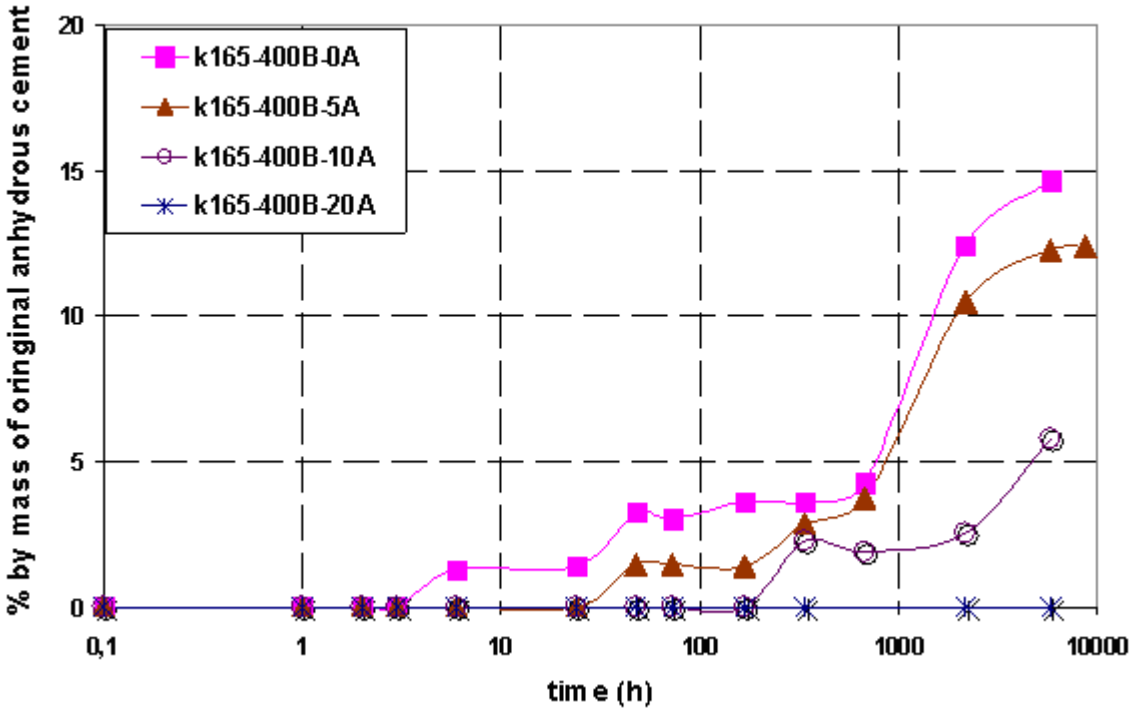

Figure 4-40: Comparison of calcium monosulfoaluminate hydrate evolution during the hydration of cement k165-400B-0A, k165-400B-5A, k165-400B-10A, k165-400B-20A in paste (w/c=0.5) during one year, in % by mass of original anhydrous cement

Time	Monosulphate	Hydrogarnet	Gibbsite	Hemicarbonate	Monocarbonate	Amorph [%]
0	0	0	0	0	0	0
5m	0	0	0	0	0	0
10m	0	0	0	0.7	0	0
15m	0	0	0	0.8	0	0
20m	0	0	0	0.5	0	0
30m	0	0	0	0.6	0	0
1h	0	0	0	0	0	0
2h	0	0	0	0	0	0
4h	0	0	0	0	0	0.2
6h	0	0	0	0	0	0
8h	0	0	0	0	0	9.4
9h	0	0	0	0	0	9.3
10h	0	0	0	0	3.0	10.8
18.5h	0	0	0	0	2.8	21.1
22h	0	0	0	0	4.0	14.9
23.1h	0	0	0	0	5.0	12.6
24h	0	0	0	0	2.8	11.9
26h	0	0	0	0	2.1	9.9
27.3h	1.5	0	0	0	0	5.2
48h	0	1.4	0	0	0	0

Table 4-3: Normalised Rietveld estimates of major hydrate phases of cement k165-400B-0A hydrated in suspension (w/c=5) during two days, in % by mass of original anhydrous cement

Time	Strätlingite	Monosulphate	Hydrogarnet	Gibbsite	Hemicarbo	Amorph
0	0	0	0	0	0	0
5m	0	0	0	0	0	0
10m	0	0	0	0	0	0
15m	0	0	0	0	0	0
20m	0	0	0	0	0	0
30m	0	0	0	0	0	0
1h	0	0	0	0	0	0
2h	0	0	0	0.1	0	0
2h15	0	0	0	0	0.3	0
2h5	0	0	0	0.2	0.7	0
4h15	0	0	0	0.7	2.1	0
5h	0	0	0	1.0	1.7	0
5.8h	0	0	0	1.3	2.8	0
10h	1.6	0	0	1.0	0.7	0
11h15	3.5	0	0	0.6	3.0	0
14h	4.2	0	0	0.7	1.0	0
16h	9.3	0	0	1.0	0.8	0
18h	13.7	0	0	0	1.2	0
22h8	32.1	0.5	0.1	0	0	0
38h30	28.3	0.8	8.5	0	0	0
47h	28.7	0.8	8.7	0	0	0

Table 4-4: Normalised Rietveld estimates of major hydrate phases of cement k165-400B-10A hydrated in suspension (w/c=5) during two days, in % by mass of original anhydrous cement

Time	Strätlingite	Monosulpho	Hydrogarnet	Gibbsite	Hemicarbo	Monocarbo	Amorph [%]
0	0	0	0	0	0	0	0
5m	0	0	0	0	0.6	0	0
10m	0	0	0	0	0	0	0
15m	0	0	0	0	0	0	0
20m	0	0	0	0	0	0	0
30m	0	0	0	0	0	0	0
1h	0	0	0	0	0	0	0
2h	0	0	0	0	0	0	0
2.3h	0	0	0	0	0	0	0.1
2.5h	0	0	0	0	0	0	0
3h	0	0	0	0	0	0	0
4h	0	0	0	0	0	0	0
6h	0	0	0	0	0	0	0.5
10.5h	0	0	0	0	0	0	0
13.5h	0	0	0	1.3	0	0	0
16h	0	0	0	1.1	0	0	0
18h	0	0	0	1.3	0	0	0
21h	0	0	0	1.3	0	0	0
30h	0	0	0	1.5	0	0	0
44h	0	0	0	1.1	0	0	0
47.8h	0	0	0	1.1	0	0	0

Table 4-5: Normalised Rietveld estimates of major hydrate phases of cement k165-400B-20A hydrated in suspension (w/c=5) during two days, in % by mass of original anhydrous cement

time	Monosulphate	Hydrogarnet	Gibbsite	Hemicarbonate	tobermorite	Amorph [%]
0	0	0	0	0	0	0
1h	0	0	0	0	0	6.8
2h	0	0	0	0	0	4.6
3h	0	0	0	0	0	10.7
6h	1.3	0	0	1.5	0	17.7
1d	1.4	0	0	3.2	0	23.0
2d	3.3	0	0	0	0	21.3
3d	3.0	2.3	0	0	0	15.5
7d	3.6	9.4	0	0	0	13.9
14d	3.6	9.9	0	0	0	14.3
28d	4.3	12.3	0	0	0	18.4
3m	12.5	12.6	0	0	4.5	32.1
8m	14.7	18.7	0	0	6.4	33.5

Table 4-6: Normalised Rietveld estimates of major hydrate phases of cement k165-400B-0A hydrated in paste (w/c=0.5) during eight months, in % by mass of original anhydrous cement

time	Strätlingite	Monosulphate	Hydrogarnet	Gibbsite	Hemicarbonate	tobermorite	Amorph
0	0	0	0	0	0	0	0
1h	0	0	0	0	0	0	6.8
2h	0	0	0	0	0	0	8.4
3h	0	0	0	0	0	0	8.6
6h	0	0	0	0	0	0	7.9
1d	0	0	0	0	0	0	8.0
2d	0	0	0	0	0	0	4.1
3d	0	0	0	0	0	0	4.2
7d	0	0	0	0	0	0	4.2
14d	3.8	1.9	0	0	0	0	3.1
28d	4.6	1.6	0	0	0	0	4.0
3m	31.1	2.0	3.2	0	0	1.5	0.00
8m	23.0	4.6	6.6	0	presence	3.9	5.4

Table 4-7: Normalised Rietveld estimates of major hydrate phases of cement k165-400B-0A hydrated in paste (w/c=0.5) during eight months, in % by mass of original anhydrous cement

time	Strätlingite	Monosulphate	Hydrogarnet	Gibbsite	Hemicarbonate	Tobermorite	Amorph [%]
0	0	0	0	0	0	0	0
1h	0	0	0	0	0	0	1.8
2h	0	0	0	0	0	0	7.2
3h	0	0	0	0	0	0	4.6
6h	0	0	0	0	0	0	2.5
1d	0	0	0	0	0	0	0
2d	0	0	0	0	0	0	0
3d	0	0	0	0	0	0	0
7d	0	0	0	0	0	0	0
14d	0	0	0	0	0	0	0
3m	0	0	0	0	0	0	3.8
8m	0	0	0	0	0	0	2.2

Table 4-8: Normalised Rietveld estimates of major hydrate phases of cement k165-400B-20A hydrated in paste (w/c=0.5) during eight months, in % by mass of original anhydrous cement

Time	CSH08	CSH09	CSH10	CSH11	CSH12	CSH13	CSH14	CSH15	CSH16	CSH17	CSH18
5m	-1.55	-1.6	-1.73	-1.79	-1.85	-1.99	-2.20	-2.49	-2.80	<-3	<-3
10m	-2.02	-2.15	-2.36	-2.51	-2.65	-2.89	<-3	<-3	<-3	<-3	<-3
15m	-2.59	-2.80	<-3	<-3	<-3	<-3	<-3	<-3	<-3	<-3	<-3
20m	-1.60	-1.61	-1.80	-1.87	-1.93	-2.08	-2.30	-2.60	-2.91	<-3	<-3
30m	<-3	<-3	<-3	<-3	<-3	<-3	<-3	<-3	<-3	<-3	<-3
1h	-1.63	-1.67	-1.80	-1.86	-1.91	-2.60	-2.27	-2.56	-2.87	<-3	<-3
2h	-1.62	-1.73	-1.92	-2.05	-2.17	-2.38	-2.64	<-3	<-3	<-3	<-3
2h18	-1.68	-1.75	-1.90	-1.99	-2.07	-2.24	-2.47	-2.79	<-3	<-3	<-3
2h30	-2.10	-2.35	-2.67	-2.94	<-3	<-3	<-3	<-3	<-3	<-3	<-3
3h	<-3	<-3	<-3	<-3	<-3	<-3	<-3	<-3	<-3	<-3	<-3
3h30	<-3	<-3	<-3	<-3	<-3	<-3	<-3	<-3	<-3	<-3	<-3
4h	<-3	<-3	<-3	<-3	<-3	<-3	<-3	<-3	<-3	<-3	<-3
6h	<-3	<-3	<-3	<-3	<-3	<-3	<-3	<-3	<-3	<-3	<-3
8h	<-3	<-3	<-3	<-3	<-3	<-3	<-3	<-3	<-3	<-3	<-3
10h30	<-3	<-3	<-3	<-3	<-3	<-3	<-3	<-3	<-3	<-3	<-3
13h30	<-3	<-3	<-3	<-3	<-3	<-3	<-3	<-3	<-3	<-3	<-3
18h	<-3	<-3	<-3	<-3	<-3	<-3	<-3	<-3	<-3	<-3	<-3
21h	-2.45	-2.52	-2.66	-2.75	-2.83	-3	<-3	<-3	<-3	<-3	<-3
38h30	-1.84	-1.99	-2.21	-3.38	-2.54	-2.79	<-3	<-3	<-3	<-3	<-3
44h	-0.89	-0.92	-1.04	-1.09	-1.14	-1.47	-1.75	-1.75	-2.05	-2.21	-3.67
47h50	-0.87	-0.88	-0.97	-1	-1.02	-1.13	-1.30	-1.56	-1.83	-2.14	-2.40
63h	-0.86	-0.86	-0.93	-0.95	-0.96	-1.05	-1.21	-1.46	-1.71	-2.01	-2.27

Table 4-15: Saturation indexes with respect to C-S-H from the aqueous phase composition recovered during K165-400B-20A hydration in suspension (w/c = 5)

*notion of different C-S-H can be found in Annex 2-11

Chapter V

Hydration of K165-400B-5A in the presence of 15% limestone

5. Hydration of BCSAF cement with limestone addition

Here, we remind the potential interactions summarized in Figure 1-6, especially the interaction of limestone with the constituents of BCSAF cement.

Interaction 11 (ye'elimite/limestone):
Limestone may accelerate the hydration of ye'elimite to form ettringite. Also, calcium monocarbo aluminate hydrate can be formed instead of calcium monosulfo aluminate hydrate.

Interaction 12 (ferrite/limestone):
Limestone may accelerate the hydration of ferrite but here we have to consider the presence or not of sulphate ions that changes the interaction.

Interaction 13: (belite/limestone):
Limestone may accelerate the hydration of C_2S if its rate depends on C-S-H nucleation.

5.1 Results and interpretation

15% by mass of a fine limestone powder was added to cement k165-400B-5A as mentioned in Chapter 2. The resulting cement was given the code k165-400B-5A-15L.

A first experiment was done in suspension by following the electrical conductivity (Figure 5-1). Compared to the evolution of the electrical conductivity observed for k165-400B-5A, the one of k165-400B-5A-15L had the same beginning in the first 5 hours. But at longer time, its value becomes smaller and the difference becomes greater and greater (at 2 days, around 9.5mS/cm for k165-400B-5A and only 7mS/cm for k165-400B-5A-15L). Therefore we supposed that the rate of hydration in the presence of calcite may be reduced and as a consequence we decided to increase the duration of the suspension experiment to 110 hours. Moreover carbonation due to CO_2 is not a problem anymore with these longer suspension experiments as some carbonate ions are also supplied by calcite dissolution.

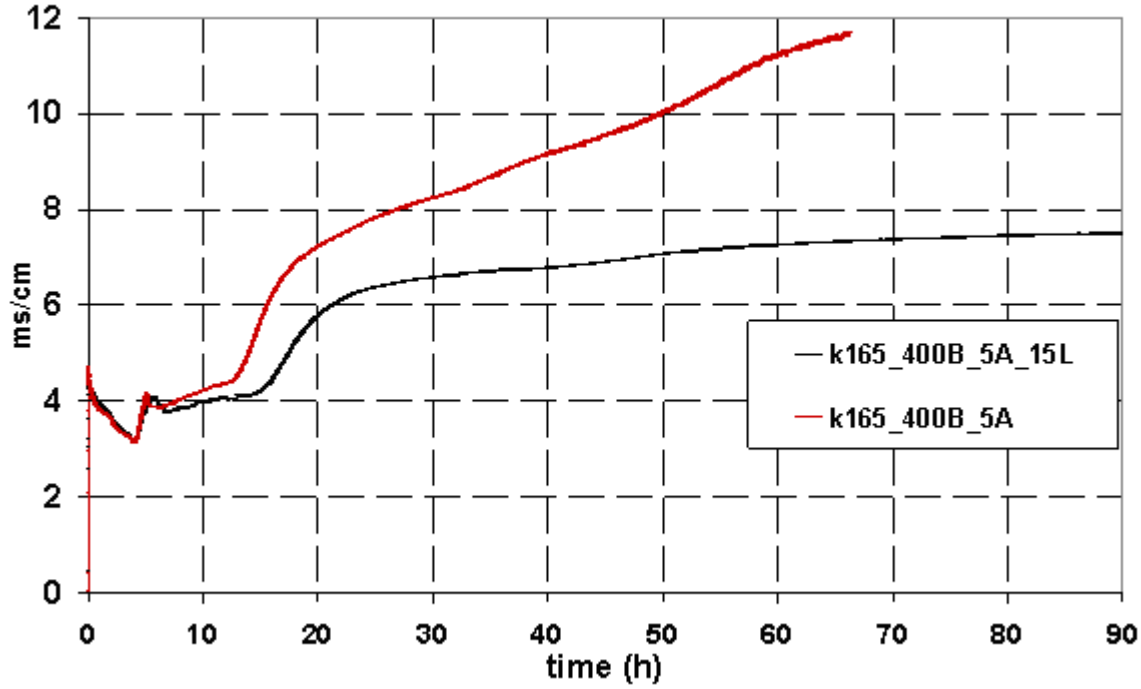

Figure 5-1: Electrical conductivity measured during the hydration of cements k165-400B-5A and k165-400B-5A-15L during 70 hours

In order to facilitate the reading, the major tables and figures of the results of cement k165-400B-5A-15L in suspension and in paste are shown at the end of this chapter. Tables 5-1 and 5-2 report the corresponding tables and figures in suspension and in paste respectively and also the corresponding ones for cement k165-400B-5A that will be used as reference.

W/C=5	Liquid phases		Solid phases		
	Major	Minor	anhydrous	major hydrate	minor hydrate
5A	Figure 3-2	Figure 3-3	Figure 3-4	Figure 3-5	Table 3-3
5A-15L	Figure 5-2	Figure 5-3	Figure 5-4	Figure 5-5	Table 5-3

Table 5-1: Figures and tables for the results of the hydration of cements k165-400B-5A and k165-400B-5A-15L in suspension

W/C=0.5	Solid phases		
	Anhydrous	major hydrate	minor hydrate
5A	Figure 3-6	Figure 3-7	Table 3-16
5A-15L	Figure 5-6	Figure 5-7	Table 5-4

Table 5-2: Figures and tables for the results of the hydration of cements k165-400B-5A and k165-400B-5A-15L in paste

5.1.1 Discussion of results

Step 1

The early hydration (before 4 hours for suspension and before 1 hour for paste) of cement k165-400B-5A-15L is similar to that of cement k165-400B-5A. The amount of anhydrite

declines to zero in parallel with ye'elimite consumption (from 28% to 15% in suspension, and from 28% to 16% in paste, relative to original mass of cement), while the consumption of belite is very slow (Figures 5-4 & 5-6). On the other hand, it seems especially for the suspension experiment, that ferrite is reacting slightly more in the presence of limestone. This point has to be made with caution as one can see that Rietveld estimates are not so precise when considering the amount of limestone that slightly increases both in paste and suspension experiments. At the same time, the amount of ettringite (Figures 5-5 & 5-7), the only crystalline phase identified by XRD, increases fast (from 0 to 20% in suspension and from 0 to 16% in paste).

The concentrations of the major chemical elements of the aqueous phase in suspension (Figure 5-2) show high sulphate, calcium and aluminium concentrations, 21mM, 12mM and 5mM respectively. This suggests a strong dissolution of anhydrite and ye'elimite once mixed with water. After that, sulphate and calcium concentrations decrease while aluminium concentration increases.

This fits well the step 1 of k165-400B-5A so limestone is not expected to have a strong effect on this step (Table 5-5).

W/C=5	Starting time	Ending time	Duration	W/C=0.5	Starting time	Ending time	Duration
5A	0H	4H	4H	5A	0H	1H	1H
5A-15L	0H	4H	4H	5A-15L	0H	1H	1H

Table 5-5: Starting and ending times and the duration of step 1 for the hydration of cements k165-400B-5A and k165-400B-5A-15L both suspension and paste

The same equations can be proposed as for k165-400B-5A to describe the reaction between ye'elimite and anhydrite:

$$C_4A_3\$ + 2C\$ + 38H \rightarrow C_3A.3C\$.H_{32} + 2AH_3 \text{ (amorphous)} \qquad (3.2)$$

Also, the reaction of alkali sulphate with ye'elimite can be written as (3.3).

$$C_4A_3\$ + 2[Ca^{2+}] + 2[SO_4^{2-}] + 38H \rightarrow C_3A.3C\$.H_{32} + 2AH_3 \qquad (3.3)$$

Belite or ferrite or both could be the calcium source, but the quantity is expected to be very small as they practically not react during this step. However limestone may have a slight effect on the ferrite hydration that seems to be not blocked as efficiently by sulphate: thus an interaction between ferrite and limestone has been added (interaction 12) to the major interactions already mentioned (paragraph 3.3 of chapter 3) (Figure 5-8).

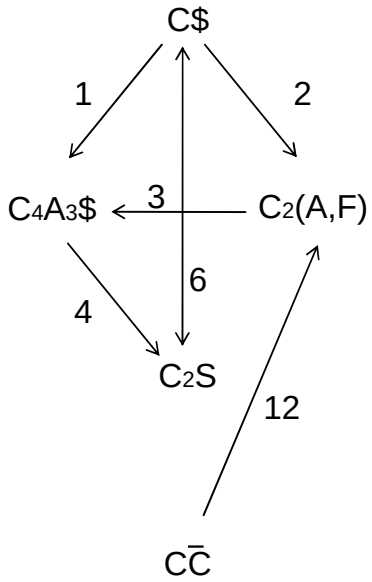

Figure 5-8: Major interactions between the involved phases in step 1 during the hydration of cement k165-400B-5A-15L

As discussed in step 1 of k165-400B-5A, ye'elimite hydration is accelerated by the presence of anhydrite (interaction 1). Belite is inhibited by the concentrations of both sulphate and aluminate (interactions 4 and 6).

Therefore, the effect of limestone on the early hydration of BCSAF is not significant. Step 1 ends when anhydrite is no more available in the system.

Step 2

When anhydrite is totally consumed in the suspension experiment, the sulphate concentration is high (15mM), then it decreases to zero quickly (Figure 5-2). At the same time, the amount of ye'elimite decreases from 16% to 5% and ettringite increases from 20% to 40% (Figures 5-4 & 5-5). The same phenomena can also be observed in paste experiment (ye'elimite passes from 15% to 7 %, Figure 5-6, and ettringite increases from 16% to 26%, Figure 5-7).

This can be explained by the equations proposed in Chapter 3:

$$C_4A_3\$ + 2[Ca^{2+}] + 2[SO_4^{2-}] + 38H \rightarrow C_3A.3C\$.H_{32} + 2AH_3 \quad (3.3)$$

After that, the hydration of ye'elimite slows down. Carbonated AFm is detected during this time, but the quantity estimated by Rietveld analysis is very small (Table 5-3). In paste experiment, calcium monosulfoaluminate cannot be detected at the hydration beginning, but some AFm carbonated phases are detected later after 2 days (Table 5-4).

Besides, the quantity of ferrite in both suspension and paste seems to decrease steadily, without any obvious sign for a coupled reaction with belite contrarily to what was observed without limestone (Figure 5-6). Therefore interaction 12 continues to be valid in this step. Moreover if we consider the duration of this step from the paste experiment (Table 5-6), the rate of reaction of ye'elimite is increased in the presence of carbonate. So we also have to consider an interaction between ye'elimite and calcite (interaction 11 on figure 5-9).

W/C=5	Starting time	Ending time	Duration	W/C=0.5	Starting time	Ending time	Duration
5A	4H	6.25H	2.25H	5A	1H	3D	3D
5A-15L	4H	9H	5H	5A-15L	1H	1D	1D

Table 5-6: Starting and ending times and the duration of step 2 for the hydration of cements k165-400B-5A and k165-400B-5A-15L both suspension and paste

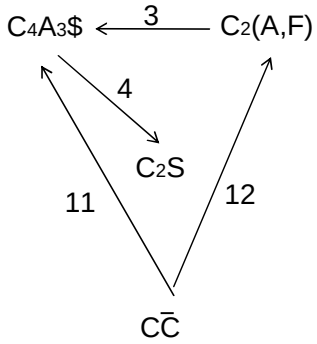

Figure 5-9: Major interactions between the involved phases in step 2 during the hydration of cement k165-400B-5A-15L

Interaction 11 (ye'elimite / calcite):
In the presence of $[CO_3]^{2-}$, small amounts of carbonated AFm phases may be formed in addition to the large amounts of ettringite and AH_3 (Table 5-4). This could slightly increase the rate of ye'elimite hydration and also free some sulphate ions useable to form ettringite. Therefore the reactions in this step can be proposed as:

$$C_4A_3\$ + 2[Ca^{2+}] + 2[SO_4^{2-}] + 38H \rightarrow C_3A.3C\$.H_{32} + 2AH_3 \quad (3.3)$$

$$C_4A_3\$ + [CO_3^{2-}] + 17H \rightarrow C_3A.C\overline{C}.H_{11} + 2AH_3 + [SO_4^{2-}] \quad (5.1)$$

Interaction 12 (ferrite / calcite):
Carbonate ions are also expected to react with the ferrite phase to form some carbonated AFm that may help an earlier restart of ferrite hydration or a less efficient blockage from the initially and rapidly formed ettringite.

Step 3

The main influence of limestone concerns step 3 corresponding to the start of belite hydration in order to precipitate C_2ASH_8 especially. This is especially true in the paste experiment: during which belite does not start to hydrate when ye'elimite is totally consumed (Figure 5-6) but some days are needed to start to nucleate C_2ASH_8. Indeed, strätlingite formation starts at around 9 hours in suspension (Figure 5-5) and at 7 days in paste (Figure 5-7). At this time, we can observe the decrease of belite. However, the rate of ferrite consumption seems to stay quasi constant until 5% is consumed. Then hydration of ferrite seems to be more coupled with belite one (Figures 5-4 & 5-6).

At longer times, strätlingite continues to increase, while ettringite stays stable and no hydrogarnet is observed in the paste even after eight months (Figures 5-5 & 5-7). At the same time, the electrical conductivity of k165-400B-5A-15L is found much lower than that of k165-400B-5A (Figure 5-1).

All the information tends to demonstrate that C_2S hydration is slower in the presence of calcite even if C_2ASH_8 is still the first hydrate that is formed: only 25% has reacted after eight months instead of 75% without limestone (after one year). Therefore, the effect interaction for k165-400B-5A should be modified in consideration of the effect of limestone on the nucleation of C_2ASH_8 that seems to delay it (Interaction 14 on Figure 5-10).

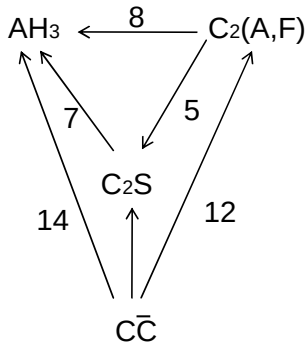

Figure 5-10: Major interactions between the involved phases in step 3 during the hydration of cement k165-400B-5A-15L

Several hypotheses can be raised to explain the effect of calcite on C_2ASH_8 nucleation. First, as ettringite is stabilised in the presence of calcite, and thus calcium monocsulfoaluminate hydrate is not formed, we can expect as said before to maintain for longer periods, higher sulphate concentrations that inhibit C_2ASH_8 nucleation. Second, the synergy between C_2S and ferrite is less efficient ferrite phase tends to form some carbonated AFm: thus it requires more calcium than providing some to the aqueous phase in order to enable the system to progressively reach higher pH and as a consequence precipitate hydrogarnet.

5.1.2 Complementary experiments done on pure phases

In order to assess further the effect of limestone on hydration of both belite and ferrite phases, some experiments have been carried out on mixtures made with pure phases:

- a belite doped with borax having a similar hydration kinetics as belite recovered by selective dissolution from K165 clinker (Annex 5-1),
- a ferrite phase having the brownmillerite composition (C_4AF) (Annex 5-2) and thus richer in aluminium compared to the ferrite phase of K165 clinker.

Two mixtures have been studied in suspension (W/C=5) and compared to pure belite:

1. 77% belite + 23% C_4AF
2. 70% belite + 20% C_4AF + 10% limestone

The experimental methods were similar as mentioned in 2.2, except that in consideration of limited materials, the experience was done a closed bottle containing 16ml of solution with a magnetic stirring to ensure the uniformity. Temperature was thermostated at 20°C.

Quantification of the solid phases by Rietveld estimates from XRD patterns has not been performed since some phases identified are not included into the database yet.

In order to facilitate reading, the major tables and figures of the results are also shown at the end of this chapter. Table 5-7 reports the corresponding tables and figures.

W/C=5	conductivity	Liquid phases	Solid phases
Belite+ferrite	Figure 5-11	Figure 5-12	Figure 5-13
Belite+ferrite+limestone		Figure 5-14	Figure 5-15

Table 5-7: Figures and tables for the results of hydration of mixtures of belite / ferrite and belite / ferrite / limestone in suspension

The change of the electrical conductivity was followed during 310 h (Fig 5-11). With limestone, the conductivity stays lower than that of the two others.

Hydration in suspension of a mixture containing 77%C_2S + 23%C_4AF

Figure 5-13 shows the solid phase evolution during the hydration of 77% C_2S + 23% ferrite. These relative amounts have been determined to have similar relative quantities than in clinker K165.

It is observed that belite hydration is slightly delayed by the presence of C_4AF.

The hydration of C_4AF that is not rapidly blocked by the presence of sulphate ions, provides some aluminate ions to the aqueous phase and thus delays slightly the hydration of C_2S as expected due to the effect of aluminate ions on C-S-H nucleation.

Nevertheless in this experiment, C_2S hydrates following the usual pathway by giving CH (portlandite) and certainly C-S-H. Portlandite precipitation is observed by the typical drop of the electrical conductivity associated with a decrease of calcium concentration (Figures 5-11 & 5-12) and also by XRD after 310 h (Figure 5-13).

Thus this experiment misses some of the interactions and especially the interaction between belite and AH_3 in the presence of sulphate ions to be able to reproduce the mechanisms of hydration in step 3 without limestone.

Hydration in suspension of a mixture containing 70% C_2S, 20%ferrite and 10% limestone

As the previous experiment without limestone, this experiment will lack of some of the major interactions to be representative of step 3 during the hydration of cement k165-400B-5A-15L. Nevertheless the addition of limestone has also a strong influence on this simpler system. Indeed in that case, belite hydration does not follow the same pathway as portlandite is not precipitated: this can be proven by the lower calcium concentrations that are reached (Figure 5-14). The different reaction pathway could be due to an increased reactivity of C_4AF with limestone knowing that belite hydration is active till the beginning of hydration. Thus contrarily to the case when sulphate is present, C_4AF hydration would not be blocked at the beginning in the presence of calcite when no sulphate is present in the aqueous phase.

The higher reactivity of C_4AF can also be observed by several iron containing hydrates that are precipitated: iron carbonate hydrate (suggested formula: $Ca_6Al_2Fe_2O_{12}CO_3(OH)$), calcium aluminium iron oxide carbonate hydroxide hydrate (suggested formula: $Fe_6(OH)_{12}CO_3$) can be found in 310 hours (Figure 5-15). Finally interestingly, thaumasite may be the only Si containing hydrate in this system.

5.2 Conclusions of Chapter 5

The mechanism of hydration of cement k165-400B-5A-15L with limestone can be summarized on Figure 5-16 in suspension and Figure 5-17 in paste.

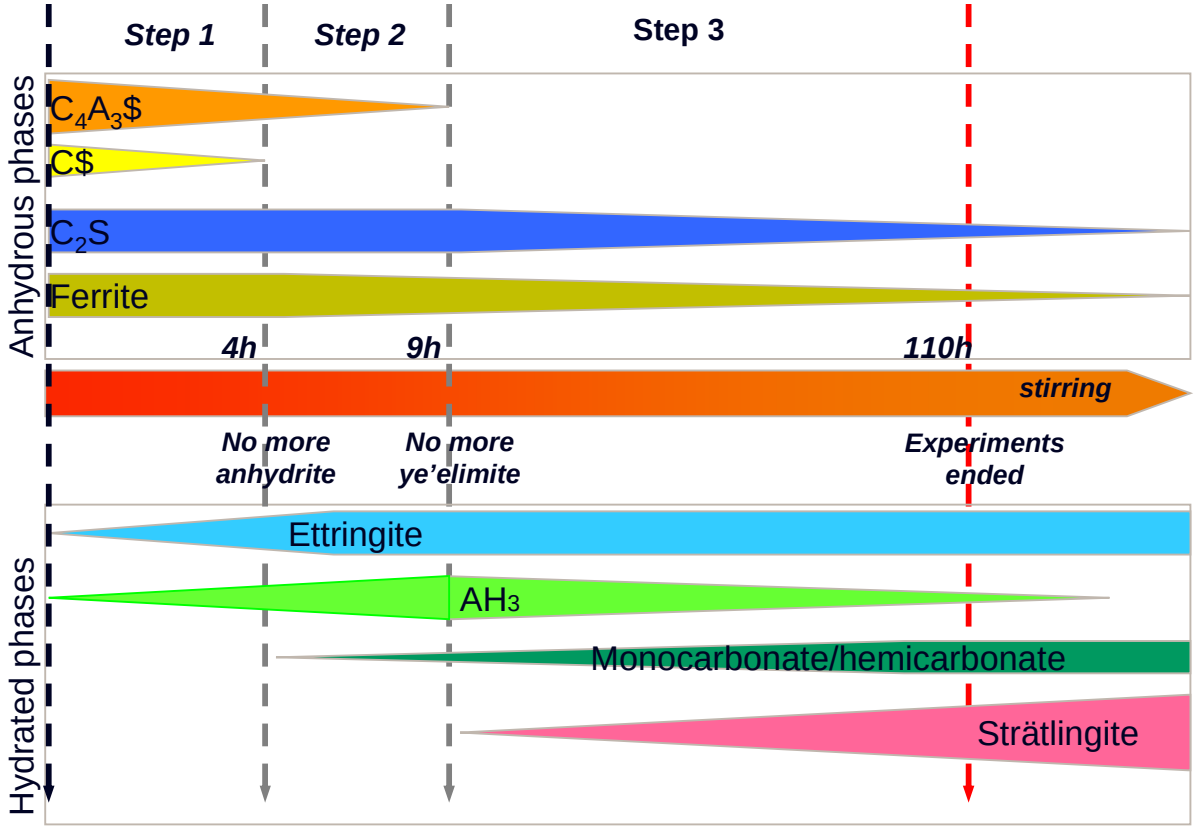

Figure 5-16: Steps observed during the hydration of k165-400B-5A-15L in suspension during 5 days

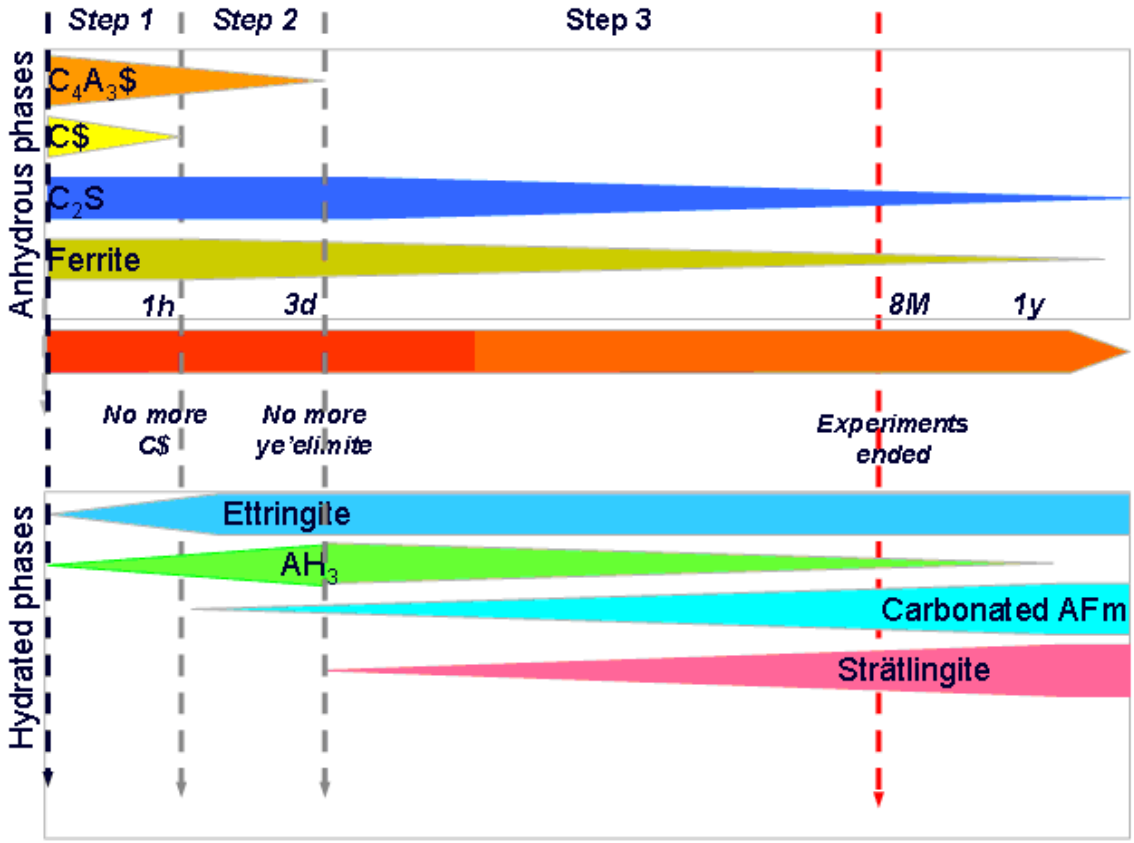

Figure 5-17: Steps observed during the hydration of k165-400B-5A-15L in paste during 8 months

The impact of limestone on the hydration of cement K165-400B-5A-15L was found to be quite different from that observed on the hydration of OPC. Indeed instead of a beneficial effect of limestone observed on OPC, a strong retarding effect is observed on step 3 during which C_2S starts to hydrate into C_2ASH_8.

The acceleration of ferrite hydration by limestone and as a consequence, carbonate AFm phase formation, can delay the occurrence of other hydrates, such as strätlingite, hydrogarnet and C-S-H. In order to make the limestone compatible with BCSAF cement, some retarders for ferrite phase, should be tested.

With the results, we can answer the question remaining in last chapter:

⇨ to check if limestone has an accelerator effect on belite hydration such in OPC,

- limestone does not have an accelerator effect on early belite hydration. On the contrary it delays the beginning of belite hydration as it retards C_2ASH_8 nucleation certainly by maintaining too high $[SO_4^{2-}]$ in relation of the stabilisation of ettringite by calcium monocarboaluminate hydrate at the expense of calcium monosulfoaluminate hydrate,
- Also by accelerating the ferrite hydration at the hydration beginning in precipitating calcium monocarboaluminate hydrate, but also at latter ages when all sulphate ions have been consumed, it reduces the synergy between belite and ferrite hydrations that enables the pH of the aqueous to increase. As a consequence, the later hydration of belite to form hydrogarnet and C-S-H (steps 4 and 5) is strongly delayed.

It has to be noticed that the quantities of carbonated AFm detected by XRD are less than expected from the previously described mechanism of hydration. The exact reason remains unclear but we may consider that the most probable hypothesis relies on badly crystallized phases.

Figures and tables of experimental results of k165-400B-5A-15L in paste and in suspension

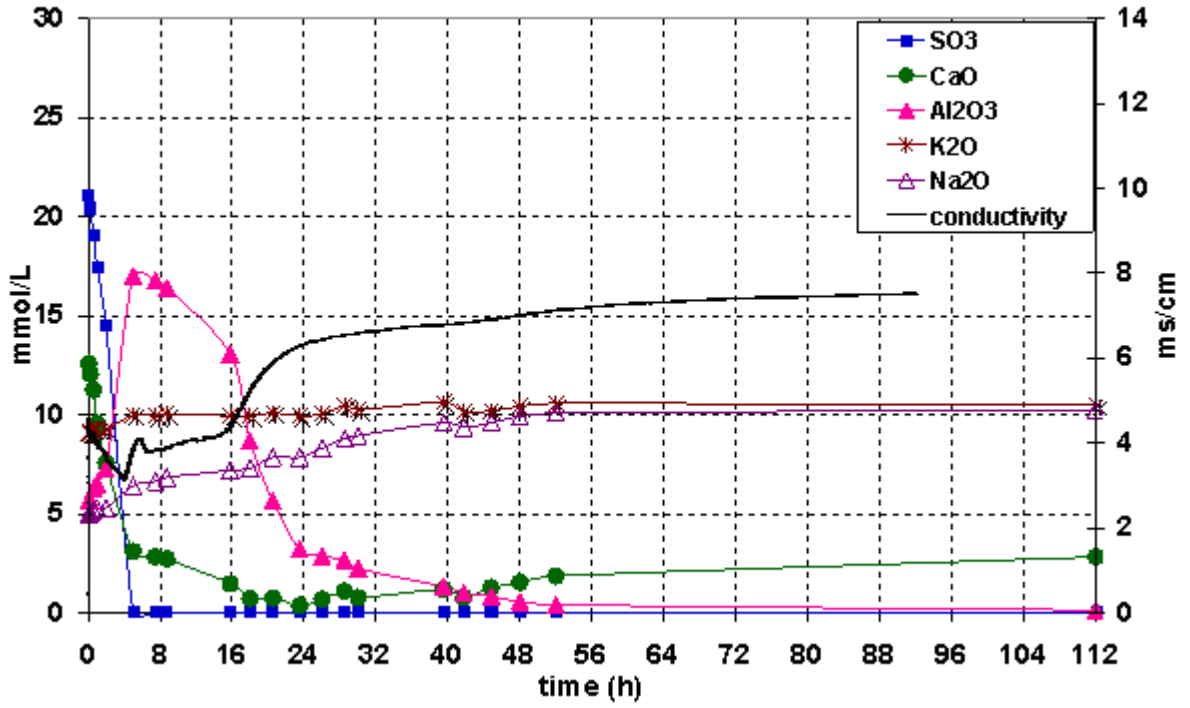

Figure 5-2: Electrical conductivity and major chemical elements of the liquid phase recovered during k165-400B-5A-15L hydration in suspension (w/c = 5) during five days

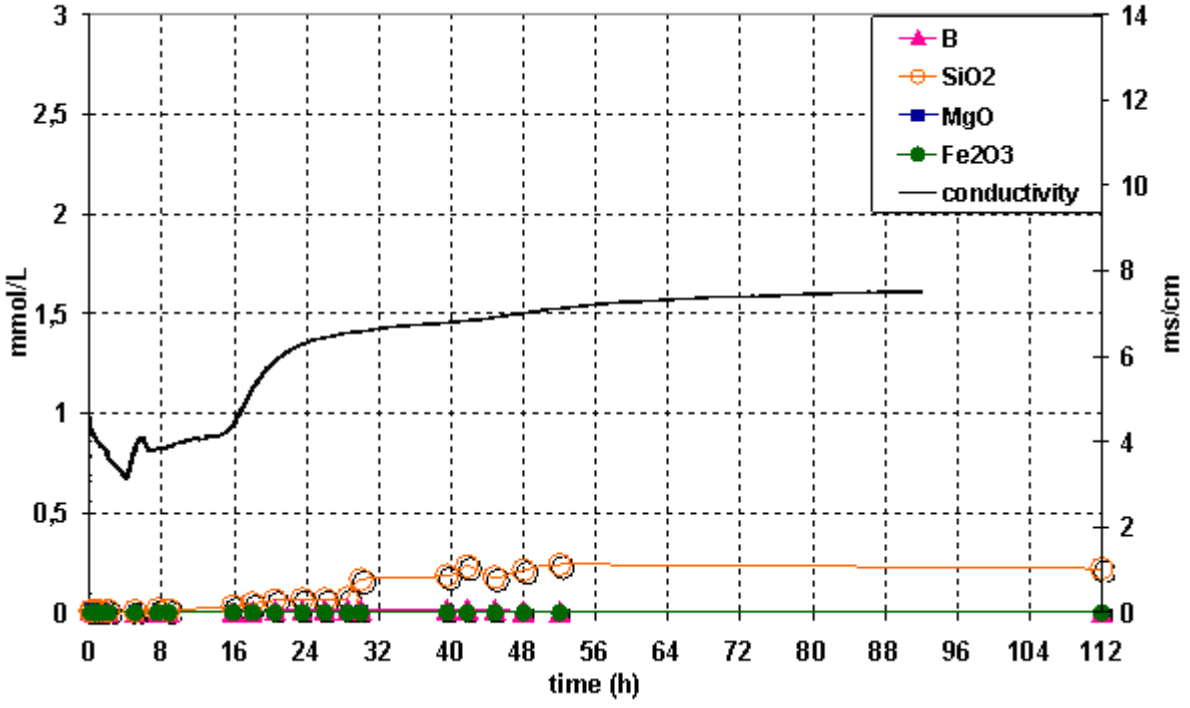

Figure 5-3: Electrical conductivity and minor chemical elements of the liquid phase recovered during k165-400B-5A-15L hydration in suspension (w/c = 5) during five days

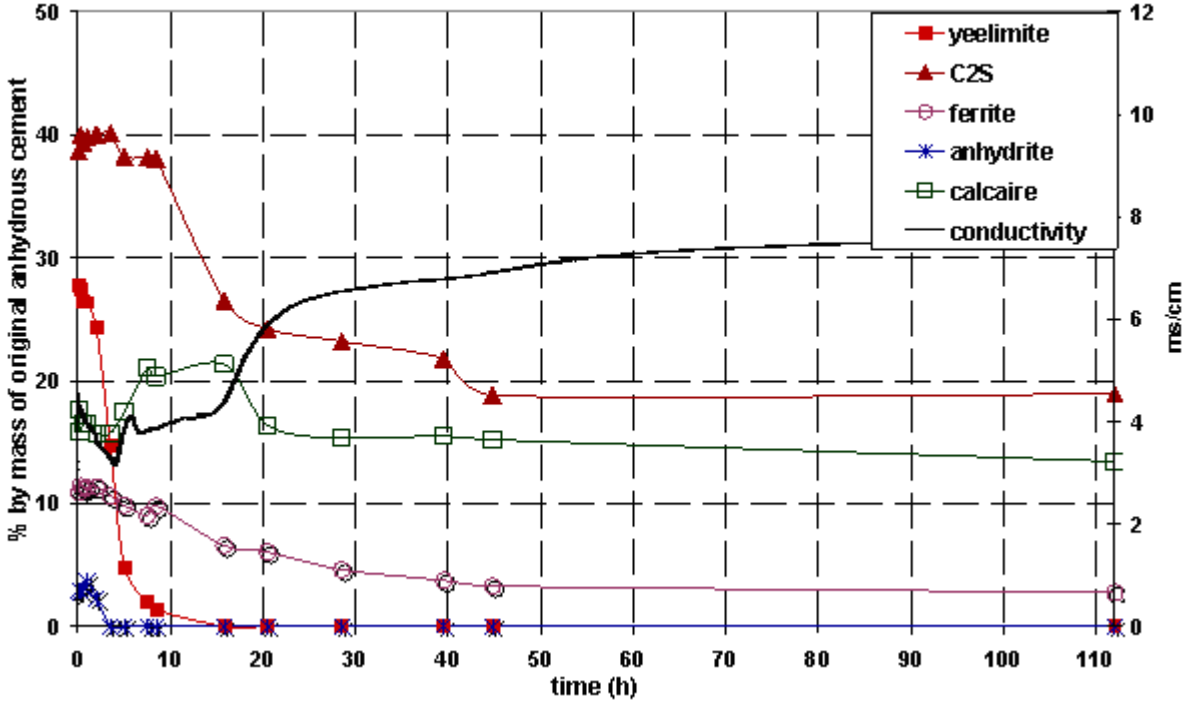

Figure 5-4: Electrical conductivity and normalised Rietveld estimates of anhydrous phases of cement k165-400B-5A-15L hydrated in suspension during five days, in % by mass of original anhydrous cement

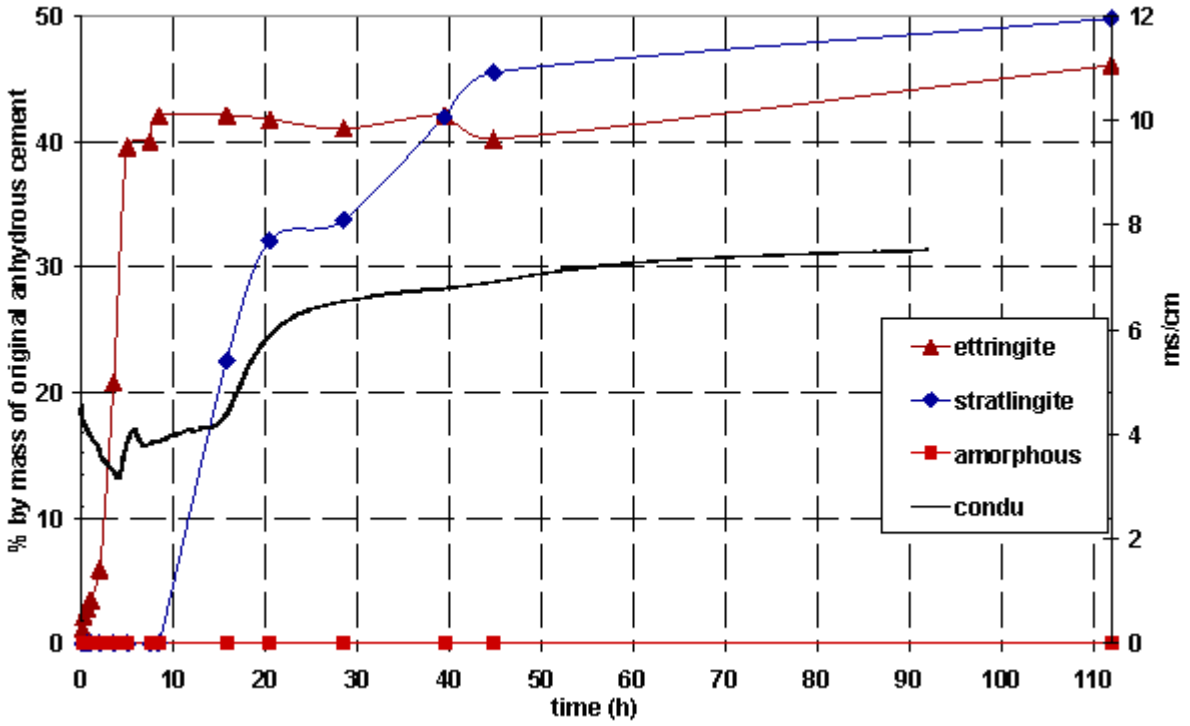

Figure 5-5: Electrical conductivity and normalised Rietveld estimates of major hydrate phases of k165-400B-5A-15L hydrated in suspension during five days, in % by mass of original anhydrous cement

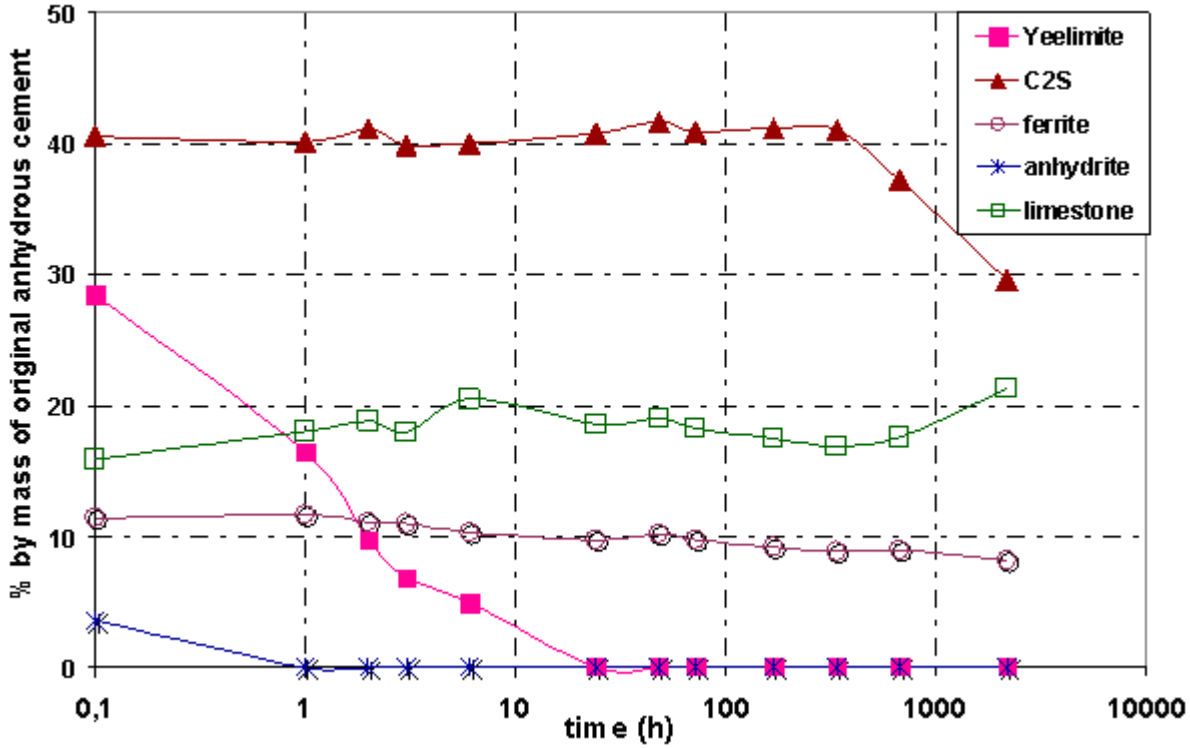

Figure 5-6: Normalised Rietveld estimates of anhydrous phases of k165-400B-5A-15L hydrated in paste during 8 months, in % by mass of original anhydrous cement

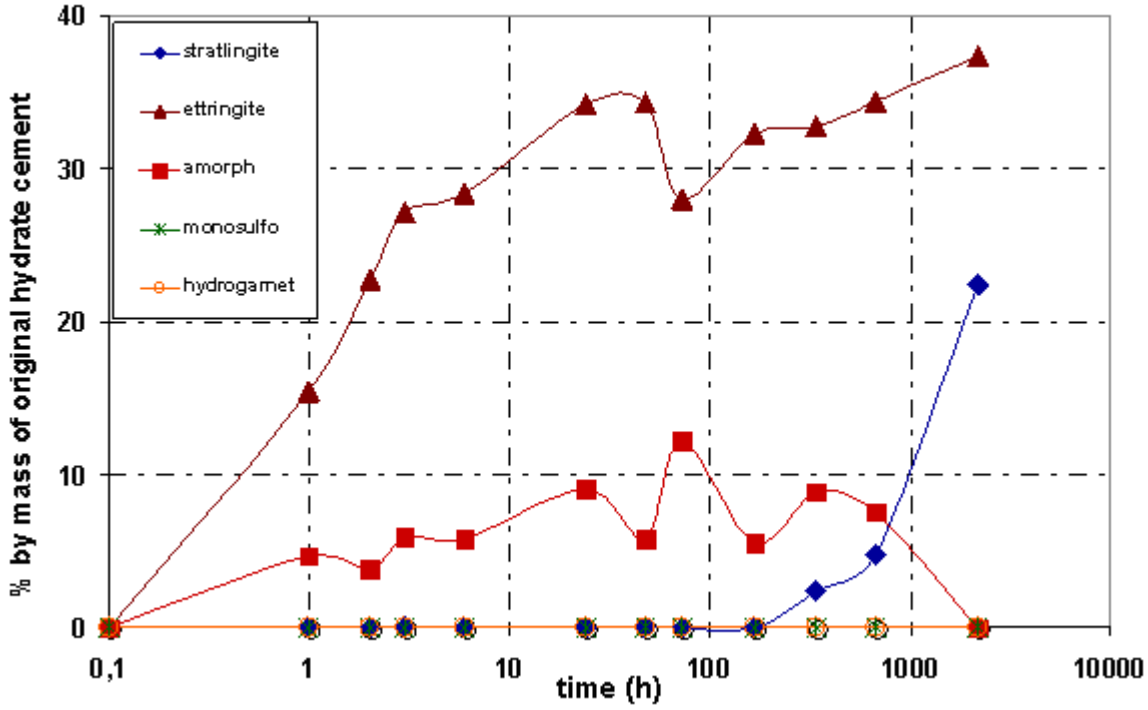

Figure 5-7: Normalised Rietveld estimates of major hydrate phases of cement k165-400B-5A-15L hydrated in pasted during 8 months, in % by mass of original anhydrous cement

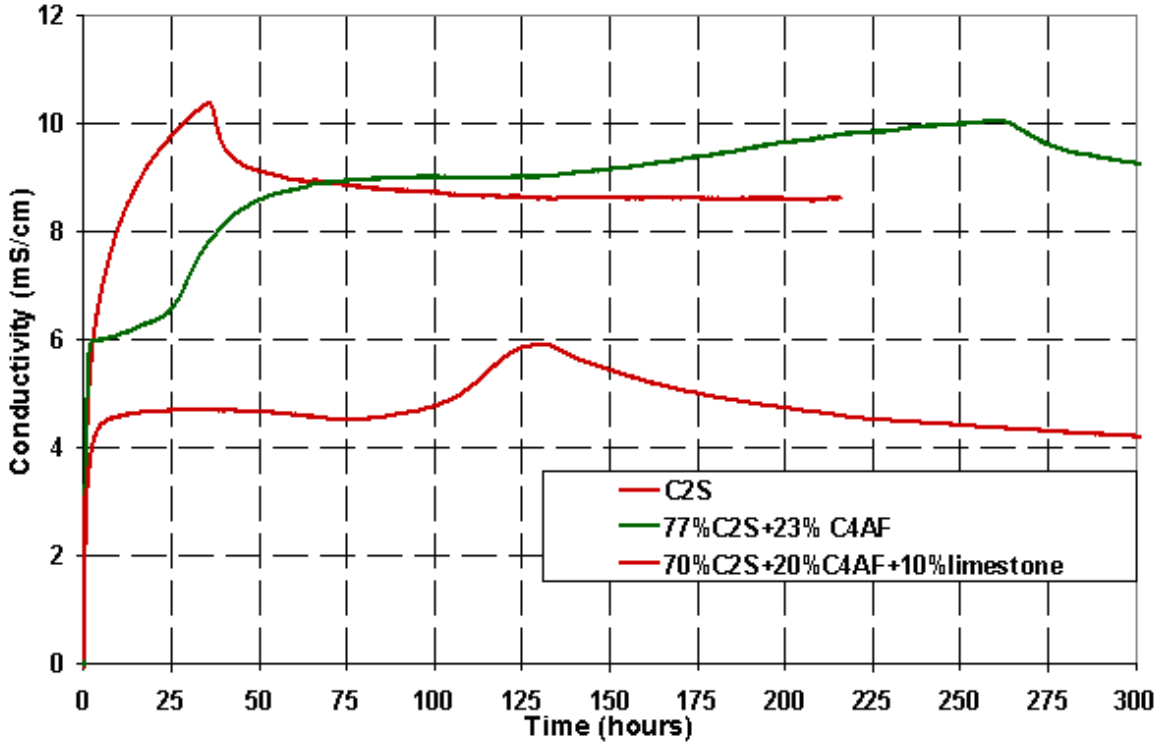

Figure 5-11: Change in electrical conductivity during hydration (W/C=5) of synthetic belite and mixtures made with it

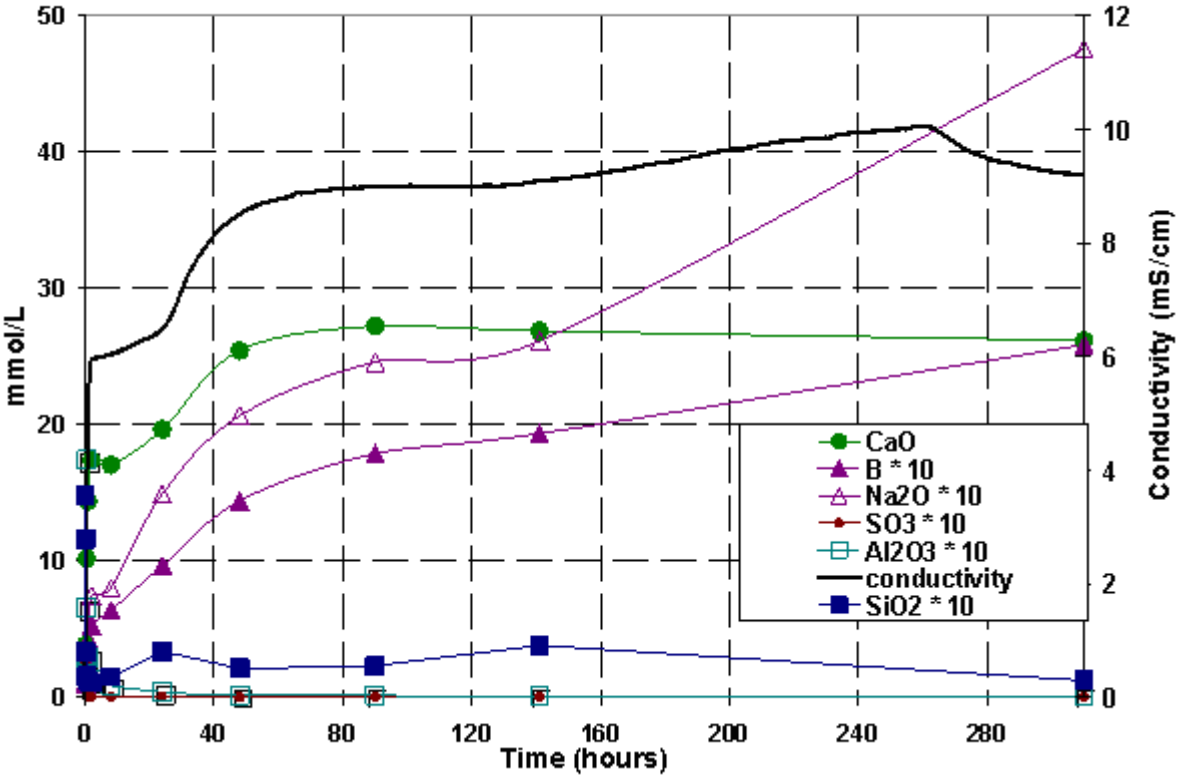

Figure 5-12: Electrical conductivity and major chemical elements of the liquid phase recovered during hydration of 77%C2S and 23%C4AF in suspension (w/c = 5) during five days

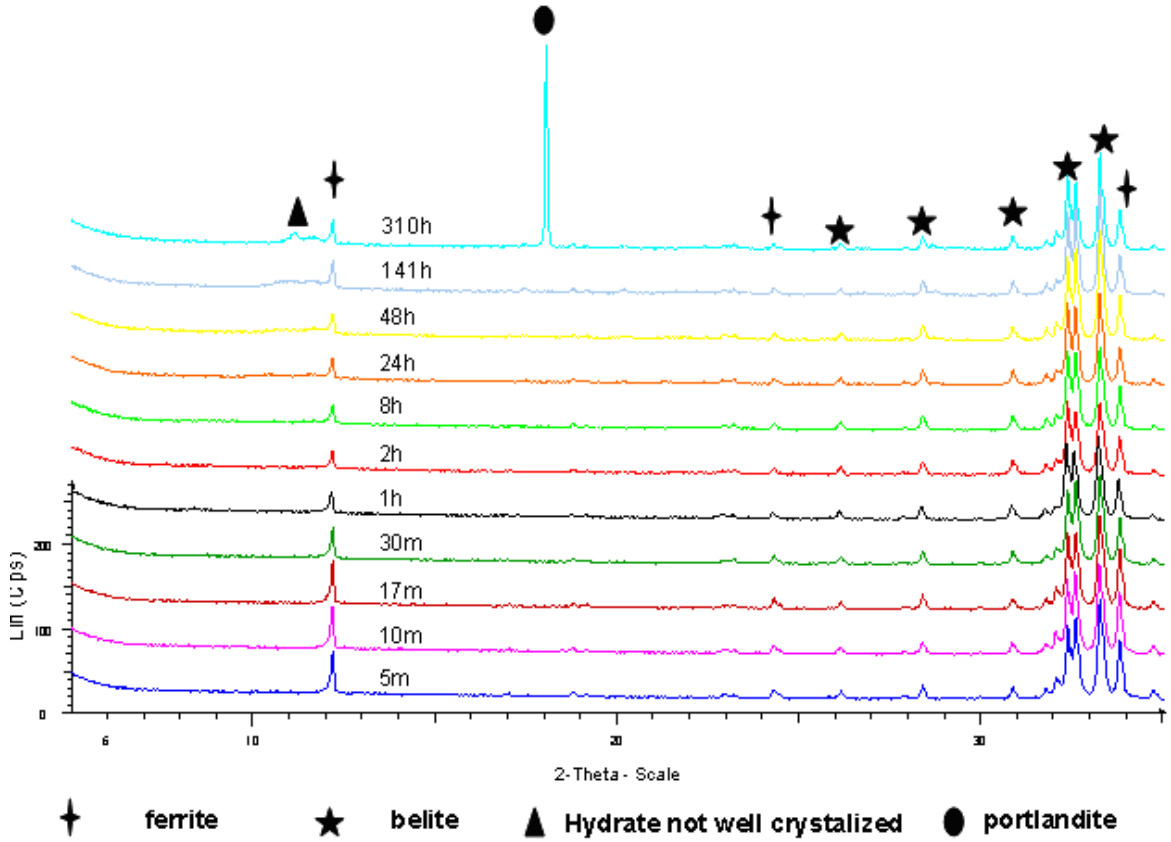

Figure 5-13: XRD patterns of the solids recovered during hydration of 77%C_2S and 23%C_4AF in suspension (w/c = 5) during five days

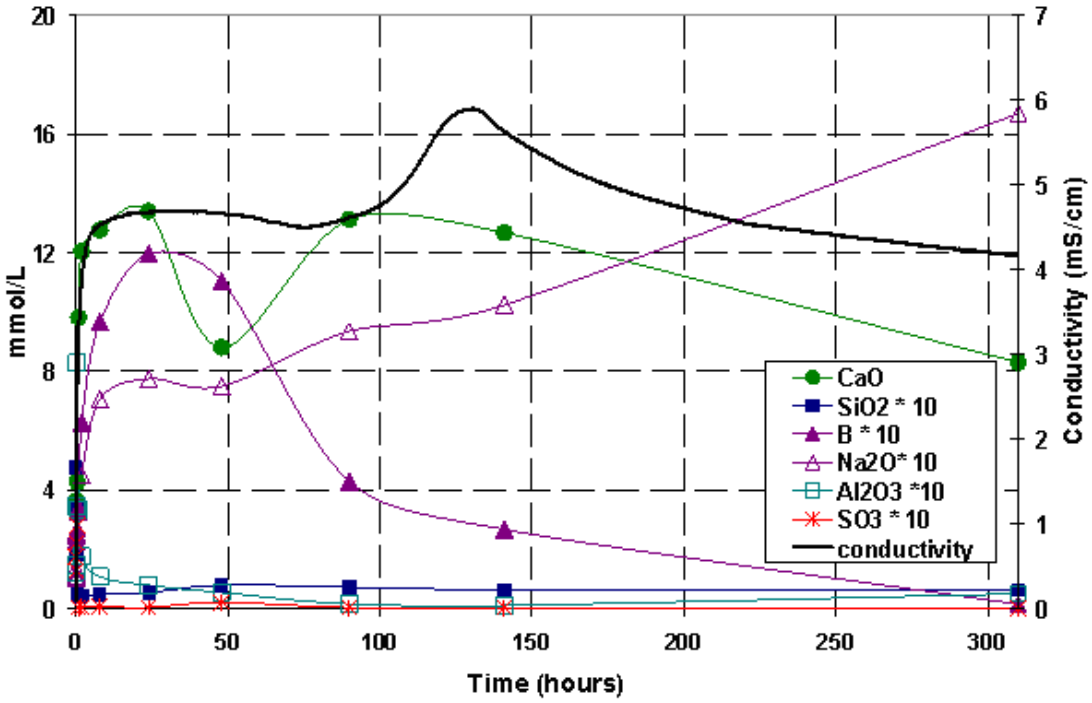

Figure 5-14: Electrical conductivity and chemical elements of the liquid phase recovered during hydration of 70%C_2S, 20%C_4AF and 10% limestone in suspension (w/c = 5) during five days

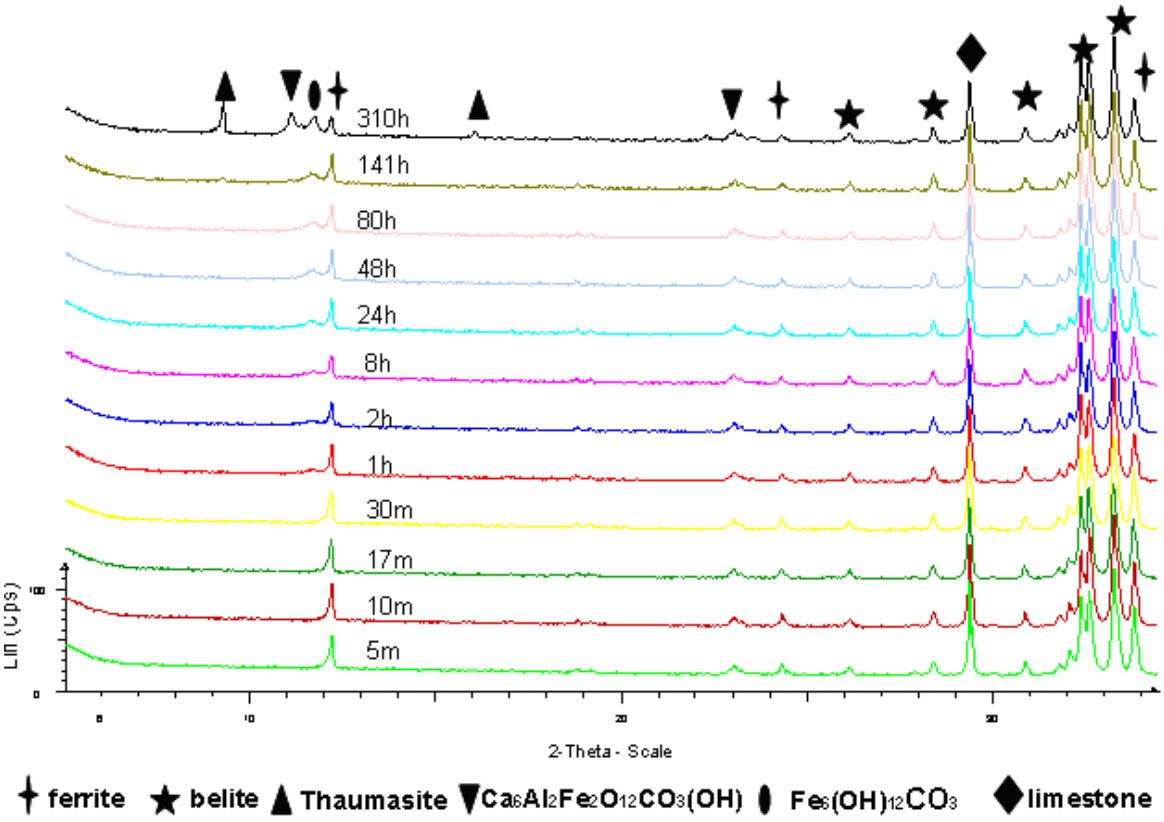

Figure 5-15: XRD patterns of the solids recovered during hydration of 70% C_2S, 20% C_4AF and 10% limestone in suspension (w/c = 5) during five days

	Minor hydrate phases						
Time	Strätlingite	Monosulphate	Hydrogarnet	Gibbsite	Hemicarbo	Monocarbon	Amorph
5m	0	0	0	0	0	0	0
15m	0	0	0	0	0	0	0
36m	0	0	0	0	0	0	0
1h	0	0	0	0	0	0	0
2h	0	0	0	0.1	0	0	0
3.5h	0	0	0	0.6	presence	0	0
5h	0	0	0	1.0	Presence	Presence	0
7.5h	0	0	0	1.0	Presence	Presence	0
8.75h	0	0	0	1.3	Presence	0.8	0
15.8h	22.5	0	0	0	presence	Presence	0
20.5h	32.1	0	0	0	Presence	Presence	0
28.5h	33.8	0	0	0	Presence	Presence	0
39.5h	41.9	0	0	0	Presence	Presence	0
44.85h	45.5	0	0	0	Presence	Presence	0
52h	46.7	0	0	0	Presence	Presence	0
112h	49.8	0	0	0	Presence	Presence	0

Table 5-3: Normalised Rietveld estimates of minor hydrates during k165-400B-5A-15L hydration in suspension for five days, in % by mass of original anhydrous cement

	Minor phases					
Time	Monosulphate	Hydrogarnet	Gibbsite	Carbonate	thaumasite	Amorph
0	0	0	0	0	0	0
1h	0	0	0	0	0	4.4
2h	0	0	0	0	0	3.6
3h	0	0	0	0	0	5.4
6h	0	0	0	0	0	5.3
1d	0	0	0	0	0	8.1
2d	0	0	0	1.4 (phase1)	0	5.1
3d	0	0	0	2.0 (phase1)	1.2	10.9
7d	0	0	0	3.0 (phase2)	0	5.1
14d	0	0	0	2.9 (phase2)	0	7.8
28d	0	0	0	4.4 (phase2.3)	0	6.6
3m	0	0	0	4.7 (phase1.2.3)	0	0

Table 5-4: Normalised Rietveld estimates of minor hydrates during k165-400B-5A-15L hydration in paste for 3 months, in % by mass of original anhydrous cement

Chapter VI

Conclusions and perspectives for future study

6. Conclusions and perspectives for future studies

With the results of chapters 3, 4 and 5, we can now answer with a good level of confidence, the five initial questions as follows:

1) to confirm that the main initial reaction is: $C_4A_3\$ + 2C\$ + 38H \Rightarrow C_6A\$_3H_{32} + 2AH_3$, whatever the content of C$

   - this is confirmed whatever the system studied even with 0% C$ as K165 contains alkali sulphate

2) to assess why and how does the quantity of the initial soluble sulfate influence the later hydration.

   - For C$ amounts less than the amount to react with all ye'elimite to form ettringite, different quantities of C$ do not change the mechanism of hydration: it makes steps 1 and 2 longer and thus it delays the beginning of C_2S hydration (step 3). Moreover the reaction rate in steps 3 and 4 (and may be 5) is slower.
   - For C$ amounts higher than the amount to react with all ye'elimite to form ettringite, the mechanism of hydration is changed: C_2S reacts till the beginning to form either a Si containing ettringite or C-S-H and thus it reacts earlier but more slowly.

3) to determine the parameters that control ferrite phase hydration,

   - C$ control ferrite hydration at the beginning by stopping it very rapidly at the beginning then it restarts as $[SO_4]^{2-}$ becomes very low.
   - Calcite reduces the blocking effect of C$ at the hydration beginning and may also accelerate ferrite hydration at later ages when the aqueous phase is sulphate depleted.

4) to determine the factors that control belite hydration and induce a retardation of its start,

   - This is the hydrate that nucleates that will control the kinetics and thus the "start" of C_2S hydration. In our systems at room temperature (at the exception of very high C$ contents i.e. k165-400B-20A), it is C_2ASH_8 nucleation rate that governs the hydration of C_2S. C-S-H does not form as the initial hydrate for belite hydration because it is not saturated in the beginning due to low calcium and silicon concentration and its formation is further delayed later by the inhibition effect of high aluminate concentration on C-S-H nucleation. The main parameter that governs the nucleation rate of C_2ASH_8 is $[SO_4^{2-}]$ that has to be low (of course [Al] has to be moderate but it is why C-S-H is not forming). As a consequence, this is indirectly the sulphate concentration that controls the beginning of belite hydration and thus the reactions leading to its reduction, mainly the hydration of ye'elimite to form ettringite. Globally it is once ye'elimite has been completely reacted that strätlingite may nucleate.
   - C_4AF can have a small acceleratory effect but after this initial step by taking into account a synergy between the reaction of belite and ferrite is found to accelerate the formation of later hydrate, hydrogarnet and C-S-H at the expense of strätlingite.

5) to check if limestone has an accelerator effect on belite hydration such in OPC,

- 15% of limestone added to a cement containing a low C$ amount, does not change the first period of hydration involving anhydrite and ye'elimite, but strongly delayed the beginning of the second period where both belite and ferrite hydrate. This may be due to a delayed nucleation of strätlingite induced by a longer period having higher $[SO_4]^{2-}$ as ettringite is stabilised by the precipitation of carbonated AFm at the expense of calcium monosulfoaluminate hydrate, thanks to the carbonate ions brought by limestone.
- By accelerating the ferrite hydration and enabling carbonated AFm phases to be formed, it reduces the synergy between hydrations of belite and ferrite. Thus it is likely htat the pH increase will be slower and thus that the beginning of steps 4 and 5, will be further delayed. As a consequence, the later hydration of belite to form hydrogarnet and C-S-H is strongly delayed.

Perspectives

This thesis represents the first detailed study of the hydration of a set of typical BCSAF cements based on a single clinker. The results show that the hydration mechanism of this new cement is very different than that of an OPC. In this respect, it particularly interesting to note that one of the principal initial hydrates of BCSAF cements, amorphous aluminium hydroxide, typically reaches a maximum concentration after only one or two days and then decreases again as its consumed to give other hydrates (principally, strätlingite). Similarly, strätlingite itself goes through a maximum and is finally largely replaced by katoite. Thus, it is important to study the hydration over very long periods of time to follow the full sequence of phase formation, and then to understand how this in turn affects microstructure and properties.

In order to improve on the work in this thesis, major improvements in well known quantitative phase-analysis techniques such as XRD-Rietveld and MAS-NMR are needed. The refinement of these techniques is difficult and time-consuming but is essential for progress.

An important finding of this work is that the hydration path completely changes when the amount of anhydrite added is greater than that needed to react with all ye'elimite in the clinker to give ettringite. We can therefore expect many other differences to occur with BCSAF cements of significantly different compositions to those studies here. This will be an important challenge to future researchers.

Durability issues are also bound to be very important in assessing the usefulness of this new class of cement. One effect that I believe is worth studying is the effect of short periods at elevated temperature at early ages, as might be expected, for example, in massive structures. Is there any risk of delayed ettringite formation, of the type known to occur with some Portland cements? Here the effects of the initial amount of anhydrite, and of soluble alkalis, are likely to be very important.

The ultimate objective of further research on BCSAF cement hydration should be to link the hydration mechanism to the final macroscopic properties via the microstructure.

Annexes

Annexes

Annex 2-1: X-ray fluorescence

Principle

X-ray fluorescence (XRF) is the emission of characteristic "secondary" (or fluorescent) X-rays from a material that has been excited by bombarding with high-energy X-rays. The phenomenon is used to determinate the elemental analysis (Si, Al, Fe, Ca, Mg, K, Na, S, Ti, Mn, P, Cr, Zr, Sr and other minor elements) in cementitious materials and raw materials.

Experimental procedure :

The samples are dried at 105°C and grounded until the size of particles is inferior to 100µm. About 3g of samples were heat at 950°C for 3 hours. Weigh the samples very quickly after ignition to prevent resumption of H_2O or CO_2, which would distort the result.

Then, the loss of ignition at 950 ° C could be expressed by:

$$\text{(\% by mass) LOI} = \frac{(M_1\text{-}M_2) \times 100}{(M_1\text{-}M_0)}$$

M_1 = mass of crucible in grams before calcination
M_2 = mass of crucible after calcination
M_0 = tare of crucible

After that, around 1.25g of residue is taken out, grounded and mixed homogeneously by a spatula with 11g of liquid mixture which is composed by 66% of lithium tetraborate ($Li_2B_4O_7$) and 34% of lithium metaborate ($LiBO_2$) by mass. Then, the solution of lithium bromide 466.7 g/L is added by a micropipette in order to avoid sticking in the crucible.

Then, the mixtures are put into the equipment 'Fluxer M4 CLAISSE' (Figure 2A1-1), heated around 1000°C and a pressed powder pellet was made. The pellet was analysed by the equipment 'BRUKER FX SRS3400'.

Figure 2A1-1: Equipment of fluxer M4 CLAISSE

The results obtained are in percentage of oxides by mass. Taken into account the loss on ignition, the final results could be calculated by the following formula:

Ex : $$\% SiO_2 = \frac{\% SiO_2 \text{ calcined} \times (100 - LOI)}{100}$$

Accuracy of results

In order to have more precise quantified results, the total percentage is always calculated. The value must be between 99.7% and 100.3% for cement and between 99.5% and 100.5% for other types of materials. Also, regularly, we compare the content of SO_3 with that measured by IR and the contents of K_2O and Na_2O with those obtained by ICP.

Also, the reproducibility of these analyses was tested on different samples by different operators each month. Here, we use the simple standard deviation, s:

$$s = \sqrt{\frac{1}{N-1}\sum_{i=1}^{N}(x_i - \overline{x})^2}$$ (where $\overline{x}$ is the mean value),

to estimate random measurement errors. Results are shown in Table 3A1-1 and Table 3A1-2:

Clinkers	SiO_2	Al_2O_3	Fe_2O_3	CaO	MgO	K_2O	Na_2O
Mean	21.09	5.26	1.91	64.72	2.5	0.69	0.14
Standard deviation(%)	0.14	0.06	0.02	0.25	0.04	0.03	0.05
Clinkers	SO_3	TiO_2	Mn_2O_3	P_2O_5	Cr_2O_3	ZrO_2	SrO
Mean	3.49	0.22	0.05	0.06	0.01	0.02	0.23
Standard deviation(%)	0.02	<0.01	<0.01	0.01	<0.01	0.03	0.02

Table 2A1-1: reproducibility of FX on clinker

Gypsum	SiO_2	Al_2O_3	Fe_2O_3	CaO	MgO	K_2O	Na_2O
Mean	3.35	0.55	0.26	31.11	3.27	0.09	0.03
Standard deviation(%)	0.05	0.01	0.01	0.11	0.02	0.02	0.01
Gypsum	SO_3	P_2O_5	Ba	SrO	TiO2	Cr ppm	Mn ppm
Mean	35.77	0.04	0.0065	0.29	0.03	14	59
Standard deviation(%)	0.24	0.01	3	0.01	0.01	2	3

Table 2A1-2: reproducibility of FX on gypsum

Here, gypsum was chosen for reproducibility tests instead of anhydrite, since analysis of gypsum have more errors (LOI of gypsum is around 20%).

Annex 2-2: ICP analysis

Principle

The analysis is done by atomic emission spectrometry ICP-AES (ICP: Inductively Coupled Plasma, AES: Atomic Emission Spectrometry). The sample is introduced into a source (plasma) whose role is to transform the sample into atomic and ionic vapour and excite the elements that constitute it. Electrons, increased to levels higher energy at the fundamental level, iron spontaneously at lower energy levels by emitting radiation that are specific. These rays are captured by a detector and can make qualitative and quantitative comparison with standards. The results obtained are expressed in percentage of oxides by mass, except P and B.

Experimental procedure

The liquid phases were acidified with HCl and diluted ten times. Then, the samples are analyzed by Varian 720-ES ICP equipped with a short torch axial piece, a nebulizer and cyclonic chamber. The experimental temperature is at 22 ± 2 °C.

Accuracy of results

The reproducibility of these analyses was tested on different samples by three different operators. Results are shown in Table 2A2-1:

	Si	Al	Fe	Ca	Mg	K	Na	S	P
Average (mg/L)	1.98	1.98	2	160	1.99	154.9	158.5	80.5	4
Standard deviation(%)	1.5	2.3	1.1	1	1.1	1	0.8	1.4	1.2

Table 2A2-1: reproducibility tests of ICP for Si, Al, Fe, Ca, Mg, K, Na, S, P elements

Calibration is also done each time before we start the experience (Table 2A2-2). Standard Plasmacal solution for each element is used.

	Si	Al	Fe	Ca	Mg	K	Na	S	P
Theoretical valeur (mg/L)	2	2	2	160	2	160	160	80	4
Errors (%)	1.01	1.01	<0.10	<0.19	0.5	3.29	0.95	0.62	<0.13

Table 2A2-2: calibration of ICP for Si, Al, Fe, Ca, Mg, K, Na, S, P elements

Annex 2-3: Rietveld estimates applied to clinker k165

Principle

The XRD can define the mineralogical nature of phases present in the solid. The principle is that a beam of X-ray penetrates the sample, and is then diffracted by crystalline plans of crystals contained in the sample. The angle of diffraction and the intensity of diffraction are characteristic of a crystalline structure. All lines of diffraction are used to identify the nature of crystals.

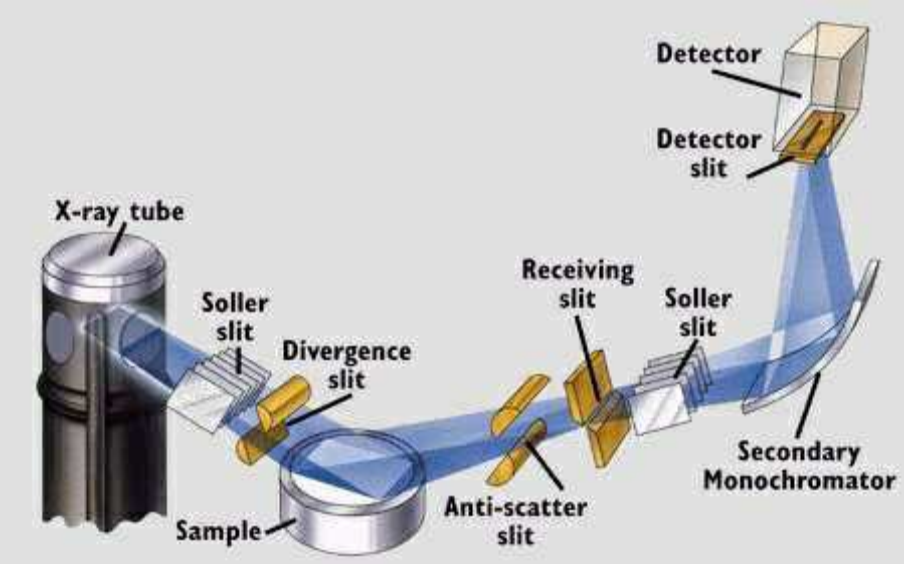

Figure 2A3-1: The principle of XRD

Quantified analyse with Rietveld method:

Rietveld method is currently the most effective procedure for analyzing powder diffraction data, when the structure of constituent phases in the sample is known. Depending on the control file used, a theoretical diffractogram is calculated. This is compared with the experimental diffractogram is "refined" by variations of many parameters such as intensity, the positions of some diffraction peaks, the modeling of the baseline, etc. The refinement stops when the difference between the diffractograms reaches its optimum.

Generally, the intensity of the ith point of the diffractogram can be expressed by:

$$\mathbf{I_i = I_{background} + S_h \Sigma S_n Y_n}$$

where S_h is the global histogram scale factor, S_n is the scale factor of the n crystalline phases, and Y_n presents the structure factor, the profile functions, the intensity correction factors, etc.

The weight percentages of phases present in the control file are calculated. The values are relative (the total is equal to 100%). If we know the quantity of phase n, then S_n / the volume of the crystalline phases = const. Given that $Y_n = X_n/V_n$, where V_n is the unit cell volume of phase n, we can get that: S_n / the number of unit celles = const. In fact, there is proportional constant between the scale factors and the calculated weight fractions:

$$K_i = \rho_i / \Sigma S_n \rho_n$$

Therefore, the weight fractions of the ith crystalline phases can be calculated as: $W_i = (S_i \rho_i)/\Sigma S_n \rho_n$, where ρ is the density of the ith phase.

To calculate the amorphous phases, we assume that in the beginning of hydration, there are no amorphous phases. The constant K calculated for the first diffractogram can be used to reconvert the scale factor of the ith phase in the jth diffratogram to a weight fraction Wj. The amorphous content is estimated as:
Wamorphous = 1 – Wj/Wi

Rutile TiO_2 is chosen both as internal and external standard since its peaks do not superimpose other crystalline phases. Here, internal standard means calculating with the diffratogram of the mixture of our sample and known quantity (eg. 20% by mass of mixture) of TiO_2, while external standard means calculating with the diffratogram which is combined with the diffratogram of known quantity (eg. 20% by mass of mixture) of TiO_2 and that of our sample. In order to avoid the problem introduced by grounding and to improve the efficiency of experiments, we use mostly external standard. Internal standard is only used to compare with the results of external standard.

Experimental procedure

The sample is grounded in a porcelain mortar until that all the powder passed through sieve < 100 microns. A pressed powder pellet (around 10g materials) was made and analysed by the equipment of Philips X'pert (Figure 2A3-2). The experimental temperature is at 22 ± 2 °C.

Figure 2A3-2: The equipment of XRD (Philips X'pert)

Accuracy of results

The reproducibility of these analyses was tested on one sample for ten times. The results are as following. Results are shown in Table 2A3-1:

phases anhydres	$C_4A_3\$$	belite	α'C2S	α'L C_2S	α'H C_2S	C_4AF	$C_{12}A_7$	C_2AS	merwinite
k165a (%)	33.0	3.2	45.0	3.9	0.0	13.8	0.0	0.7	0.4
k165b (%)	32.9	3.1	44.9	4.1	0.0	14.2	0.0	0.5	0.3
k165c (%)	33.4	2.9	44.0	4.0	0.0	13.9	0.0	0.9	0.8
k165d (%)	32.8	3.1	44.9	3.9	0.0	13.8	0.0	0.6	0.8
k165e (%)	32.8	3.2	45.1	3.9	0.0	14.2	0.0	0.6	0.3
k165f (%)	33.3	3.3	43.7	3.3	1.0	14.0	0.0	0.6	0.7
k165g (%)	33.0	2.8	45.2	4.0	0.0	14.1	0.0	0.6	0.3
k165h (%)	33.0	3.3	44.4	4.3	0.0	13.5	0.0	0.8	0.8
k165i (%)	33.2	3.3	45.3	3.9	0.0	13.7	0.0	0.5	0.2
k165j (%)	33.0	2.8	44.7	3.9	0.0	14.2	0.0	1.0	0.5
Mean (%)	33.0	3.1	44.7	3.9	0.1	13.9	0.0	0.7	0.5
Standard deviation(%)	0.2	0.2	0.5	0.3	0.3	0.2	0.0	0.2	0.2

Table 2A3-1: reproducibility tests of Rietveld calculation for k165

Here, C_2AS and merwinite is estimated less than 1 %. Meanwhile, in the diffratogram, there is no obvious corresponding peak (2 Theta of C_2AS and merwinite, respectively, 32.72° and 35.22°), therefore, we estimate that the quantity of two phases equals zero (Figure 2A3-3).

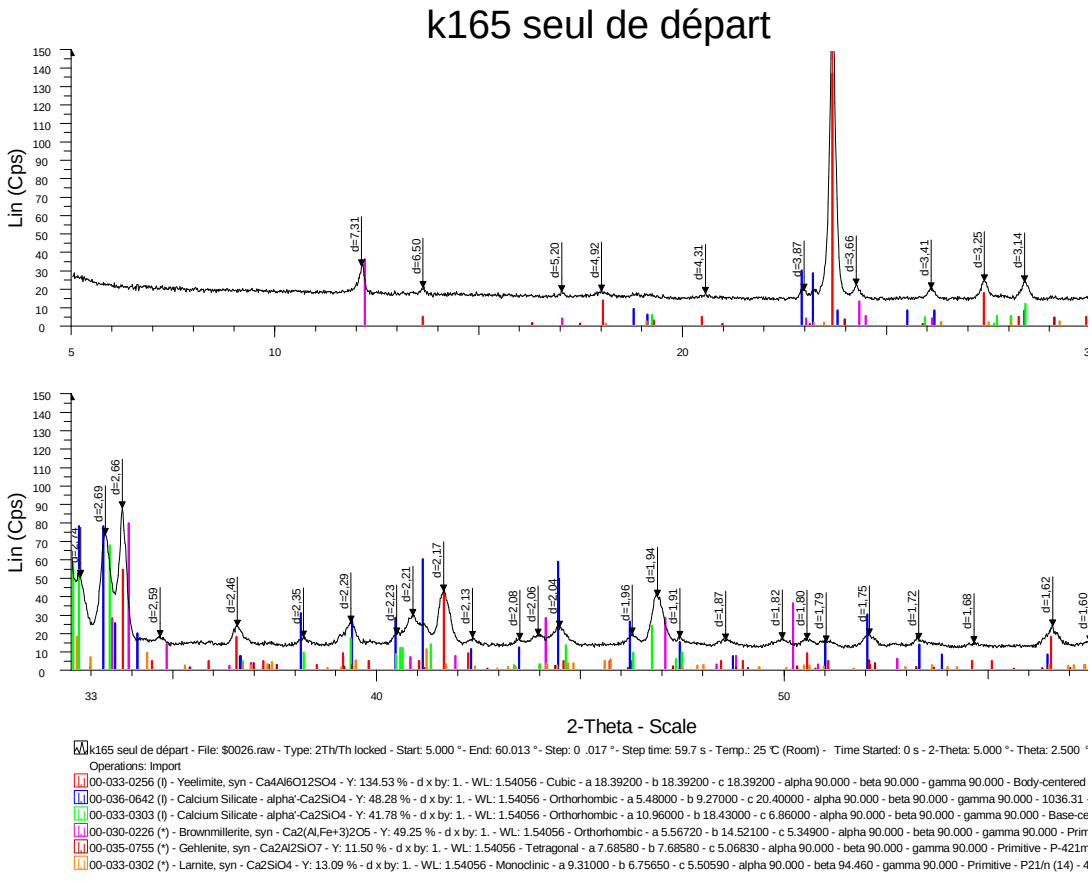

Figure 2A3-3: XRD pattern for clinker k165

Annex 2-4: FEG-SEM

Principle

The scanning electron microscope (SEM) is a type of electron microscope that images the sample surface by scanning it with a high-energy beam of electrons in a raster scan pattern. The electrons interact with the atoms that make up the sample producing signals that contain information about the sample's surface topography, composition and other properties such as electrical conductivity.

A field emission gun (FEG) is a type of electron gun in which the emitter tip is held at several kilovolts negative potential relative to a nearby electrode, so that there is sufficient potential gradient at its surface to cause field emission of electrons.

In field Scanning Electron Microscope (SEM), a field emission gun (FEG) is used to produce an electron beam that is smaller in diameter, more coherent and with up to three orders of magnitude greater current density or brightness than can be achieved with conventional thermionic emitters such as tungsten or lanthanum hexaboride (LaB6)-tipped filaments. The result in both scanning and transmission electron microscopy is significantly improved signal-to-noise ratio and spatial resolution, and greatly increased emitter life and reliability compared with thermionic devices.

Our experiences of SEM-FEG are mainly done in “Ecole des Mines de Douai”. The sample was stuck for the fracture observation and the sample was polished with diamond slurry after impregnation in an epoxy resin for the polished section. For both cases, a carbon film is covered on the surface of samples to make them conductive to get better results.

The working conditions were noted in the bottom of the image: electron accelerating voltage (kV), working distance (WD), the magnification and the scale.

Annex 2-5: Selective dissolution to remove the aluminate phases

The selective dissolution undergoes by the three following steps:

- remove aluminates by selective dissolution
- remove the remaining sucrose and decompose hydrate phases (eg CSH) by heating at 1000°C
- eliminate the free lime formed by calcination of hydrates.

These steps can be detailed as below:

Step 1:

The clinker is grounded around 400m²/kg Blaine.

A solution composed of 150ml demineralised water, 20g KOH and 20g sucrose is heated to 95°C with stirring in a 500 ml beaker with a glass cover. After around 30 minutes, it becomes brown-yellow. Then add 10g of clinker powder and keep stirring for 1 hour (55 minutes may be sufficient).

After that, filter the solution with Whatman system (Whatman filter with diameter 90mm with Teflon support). During the filtration, keep the temperature of the mixture high enough to ensure that the sucrose doesn't freeze.

Once the filtration is finished, continue to add minimum volume of water to eliminate the sucrose. Then, rinse twice with 100ml of isopropyl alcohol to remove water. When the samples become sec, get the residue and mash it to break the agglomerated particles with a spatula.

Step 2:

Hydrate (mainly CSH) could be formed during the dissolution of aluminate phase by reaction between the silicate phases and water. These hydrates decompose into free lime by heating at into 1000°C in a crucible in an oven for one hour.

After one hour, turn off oven, and wait about 10 minutes until the temperature drops to 400°C. Then take out the crucibles from the oven and place on steel tanks located near the oven.

Step 3:

Mash with a spatula to break up agglomerated parties.

Mix the residue with 100ml of ethylene glycol in a 500 ml beaker, cover with glass cover and heat at 110°C for 30 minutes, then filter with Whatman system. After that, rinse three times with 100 ml of ethanol. Evaporate the solvent up under the hood. Then get the powder without taking off the pull of piece of filter paper and mash with a spatula to break up agglomerated parties.

Verification of results by XRD:

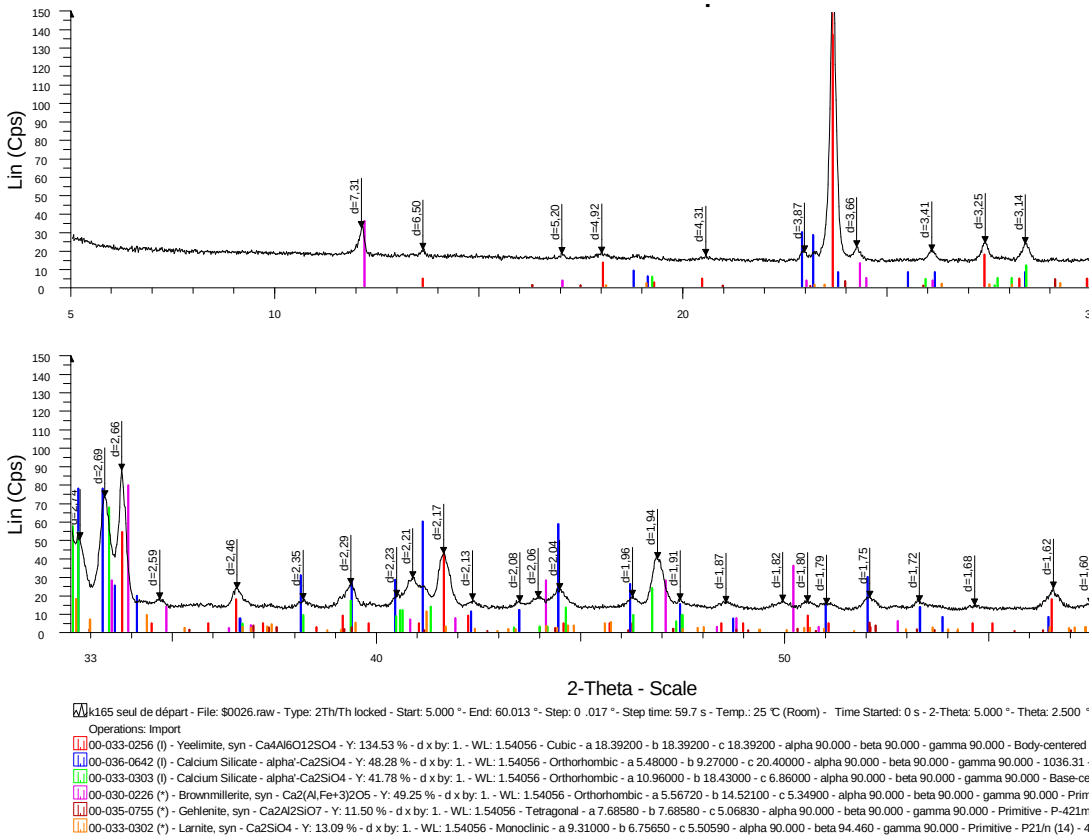

Figure 2A5-1: XRD patten for clinker k165

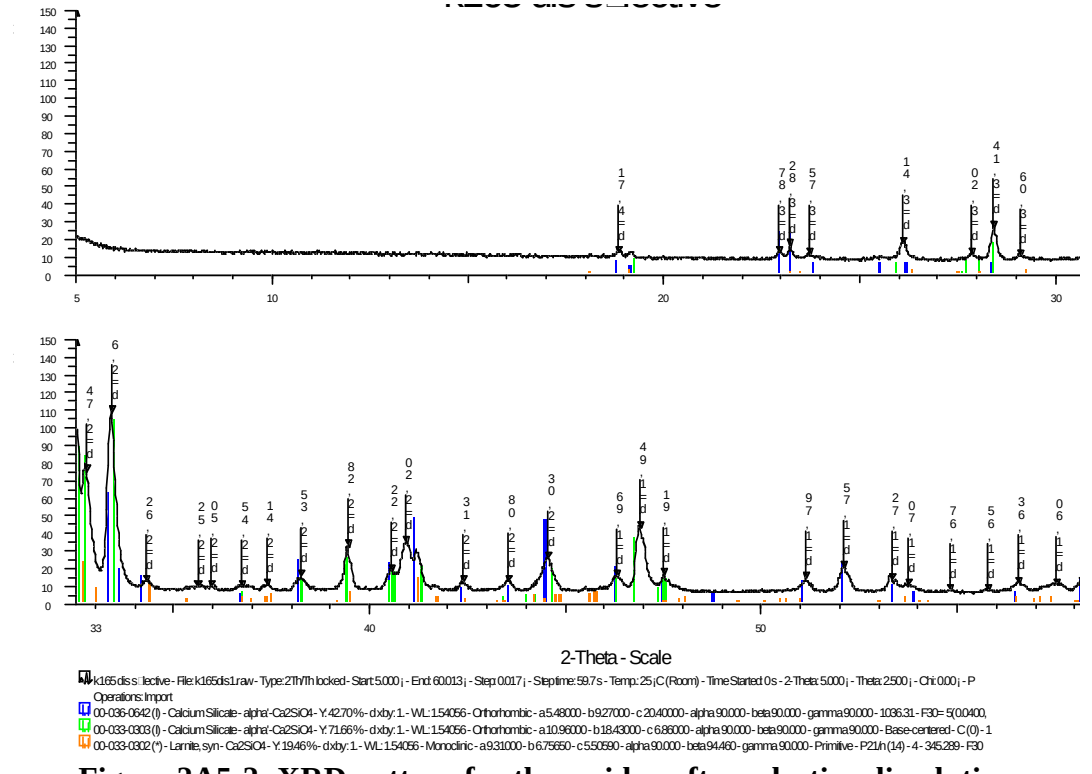

Figure 2A5-2: XRD pattern for the residue after selective dissolution

In comparing the XRD pattern of clinker k165 and the residue after selective dissolution, we can see that $C_4A_3\$$ (2 Theta = 23.6°) and ferrite (2 Theta = 12.2°) are completely gone and there are no hydrates (ettringite, 2 Theta = 9.08°) formed during the operation.

Figure 2A5-3 and Figure 2A5-4 shows a backscattered electron image of a polished section of the clinker and the residues after selective dissolution obtained using a FEG-SEM.

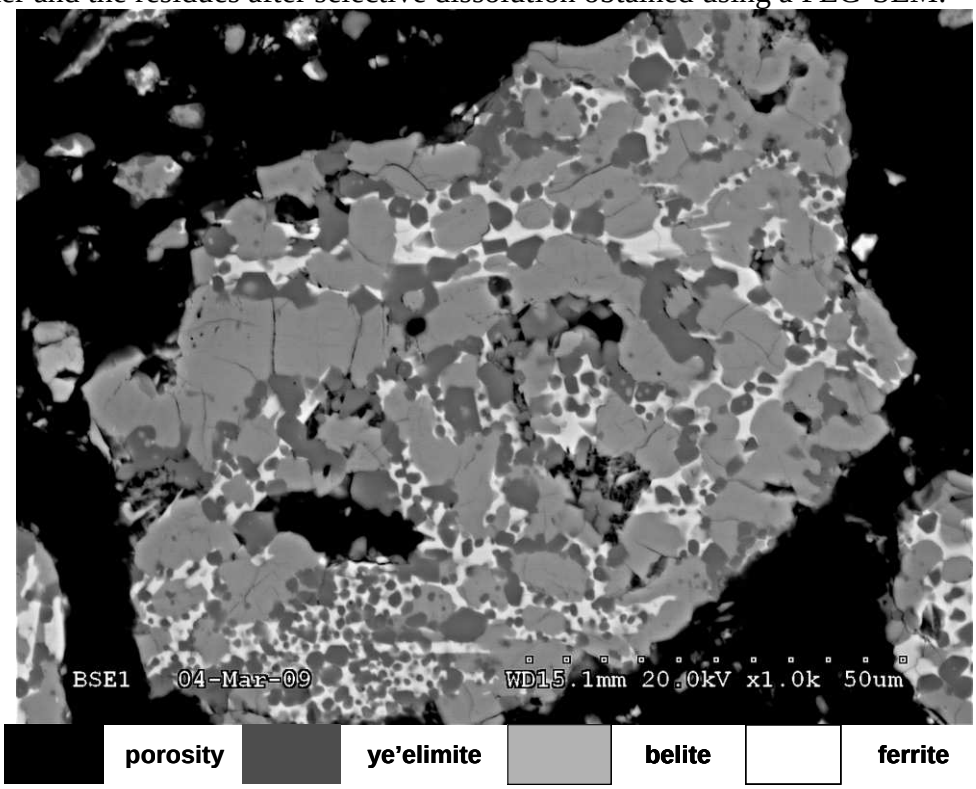

Figure 2A5-3: Typical FEG-SEM BSE image of clinker k165

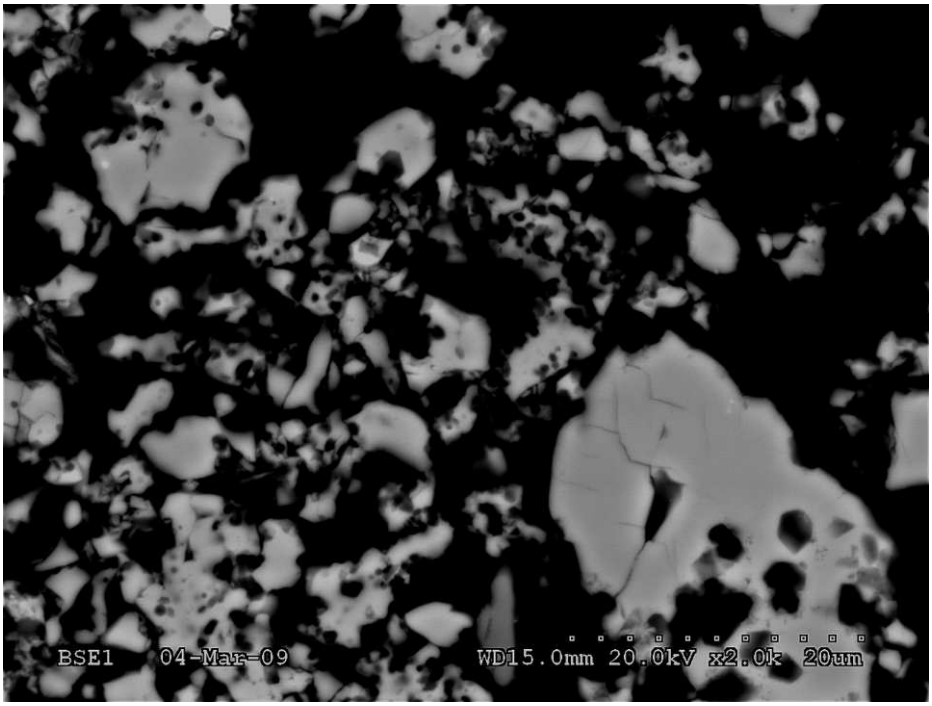

Figure 2A5-4: FEG-SEM BSE image of residue after selective dissolution

We can see that only one phase remains after the selective dissolution. Further discussion of analytical results is done in 2.1.1.1.

Annex 2-6: selective dissolution to remove C2S and ye'elimite

The selective dissolution undergoes by the three following steps:

- selective dissolution to remove silicate phases
- selective dissolution to remove ye'elimite
- heat at 1000°C to decompose the hydrate $CaCO_3$ into CaO
- eliminate the free lime by filtering with ethylene glycol.

Four steps can be described and detailed below:

Step 1:

Prepare the mixture with 10g of clinker powder, 130 ml methanol and 60g salicylic acid. Then stir the mixture in a 500 ml beaker with a glass cover for around 50 minutes.

After that, filter the mixture with Whatman system (Whatman filter with diameter 90mm with Teflon support). Analyse of XRD shows that silicate phase is totally removed from the clinker.

Step 2:

With the residue taken from step 1, prepare the mixture with the solution of 5% Na_2CO_3. The ratio is 1g solution with 60ml solution. The mixture is stirred for 15 minutes, and filtered with Whatman system. Then, rinse three times with the solution of ethanol and water (volume ratio=1:1).

Take the solid residue when it is sec.

Step 3:

The residue of sample is heated at 1000°C for 1 hour. Mix the residue with 100ml of ethylene glycol in a 500 ml beaker, cover with glass cover and heat at 110°C for 30 minutes, then filter with Whatman system. After that, rinse three times with 100 ml of ethanol. Evaporate the solvent up under the hood. Then get the powder without taking off the pull of piece of filter paper and mash with a spatula to break up agglomerated parties.

Verification of results by XRD

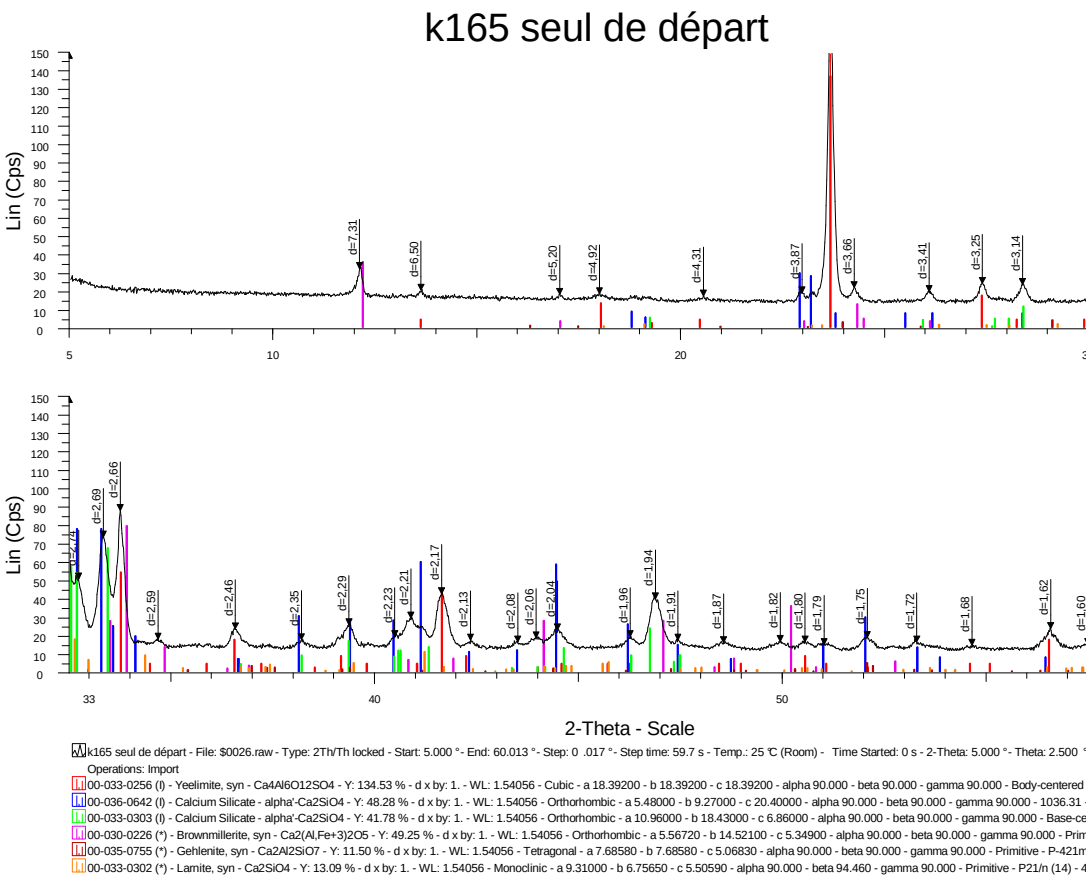

Figure 2A6-1: XRD pattern for clinker k165

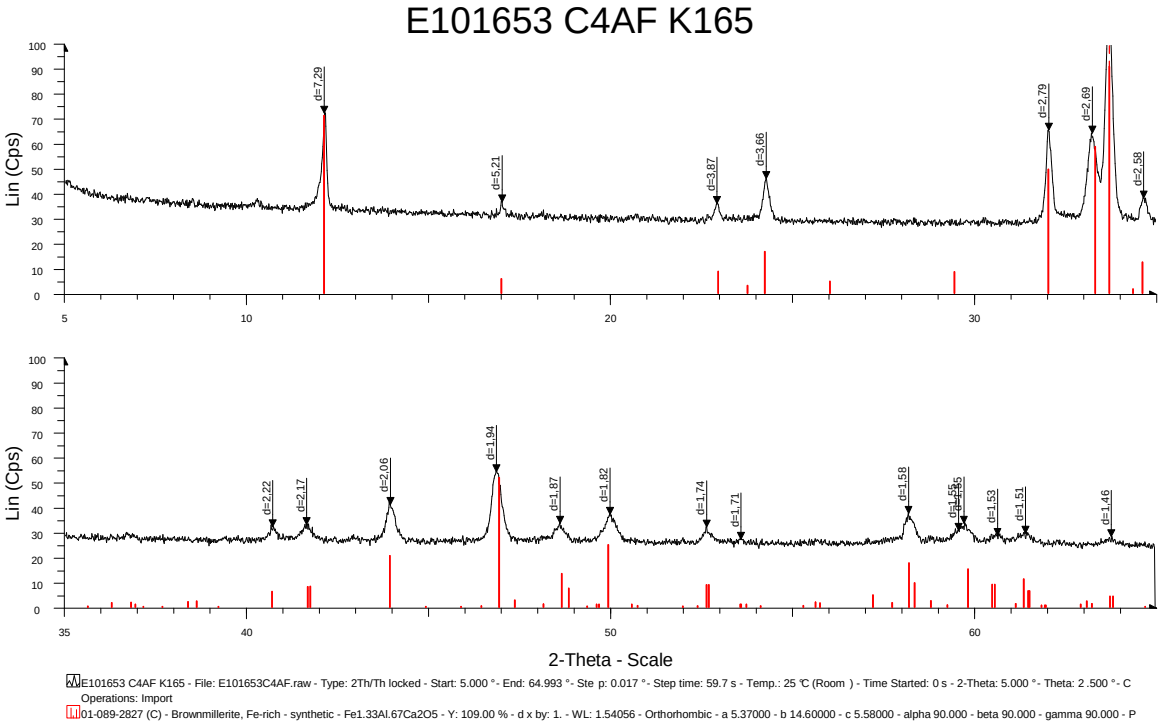

Figure 2A6-2: XRD pattern for the residue after selective dissolution

Figure 2A6-2 shows the results of XRD analysis of the selective dissolution residue after the removal of C_2S and ye'elimite from the clinker. We can see that $C_4A_3\$$ (2 Theta = 23.6°) and C_2S (2 Theta = 12.2°) are completely gone and there are no hydrates (e.g. ettringite, 2 Theta = 9.08°) formed during the operation.

Annex 2-7: Granulometry LASER MS 2000

Principle

Granulomery laser is a technique which allows measuring the distribution of particle size between 0.02 and 2000 microns in a mixture. The principle is based on the diffraction of laser.

Experimental procedure

The materials are measured by means of laser granulometry measurement with Malvern MasterSizer 2000 according to LCR-MO-041 using the complex diffractive index of cement: 1.68 + 0.1i. The measurement is carried out with agitation speed of 800 rpm and pump speed 2000 rpm. Dispersion with ultrasound is not necessary for the relatively coarse samples.

Annex 2-8: Grinding in the ball mill

Principle

Materials are grounded into a lab ball mill with steel balls with the requirement of Blaine specific surface area.

Experimental process

- Determine at first the density of the clinker, which will be used for measuring the Blaine surface.
- Insert the quantity of clinker in the mill and run 500 rounds.
- Open the door and clean around.
- Close the door, run 500 rounds again.
- Open the door and take out the samples to measure the fineness Blaine (take at 3 different places at the bottom of the grinder and mix)
- Measure and note the Blaine fineness value.
- Adapt the number of rounds to run for the next step (depend on the measured value and expected value in Blaine).

Annex 2-9: Blaine specific surface measurement

Principle

The SSB (Blaine specific surface) is an estimation of the surface area per unit mass of a powder. It is used to characterize the fineness of a powder and is expressed in cm²/g.

SSB is determined indirectly by measuring the time of a known volume of air passing through a pellet of powder with an effective pressure. Then, according to the following equation, we can calculate the SSB:

$$\mathbf{S} = \frac{\mathbf{K}}{\mathbf{MV}} \times \frac{\sqrt{e3}}{1-\mathbf{e}} \times (-0.9708 \times \theta + 760.7) \times \sqrt{\mathbf{t}}$$

where:

K = constant of the equipment
e = is the volume porosity of the bed (dimensionless)
t = time of passage of air (s)
MV = density (g/cm3)
θ = temperature of ambient air
S = specific surface Blaine (cm²/g)

Experimental process

- Determine the density of sample
- Weigh the quantity of the sample (m) to obtain the volume density of the bed (e = 0.500) with the following formula: m = 0.5 x MV x V(g).
  where:
  MV = density of the sample in g/cm^3
  V = Volume of cell

- Put the total amount of material into the cell with a funnel
- Put a second filter paper on the sample, and insert the plunger slowly until the plunger comes into contact with the cell. While maintaining pressure, rotate the plunger 90°.
- Slowly remove the piston and measure the time.

Accuracy of results

- Check the oil level in the tube and fill if necessary.
- With standard samples of Portland cement 114P, measure four times of passage of air (t) and then use the average value to calculate the SSB.
- If the error is ± 58 cm²/g compared to the standard value is 3774g/cm², the calibration is considered good
- If not, value K (constant of the equipment) should be calculated as following equation:

$$\mathbf{K} = 1.414 \times \mathbf{S} \times \mathbf{MV} \times \frac{\sqrt{0.1\eta}}{\sqrt{\mathbf{t}}}$$

Where, η is the viscosity of air (refer to the instruction manual to know its value)

Annex 2-10: pH measurement

Experience

In suspension experiments, pH values were measured continuously with pH meter PHM210 standard Meterlab. Each time before the experience, the pH meter is calibrated with the standard solution pH 4.00 and pH 10.00.

Precision

Measured values of pH during the hydration of cement k165-400B-5A in suspension (E/C=5) were compared with the calculated values by CHESS. It was found that with measured values was high and almost in parallel with the calculated ones, this probably due to the precipitation of some hydrates which were found in the surface of sensors.

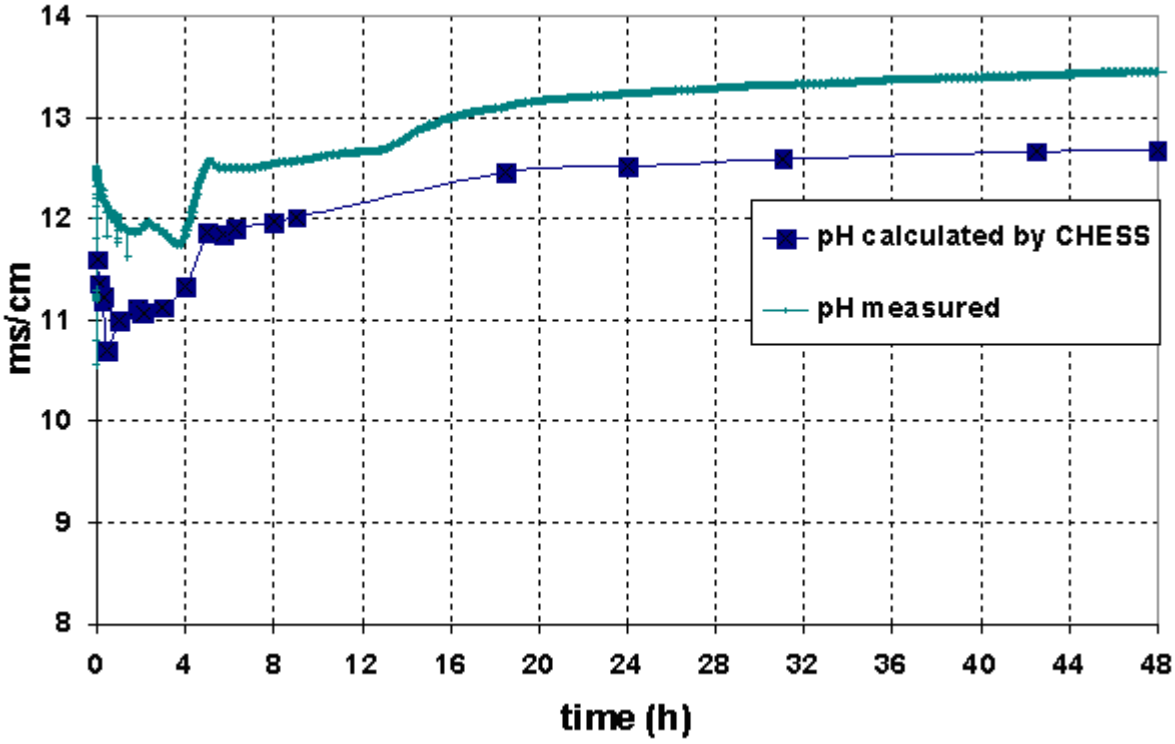

Figure 2A10-1: comparison of pH values measured during the hydration of cement k165-400B-5A is suspension (E/C=5) and values calculated by CHESS with the given concentration of ions in the solution

Annex 2-11: Rietveld-XRD method (hydrate cement)

Principle (Same as Annex 2-3)

Quantified analyse with Rietveld method (Same Annex 2-3)

Experimental procedure

Different methods are used to stop the hydration. In consideration of efficiency and accuracy, the solvents are used to dry the samples as following steps:

- Prepare in a Whatman system (Whatman filter with diameter 90mm with Teflon support) with filter (No. 542 retention 2.7 microns).
- First time quickly rinse with acetone (the volume of solvent is 2-3 times than that of solid) and mix with a spatula slowly (not to damage the filter).
- Wait until the residue is as dry as possible (sometimes, a few cracks are starting to appear).
- Second rinse with acetone, but very slowly (drop by drop).
- Once the dough is dry, a third rinse with ether, also very slowly.
- Wait until the sample is completely dry (cracks).
- Store the sample in a sealed plastic tube, then in a desiccator with silica gel.
- X-ray diffraction analysis

In fact, different solvents (2*acetone/ether, 3* isopropanol, 3*methanol) are used, and the results are compared.

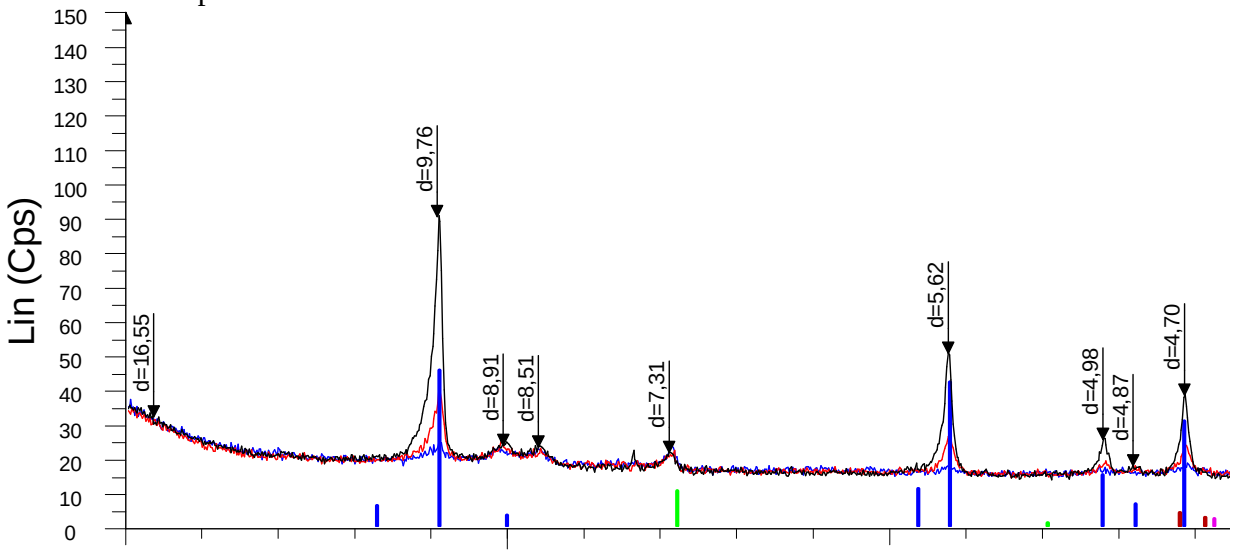

Figure 2A11-1 : comparaison of XRD patterns of samples at 1 month dried by different solvents

In the diagram, we can observe that the peaks of ettringite according to the various stoppages don't have the same intensity. With the stoppage with acetone/ether, the peaks of ettringite are intense while with isopropanol and ethanol, its peaks have lost their intensity and are shifted significantly.

The decrease and shift of the peaks of ettringite lattice (9.76 Å) have already been observed in the report of the Core project 4[73]. The reason is probably the dehydration of ettringite.

Accuracy of results

Mass balance is used to estimate the precision of quantified results of hydration phases in section 3.1. It shows that the results can be only used for semi-quantified. All the parameters are kept the same for all the experience in order to compare between them.

Annex 2-12: Thermodynamic database of CHESS (hydrate cement)

Arcanite {composition = 1.0 SO4[2-] 2.0 K[+], logK = 2.25101(0), 1.86369(25), 1.3628(50), 1.25589(75), 1.01307(100) }

Anhydrite {composition = 1Ca[2+], 1SO_4[2-], logK = 4.1043(0), 4.3064(25), 4.7587(60), 5.3851(100), 6.2741(150), 7.2829(200), 8.4644(250), 9.9598(300), vol.weight = 2963.47 kg/m^3}

Gypsum {composition = 1Ca[2+], 1SO_4[2-], 2H_2O, logK = 4.5331(0), 4.4823(25), 4.6094(60), 4.9035(100), 5.4299(150), 6.1266(200), 7.0386(250), 8.3003(300), vol.weight = 2305.16 kg/m^3}

Calcite {composition = -1H[+], 1Ca[2+], 1HCO_3[-], logK = -2.2257(0), -1.8487(25), -1.333(60), -0.7743(100), -0.0999(150), 0.5838(200), 1.3262(250), 2.2154(300), vol.weight = 2709.89 kg/m^3}

Ettringite {composition = 6Ca[2+], 2Al[3+], -12H[+], 38H_2O, 3SO_4[2-], logK = -56.8566, vol.weight = 1774 kg/m^3}

Gibbsite {composition = -3 H[+], 1 Al[3+], 3 H_2O, logK = -9.3787(0), -7.756(25), -5.8286(60), -3.9979(100), -2.0853(150), -0.4377(200), 1.0575(250), 2.4754(300), vol.weight = 2440.97 kg/m^3}

Monosulfoaluminate {composition = 4Ca[2+], 2Al[3+], -12H[+], 18H_2O, 1SO4[2-], logK = -72.5066, vol.weight = 2014 kg/m^3}

C_4AH_{13} {composition = 4Ca[2+], 2Al[3+], -14H[+], 20H_2O, logK = -104.3666, vol.weight = 2044 kg/m^3}

C_2AH_8 {composition = 2Ca[2+], 2Al[3+], -10H[+], 13H_2O, logK = -60.2066, vol.weight = 1946 kg/m^3}

C_3AH_6 {composition = 3Ca[2+], 2Al[3+], -12H[+], 12H_2O, logK = -80.9266, vol.weight = 2521 kg/m^3}

CAH_{10} {composition = 1Ca[2+], 2Al[3+], -8H[+], 14H_2O, logK = -38.2666, vol.weight = 1742 kg/m^3}

Gehlenite {composition = -10.0H[+], 1.0$Si(OH)_4$(aq), 2.0Al[3+], 2.0Ca[2+], 3.0H_2O, logK = -64.62455(0) -56.57347(25) -49.76782(50) -43.93957(75) -38.89228(100) }

Thaumasite {composition = 6Ca[2+], 2HCO_3[-], -6H[+], 32H_2O, 2$Si(OH)_4$(aq), 2SO_4[2-], -4 H_2O, logK = -18.61, vol.weight = 1890 kg/m^3}

Strätlingite {composition = 2Ca[2+], 2Al[3+], -10H[+], 11H_2O, 1 $Si(OH)_4$(aq), logK = -49.2291, vol.weight = 1936 kg/m^3}

Si-Hydrogarnet {composition = 3Ca[2+], 2Al[3+], -12H[+], 8.8H_2O, 0.8$Si(OH)_4$(aq), logK = -68.6586, vol.weight = 2779 kg/m^3}

CSH08 {composition = -1.6H[+], 0.8Ca[2+], 1$Si(OH)_4$(aq), -0.4H_2O, logK = -10.94, vol.weight = 2230 kg/m^3}

CSH09 {composition = -1.8H[+], 0.9Ca[2+], 1$Si(OH)_4$(aq), -0.2H_2O, logK = -12.96, vol.weight = 2230 kg/m^3}

CSH10 {composition = -2.0H[+], 1.0Ca[2+], 1$Si(OH)_4$(aq), logK = -15.06, vol.weight = 2230 kg/m^3}

CSH11 {composition = -2.2H[+], 1.1Ca[2+], 1$Si(OH)_4$(aq), 0.2H_2O, logK = -17.10#-17, vol.weight = 2230 kg/m^3}

CSH12 {composition = -2.4H[+], 1.2Ca[2+], 1$Si(OH)_4$(aq), 0.4H_2O, logK = -19.13, vol.weight = 2230 kg/m^3}

CSH13 {composition = -2.6H[+], 1.3Ca[2+], 1$Si(OH)_4$(aq), 0.6H_2O, logK = -21.25, vol.weight = 2230 kg/m^3}

CSH14 {composition = -2.8H[+], 1.4Ca[2+], 1$Si(OH)_4$(aq), 0.8H_2O, logK = -23.43, vol.weight = 2230 kg/m^3}

CSH15 {composition = -3.0H[+], 1.5Ca[2+], 1$Si(OH)_4$(aq), 1.0H_2O, logK = -25.70, vol.weight = 2230 kg/m^3}

CSH16 {composition = -3.2H[+], 1.6Ca[2+], 1$Si(OH)_4$(aq), 1.2H_2O, logK = -27.98, vol.weight = 2230 kg/m3}

CSH17 {composition = -3.4H[+], 1.7 Ca[2+], 1 $Si(OH)_4$(aq), 1.4H_2O, logK = -30.3, vol.weight = 2230 kg/m^3}

CSH18 {composition = -3.6H[+], 1.8 Ca[2+], 1 $Si(OH)_4$(aq), 1.6H_2O, logK = -32.58, vol.weight = 2230 kg/m^3}

$Fe(OH)_3$ { composition = -3H[+], 1Fe[3+], 3H_2O, logK = -6.9971(0), -5.6556(25), -4.1038(60), -2.6878(100), -1.2773(150), -0.1146(200), 0.913(250), 1.8839(300), vol.weight = 3110.27 kg/m^3}

Portlandite {composition = -2H[+], 1Ca[2+], 2H_2O, logK = -22.85, vol.weight = 2241.43 kg/m^3}

Annex 2-13: NMR

Experience

Solid state NMR for 27 Al and 29Si were done at E.S.P.C.I. (Ecole Supérieure de Physique et de Chimie Industrielles de la Ville de Paris).

The solid state 27Al nuclear magnetic resonance spectra were recorded on a Bruker DRX spectrometer in 4mm zirconia rotors with the frequency 14.1 kHz for about 5 hours.

The solid state 29Si nuclear magnetic resonance spectra were recorded on a Bruker DRX spectrometer in 4mm zirconia rotors with the frequency 5 kHz for about 17 hours.

Precision

In fact, the frequency and the time during of experience could influence a lot the intensity of signal. However, in both case, optimisation of relaxation time and the time during of experience was not done due to the budget restraint. The results are only qualified.

Annex 2-14: DTA (Differential Thermal Analysis)

Principle

Temperature measurements were made by two thermocouples connected in opposition which plunge respectively into the heart of the sample and reference. This arrangement gives a very good sensitivity to thermal phenomena occurring in the sample. The material chosen for the reference should be inert in the temperature range of work (in our case alumina).

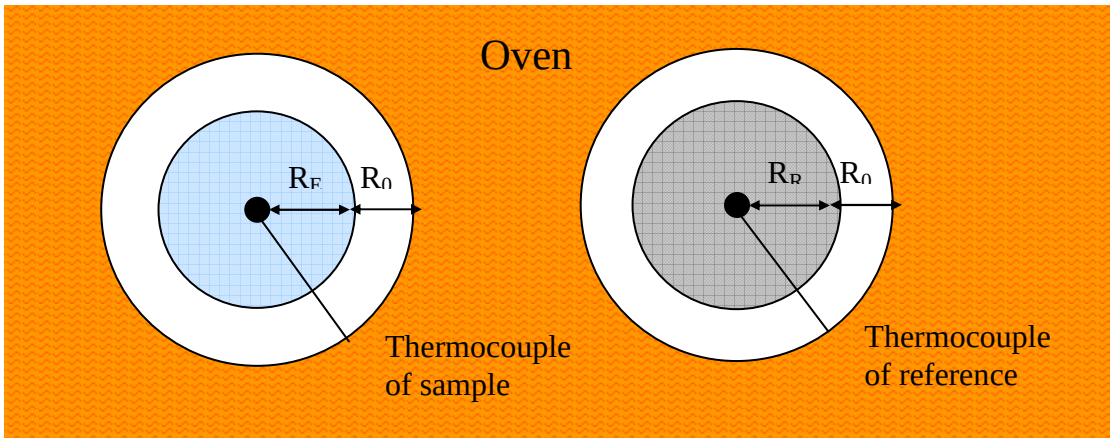

Figure 2A14-1: schema of DTA equipment

Procedure

Weigh between 20 and 60 mg of powder sample. Depending on the density of the sample, the glass tube should be filled approximately to one third. The powder in the tube is then tapped to compact the sample.

In the case of spatial analysis of the same nature, try to have the same amount for all the samples so that the results are more comparable.

Annex 5-1 Synthesis of a'-C_2S with $Na_2B_4O_7$

Mixture is made by pure calcite and silicon oxide powder according to the stoichiometric mix of 2 mol CaO and 1 mol SiO_2. $Na_2B_4O_7$ is used to stabilized C_2S into a'-form.

	$CaCO_3$	SiO_2	$Na_2B_4O_7$
a'-C_2S	116.215	34.884	3.902

Table 5A1-1: mix composition in g for 100g of final product

The sintering procedure is 1 hour 45 minutes heating ramp to 1450°C, then holding for 4 hours. Subsequently the sample is quenched into the air.

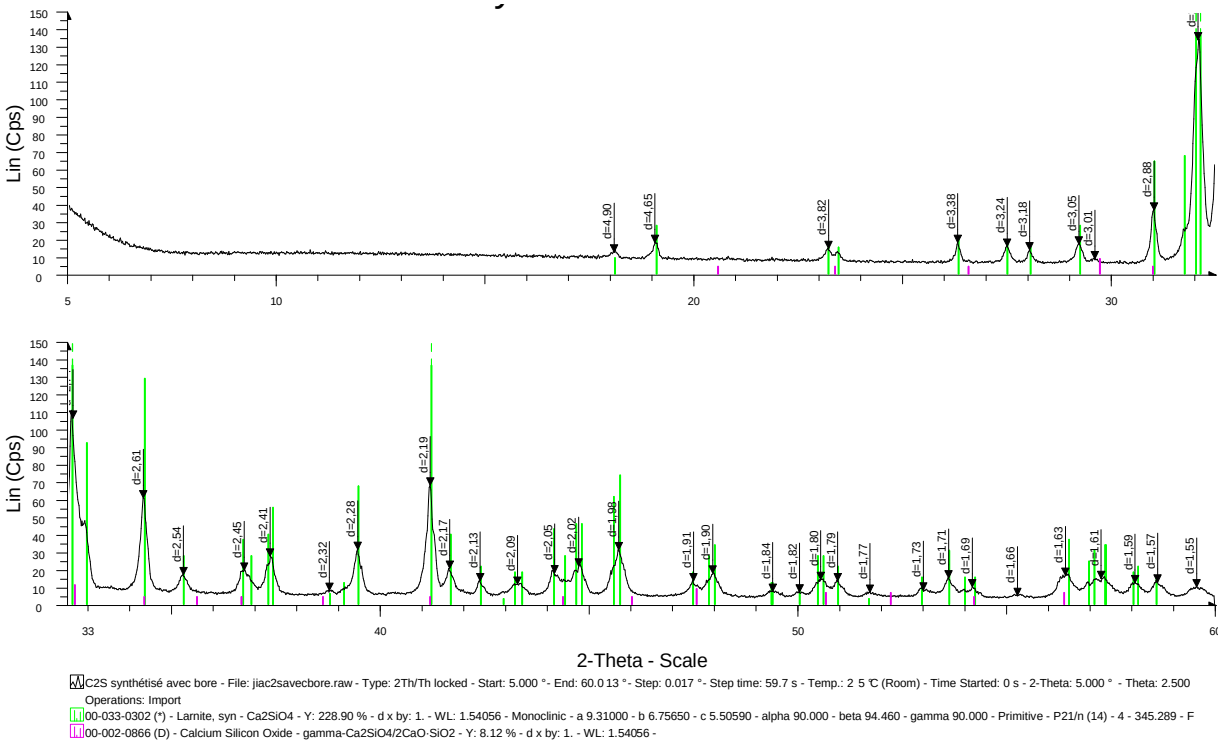

Figure 5A1-1: XRD pattern of synthesized C_2S

XRD analyse shows that synthesized C_2S is in a'-form.

Annex 5-2 Synthesis of C_4AF

Mixture is made by pure calcite, aluminium oxide and iron oxide according to the stoichiometric mix of 4 mol CaO, 1 mol Al_2O_3 and 1 mol Fe_2O_3.

	$CaCO_3$	Al_2O_3	Fe_2O_3
C_4AF	82.38	20.982	32.861

Table 5A2-1: mix composition in g for 100g of final product

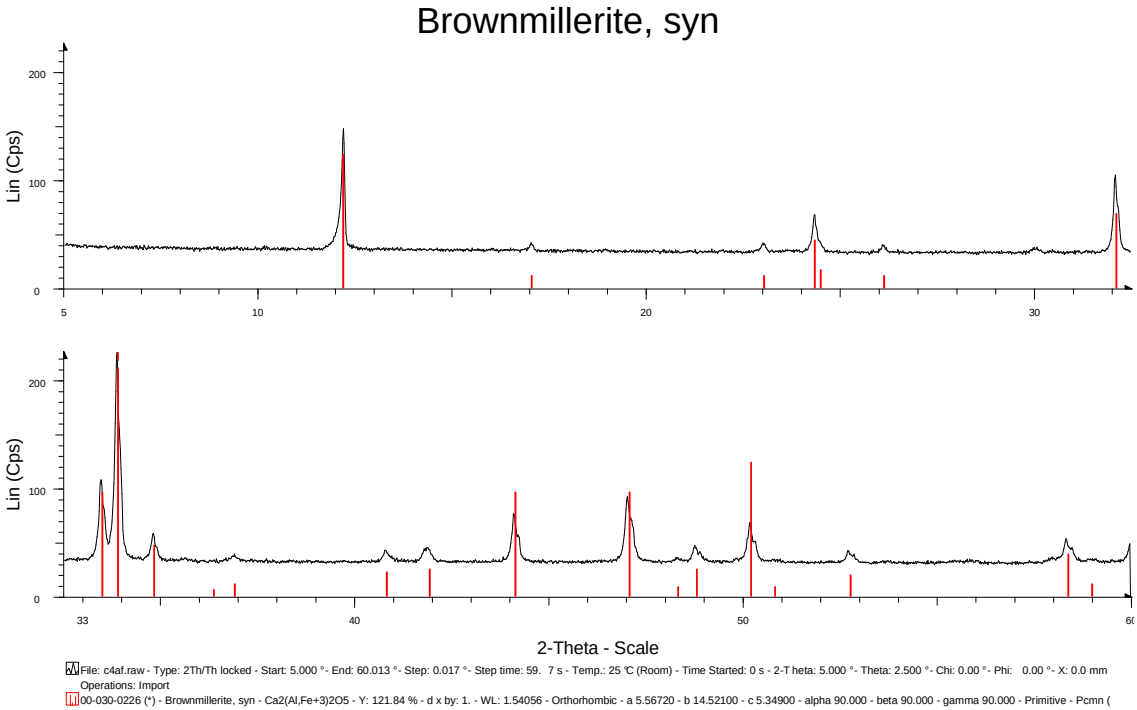

Figure 5A2-1: XRD pattern of synthesized C_4AF

The sintering protocol is 1 hour 30 minutes heating to reach 1300°C, then holding for 2 hours. If the sample shows severe melting or sticks to the surface of the crucible, sintering at 1250°C for 3.5 hours should be tried. Subsequently the sample is quenched in the air.

Bibliography

[1] http://www.ifremer.fr/lpo/cours/nao/climat_sat100-1000.html
[2] E. Gartner, Industrially interesting approaches to "low-CO_2" cements, Cem Concr Res 34, 2004,1489-1498.
[3] Wang, Y.M, Su, M.Z, Zhang, L, " Sulfoaluminate cement" in Chinese, China Building industry press, 1999
[4] F.Raupp-Pereira, A.M.Segadaes et J.A. Ladrincha, New clinker formulations made of industrial waste, University of Aveiro, Averio, Portugal, 2007.
[5] Zhang L. Su Muzhen, Wang Yanmou, Development and use of sulfo and ferro aluminate cements in China, Advances in cement research, 1999, vol. 11, no1, pp. 15-21 (6 ref.)
[6] DIAO J. Actuality and perspective of Chinese CSA development, Journal of Chinese Concrete and Cement Association, 2008, in Chinese
[7] Li, G.S., and Gartner, E.M., "High belite sulfoaluminate clinker: fabrication process and binder preparation," French patent application 04-51586, 27/01/2006
[8] G.S.Li, E.Gartner, G.Walenta, D.Sorrentino, V.Broyer, Lafarge Research Centre, Saint Quentin Fallavier, France, 2004
[9]Sulphoaluminate cement (in Chinese), Yanmou WANG, Muzhen SU, Liang ZHANG, Beijing Industial University Press, 1999, page 37.
[10] F. Canonico, G. Bernardo, al, Microstructural inverstigation on hydrated high-performance cements based on calcium sulfoaluminate, University of Basilicate, Potenza, Italy, 2006
[11] J.Zhang, Z.Li, Comparaison of early age resistivity development between ordinary Portland and calcium sulfoaluminate cement, the Hongkong University of Science and technology, Clear Water Bay, Kowloon, Hong Kong, China, 2007
[12]Martin T. Palou and Jan Majling, Hydration of the model sulfoaluminate-belite cements composed of blends of minerals with classified particle sizes, Ceramics-silikaty, 41(4), pp125-133, 1997
[13]Martin T. Palou and Jan Majling, Hydration in the System C_4A_3\$-C\$$H_2$-CH-H, Journal of Thermal Analysis, vol.46, n°2, pp.557-563, 1996.
[14] A., Nguyen, V.H., Divet, L., Feraille, A. and Le Roy, R. Experimental studies of hydration mechanism of sulfoaluminate clinker, in 12th International Congress on the Chemistry of Cement, Montreal, Canada, 2007b
[15] Peysson, S., Contribution à l'étude de la stabilization de déchets par du ciment sulfo-alumineux, Thèse de doctoorat, INSA de Lyon, 2005
[16] Wang, Y., Su, M., Yang, R. and Lui, B. A quantitative study of paste study microstructures and hydration characteristics of sulfoaluminate cement, 9th, International Congress on the Chemistry of Cement. New Delhi India 1993, pp 454-459.
[17] Production and application of Chinese CSAs (in Chinese), DIAO Jiangjing, Chinese Buidling material industrial press, 2006
[18] Philippe BEYLERIAN, Etude de Ciment Bélite Sulfoalumineux, Laboratoire central de recherche, Université Claude Bernard Lyon1 UFR Chimie et Biochimie, 2003
[19] HFW Taylor, Cement Chemistry, 2nd ed. 1997
[20] Ishida H. and Mitsuda T., Highly reactive β-Ca_2SiO_4, Special volume edited in 1995.
[21] Struillou R and M. Arnould M, Synthesis at about 750°C and properties of a sulfated C_2S, 7th ICCC, Paris, III, V-75-9
[22] Bouniol P, Synthese, mineralogie et hydraulicite du silicate dicalcique sulfate. These de l'Université Paris VI, 1983.

[23] Kasselouri, V., Tsakiridis, P., Malami, C., Georgali, B. and Alexandriou, C.A, Study on the hydration products of a non-expansive sulfoaluminate cement, Cement and concrete research, Vol. 25, No. 8, 1995, pp 1725-1736.
[24]Bernardo,G., Telesca,A. and Valenti,G.L. A porosimetric study of calcium sulfoaluminate cement paste cured at early ages, Cement and concrete research, Vol.36, No. 6, 2006, pp.1042-1047.
[25] Zhang, L. and Glasser, F.P. Hydration of calcium sulfoaluminate cement at less than 24h, Advance in Cement Research, Vol. 14, No.4, 2002, pp. 141-155.
[26] Andac, M. And Glasser, F.P. Pore solution composition of calcium sulfoaluminate cement, Advances in Cement Research, Vol. 11, No. 1, 1999, pp. 23-26
[27] Poisoning of tricalcium silicate hydration by soluble alumina, COTTIN B., VIBERT C. Cem. Wapno Gips, 1976, 7, 193-196
[28] Investigation technics to Analyse Hydration Characteristics of CSA Cements, A. CAPMAS, J.P. BAYOUX, M TESTUD, SU MUZHEN, ZHANG LIANG, The 3rd Beijing Inter Symp on Cement and Concrete Beijing, China, Vol 3, p 11
[29]Action de CaCO3, CaSO4 et CaSO4 · 2H2O sur l'hydratation de C3S, L. Montanaro, A. Negro and M. Regourd, Cement and Concrete Research, Volume 18, Issue 3, May 1988, Pages 431-437
[30] Drabik M., Smrcok L, Stevula L and Kapralik I., Study of brownmillerite prepared at 1200°C, Silikaty, 1987, 31, 299-307
[31]GUO,Y. Master report: role of ferrite in Chinese ferro sulfoaluminate cement, Chinese, 1987
[32] Sharp, J.H., Lawrence, C.D. and Yang, R. Calcium sulfoaluminate cements – low-energy cements, special cement or what?, Advances in Cement Research, Vol. 11, No. 1, 1999, pp. 3-13.
[33] Su Muzhen, W Kurdowski & F Sorrentino : Developments in non Portland cements. In 9th, International Congress on the Chemistry of Cement. New Delhi India 1993, pp 317-354.
[34] Wang, Y., Deng, J. and Su, M., in 8th ICCC, Vol.3, p.300 (1986)
[35] Tang, F.J. and E.M. Gartner, Influence of sulphate source on Portland cement hydration. Advances in Cement Research, 1988. 1(2): p. 67-74.
[36] Regourd, M., in 8th ICCC, Vol.1, p.199 (1986)
[37] HFW Taylor, Cement Chemistry, 2nd ed. 1997, page 189
[38] W. Jia, hydration study of BCSAF cement, in French, 2007
[39] W Jia, G. Ellis, D Denis, S Tongbo, thesis proposal of Jia WANG, Sep 2007
[40] Wang, Y.M, Su, M.Z, Zhang, L, " Sulfoaluminate cement" in Chinese, China Building industry press, 1999, page 44
[41] Neubauer, J. and Mayerhofer, W. "Solid solution series of ferrate and aluminate phases in OPC: Part I. The Ferrate phase". in 22nd International Conference on Cement Microscopy. 2000. Montreal, Canada.
[42] Yamaguchi, G. and Takagi, S. in 5th ISCC. 1969
[43] Marino, M.B. and Glasser, F.P., Cem. Concr. Res., 1984. 14: p. 360
[44] Bergstrom, T.B., Hall, C., and Scrivener, K.L., Adv. Cem. Res., 1991. 4: p. 141.
[45] Hall, C. and Scrivener, K.L., Adv. Cem. Based Mater., 1997.
[46] http://chess.ensmp.fr/
[47]. Thermodynamic investigation of the $CaO-Al_2O_3-CaSO_4-K_2O-H_2O$ system at 25°C. DAMIDOT D., GLASSER F.P, 1993, CCR 23, 5, 1185-1204.
[48] Thermodynamic investigation of the $CaO-Al_2O_3-CaSO_4-H_2O$ system at 25°C and the influence of Na2O, DAMIDOT D., GLASSER F.P, 1993, CCR 23,1, 221-238.

[49]Thermodynamic investigation of the $CaO-Al_2O_3-CaSO_4-H_2O$ system at 50°C and 85°C, DAMIDOT D., GLASSER F.P, 1993, CCR 22,6,1179-1191
[50]The effect of metakaolin on the reaction products and microporosity in blended cement pastes submitted to long hydration time and high curing temperature, M. Frıas, Advances in Cement Research, 2006, 18, No. 1, January, 1–6
[51] Stéphane BERGER, Etudes des potentialité des ciments sulfo-alumineux bélitiques pour le conditionnement du zinc de l'hydration à la durabilité, thesis report, University of Lille1, 2009
[52] Poisoning of tricalcium silicate hydration by soluble alumina, COTTIN B., VIBERT C. Cem. Wapno Gips, 1976, 7, 193-196
[53] Investigation technics to Analyse Hydration Characteristics of CSA Cements, A. CAPMAS, J.P. BAYOUX, M TESTUD, SU MUZHEN, ZHANG LIANG, The 3rd Beijing Inter Symp on Cement and Concrete Beijing, China, Vol 3, p 11
[54] Study of alite containing aluminium hydration, F. BEGARIN, S. GARRAULT, A. NONAT, L. NICOLEAU, Ann. Chim. Sci. Mat., 2008, 33, pp.251-258
[55] Thermodynamic investigation of calcium silicate hydrate/aluminium equilibria, X. CHEN, I. POCHARD, A. NONAT, ANN. Chim. Mat., 2008, 33, pp. 267-274
[56] Laszlo J. Csetenyi and F.P. Glasser, borate substituted ettringites, Mat. Res. Soc. Symp. Proc. Vol. 294, 1993
[57]D. Damidot et F.PG. Glasser "Investigation of the $CaO-Al_2O_3-SiO_2-H_2O$ system at 25°C by thermodynamic calculations", Cem. Conc. Res., 25(1) 22-28, 1995
[58] Quantitive aspects of 27Al MAS NMR of Calcium Aluminoferrites, Advn Cem Bas Mat, 1998, 7, 57-59
[59] Incorporation of aluminium in the calcium silicate hydrate (C-S-H) of hydrated Portland cements: a high-field 27Al and 29Si MAS NMR investigation, ANDERSEN M.D., JAKOBSEN H.J., SKIBSTED J, 2003, Inorg. Chem. 7, 2280-2287
[60] Silicon substitution for aluminum in calcium silicate hydrates, FAUCON P., PETIT J.C., CHARPENTIER T., JACQUINOT J.F., ADENOT F, 1999, J. Am. Ceram. Soc. 5, 1307-1312
[61] Thermal decomposition of mechanical activated gibbiste, K.J.D. MacKenzie, J. Temuujin, K. Okada, 1989, Thermochimica acta, 103-108
[62] Tobermorite as the final product of beta-C_2S hydration, Shebl F.A.,Helmy F.M. CCR, 1985, 15, 4, 573-580.
[63] 29Si and 27Al MASNMR Study of Stratlingite, Stephen Kwan, Judith LaRosa, Michael W. Grutzeck , J. Am. Ceram. Soc. 78, 7, 1921-1926.
[64] Solid-state 27Al and 29Si NMR investigations on Si-substituted hydrogarnets, J. Rivas Mercury, P. Pena, A. De Aza, X. Turrillas, I. Sobrados, J. Sanz, *Acta Materialia*, Volume 55, Issue 4, Pages 1183-1191
[65] Fisher, R and Kuzel, H.-J. (1982), Cem. Concr. Res. 12, 517
[66] Roberts, M.H., in 5th ISCC, Vol.2, 9.104 (1969)
[67] T. MATSCHEI, B. LOTHENBACH AND F.P. GLASSER, The AFm phase in Portland cement, 2007, Cement and Concrete Research, Volume 37, Issue 2 , February 2007, Pages 118-130 Volume 37, n° 2 , pp 118-130
[68] T. MATSCHEI, B. LOTHENBACH AND F.P. GLASSER, Thermodynamic properties of Portland cement hydrates in the system $CaO–Al_2O_3–SiO_2–CaSO_4–CaCO_3–H_2O$, 2007, Cement and Concrete Research , Volume 37, Issue 2 , February 2007, Pages 118-130 Volume 37, n° 2 , pp 118-130
[69] M. Balonis and F.P. Glasser, The Density of Cement Phases, Cement and Concrete Research, Volume 39, Issue 9, September 2009, Pages 733-739

[70] American Mineralogist, volume 072, pp. 226-227(1987)
[71]Calorimetric and thermogravimetric study on the influence of calcium sulfate on the hydration of ye'elimite, Frank Winnefeld and Stefan Barlag, Journal of Thermal Analysis and Calorimetry, DOI: 10.1007/s10973-009-0582-6
[72] Substitution of Si in the lattice of ettringite, W. Lukas, Cement and Concrete Research, Volume 6, Issue 2, March 1976, Pages 225-233
[73] V.Kocaba, G.Le Saoût, K.L.Scrivener, reactivity of blended cements with SCMs, Ecole Polytechnique Fédérale de Lausanne, Suisse, page 22